LABORATOIRE REACTIONS ET GENIE DES PROCEDES, CNRS UMR 7274
ECOLE DOCTORALE :
Sciences et Ingénierie des Ressources, Procédés, Produits, Environnement

THESIS

Presented and defended publicly on:
September 25th 2017
for obtaining a:

PhD title from the University of Lorraine
In Process and Product Engineering

by

David TORRADO

Effect of carbon black nanoparticles on the explosion severity of gas mixtures

Composition of the Jury:

Referees:	Dir Rech. Armelle CESSOU	(CORIA – Rouen)
	Pr. Phillipe GILLARD	(PRISME–Université d'Orleans-Bourges)
Members:	Dr. Wassila BENAISSA	(Solvay - Saint-Fons)
	Dr Agnès JANES	(CRAMIF - Paris)
	Dr. HdR. Michel MOLIERE	(UTBM - Belfort-Montbéliard)
	Dir Rech. Pierre-Alexandre GLAUDE	(LRGP– Thesis Co-Director)
	Pr. Olivier DUFAUD	(Université de Lorraine – Thesis Director)

CONTENTS

List of Figures

List of Tables

ACKNOWLEDGEMENTS

Behind any professional or personal achievement there is a group of key people who helped - in many instances without acknowledging it- to make it possible. This doctoral work has obviously not been the exception. It is for this reason that I would like to express my most deeply gratitude to some of the people who has participated in what began as a project a few years ago and what has become a reality today.

TO MY FAMILY

First of all, I would sincerely like to express my infinite gratitude to Ana Lucia Beltran and Juan de Dios Torrado, my parents. All what I have achieved until this day, no matter the size, is thanks to you. Since passing the very early exams (some of them that deserved to be stick on the refrigerator) until this doctorate title are the product of your wise advice, supervision and support. Even at more than 10 thousand kilometers away, I have felt your presence and company every day. To my two brothers, Juan Manuel and Julian, thank you very much. The constant talks and advices proved very helpful. You managed to transmit to me that healthy ambition to conquer every challenge. No matter how difficult it could be, with hard work, discipline and hope everything it's possible. You have always been an extraordinary model and example. I can finally claim that I have beaten you two for the first time regarding an academic achievement, perhaps because you have never decided or attempted to pursue a PhD…. but it, nevertheless, does not matter, I am the first 'doctor' in the family ☺.

Many thanks to my uncles and cousins, you have always been very supportive looking out for my well-being. Every Sunday night talk we had worked as a revitalizer for the coming challenges of the week.

TO LAURA

I would also like to thank my girlfriend, Laura Fonseca, an unconditional partner in uncountable battles. The only thing more challenging than doing a PhD alone is to make it while maintaining a long-distance relationship. But we did it… incredibly we did it! Thank you so much for every tip, gift, laugh and support. Thank you for each conversation that helped me to shape and reshape my ideas, to decide how to face every challenge and to recharge energies for the future. I hope we can together continue sharing many more achievements and demonstrating everyone that boundaries do not exist.

TO THE MEMBERS OF THE JURY AND THESIS DIRECTORS

I would like to thank the members of the jury for kindly agreeing to evaluate this work, rising interesting scientific inquiries and providing in depth perspectives for this research.

I am deeply grateful to my two thesis directors Olivier Dufaud and Pierre-Alexandre Glaude. All your supervision, grounded advice and discussions significantly contributed to the success of this work, paralleling enhancing my critical spirit and professional skills. Thanks for all those good conversations which, besides their deep scientific content, allowed me to learn a lot about the French culture and some of the world curiosities, all memories that I will always carry with me.

I would also like to acknowledge Professor Felipe Muñoz for giving me the opportunity to work in collaboration with the University of Los Andes and to help me addressing the project's framework for its good development.

TO THE MEMBERS OF THE 'SAFE' AND LRGP LABORATORY

The quotidian work in the laboratory would not have been that interesting and pleasant without the charisma and good attitude of all the members of the SAFE team. The conversations held during our coffee gatherings had a positive impact on my day.

Thank you for all the cooperation and interest shown during the course of this research. I want to express my gratitude to Dominique Thomas and Augustin Charvet for your constant collaboration in all the dispersion stability experiments. Likewise, I would like to express my gratitude to Stéphanie Pacault and Jean-François Remy for the help provided in the different laboratory tests carried out during the development of this work. I want to thank the people who directly worked on this project: Nicolás Cuervo, Carlos Murillo, Valentina Buitrago, Mariangel Amín and Andrés Pinilla.

In addition, I would like to thank Charly Koenig, Christian Blanchard and the workshop team for the help with the modifications of the 20L sphere and the propagation tube and the implementation of the Schlieren system.

TO MY FRIENDS

The life inside and outside the laboratory has been very pleasant thanks to the contribution and support of all my friends. Thanks to my "parceros" since the school, Daniel Flórez, Adriana Flórez, Jairo Tulande, Juan Carlos Cortés, Juan Gabriel Camelo, Laura Celis, Pio, Mario, Aleja and Andres Hernández, who despite the distance were always taking care of my me.

To my Colombian family in Nancy that accompanied me on this trip. Thanks to Nicolás, David R., Carlos, Daniela and Fabio. Our everyday talks were very useful to clarify my ideas in addition to having a good time. Many thanks to Wilmar, Deisy, Alejandra, Álvaro, Camilo, Felipe Buendía, Felipe Melo, Diana 'Caleña', Diana Guerrero, Andrés Alejo, Giovanny and all the people with whom I shared good moments in Nancy.

To my friends in the lab, thank you so much: Guillemette, Kevin, Marc, Selven, Miriam, Loïc, François and Quentin. All your help during my doctorate work and all the good moments we lived together were terrific. I also want to thank all the doctoral students with whom I had the opportunity to share in the different events organized in the laboratory. I also want to thank Edouard, Zineb and all the friends outside the lab, each one of them ready to share a "cervecita" and enjoy a good time together. My gratitude also goes out to all of the others who I am failing to mention by name, but who have made valuable contributions as well.

ABSTRACT

Nanoparticles have been progressively used in a wider variety of applications because of their special properties compared to bulk material. Atmospheres with dispersed nanoparticles and combustible gases are commonly generated either during the production of carbon black nanoparticles or during industrial applications that involve incomplete combustion, leading to the formation of hazardous explosive hybrid mixtures. Common examples of hybrid mixtures are coal/gas mixtures in mines, natural gas/fly ash in power plants or hydrocarbons/resins in plastics manufacturing. Up to now, flammable gas/solid mixture explosions are not well understood because of the intrication of the thermal transfer process, the combustion kinetics mechanisms and the interactions between turbulence and combustion. The main objective on this work is to study the explosion severity and flame burning velocities of carbon black nanoparticles/methane to better understand the influence of added nanopowders in gas explosions, and to unnravel the influence of dispersed nanoparticles on the combustion reaction, heat transfer and flame stretching.

Two grades of carbon blacks nanoparticles ranging from 20 to 300 nm average diameter have been mixed with methane. The powder has been characterized by scanning electron microscopy and BET. The dust dispersion has been characterized by using laser diffraction and particle image velocimetry (PIV). Tests have been performed in a flame propagation tube and in the standard 20 L explosion sphere. The influence of carbon black particles on the explosions severity and in the front flame propagation has been appreciated by comparing the results obtained for pure gas mixtures. The influence of the initial turbulence level and of the elementary particle size of the nano-sized carbon black have been also studied. It appeared that the carbon black nanoparticles insertion increases around 10% the explosion overpressure for lean methane mixtures at low initial turbulences. Similar results were obtained for high initial turbulent systems. Therefore, it seems that nanoparticles has an impact on the severity of the explosion even for quiescent systems, contrary to systems involving micro-sized powders that requires a dispersion at high turbulence levels. Concerning the maximum rate of pressure rise, the insertion of carbon black nanoparticles increase around 15% this variable for lean fuel mixture. However, this behavior is only observed at high initial turbulence levels. The increment on the maximum rate of pressure rise is higher for powders with lower elementary particle diameter, which is notably due to the fragmentation phenomena that promote the heat exchange. The burning velocity of gaseous mixture seems to increase when the initial turbulence is augmented. However, for significant initial turbulence levels, the flame velocity seems to decrease. The results showed that the addition of low concentrations of nanoparticles modifies the flame propagation.

A flame propagation numerical model associated to a gas/carbon black mixture has been developed to examine the influence of carbon blacks on the flame propagation and on the thermal heat transfer, especially on radiative transfer. The results of the numerical model suggest that the radiative heat contribution promotes the flame acceleration due to the increase of the temperature on the flame zone. This result is consistent with the experimental increase on the explosion severity for some hybrid mixtures.

RÉSUMÉ

Les nanoparticules ont été progressivement utilisées dans une grande variété d'applications en raison de leurs propriétés spécifiques comparées aux particules micrométriques. Des mélanges de nanoparticules dispersées dans des gaz combustibles sont communément générées lors de la production de nanoparticules de noir de carbone, ou dans des applications industrielles impliquant une combustion incomplète, entraînant la formation de mélanges hybrides explosifs dangereux. Des exemples courants de mélanges hybrides sont les mélanges charbon/gaz dans les mines, gaz naturel/cendres volantes dans les centrales électriques ou hydrocarbures/résines dans la fabrication des plastiques. Les explosions de mélanges de gaz inflammables/solides combustibles ne sont pas bien comprises en raison de la complexité des transferts thermiques, des mécanismes de cinétiques et des interactions entre la turbulence /combustion. L'objectif principal de ce travail est d'étudier la sévérité des explosions des nanoparticules de carbone noir / méthane afin de comprendre l'influence de l'insertion des nanoparticules sur les explosions de gaz. En outre, la mesure de la vitesse de combustion des mélanges hybrides permet d'analyser l'influence possible des nanoparticules dispersées sur la réaction de combustion, le transfert de chaleur et l'étirement de la flamme.

Deux types de nanoparticules de noirs de carbone allant de 20 à 300 nm de diamètre moyen ont été étudiés. La poudre a été caractérisée par microscopie électronique à balayage et BET. La dispersion de poussière a été caractérisée par diffraction laser et vélocimétrie d'image de particule (PIV). Des tests ont été effectués sur ces mélanges dans un tube de propagation de la flamme et dans une sphère d'explosion standard de 20 L. L'influence de la turbulence initiale et de la taille de particule élémentaire du noir de carbone a également été étudiée. Il semble que l'insertion de nanoparticules de noir de carbone augmente d'environ 10% la surpression d'explosion pour les mélanges pauvres en méthane à des turbulences initiales faibles. Des résultats similaires sont obtenus pour des systèmes avec une turbulence initiale élevée. Par conséquent, il semble que les nanoparticules ont un impact sur la gravité de l'explosion même pour les systèmes à basse turbulence, contrairement aux systèmes impliquant des poudres de taille micrométrique qui nécessitent une dispersion à des niveaux élevés de turbulence. En ce qui concerne la vitesse maximale de montée en pression, l'insertion de nanoparticules de noir de carbone augmente d'environ 15% cette variable pour les mélanges pauvres en méthane. Cependant, ce comportement n'est observé qu'à des niveaux élevés de turbulence initiale. L'augmentation du taux maximal de montée en pression est plus élevée pour des poudres avec une petite taille élémentaire de particule, notamment en raison des phénomènes de fragmentation qui favorisent les échanges de chaleur. La vitesse de combustion du mélange gazeux semble augmenter lorsque la turbulence initiale augmente. Les résultats ont montré que l'ajout de faibles concentrations de nanoparticules modifie la propagation de la flamme.

En outre, un modèle numérique de propagation de front de flamme associé à un mélange gaz / noir de carbone a été développé pour examiner l'influence du noir de carbone sur la propagation de la flamme et sur le transfert thermique, en particulier sur les transferts radiatifs. Les résultats du modèle numérique suggèrent que la contribution de la chaleur radiative favorise l'accélération de la flamme due à l'augmentation de la température sur la zone de flamme. Ces résultats sont en accord avec les résultats expérimentaux de sévérité de l'explosion pour certains mélanges hybrides.

INTRODUCTION

The study of dust explosions has become of great importance due to its frequent occurrence in the industry and to fatal consequences to persons, to environment and financial loss that may be generated. A first well documented dust explosion was registered in 1785 at a flour warehouse in Turin (Amyotte and Eckhoff, 2010), since then, the occurrence of such accidents has been continuously growing in the industry processes. In the last two centuries, around 2000 dust explosions had been registered worldwide in different types of industries, as petroleum, mining, pharmaceuticals or agriculture (Yuan et al., 2015). In the United States, between 1980 and 2007, 109 fatalities and 592 injuries occurred as a result of 197 accidental dust fires (Joseph, 2007). In China, between 1981 and 2011, 106 coal mine accidents were recorded (Yan and Yu, 2012). In France, the Bureau of Risk Analysis and Industrial Pollution (BARPI in French) reported 190 dust explosions between 1903 and 2010 (Janès and Chaineaux, 2010). In Figure 1, a classification of the accidents by type of dust is observed, in which the metal and wood particles represents around 44% of the worldwide dust explosions.

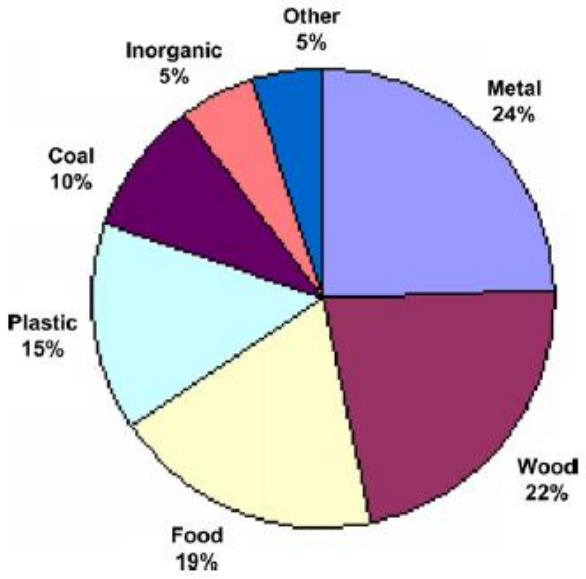

Figure 1. Distribution of dust explosion by type of material (Joseph, 2007).

Nevertheless, explosion of simultaneous dust and gaseous fuel have been also registered. For instance, over 25 methane/coal explosions have been recorded since 1976 in the United States (Zipf et al., 2013). This type of systems has been defined as *hybrid mixtures*, i.e. an explosive mixture of a flammable gas and combustible dust, in which the gas may be present below its lower flammability (or explosivity) limit (LEL) and the powder may be below its minimum explosive concentration (MEC). The explosion severity and sensitivity parameters of hybrid mixtures can considerably change in comparison to parameters of pure gases or dusts, generating under estimations in the design of protection devices such as rupture disks. In addition, their explosion parameters are still difficult to predict and depend on the interaction of the reaction mechanisms of both fuels, the heat transfer modifications and flow modifications due to the presence of dispersed particles. Owing to these difficulties, further studies of the explosive properties of such

atmospheres must be conducted (Amyotte and Eckhoff, 2010; Jiang et al., 2014; Worsfold et al., 2012).

In previous studies of hybrid mixture explosions, the influence of gas concentration in dust explosions has been analyzed (Amyotte et al., 2009; Cuervo et al., 2017; Dufaud et al., 2008, 2009; Khalili et al., 2012). However, the opposite case of the influence of dust concentration on gas explosions had not been widely investigated, even if in various industrial processes this type of hybrid mixtures can be encountered, for instance, methanation facilities, biofuel plants, during the combustion of fuel rich mixtures (generation of soot), during the combustion of organic dust particles (pyrolysis gases + nanoparticles) or during the production of some carbonaceous nanoparticles. Some hybrid mixtures consist of nanometric combustible particles with specific dispersion and reactive properties that must be characterized. In this work, the influence of the addition of low concentrations of carbon/black nanoparticles in methane/air mixtures is addressed. In the following paragraphs, the industrial processes in which these systems can occur and the interest of studying such specific hybrid mixtures involving dispersed nanoparticles will be developed.

Dispersed particles in previous accidents: Buncefield Explosion

The influence of dispersed particles on the flame propagation is not well understood and in some accidents, it could explain the acceleration of the flame. The Buncefield oil storage explosion can be an example of this phenomenon. On Sunday 11 December 2005, two explosions followed by fires of 23-fuel storage took place in this industrial site. No fatalities were registered but 43 injured and several damages to properties were obtained. The fire burnt during 5 days and a large quantity of smoke was emitted (Bradley et al., 2012).

Some studies have been performed in order to elucidate the phenomena that took place in the explosion and which explains the damages around the site. The results suggest that the damages observed in different directions around the storage site were the consequence of the deflagration of a vapor cloud, during which an acceleration of the flame was presented and leads to a DDT - deflagration to detonation transition (Bradley et al., 2011, 2012). The causes that generated the flame acceleration are not well understood. The confinement/congestion around the ignition point may explain the transition (i.e. the presence of trees along the alleys is supposed to have increase the congestion and to have led to a flame acceleration). However, it is not clear how the detonation could be sustained in open space (Bradley et al., 2011, 2012). Multiple mechanisms and flame propagation characteristics have been proposed to explain the acceleration of the flame, as for example, multiple ignitions, stratified explosion, inhomogeneous fuel concentration, etc. Among the previous explanations, it has been suggested that the flame speed can be increased as a result of the radiative transfer between a burnt mixture (gas + fine particles) and the reactants (Bradley et al., 2012). In addition, the presence of fine particles and aerosol droplets may enhance the flame speed due to the instabilities generated in the flame front (Lawes and Saat, 2011), which results in a flame wrinkling extended to greater length scales.

As a result, the effect of fine particles (as carbon black particles) ahead the flame front must be studied in order to understand the probable acceleration due to radiation and perturbations induced by these particles.

Hybrid mixture generation

In various industrial processes, simultaneous generations of fine carbonaceous particles and fuel gas occur. Thus, it is necessary to study and quantify the risk of a hybrid mixture explosion. The

gasification process is an example of this type of industrial processes. The development of gasification processes has been growing up as a consequence of the effect of fossil fuel on the emission of pollutant (which has a possible influence on climate change) and due to the increasing price of oil (Molino et al., 2016; Tilghman and Mitchell, 2015). In such processes, the conversion of organic solid/liquid is performed in order to obtain a gas phase (i.e. usually defined as syngas) and solid phase (i.e. called char). The mains stages of gasification processes are the oxidation, drying, pyrolysis and reduction. The first oxidation stage is necessary to obtain the required energy for the endothermic stages of the gasification processes. The pyrolysis stage consists in the thermal decomposition of the biomass and during the reduction step, the products generated in the previous stages (mainly oxidation and pyrolysis) react in order to obtain the final syngas (Molino et al., 2016). During the different stages, carbonaceous particles and combustible pyrolysis gases are generated simultaneously. Then, it is important to quantify the risk of hybrid mixtures explosion for such systems.

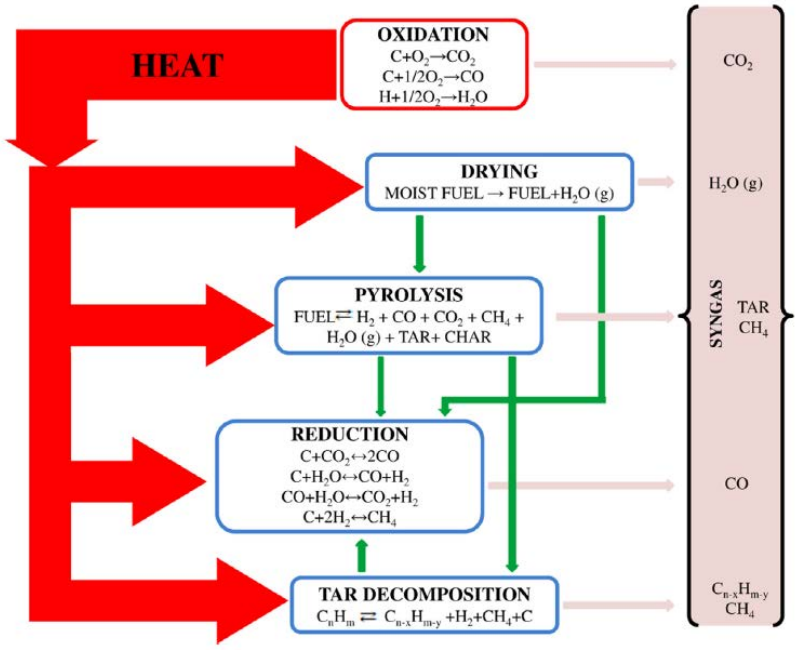

Figure 2. Main stages of the gasification process (Molino et al., 2016).

Another example of this type of hybrid mixture atmospheres can be found in coal mines. The effect of dispersed carbonaceous particles in the explosion of methane in coal mines is still not clear, due to the non-uniformity of an heterogeneous concentration of two fuel combustible systems consisting of methane, air and coal dust (Vasil'ev et al., 2017).

Specificities of nanoparticles/gas hybrid mixture explosions

As it has been previously highlighted, hybrid mixture explosions can present lower ignitability parameters and higher explosion severity properties due to the simultaneous presence of fuel gas and combustible particles (Ajrash et al., 2016; Pilão et al., 2006). The complex reaction mechanisms, the heat exchange in a heterogeneous media and the turbulent gas flow modifications can explain this trend. However, the contribution of each phenomenon and the influence of the dust and gas properties on this type of mixtures is not well defined. The study of nanoparticles/gas mixture allows to analyze the influence of the particle diameter on the explosion and to better understand the effect of the total surface of particles on the flame propagation. In other words, a

better understanding of the flame dynamic can be achieved through the dispersion of particles with a high specific surface and a promoting or inhibiting contribution of particles can be highlighted.

Furthermore, turbulence is needed for the dispersion of the dust (one of the conditions of the explosion hexagon), and may modify the reaction and the heat exchange during the explosion. This turbulence/reaction interaction becomes a challenge in the understanding of the influence of particles in gas explosions. However, the high stability at dispersion of nanoparticles can be an advantage in order to study hybrid mixture explosions at low turbulence levels and try to isolate the contribution of the turbulence from the reaction.

Combustion processes: influence of soot in fuel combustion

The soot release encountered during fossil combustion processes has been of great interest in the past years because it represents a problem as a contributor to the global pollution and also has become a significant health problem, associated to respiratory illnesses. From a thermodynamic point of view, the generation of soot induces an energy loss associated to incomplete reaction (Puri, 1993). The kinetics of soot formation has been greatly studied in order to address this problem (Agafonov et al., 2007; Appel et al., 2000; Saggese et al., 2014). However, a lot of questions are still present about the influence of initial concentrations of soot particles on the combustion reaction. It is not well understood what could be the effect of initial soot in combustion chamber on the growth of soot particles, as well as the possible effects of the soot oxidation and subsequent modifications in the fuel reaction mechanisms

In addition, the effect of the radiative properties of soot particles is of great importance in the risk evaluation of industrial fires as well as in the design of combustion chambers. In order to evaluate the consequences of a fire to the structure and people, empirical correlations are applied in order to estimate the heat loss due to radiative transfers between the flame ant soot particles present in the smoke emitted during the fire (Laurent, 2003). As a consequence, the study of the radiative heat transfer generated by soot particles is necessary to avoid underestimation of damages generated in this type of accidents.

Assimilating the carbon black nanoparticles to soot particles, the severity tests (i.e. determination of the maximum overpressure, maximum rate of pressure rise and the burning velocity) could be an approach to understand the influence of initial soot particles on the combustion reaction and on the flame propagation.

Objectives of this work

This present work aims to study the influence of carbon black nanoparticles to the explosion severity parameters of methane/air explosions. The explosion characteristics of nanoparticles/methane hybrid mixtures are studied and compared with the pure gas explosion. In addition, this thesis is an effort to understand the effect of dispersed nanoparticles on the flame propagation, radiative heat transfers and chemical reaction contribution. Moreover, low turbulence systems are analyzed in order to try to isolate the turbulence/reaction interactions present during hybrid mixture explosions.

This work is divided in four chapters, which describe the context of this type of systems, the experimental methodology implemented and the results of the explosion severity parameters.

Initially, the first chapter presents the main definitions and state of the art dust explosions, the specificities of nanoparticles systems and the hybrid mixture explosions studies previously performed. In addition, the different studies on the influence of some variables of interest in this

work are summarized and analyzed. Finally, a brief description of the interest of the study of hybrid mixtures burning velocity is presented and the recent efforts to measure the burning velocity of combustible powders are summarized.

In the second chapter, the experimental characterization of the dust properties and its dispersion characteristics are presented. Then, the turbulent flow developed in the experimental set-ups will be characterized by Particle Image Velocimetry (PIV). Moreover, the study of the influence of carbon black nanoparticles on the explosion severity parameters measured on a 20-L sphere is analyzed. The effect of the turbulence level, dust concentration, gas concentration and elementary particle diameter is also studied. In addition, the reaction contribution of carbon black nanoparticles is analyzed by micro gas chromatography. Finally, the explosion severity results for carbon black nanoparticles and methane/air mixtures will be compared to inert alumina nanoparticles/methane/air mixture, aiming to isolate the possible chemical contribution from the turbulence and heat radiation effect on the explosions.

In Chapter 3, the experimental determination of the burning velocity of methane/air and hybrid mixtures is developed in a propagation tube. In addition, the influence of nanoparticles concentration and of the initial turbulence level on the burning velocity is also analyzed. The influence of nanoparticles dispersion is developed now by analyzing the potential modifications on the flame surface, stretch and radiative heat transfer, which was not possible using the standard 20 L explosion sphere. The burning velocity determined using the flame propagation tube has been compared to the estimations of the flame velocity obtained with the explosions severity test results.

In Chapter 4, a numerical model aiming to determine the flame velocity of a gas mixture explosion through a two-phase media containing nanoparticles is presented. Firstly, the results of the simulation and the comparison with the experimental data are presented. Finally, the influence of radiative heat transfer and carbon reaction are analyzed.

References

Agafonov, G.L., Naydenova, I., Vlasov, P.A., Warnatz, J., 2007. Detailed kinetic modeling of soot formation in shock tube pyrolysis and oxidation of toluene and n-heptane. Proc. Combust. Inst. 31, 575–583.

Ajrash, M.J., Zanganeh, J., Moghtaderi, B., 2016. Effects of ignition energy on fire and explosion characteristics of dilute hybrid fuel in ventilation air methane. J. Loss Prev. Process Ind. 40, 207–216.

Amyotte, P., Lindsay, M., Domaratzki, R., Marchand, N., Di Benedetto, A., Russo, P., 2009. Prevention and mitigation of dust and hybrid mixture explosions. Process Saf. Prog. NA-NA.

Amyotte, P.R., Eckhoff, R.K., 2010. Dust explosion causation, prevention and mitigation: An overview. J. Chem. Health Saf. 17, 15–28.

Appel, J., Bockhorn, H., Frenklach, M., 2000. Kinetic modeling of soot formation with detailed chemistry and physics: laminar premixed flames of C2 hydrocarbons. Combust. Flame 121, 122–136.

Bradley, D., Chamberlain, G.A., Drysdale, D.D., 2012. Large vapour cloud explosions, with particular reference to that at Buncefield. Philos. Trans. R. Soc. Math. Phys. Eng. Sci. 370, 544–566.

Bradley, D., Chamberlain, G.A., Drysdale, D.D., 2011. The Buncefield Explosion. Presented at the Proceedings of the Sixth International Seminar on Fire and Explosion Hazards, Research Publishing Services.

Cuervo, N., Dufaud, O., Perrin, L., 2017. Determination of the burning velocity of gas/dust hybrid mixtures. Process Saf. Environ. Prot. 109, 704–715

Dufaud, O., Perrin, L., Traoré, M., 2008. Dust/vapour explosions: Hybrid behaviours? J. Loss Prev. Process Ind. 21, 481–484.

Dufaud, O., Perrin, L., Traore, M., Chazelet, S., Thomas, D., 2009. Explosions of vapour/dust hybrid mixtures: A particular class. Powder Technol. 190, 269–273.

Janès, A., Chaineaux, J., 2010. Explosions de poussières dans les lieux des travail: Recensement et analyse. ND - 2331- 220 -10- INRS - Hygième Est Sécurité Trav.

Jiang, J., Liu, Y., Mannan, M.S., 2014. A correlation of the lower flammability limit for hybrid mixtures. J. Loss Prev. Process Ind. 32, 120–126.

Joseph, G., 2007. Combustible dusts: A serious industrial hazard. J. Hazard. Mater. 142, 589–591.

Khalili, I., Dufaud, O., Poupeau, M., Cuervo-Rodriguez, N., Perrin, L., 2012. Ignition sensitivity of gas–vapor/dust hybrid mixtures. Powder Technol. 217, 199–206.

Laurent, A., 2003. Sécurité des procédés chimiques. Connaissances de base et méthodes d'analyse de risques. TEC & DOC.

Lawes, M., Saat, A., 2011. Burning rates of turbulent iso-octane aerosol mixtures in spherical flame explosions. Proc. Combust. Inst. 33, 2047–2054.

Molino, A., Chianese, S., Musmarra, D., 2016. Biomass gasification technology: The state of the art overview. J. Energy Chem. 25, 10–25.

Pilão, R., Ramalho, E., Pinho, C., 2006. Explosibility of cork dust in methane/air mixtures. J. Loss Prev. Process Ind. 19, 17–23.

Puri, I.K., 1993. Environmental Implications of Combustion Processes. CRC Press.

Saggese, C., Sánchez, N.E., Frassoldati, A., Cuoci, A., Faravelli, T., Alzueta, M.U., Ranzi, E., 2014. Kinetic Modeling Study of Polycyclic Aromatic Hydrocarbons and Soot Formation in Acetylene Pyrolysis. Energy Fuels 28, 1489–1501.

Tilghman, M.B., Mitchell, R.E., 2015. Coal and biomass char reactivities in gasification and combustion environments. Combust. Flame 162, 3220–3235.

Vasil'ev, A.A., Pinaev, A.V., Trubitsyn, A.A., Grachev, A.Y., Trotsyuk, A.V., Fomin, P.A., Trilis, A.V., 2017. What is burning in coal mines: Methane or coal dust? Combust. Explos. Shock Waves 53, 8–14.

Worsfold, S.M., Amyotte, P.R., Khan, F.I., Dastidar, A.G., Eckhoff, R.K., 2012. Review of the Explosibility of Nontraditional Dusts. Ind. Eng. Chem. Res. 51, 7651–7655.

Yan, X.-Q., Yu, J.-L., 2012. Dust explosion incidents in China. Process Saf. Prog. 31, 187–

Yuan, Z., Khakzad, N., Khan, F., Amyotte, P., 2015. Dust explosions: A threat to the process industries. Process Saf. Environ. Prot. 98, 57–71.

Zipf, R.K., Gamezo, V.N., Sapko, M.J., Marchewka, W.P., Mohamed, K.M., Oran, E.S., Kessler, D.A., Weiss, E.S., Addis, J.D., Karnack, F.A., Sellers, D.D., 2013. Methane–air detonation experiments at NIOSH Lake Lynn Laboratory. J. Loss Prev. Process Ind. 26, 295–301.

CHAPTER 1: Dust nanoparticles – gas hybrid mixture explosions

1.1. Dust explosions

An explosion is defined as the sudden liberation of chemical energy of an exothermal reaction that, under constant volume conditions, may generate a significant pressure rise or the liberation of a pressure wave (Eckhoff, 2003; Skjold, 2003). Many solid materials in bulk form are not flammable, but when subdivided, are highly explosive. Dust explosion is one of the most serious hazards in the process industry including the gas explosions and boiling liquid expansion vapor explosions – BLEVE (Abbasi and Abbasi, 2007). These accidents are of main interest in the process industry due to their fatal consequences to personnel and the financial loss that may be generated. Furthermore, dust explosion incidents can occur on wood, food, metal, power generation, polymers, mining, textiles and chemical process industries (Amyotte and Eckhoff, 2010). The fatal consequences of dust explosions imply the necessity of the comprehension of the hazard associated to the use of subdivided powder, as well as the design of protection devices and prevention procedures.

In order to generate a dust explosion, six requirements must take place, as shown in Figure 3.

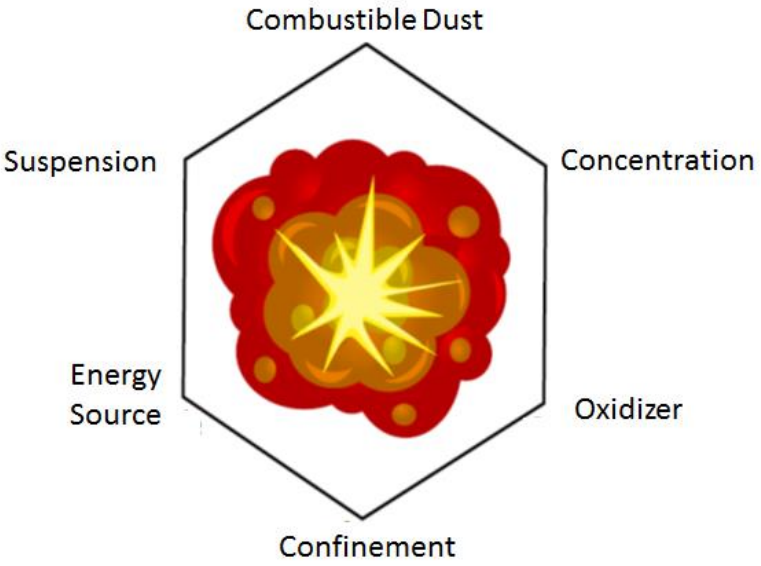

Figure 3. Dust explosion hexagon (Eckhoff, 2003)

A dust explosion is likely to occur if the combustible powder is dispersed in a confined site at the explosive concentration with a simultaneous presence of an ignition source. Even if the confinement is considered as a necessary element to have a dust explosion, some accidents demonstrate that this condition increases the likelihood and the severity of an explosion but is not compulsory, e.g. in the "Color Play Asia" party (2015) in Taiwan dust explosion, resulting in 15 deaths and 497 injuries (Chan and Chong, 2016; Cheng et al., 2016).

Eckhoff (2003) listed the major factors that will influence the sensitivity and the severity of dust cloud explosions (Table 1). The ignitability or ignition sensitivity describes the probability of occurrence for a dust explosion. The explosivity or explosion severity characterizes the violence of the phenomenon, which usually is described by the explosion overpressure or the burning velocity.

Table 1. Factors influencing the ignition sensitivity and explosion violence of dust clouds (Eckhoff, 2003)

#	Factor
1	Chemical composition of the dust
2	Chemical composition, initial temperature and pressure of the gas phase
3	Distribution of sizes and particle's shapes
4	Distribution of dust concentration
5	Initial turbulence
6	Possibility of a generation of explosion-induced turbulence in the still unburnt part of the cloud
7	Possibility of flame front distortion by mechanism other than turbulence
8	Possibility of significant radiative heat transfer

In addition to the chemical properties of the dust and to the dynamic conditions of the system at the moment of the ignition, the heat radiation transfer may contribute to the heat exchange between the flame and the unburnt mixture, and resulting in considerable modifications of the explosion severity (Abbasi and Abbasi, 2007). Especial attention will be addressed to this point in this work due to the high emissivity of carbon black particles. Despite numerous specifities of dust explosions, it should be pointed out that explosive gas and dust clouds exhibit similar ignition and combustion properties (Eckhoff, 2006):

- Flammability/explosive limits
- Laminar burning velocities and quenching distances
- Response of the burning velocity to the turbulence
- Detonation phenomena
- Adiabatic explosion pressures of similar magnitudes
- Well-defined minimum ignition levels
- Minimum ignition temperatures

Nevertheless, Eckhoff, (2006) highlighted the main differences between dust and gas explosions, emphasizing the necessity of further understanding of the specifities of each type of system. Firstly, the physics of the generation and modifications of a gas and dust cloud are substantially different, which means that at the conditions where accidental gas clouds are generated, a dust cloud is unlikely to be formed. Secondly, the ignition sensitivity of dust clouds is not only dependent of the

concentration limits, but also the state of stagnant layers and deposits constitute additional contributions to the flame propagation.

Another important difference is related to the homogenous concentration of the dust cloud, for instance, if a gas cloud has been generated assuming a perfect mixture, the concentration will stay unchanging due to molecular random motion. However, in dust cloud, gradient concentrations are likely to be obtained due to the inertial forces, including gravity. (Eckhoff, 2006). In addition, two different combustion mechanisms can control the dust explosions: homogeneous and heterogeneous. Small particles having a low vaporization temperature react with a homogeneous mechanism (for instance, starch particles with an average diameter lower than 20 μm), whereas, non-volatile particles and/or with a great particle sise will evidence a heterogeneous reaction mechanism (e.g. carbon black, metal powders with a great particle diameter) (Di Benedetto et al., 2010; Fumagalli et al., 2016). On the one hand, homogeneous combustion process usually involves a first step of particles heating, that leads to the volatilization and mixing of combustible gases (pyrolysis gases or metal vapors) with the air and finally a homogeneous combustion is present. On the other hand, in the case of a heterogeneous combustion, the diffusion of oxygen into a molten or solid core is necessary, and then, the heterogeneous oxidation takes place (Rockwell and Rangwala, 2013).

1.1.1. Explosion parameters

In industrial processes involving powders, the risk related both to the ignitability and explosivity of the material must be assessed. The principal properties describing the sensitivity and the severity of the explosion are explained in the following paragraphs.

1.1.1.1 Explosion sensitivity

Minimum explosive concentration (MEC)

The minimum explosive concentration is the lowest concentration of a dust homogeneously dispersed that ignites and that leads to flame propagation. The MEC of a combustible powder is measured following international standards in order to assure a standard characterization of the dust (ASTM E1515-14, 2014; NF EN 14034-3, 2011). During the test phase, conditions as the initial temperature, pressure and moisture are kept constant in order to avoid an influence on this limit. A dust cloud is dispersed in the 20-L sphere and ignited at a specific ignition delay time (i.e. delay time between the dispersion and the ignition of the dust) at the center of the chamber and at a suggested energy of 2.5 or 5 kJ. Since the MEC change with the ignition delay time and energy of the pyrotechnic igniter, the concentration limit should be considered a relative rather than absolute measurement.

Minimum Ignition Temperature (MIT)

The dust explosion could be generated in some industrial units when a combustible dust is in contact with hot surfaces. Thus, the minimum temperature of a hot surface that produces the ignition of a dust in contact with air must be estimated. This property, however, is not an intrinsic parameter for a given dust cloud and depends on the geometry of the hot surface and the dynamic state of the dust cloud (Eckhoff, 2003). Therefore, this temperature will change if the hot surface is in contact with a dust layer or a dust cloud, and both temperatures of the dust should be reported.

In order to determine the MIT of a dust cloud, the minimum temperature of the internal wall of a furnace that will generate the ignition of the dust is measured. The dust concentration and turbulence of dispersion are modified in order to follow the modifications on the MIT. The vertical

Godbert-Greenwald furnace is used for this measure and had been designed to avoid the fast sedimentation of particles. (ASTM E1491 - 06, 2012; Laurent, 2003).

Minimum Ignition Energy (MIE)

This parameter corresponds to the minimum electrical energy that generates an explosion of the most easily ignitable concentration under specific conditions. Smaller values of the MIE could be obtained modifying the spark discharge system or optimizing the number of repetitions, so this limitation must be taken in account when using this limit on the explosion prevention system (ASTM E2019 − 03, 2007). The dust is dispersed in the chamber and the energy is delivered after an ignition delay time (i.e. Δt between the dispersion and the ignition), a visual observation of the flame away of the spark gap is registered as inflammation. The modified Hartmann tube (0.5 and 1.2L) and the 20L sphere apparatus are used for the determination of the MIE (IEC 1241-2-3, 1994).

Minimum Oxygen Concentration (MOC)

In addition to the Minimum Ignition Energy, Minimum Explosive Concentration and the Minimum Ignition Temperature, the explosion sensitivity of a dust could be analyzed changing the oxygen concentration in the mixture. The minimum oxygen concentration or limiting oxygen concentration is defined as the minimum concentration of oxygen that allows the flame propagation of the dust cloud deflagration. This parameter is indispensable to study the influence of the equivalence ratio on the ignitibility of a dust cloud, especially for the design of inerting system units (Amyotte and Eckhoff, 2010; Eckhoff, 2004).

1.1.1.2 Explosion Severity

Explosion pressure characteristics

The explosion severity is usually characterized measuring the maximum overpressure and the maximum rate of pressure rise in a closed vessel. However, these parameters are not only a result of the intrinsic reaction properties of the combustible dust, but also they depend on the test volume. A particular attention had been paid in establishing the most appropriate vessel dimensions and test conditions that will reproduce the conditions probably obtained in industrial dust explosion. Two main explosion vessels had been designed for the explosion severity determination: a 20L and 1 m^3 explosion vessel. Figure 4 shows the 20L explosion sphere, which had been used for the explosion severity study of this work.

Figure 4. 20L sphere explosion apparatus (KUHNER Safety, 2015)

Maximum explosion pressure

A deflagration of a dust clouds at constant volume conditions generates an increment of the pressure over the time until a maximum value P_m (Figure 5). This parameter is related to the thermodynamic properties of the combustible mixture and it can be linked to the adiabatic temperature under ideal conditions.

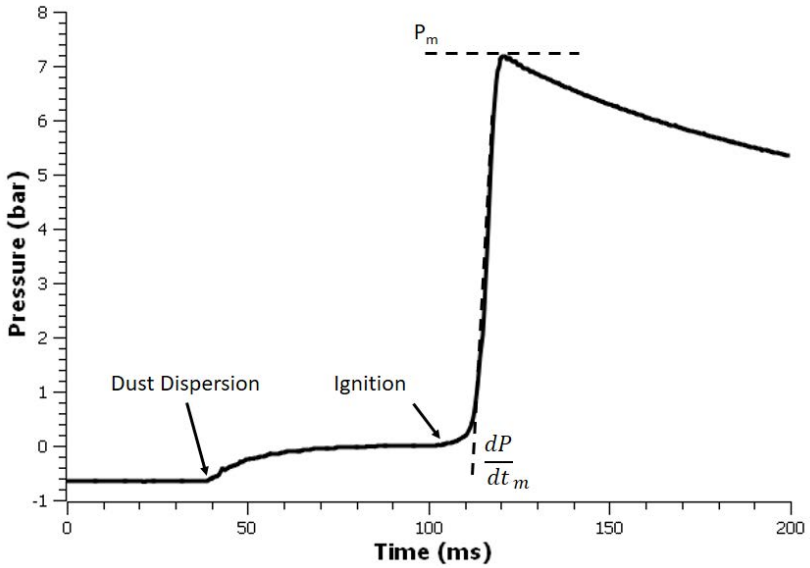

Figure 5. Pressure evolution inside the 20L sphere during a carbon black/methane/air hybrid mixture explosion.

Maximum Rate of Pressure Rise

The rate of pressure rise increases until a maximum value of $(dP/dt)_m$. If different tests are made under similar conditions, this variable allows the classification of the dust in different categories. Under confined conditions, the maximum overpressure is independent from the volume; however,

it is not the case for the maximum rate of pressure rise. Therefore, the normalized rate of pressure rise is calculated as:

$$K_{st} = \left(\frac{dP}{dt}\right)_m V^{1/3} \qquad \text{Eq 1}$$

Eckhoff (2003) pointed out that this "cubic law" is an approximation of a single point of the pressure explosion curve. This approximation is developed assuming that the flame thickness is negligible compared to the vessel size (Cashdollar, 2000). Further authors had analyzed the conditions under which the cubic root law could be used to properly estimate the severity parameters of the explosion at industrial conditions and its application is still questionable (Dahoe et al., 2002; Eckhoff, 2003).

The ignitability of a dust may be regarded as increasing as the minimum explosive concentration, the minimum ignition temperature and the minimum ignition decrease, and the explosivity greater when the burning velocity and the maximum rate of pressure rise increase (Mannan and Lees, 2005).

As previously described, the dust ignatibility and explosion severity parameters depend on the environmental conditions and industrial operating conditions. Hence, in the following subsections, a general panorama of the influence of the operation conditions and dust properties on hybrid mixtures explosions will be developed.

1.1.2. Turbulence

The turbulence level of the system before the ignition is a relevant parameter for the magnitude of the explosion severity. A high turbulence level will favor the combustion reaction and/or heat transfer. Similarly, an important combustion reaction, followed by a great energy liberation can increase the turbulence system. A key problem on the understanding of the effect of the initial turbulence level is the turbulence/reaction interactions observed during the dust and hybrid mixture explosions. In this work, the effect of the initial turbulence on the explosion severity of hybrid mixture carbon black nanoparticles/methane is of great interest, because the high stability of dispersion allows studying hybrid mixture explosions at low turbulence levels.

Turbulence is needed for the dust dispersion (one of the conditions of the explosion hexagon) and turbulence will be generated during the flame propagation (Skjold, 2003). As a consequence, two types of turbulence should be differentiated for dust explosion applications: an initial turbulence related to the dust cloud process generation (also called cold turbulence), i.e. air blast, mechanical agitation or vibrations for industrial conditions, and a second turbulence generated by the explosion itself, it means the expansion of the unburnt gases ahead of the propagating front flame. It should be stressed that the vessel geometry and internal obstacles enhance the turbulence after the ignition (Eckhoff, 2003).

The turbulence is a property of the flow (not of the fluid), which principal characteristics are:

- It is a continous phenomenon governed by the equations of continuum fluid mechanics. The smaller turbulent scale is larger than the molecular length scale.
- Turbulent flows contain structures, called turbulent eddy, to refer to the rotating structures of the flow, each one with an associated length and time scale. Different length scale are used to characterize the turbulent flow: the spatial length scale is determined by the physical boundaries, the integral length scale is characteristic for eddies containing mostly kinetic

energy, the Kolmogorov length scale is the smallest eddy size in a turbulent flow and the Taylor's length scale is an intermediary scale between the integral and Kolgomorov's scale (Skjold, 2003). The different flame regimes in function of the length scale are shown in the Borghi-Peters diagram (Figure 6).

- The turbulence is an intrinsic random phenomenon, and because of its irregularity, it is impossible to describe the motion as a function of time and space coordinates.
- The vorticity is an intrinsic property of a turbulent flow, and it is defined as the curl of the fluid field.
- Turbulence increases the rate of momentum, heat and mass transfer.

Figure 7 shows the influence of the initial turbulence level on the explosion severity parameters in a closed vessel. At very early stages after the dispersion the turbulence level is very important, but it decreases with time after the dispersion i.e. it should be reminded that at lower ignition delay times, the "cold" turbulence is higher. The initial turbulence level is modified by performing explosions at the same concentration, in the same vessel, but igniting the mixture at different times after the dispersion. The maximum rate of pressure rise decreases markedly when the ignition delay time increase. However, the maximum overpressure remains constant up to 200 ms, after which a considerable decrease is observed. This trend shows once again that the maximum pressure is a thermodynamic property, rather than the maximum rate of pressure rise, which has a strong kinetic component (Eckhoff, 2003). At high turbulence levels, the turbulence enhances the mixing of the hot gases with the unburnt gases, burning faster compared to a mixture under quiescent conditions. As a consequence the decay of the turbulent fluctuations over the time induces a reduction on the explosion violence (Eckhoff, 2003; Tamanini, 1990, 1998).

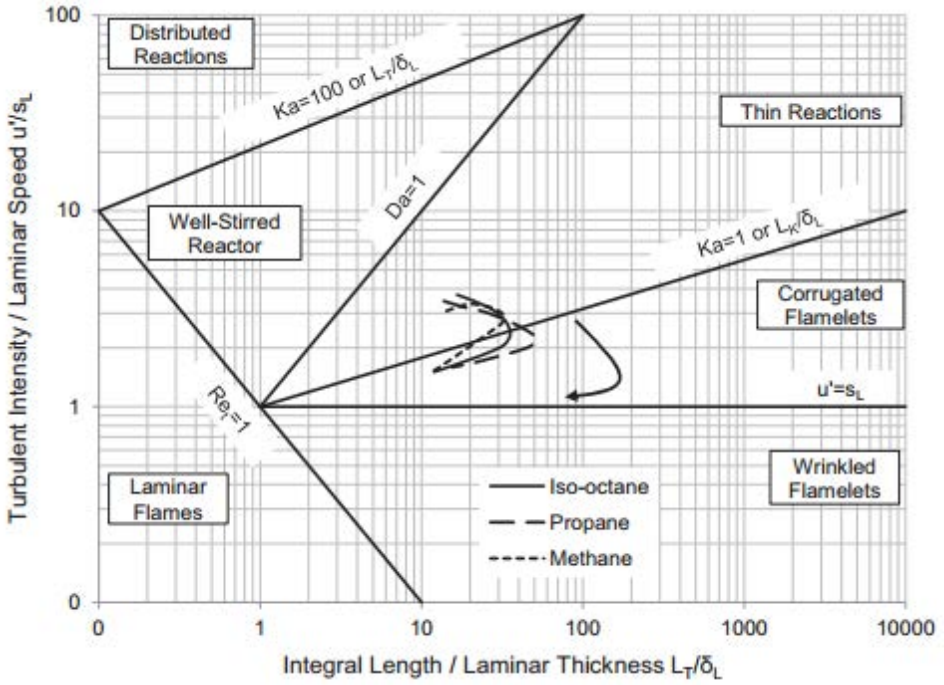

Figure 6. Borghi-Peters diagram showing the combustion regimes for three fuels (Demesoukas et al., 2016)

In addition, the uncertainties on the measure of the maximum rate of pressure rise increase for high turbulence levels (i.e. for ignition delays times lower than 100 ms) as shown in Figure 7. This trend

could notably be explained by the destabilization of the flame front at high turbulence levels, generating heat losses in the reaction zone by forced convection and even producing turbulent quenching of the flame. Regarding the ignition sensitivity, higher ignition energies are required to obtain a dust explosion for high turbulent systems compared to mixtures at quiescent conditions. Eckhoff (2003) reported an increase of several orders of magnitude on the minimum ignition energy when the ignition delay time was reduced from 120 to 60 ms. This is a positive result in the safety context, because the electrostatic discharge is usually obtained during turbulent motion (Eckhoff, 2003).

Explosion test vessels work with an initial turbulence created by an air blast. Nevertheless, in order to extrapolate the results of the explosion parameters measured on laboratory tests at industrial conditions, the turbulent flow must be characterized. Recent efforts have been made to characterize the turbulence level inside the explosion test vessels as a function of the ignition delay time. For instance, Cuervo (2005) measured the turbulence intensity and the root-mean-square velocity in a modified Hartmann tube using Particle Image Velocimetry (Figure 8). In his work, the vertical and horizontal root-mean square velocity fluctuacions ($u'_{rms}\ and\ v'_{rms}$) had been measured at different positions of the modified Hatmann tube. Similar tests have been performed for the characterization of the turbulence intensity in the 20L sphere explosion test (Dahoe, 2000; Murillo, 2016). By this means, explosion tests performed in a 20L sphere could be compared to larger geometries if the turbulence level is comparable.

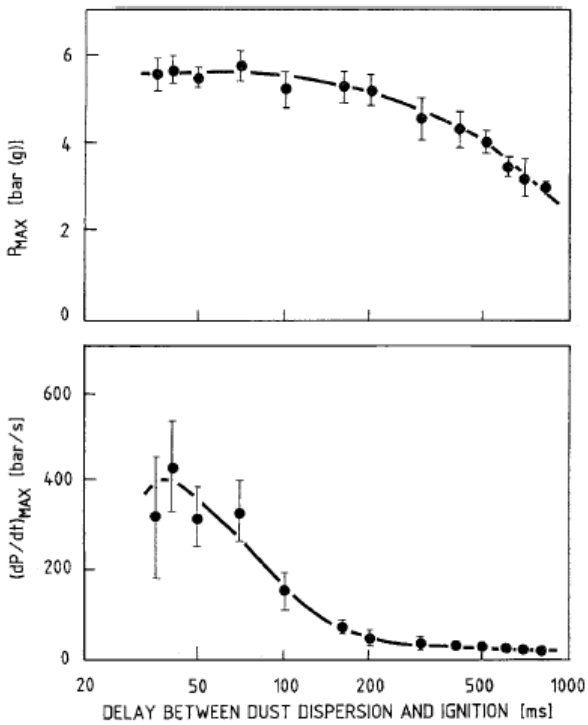

Figure 7. Influence of the delay time between dust dispersion and ignition on the explosion severity of lycopodium in air in a 1.2L Hartmann tube (Eckhoff, 2003).

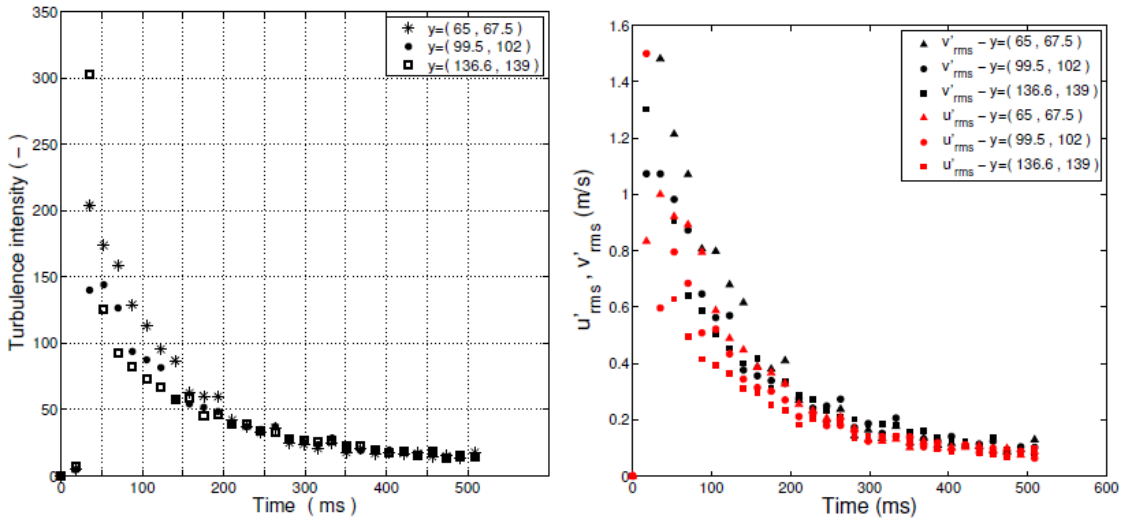

Figure 8. Evolution of the turbulence intensity (right) and the horizontal and vertical root-mean-square-velocities u'_{rms} and v'_{rms} (left) as a function of time (Cuervo, 2015).

1.1.3. Dust dispersion characteristics

As previously discussed, the dusts dispersion is compulsory in order to obtain a dust explosion, and the explosion properties will considerably depend on the characteristics of the dispersion. In order to obtain a reliable assessment of the explosion severity and ignition sensitivity, a homogeneous dispersion of the powder should be obtained in the explosion vessel. The poor reproducibility obtained for very turbulent systems (i.e. ignition delay time (tv) < 60 ms in Figure 7) is directly related to the difficulties to assure a homogeneous distribution of the dust in the 20 L vessel. In addition to the dust cloud homogeneity, during the dispersion process complete dust deagglomeration should be attained. A stable agglomerate behaves generally as a larger single particle, generating long burning time even for a very small elementary particle diameter (Eckhoff, 2003). Figure 9 illustrates the difference between a 'perfect' dust dispersion and a poor dispersion of agglomerates.

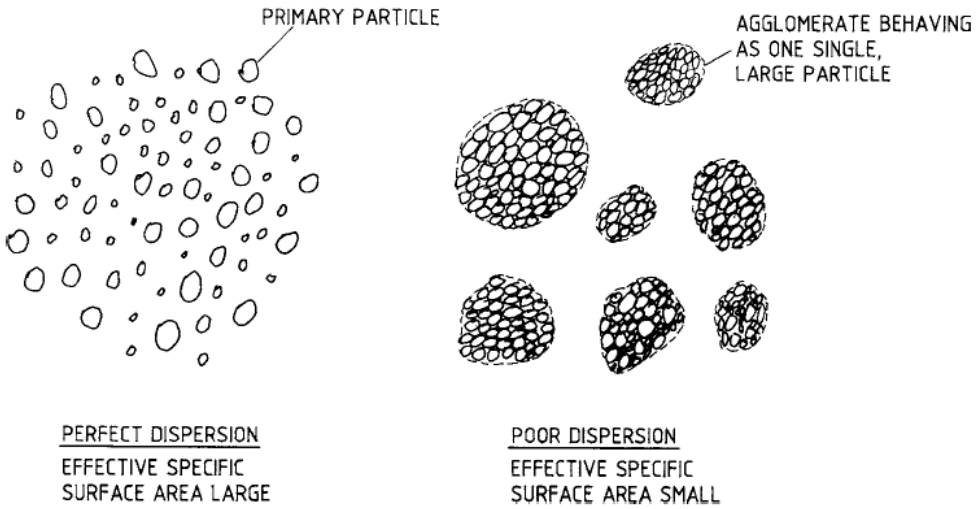

Figure 9. Illustration of a 'perfect' dust dispersion and a poor dust dispersion (Eckhoff, 2003)

Murillo (2016) studied the evolution of gas velocity during the dispersion of dust in a 20L explosion sphere (Figure 10). In his work, the influence of the nozzle position on the gas velocity over the time was analyzed (i.e. the perpendicular and parallel position represents the position of the standard nozzle with respect to the light beam of the laser used for the velocity determination). The dust dispersion could be divided in three different stages (i.e. dahs vertical lines in Figure 10) that will impose the powder fragmentation and the homogeneity of the solid phase in the vessel:

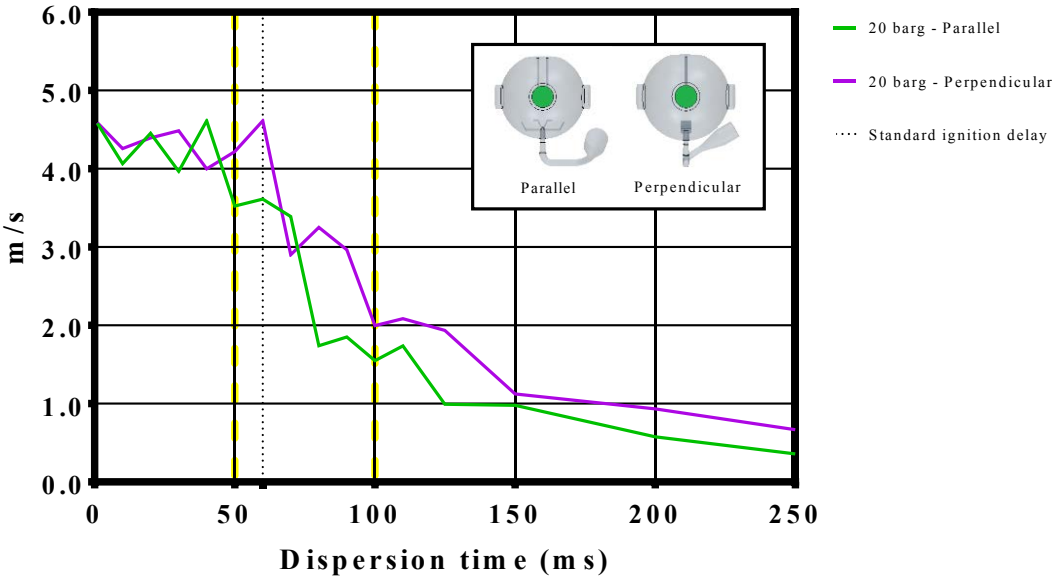

Figure 10. Mean vertical velocity fluctuations of the gas velocity of a dispersion test in a 20L explosion sphere (Murillo, 2016).

Instability stage: During this initial stage, the dust cloud was characterized by a high turbulence, at which the velocity fluctuations could reach values of 20 $m.s^{-1}$ (with a mean value of 4.5 $m.s^{-1}$ approximately). Dust deagglomeration may mostly occur at this stage, and the dispersion of the elementary particles will depend on the turbulence level achieved during the initial dispersion.

Transition stage: Most of the sample has been discharged into the vessel and the mean values of the fluctuations start to decrease. The gas velocity is still considerable but a rapid decrease of the turbulence level is evidenced.

Stable stage: The mean velocity fluctuations have decreased to values lower than 1 $m.s^{-1}$. Therefore, the turbulence level is not high enough to sustain the chaotic behavior of the dispersed particles.

These results show that the ignition delay time imposed by the standard tests (ASTM E1515-14, 2014; ASTM E2931 − 13, 2013; ISO 6184-1, 1985) occurs during the transition and stable stages, at which the dust cloud may be affected by the decrease of the turbulence level. For this study, the dust dispersion is an essential parameter to understand the effect of nanoparticles in hybrid mixtures explosions. Firstly, if the explosion is performed under an instable stage, the nanoparticles deagglomeration should be promoted and changes on the total surface can influence the flame propagation. Secondly, the nanoparticles stability at dispersion allows studying hybrid mixtures at low turbulence levels.

In addition, the gas flow depends on the geometry of the nozzle used to perform the explosion test. The rebound nozzle proposed on the standard test does not promote a homogeneous dispersion of the dust due to the initial flow characteristics of the gas, compared to the symmetric nozzle proposed by Murillo (2016) or Dahoe (2000). The authors suggest an evaluation of the standard test because the imposed conditions may not assure the adequate dust dispersion and in consequence the reproducibility of the result could not be assured.

1.1.4. Radiative heat transfer

In gas explosions, it is usually assumed that the influence of the radiative heat transfer can be neglected because the unburnt mixture is a transparent media, limiting the heat exchange with the propagating flame (this hypothesis is not valid for rich fuel mixture, conditions at which soot particles are generated). Nevertheless, radiative heat transfer is a very important factor influencing the flame propagation and the explosion properties of a dust explosion (Julien et al., 2017; Proust et al., 2017). In addition, the radiative heat transfer is greatly modified by the turbulence level and the homogeneity of the dust cloud. For these reasons, some studies have been carried out in order to measure the radiation heat exchange and to determinate its influence on the ignition sensitivity and explosion severity, especially for carbonaceous and metallic dusts.

Cao et al. (2014) measured the flame velocity and estimated the radiative heat transfer for two coal dusts with different volatility, using a high-speed video camera and thermal infrared imaging. Even if some differences between the radiation thermal transfers of both coal dust have been measured, similar flame propagation behaviors were observed. Radiative heat transfer has also been studied by Proust et al. (2017), by means of a propagation tube where a set of transducer are installed for heat flux estimations (i.e. high voltage ionization gage, a collimated infrared phodiode and a fast response fluxmeter). The amount of heat radiated by the flame has been estimated for methane/air, SiC and aluminum dust; however, not direct relation with the flame velocity could be proposed.

On the other hand, some analytical models have been proposed in order to calculate the flame velocity of lycopodium and metallic dust, taking in account the influence of the heat radiation (Bidabadi et al., 2011, 2013, Haghiri and Bidabadi, 2010, 2011). The models are based on the mass, species and energy conservation equations, in addition to the relation describing the heat radiation transfer. Bidabadi et al. (2013) considered that the radiation occurs between the propagating flame and a gray two-phase environment, including the absorption, emission and scattering of thermal radiation intensity:

$$\frac{dI}{dx} = K_a I + K_s I - K_a I_b - \frac{K_s}{4\pi}\int_{4\pi} I(\Omega)\, P d\Omega \qquad \text{Eq 2}$$

Where Ω, I, I_b, K_a and K_s are the solid angle, thermal intensity, the thermal intensity of a black body, the absorption coefficient and the scattering coefficient respectively The integration problem has been divided into the preheat zone, the reaction zone and the post flame zone (for organic powders a vaporization zone is added, as shown in Figure 11). Some simplifications have been proposed at each zone in order to solve analytically the equations (Bidabadi et al., 2013; Haghiri and Bidabadi, 2011). Therefore, radiation plays an important role on the acceleration of the burning velocity due to the increase of the temperature in the preheat zone compared to a system involving only conduction thermal transfer (Haghiri and Bidabadi, 2010). Similar results have been found experimentally for aluminum dust explosions on a vertical tube, in which higher flame velocities

were obtained for higher radiating systems due to the preheat zone temperature increment (Droujko et al., 2016).

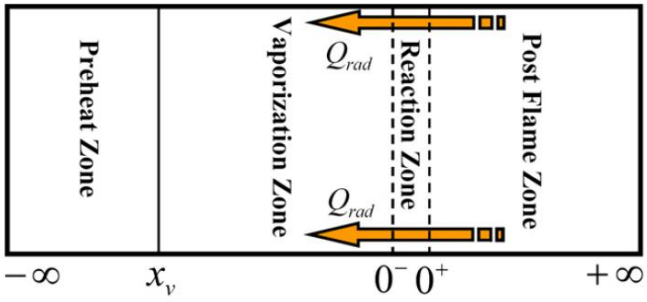

Figure 11. Schematic of the front flame propagation divided on four zones for organic fuel particles in air (Haghiri and Bidabadi, 2010).

However, the overall influence of the radiation thermal transfer on dust explosions is not totally understood because of the combined effects of turbulence, particle size distribution and complex combustion mechanisms.

1.1.5. Particle size and shapes

The explosion parameters are directly dependent on the Particle Size Distribution (PSD) of the dust, because this parameter will impose the dust cloud generation, the particle velocity, fragmentation and interactions between particles. Due to the complex influences of the particle size distribution on the combustion reaction, on the gas-solid and solid-solid interactions, on the energy and mass transport phenomena, the characterization of the particle size and its effects on the ignition sensitivity and explosion severity have been addressed on different studies. The influence of the particle size on the explosion parameters will be briefly developed in the next paragraphs.

As it has been developed by Eckhoff (2003), the effect of the PSD on the explosion parameters depends on the chemical properties of the dust. For organic powders, the devolatilization process is improved with the decrease of the particle size. Nevertheless, there is a critical particle size at which the combustion rate ceases to increase because the gas mixing and gas phase reaction will limit the overall reaction rate.

In general, the ignition sensitivity and explosion severity increase when the average particle diameter of the dust decreases until a limit value. This trend is explained by the increase of the total surface area of the dust and because of the modifications on the limiting combustion regime. Figure 12 shows the diminution of the Minimum Explosive Concentration (MEC) and the Minimum Ignition Energy (MIE) as a function of the mean particle diameter. The difference of the dust devolatilization is evidenced on the minimum explosive concentration (Figure 12 – left), obtaining lower values for a highly volatile coal. Regarding the minimum ignition energy of aluminium, a considerable reduction is obtained when the mean particle diameter is reduced from 100 to 10 µm. As a result, aluminum with very small particle diameter has comparable minimum ignition energies to combustible gas such as methane or propane.

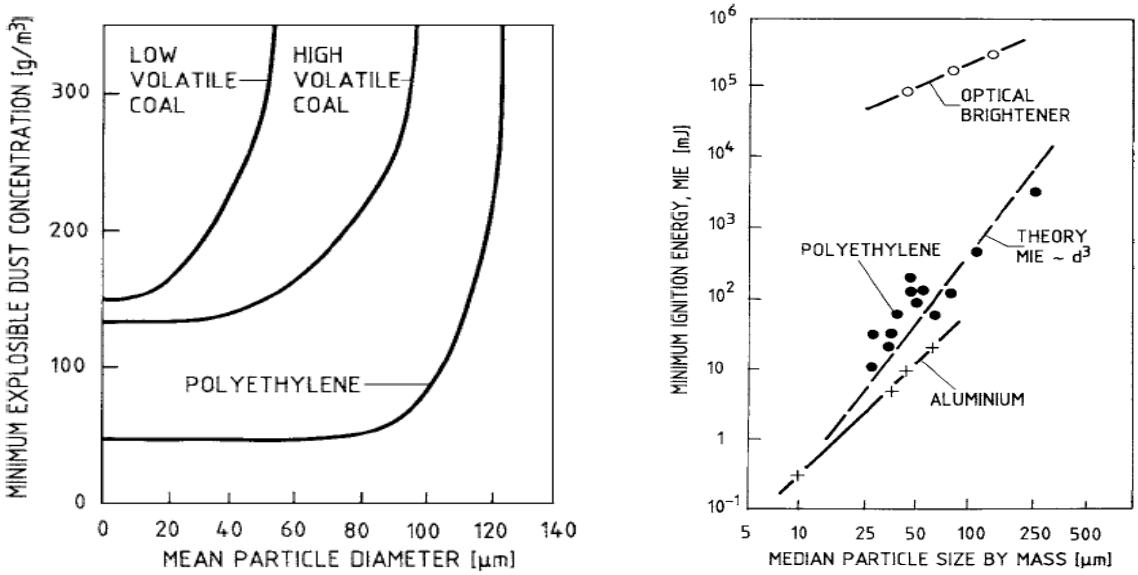

Figure 12. a) Influence of the mean particle diameter on the minimum explosible concentration for three different dust b) Influence of mean particle diameter on the minimum ignition energy of polyethylene, aluminum and optical brightener (Eckhoff, 2003).

Figure 13 shows the influence of the mean particle diameter on the maximum rate of pressure rise for different types of particles. A considerable increase of the dP/dt_{max} for silicon and atomized aluminum is observed for smaller particle size. This trend suggests that the particle size has a considerable effect on the explosion severity and in consequence, may modify the design of the protection devices.

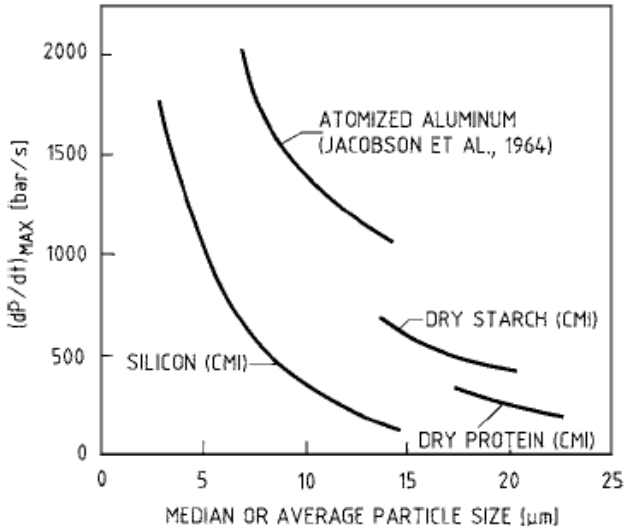

Figure 13. Maximum rate of pressure rise for silicon, aluminum and organic powders measured on Hartmann tube (Eckhoff, 2003).

The shape and porosity of dust particles have a significant influence on the explosion parameters because they are directly related to the surface area available for the combustion reaction. Eckhoff (2003) reported a significant difference on the maximum rate of pressure rise for atomize aluminum

particles and aluminum flakes, which were around 400 bar.s^{-1} for the coarse aluminum and 2600 bar s^{-1} for aluminum flakes. This is due to the degree of dispersion, deagglomeration and total surface of the dust. In order to take into account the influence of the particle size, porosity and shape, some authors suggest studying the influence of the surface area modifications on the ignition sensitivity and explosion severity parameters (Bouillard et al., 2010; Eckhoff, 2003).

As presented, the evolution of the safety parameters is not always linear towards the nanoscale. For this reason, in the following section the particularities of nano-dust explosion will be developed and an overview of the nanoparticles explosion studies will be presented.

1.2. Nanoparticles explosion

Dust materials industrial applications are numerous, involving different type, size and shapes of materials. Nanoparticles have been progressively used in a wider variety of applications because of the different properties they have compared to those of bulk materials (Figure 14). The chemical, electrical and physical properties change when the dust particle size falls down to the nanoscale size. For example, materials that are usually conductors become insulators at the nanoscale (Pritchard, 2004). Nanoparticles are used to modify certain properties, particularly resistance, rheology, hardness and magnetization. Moreover, due to their greater surface area, they appear better suited for catalysis and biological applications (Stark et al., 2015). The past few years have witnessed a transition in the production of certain products from traditional processes to nanoscale level manufacturing. Such materials are now widely used in cosmetics, paints, tires, catalysts and pharmaceuticals (Bouillard et al., 2009; Eckhoff, 2011). In Table 2, a summary of nanoparticles industrial applications is presented.

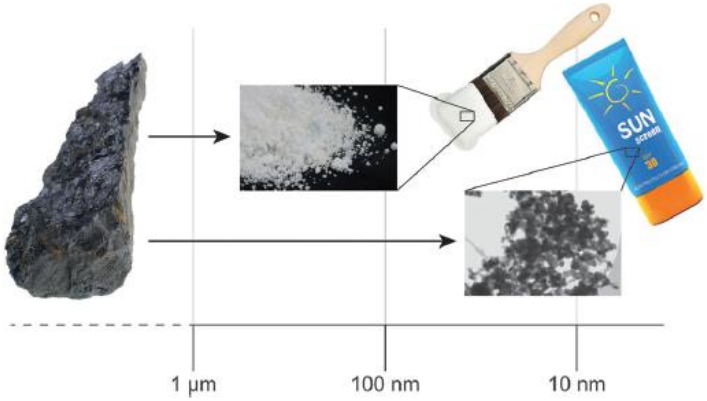

Figure 14. TiO_2 used as a pigment at micrometric size and as sunscreen protector at nanoscale size (Stark et al., 2015)

The European Commission defines a nanomaterial as a material in which more than 50% of the particles in the number size distribution (in unbound state, in agglomerates or aggregates) have a size between 1 nm and 100 nm – Recommendation 2011/696/EU (European Comission, 2011). The steady increase of needs is accompanied with larger production, handling and processing facilities for nanostructured materials and higher tonnage of nanomaterials (Kuhlbusch et al., 2011). The increased production of nanoparticles imposes the study of the potential risks related to their production and manipulation. On the one hand, the principal concern of the nanotechnology is the potential routes of exposure (i.e. dermal, oral, respiratory and parenteral) and the toxicity of the particles inside the body (Hoet et al., 2004; Kuhlbusch et al., 2011; Oberdörster et al., 2005; Stern and McNeil, 2007). On the other hand, the increased dispersibility and reactivity of

nanoparticles implies also an impact on their explosion hazards (Bouillard et al., 2009; Pritchard, 2004). However, there is still a limited amount of data and analysis on the explosion properties in this field (Amyotte, 2014). In the following sections the main properties of nanoparticles explosions are highlighted.

Table 2. Principal applications of nanopowders (Pritchard, 2004; Stark et al., 2015)

Application	Description
Catalyst	Catalysts composed by nanosized materials have greater performance, due to the higher surface area.
Coatings	Anti-scratch surfaces and self-cleaning materials are made with nanocomposite materials.
Cosmetics	Sunscreen protectors and lotions are made with nanoparticles of Titanium or Zinc (Figure 14)
Explosives	Nanopowders enhance the burning properties of explosives and pyrotechnic materials.
Energy	Batteries, fuel cells, solar cells are some example of applications where the nanodust is being used instead the micro-sized particles. Hard-disc with nanostructured magnetic multi-layers dominate the market.
Filtration	Nanofibers have been found efficient to trap viruses, bacterias, endotoxins and macromolecules.
Lubricants	The lubricant properties of some oils are improved with the addition of diamond nanopowders.
Medical uses	The surface properties of nanocomposite are being used to promote the cell growth on medical implants and improving the compatibility of the material. Moreover, the nanosized drug delivery devices have been found interesting to deliver the medical treatment at specific body places within the correct doses. Gold nanoparticles are applied on diagnostic tools (i.e. pregnancy test).
Separation	Efficient porous membranes are being manufactured by the film formation and nanopore generation, used water treatment.
Sports	Different sports accessories are being enhanced with nanocomposites (tennis racquets, ski devices, running shoes)

1.2.1. Combustion regimes of nanopowders

The study of the explosion hazard of nanoparticles is associated with modifications in the heat transfer, dispersion and reaction due to the size and surface of the elementary particles. For instance, the combustion is greatly modified when the particle size decreases to the nanoscale, as is shown in Figure 15. Bouillard et al. (2010) argument that the combustion regime of micrometric particles is controlled by the diffusion of oxygen into the particles (diffusion regime) and it is kinetically controlled for nanoparticles, explaining the differences on the combustion time.

The combustion mechanism has a direct effect on the combustion time of the reaction. For micrometric aluminum particles, the combustion time follows a d_p^n law with n ranging from 1.5 to 2 (Beckstaed, 2002; Bouillard et al., 2010). However, further studies have shown that the values of n range between 0.3 and 1.6 for nanometric particles, indicating a faster reaction (Beckstaed, 2002; Bouillard et al., 2010). Such modifications of the combustion mechanism may generate modifications on the ignitability and explosivity of the powder as it will be shown in the following sections.

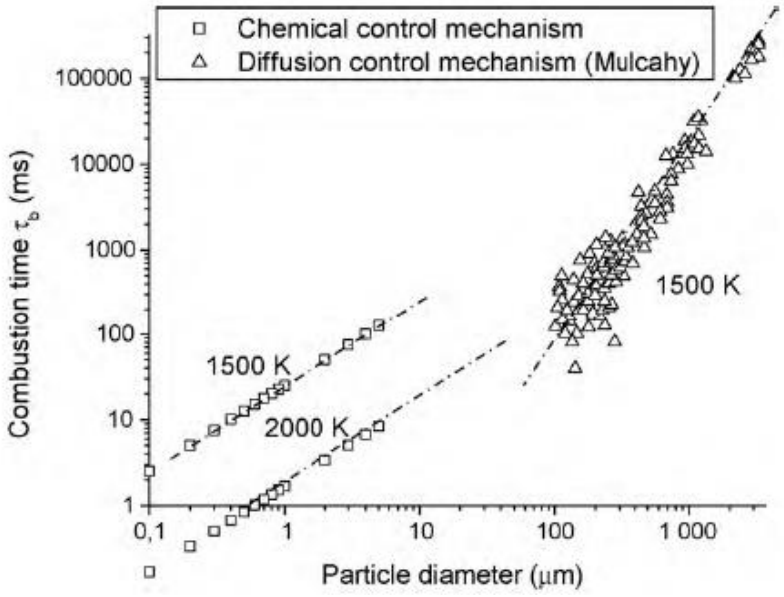

Figure 15. Combustion characteristic time as a function of particle size for carbonaceous particles (Bouillard et al., 2010).

1.2.2. Dispersion properties of nanoparticles

The dispersion of the combustible dust is a compulsory condition to obtain a dust explosion, as shown in Figure 3. When the primary particle size diminishes, a stable dust cloud is likely to take place. However, if the elementary particle diameter reaches the nanoscale, the dust will be composed of agglomerates and aggregates. Primary particles attached by van der Waals, or other physical forces constitute agglomerates while particles bond together by chemical forces are defined as aggregates (Eggersdorfer and Pratsinis, 2014). Therefore, the generation of a homogeneous dust cloud of elementary nanoparticles will depend on the fragmentation and deagglomeration generated by the forces that produce the dust dispersion (Henry, 2013).

Nanoparticles have different dispersion properties compared to micro-particles. Nanoagglomerates presents strong chemical bonds opposed to physical van der Waals forces, and in consequence, a

complete dispersion of primary particles cannot be achieved for high concentrations of nanoparticles, especially greater than MEC (Wengeler and Nirschl, 2007). Similar conclusions were exposed by Eckhoff (2012, 2011), who affirms that during normal operating conditions in industrial processes, the formation of a well-dispersed nanometric primary particle cloud from bulk powder is extremely difficult because the existence of strong interparticle cohesion forces. In contrast, at laboratory conditions, a homogeneous cloud may be generated, but the delay time between the dispersion and the ignition of the cloud, and the dust concentration are decisive for the extent of the re-agglomeration. Even if it has been established that dust cloud of elementary nanoparticles is unlikely to occur, further studies should be performed in order to understand the influence of dust fragmentation and the changes of dust size distribution on the explosivity parameters.

1.2.3. Explosion severity

Some authors have been interested in the explosion violence of nanodust compared to micrometric dust. As it has been shown in section 1.1.5, the explosion severity is directly dependent on the particle size distribution, increasing for smaller elementary particles. Nevertheless, the severity of the explosion seems to be greatly modified for the nanoscale, and the explosion violence trends may depend on further variables, as the dispersion turbulence and the combustion regime of the powder. For this reason, tests showing the differences between the explosion severity of nanometric and micrometric dust particles have been performed in the past years. Jiang et al. (2011) compared the explosion severity of aluminum dust with 75µm and 100 nm in a 20L sphere, at dust concentrations between 0.06 and 1.7 $kg.m^{-3}$. Higher values of the maximum overpressure and the maximum rate of pressure rise for the nano-sized aluminum has been found for all the studied concentrations (Jiang et al., 2011). However, it must be highlighted that the tests have been performed with an ignition delay time of 200 ms, time at which the sedimentation of the micrometric particles could be noticeable and may generate very low values on the maximum rate of pressure rise. Nevertheless, the results show that the 100 nm aluminum powder is still suspended at 200 ms after the dispersion.

Similarly, Mittal (2014) studied the explosion of micro-size (1, 10, 22, 38, 74, and 125 µm) and nano-size (30, 50, 100, 150, 200 and 400 nm) magnesium powders for concentrations ranging between 20 - 2500 $g.m^{-3}$. On this study, the maximum overpressure P_{max} and the K_{st} were measured in a 20L explosion chamber using standard procedures (BS EN 14034-1, 2004), i.e. at 60 ms ignition delay time and an energy equivalent to 10 kJ. Nevertheless, pre-ignition of the powder without ignition source was present for nano-sized dust with mean particle diameter between 30 and 150 nm, generating lower values of the explosion severity parameters (i.e. P_{max} and K_{st}) and in consequence, no direct comparison with micro-particles could be done. For particle diameter between 200 nm and 125 µm, Mittal (2014) observed that the optimum dust concentration at which the maximum explosion severity occurs is higher for micro-particles dust than that for nano-sized particles, because a higher concentration of micro-dust is necessary to have the same total surface of magnesium particles. In addition, Figure 16 shows the evolution of the explosion severity when the particle diameter moves from micro- to nano-size for magnesium powders at the experimental stoichiometric concentration. It has been found in this study that the explosion severity increases when the particle size is reduced from 150 µm until 400 nm, but it decreases for the nanometric interval between 30 and 200 nm, due to agglomeration phenomenon (Mittal, 2014).

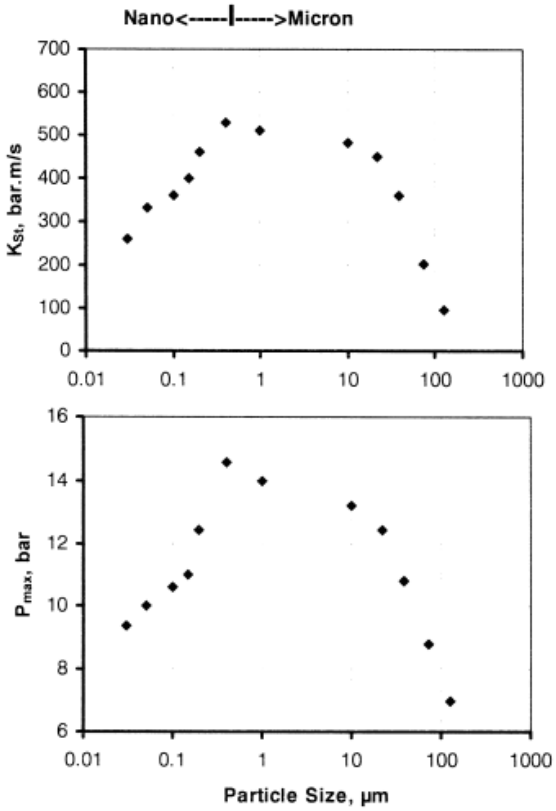

Figure 16. Effect of moving from micron- to nano-size particles on the explosion severity for magnesium powders (Mittal, 2014).

Boilard et al. (2013) had also studied the explosivity of micro- and nano-size titanium powder on a Siwek 20L explosion chamber. As Mittal (2014) had found, pre-ignition of titanium nanodust is caused by a frictional or static spark during the dispersion in the chamber, corresponding to a different ignition energy and ignition delay time compared to standardized tests. Consequently, a direct comparison could not be proposed between micrometric and nanometric dust for metallic powders (Boilard et al., 2013; Mittal, 2014). In the same way, the explosion severity of aluminum nanoparticles and carbon black nanoparticles have been studied by Bouillard et al. (2010). For aluminum, the authors found that the dust with particle diameter of 200 nm exploded more violently than 100 nm particles (Figure 17a), highlighting the importance of the degree of agglomeration on the explosion severity parameters. Regarding the carbon black nanoparticles, the explosion severity of the 4 types of carbon black particles with different mean diameter and specific surface was very close, suggesting that the specific surface should not be taken as the main factor influencing the dust explosivity (Bouillard et al., 2010; Dufaud et al., 2011; Vignes et al., 2009). Therefore, the similarities between the explosion severity parameters of nanometric and micrometric dust are mainly caused by the extremely fast agglomeration process present after the dispersion of nano-sized particles, phenomenon that is more important for small particles and high turbulence levels. This implies that dust explosion venting, suppression and isolation should be just as feasible with nanometric primary particles as with micronsize primary particles (Eckhoff, 2011, 2012, 2013; Worsfold et al., 2012).

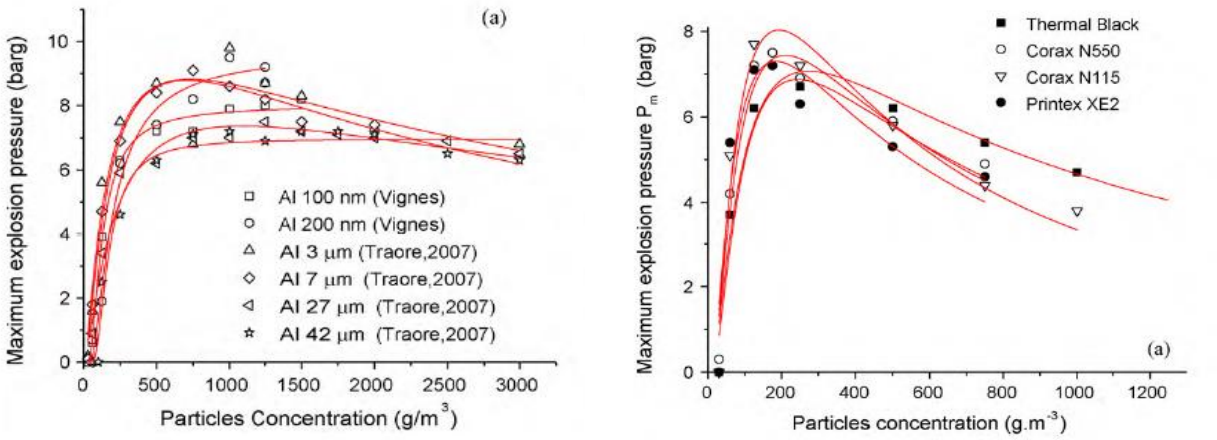

Figure 17. a) Experimental evolution explosion overpressure for Aluminum particles. b) Evolution of explosion overpressure or carbon black nanoparticles (Bouillard et al., 2010).

1.2.4. Ignition sensitivity

As it has been previously discussed, an auto-ignition of nanometric magnesium and titanium particles was observed during the dispersion of the particles on the explosion severity test, evidencing a higher ignition sensitivity for nano-dust compared to micrometric particles (Boilard et al., 2013; Mittal, 2014). Regarding magnesium nanoparticles, the minimum ignition temperature and the minimum ignition concentration seems to slightly decrease in the nano-size range compared to the micrometric tested particles. Mittal (2014) found that the minimum ignition energy decreases when the particle size moves from the micrometric to nanometric range, but once within the nano-range, this variable stay almost constant. Boilard et al. (2013) performed similar measures for titanium particles, evidencing very low minimum ignition energies for micro- and nano-size, but with the fundamental difference that lower dust loadings are necessary for nanometric dust. In addition, the minimum ignition temperature for nano-titanium was around 240-250ºC compared to a temperature around 450ºC for micro-size titanium. This clearly demonstrates the enhanced potential of ignition of nanoparticles dust by hot surfaces (Boilard et al., 2013). As a conclusion, the minimum ignition energy values of some metals are lower for dust clouds of nanometric primary particles than for clouds of micrometric primary particles. Eckhoff (2012, 2011) proposed a possible explanation of this phenomenon: particle agglomerates that would retain their integrity in the main flame propagation process might disintegrate into primary nanoparticles if located very close to the spark plasma channel due to the high temperature. This could produce a tiny cloud zone of well-dispersed nanoparticles just adjacent to the spark, which could be ignited instantaneously due to higher reaction surfaces (Eckhoff, 2012). This means that the possibility of ignition by subtle electrostatic spark discharges of very low energies have to be considered for nanometric particles with very low ignition energies.

In contrast, Bouillard et al. (2010) have found higher minimum ignition temperatures for carbon black nanoparticles (i.e. Corax N115 and Printex XE2, with elementary particle diameter of 75 and 3 nm respectively) compared for larger carbonaceous particles. This result is related to the strong attractive interaction between very small particles, generating agglomeration/aggregation, which may need higher energy to ignite compared to isolate micrometric particles (Figure 18). Additionally, the minimum ignition concentration reaches a plateau when the particle size decreases from micrometers to nanometers. Theses results show the complexity of interactions

between the combustion reaction, the turbulence of the system and the interaction between particles during the dust dispersion. Without agglomeration/aggregation phenomena, the turbulence will increase the combustion rates, but in contrast, increasing the turbulence level will promote the agglomeration of particles, reducing the total surface, modifying the heat radiation transfer and in consequence, decreasing the combustion rate (Eckhoff, 2011, 2012).

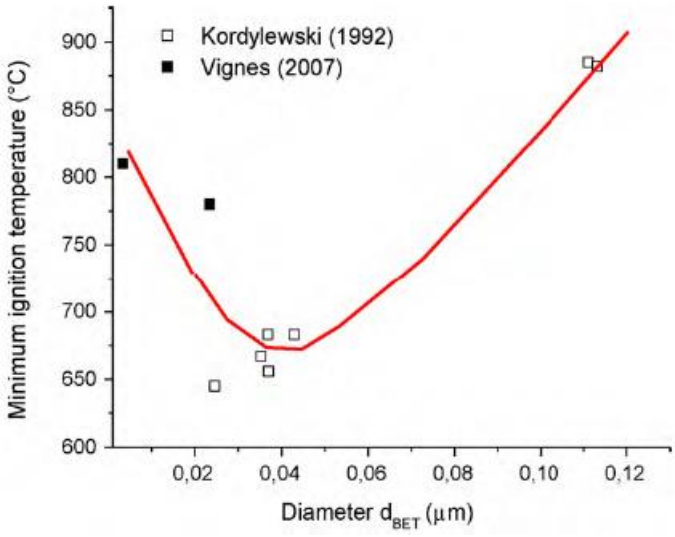

Figure 18. Minimum ignition temperature of carbon black nanoparticles compared to larger carbonaceous particles (Bouillard et al., 2010).

1.3. Hybrid mixture explosion

As it has been previously highlighted, due to the very fast agglomeration of nanoparticles, an increase in the explosion severity parameters may be not evidenced in comparison with micrometric particles. However, if a dispersion of a low concentration of nanoparticles is achieved, the agglomeration of the particles is reduced and they may have an influence of the explosion characteristics of a combustible gas simultaneously present in the system. Due to this reason, this work is focused in the explosion severity characteristics of nanoparticles/gas hybrid mixtures.

A hybrid mixture consists of an explosive mixture of a flammable gas and combustible dust, in which the gas may be present below its lower flammability (or explosivity) limit (LEL) and the powder may be below its minimum explosive concentration (MEC). Despite an increasing knowledge and efforts to propose accurate and efficient solutions to prevent these kinds of events, hybrid mixture explosions still occur in different types of industries (e.g. food, mining, pharmaceuticals, chemicals). Some examples of hybrid mixtures are coal/gas mixtures in underground mining, natural gas/fly ash in power plants or hydrocarbons/resins in plastics manufacturing (Amyotte et al., 2009; Amyotte and Eckhoff, 2010). Additionally, technical causes should also be considered to explain this occurrence: more and more processes involve the simultaneous presence of combustible gas and dusts, as is in composting or methaniation facilities, biofuel plants, or during the generation of some carbonaceous nanoparticles. As a consequence, further studies of the explosive properties of such atmospheres must be conducted (Amyotte, 2014; Amyotte and Eckhoff, 2010; Jiang et al., 2014; Worsfold et al., 2012).

Hybrid mixture explosions present different interactions between the solid and gas phases, different heat exchange and also, particularities on the reaction combustion regimes. Because of this reason,

hybrid mixture explosions have been particularly studied in the past few years due to their different severity and sensitivity variables when compared to those of pure dust or gas explosions (Denkevits, 2007; Dufaud et al., 2008; Khalili et al., 2012). The main characteristics of hybrid mixture ignition sensitivity and explosion severity will be highlighted on the next sections.

1.3.1. Ignition sensitivity

The studies of the ignition sensitivity of hybrid mixtures focus on the modifications in the Minimum Ignition Energies (MIE) when low concentrations of combustible gas are added to the system. Khalili et al. (2012) studied the evolution of the MIE of oil cakes/hexane and starch/hexane at different concentrations of combustible gas (Figure 19) in a modified Hartman tube according to IEC1241-2-3 standard. The authors reported a significant decrease of the MIE from 67 mJ for starch powder to 4 mJ when only 1% of hexane is added to the system (Khalili et al., 2012). Similar results have been found by Addai et al. (2016) for eight different combustible dusts and two flammable gases, obtaining lower values of MIE upon the addition of small amounts of gas, even below the Lower Inflammability Limit (LEL). For example, the ignition energy of starch decreases from 40 to 4.1 mJ when 4% of methane was added to the system (Addai et al., 2016). As a consequence, an electrostatic discharge may be sufficient to ignite hybrid mixtures at low concentration of gas.

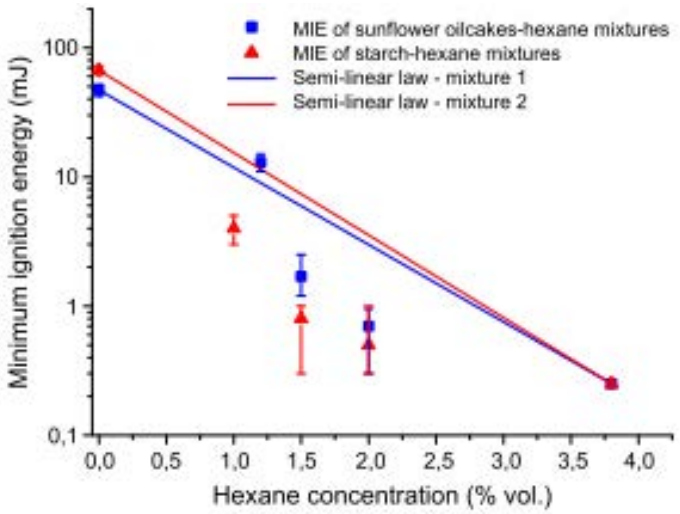

Figure 19. Evolution of the minimum ignition energy oil cakes/hexane and starch/hexane hybrid mixtures (Khalili et al., 2012).

Different simple mathematical relations have been proposed to estimate the lower explosive limit of a hybrid mixture (LEL_{Hybrid}) -e.g. Le Chatelier or Bartknecht equations (Table 3)- but certain studies have also demonstrated that for some hybrid mixtures such calculated value is not always the safest estimation (Addai et al., 2015; Khalili et al., 2012). Addai et al. (2015) obtained the ignition of starch/methane mixtures where the dust concentration was below the MEC and methane concentration below the LEL, lying in the 'no ignition zone' predicted by the Le Chatelier and Barktnecht's law.

Table 3. General correlations for the LEL of hybrid mixtures, where c is the dust concentration, y the gas fraction, MEC the minimal explosive concentration and LFL the lower flammability limit.

Le Chatelier Law	Bartknecht Equation
$\frac{c}{MEC} + \frac{y}{LFL} = 1$	$\frac{c}{MEC} = \left(\frac{y}{LFL} - 1\right)^2$

Prugh (2008) has proposed a correction of the LEL for hybrid mixtures by taking into account that its estimation is usually made at room temperature, whereas it must be recalculated at the flash point temperature. Another formula to estimate the lower flammability of the mixture has been proposed and validated by Jiang et al. (2015, 2014) using a 36-L explosion apparatus. A good prediction of the non-explosion/explosion zones have been obtained for several hybrid mixtures (Figure 20) and the results seems independent of the turbulence level and ignition energy (Jiang et al., 2015). However, the proposed zone prediction depends on the K_G and K_{st} (i.e. K_G is determined as well using the Eq 1 for the gas explosion), which are high variable at high turbulence levels.

$$\frac{c}{MEC} = \left(\frac{y}{LFL} - 1\right)^{(1.12 \pm 0.03)\frac{K_{st}}{K_G}}$$

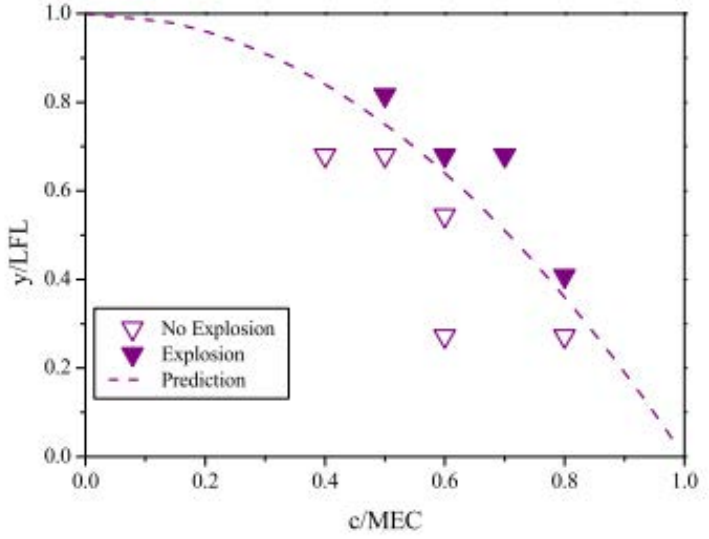

Figure 20. Explosion and non-explosion limits for niacin/methane mixtures (Jiang et al., 2015).

This result suggest that the explosion severity parameters does not follow a linear behavior and depend on the explosive properties of both solid and gas. In addition, further studies had mainly focused on the influence of the presence of gas in dust explosion properties. However, there is still necessary to study the influence of dust dispersion on gas explosions.

1.3.2. Explosion severity

When compared to the pure compound explosion parameters, the synergetic effect on the explosion severity of hybrid mixtures seems to strongly depend on the physical or chemical properties of the compounds. Pilão et al. (2006) reported non-significant changes on the maximum overpressure P_{max} and dP/dt_{max} variables of cork dust/methane hybrid mixtures when compared to those of dust explosions, even if a significant reduction in the minimum dust explosion concentration is obtained. Nevertheless, the ignition of niacin/diisopropyl ether mixtures showed an increase on the explosion severity when a low concentration (i.e. between 0 and 3% v. concentration) of vapor was added in

the system (Dufaud et al., 2008, 2009). For instance, Figure 21 shows that the maximum rate of pressure rise of a dust concentration of 300 g/m^3 reaches 800 bar.s^{-1}, and increases to 1600 bar.s^{-1} when 1.5% molar fraction of gas is added to the system.

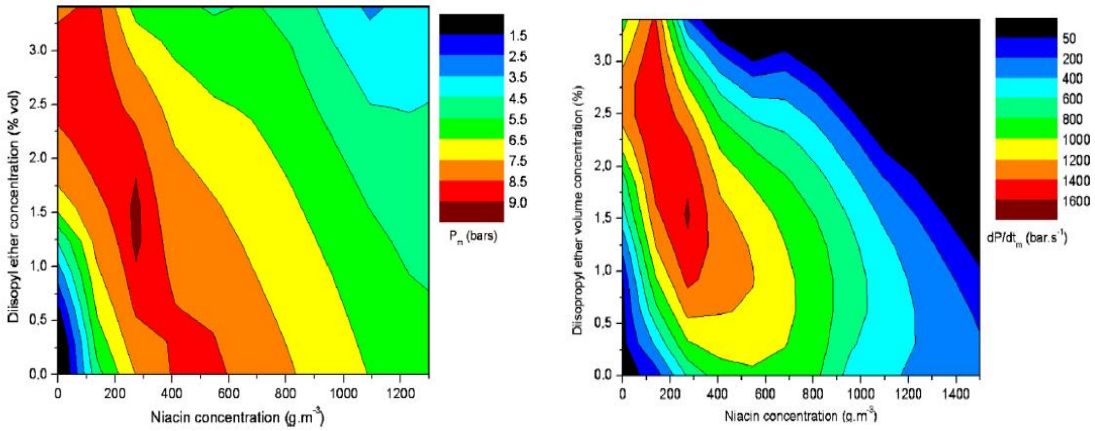

Figure 21. Maximum Overpressure Pmax and Maximum rate of pressure rise for niacin/diisopropyl ether hybrid mixtures (Dufaud et al., 2008).

Ajrash et al. (2016a, 2016b) found similar results for coal dust/methane explosions, for which higher P_{max} and K_{st} values were obtained when methane concentrations between 0.75 – 1.25% were present in the system. However, the gas concentration that generates higher explosion overpressure of hybrid mixture is greatly modified by the igniter energy. Moreover, the flame propagation velocity and the maximum flame temperature were higher for coal/methane mixtures than for coal dust or other dust flames (Liu et al., 2007).

Considering the variability of the severity experiments, Garcia-Agreda et al. (Garcia-Agreda et al., 2011) identified five different regimes for hybrid mixtures at different dust and gas concentrations (Figure 22):

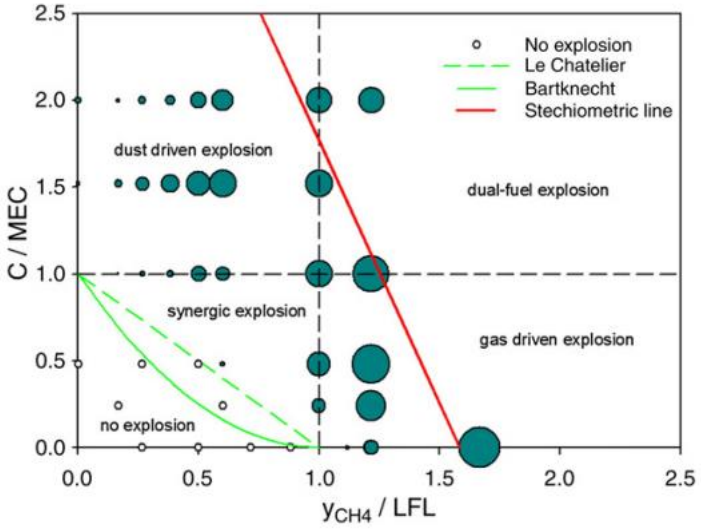

Figure 22. Explosion regimes of a Methane/Nicotinic acid hybrid mixture(Garcia-Agreda et al., 2011)

No explosion regime: The dust concentration is below it minimal explosive concentration and the gas fractions is also below the lowest explosive limit, which means that the combustible concentration lies below the Le Chatelier curve (Table 3)

Synergic explosion regime: This zone is limited by the Le Chatelier curve, the Minimal Explosive Concentration of the dust and the Lower Explosive Limit of the gas. It is defined as the synergic regime because ignition is obtained even at concentration of one component below the explosive limit.

Dust driven explosion: Dust concentration lies above the MEC, but the gas fraction is below the LEL. In this zone, the explosion characteristics are dominated by the explosion characteristics of the dust.

Gas driven explosion: Dust concentration lies below the MEC, but the gas fraction is above the LEL. In this zone, the explosion characteristics are dominated by the explosion characteristics of the gas.

Dual fuel explosion regime: Both combustible compounds have an effect on the explosion characteristics of the mixture.

Regardless the recent efforts to describe the particularities of hybrid mixtures explosions (Cuervo, 2015), the simultaneous phenomena of complex thermal transfers, combustion kinetics and turbulence/combustion interactions are still not well understood.

It is interesting to modify the particle size in order to identify the influence of the particles surface on these phenomena. It has previously been demonstrated that the elementary particle size has an influence on the severity of the explosion of hybrid mixture systems (Khalili, 2012; Khalili et al., 2012). Kosinski et al. (2013) studied the explosion severity of carbon black nanoparticles/propane/air mixtures. According to this study, the propane concentration must be higher than the lowest explosion limit in order to cause an explosion. However, in comparison with pure propane, the explosion severity was higher for low concentrations of carbon black nanoparticles and lower for high concentrations. These results suggest that the combustion process is modified by the heat loss generated by the carbon black nanoparticles (Kosinski et al., 2013). The study of hybrid mixtures explosions involving nanometric-sized dust allows to isolate the turbulence and combustion interactions, as they are highly stable at dispersion, and to work at low turbulence levels, which is not possible when working with micrometric-sized dust due to the sedimentation phenomenon. In addition, the dispersed nanoparticles may produce modifications on the burning velocity and front flame surface, allowing to study the possible perturbation occasioned by the burnt particles to the flame propagation. In the following section, the burning velocity determination for dust and hybrid mixture explosions will be highlighted.

1.4. Burning velocity

The explosion severity parameters depend on the specific chemical properties of the dust-air mixture, but also on the flow properties of the dust cloud and the characteristics of the explosion vessel (mainly the volume). Due to the absence of a description of the transient behavior of the dust-air combustion, the explosion severity tests (20L and 1m^3 sphere explosion vessels) have been chosen as the alternative to predict the consequences of a similar mixture exploded at industrial conditions (Dahoe et al., 2002). This has currently been done with the cubic root law (Eq.1).

Knowing the K_{st} of a dust explosion let estimate the explosion severity of the same mixture on a plant unit, which the input for the design for safety protection devices (i.e. explosion relief valve, rupture disc). Some authors had analyzed the conditions under which the cubic root law could be used to properly estimate the severity parameters of the explosion at industrial conditions (Dahoe et al., 2002):

- First, the mass burning rate must be the same between the laboratory test and industrial vessel at the moment where the rate of pressure rise achieves its maximum value. This condition is fulfilled when both vessels are spherical, and the mixture is ignited at the center of the vessel. In addition, the pressure and temperature changes of the unburnt mixture must have the same effect on the burning velocity and the turbulent flow should be identical in both vessels. Moreover, in industrial conditions, the turbulence level is generally unknown, so it is assumed that if the turbulence intensity is high enough on the laboratory test, the results will let to conservative estimations of the conditions at a plant unit.
- Secondly, the flame thickness must be negligible with respect to the radius of the explosion vessel. The cube root law does not take into account the effect of the flame thickness, becoming inaccurate in predicting the maximum rate of pressure rise when the flame thickness become appreciable with respect to the radius of the vessel.

While the cube root-law uses a single instant of the rate of pressure rise, balance integration models take in account the entire pressure evolution during explosion (Dahoe et al., 2002; Eckhoff, 2003). More importantly, since their derivation is based on fundamental relationships between the pressure development and the mass burning rate at any instant, the effect of all external parameters on the transient combustion process is included in the model. In the case of premixed gases, the burning velocity and the flame thickness are defined as fundamental measures of the combustion process and these quantities have been used with success to model the mass burning rate (Dahoe et al., 2002).

The burning velocity, S_u, is the rate of flame propagation relative to the unburnt gas ahead of it. The flame speed, S_b, is relative to a fixed reference point. The laminar flame velocity is a mixture's intrinsic property that describes the severity of the explosion and it is a necessary input for the CFD simulation of the systems and the protection devices dimensioning.

1.4.1. Laminar burning velocity

In a premixed flame, the upstream mixture approaches the flame with a velocity $u_u=S_u$ and leaves the flame with a velocity u_b and temperature T_b. Assuming the mixture non-stoichiometric, the reaction is governed by the concentration (Y_u) of the limiting reactant and obtaining a complete consumption crossing the flame $Y_b= 0$ (Figure 23). At a hydrodynamic level, the flame is considered as an interface dividing the unburnt from the burnt gases at equilibrium conditions. In this model, the flame is a discontinuity between the unburnt and burnt gas properties (Law, 2006).

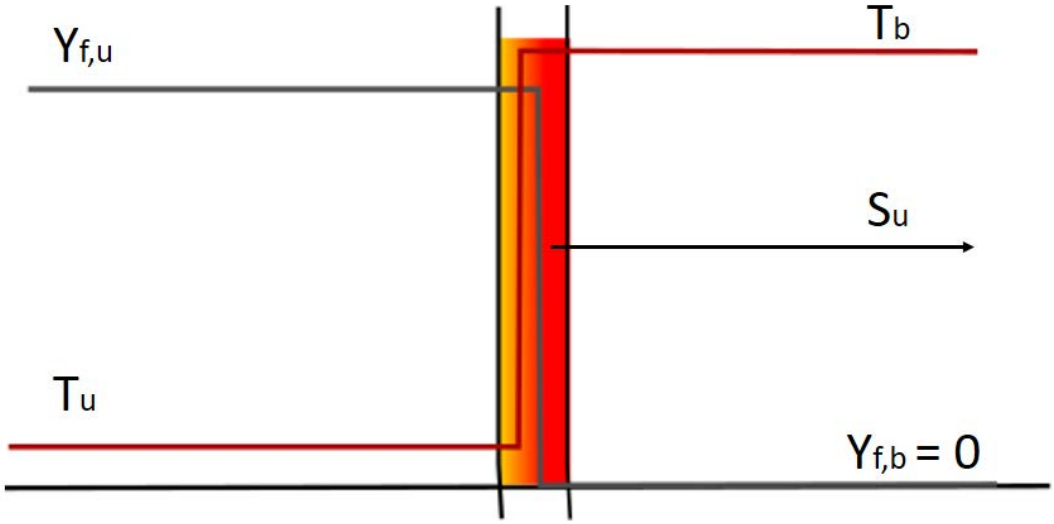

Figure 23. Simplest model of one-dimensional planar flame.

At a transport-diffusive level, the flame interface is expanded in a preheat zone with a characteristic thickness. As the mixture approaches the flame, it is gradually heated by the heat conducted from the reaction sheet, generating a continuous increase on the temperature until reaching T_b. The continuous heating of the mixture will eventually lead to its ignition and subsequent reaction. At the reaction interface, the reactant fraction and temperature are continuous and reaches their respective burnt values. In addition, the diffusion of the chemical species from the unburnt gases to the reaction sheet plays a fundamental role in the burning velocity. Furthermore, for mixture with a Lewis number equals to one (Le = 1, i.e. the thermal diffusivity and mass diffusivity are assumed equivalent), the similar values between the heat and mass diffusivities lead to a similar rate of temperature rise and decrease of reactant concentration.

$$Le = \frac{\lambda}{\rho D_i C_p} \qquad \text{Eq 3}$$

The flame structure consists of two different zones: the preheat zone in which convection and diffusion dominate, and a reaction zone where the reaction and diffusion dominate the phenomenon (Law, 2006). Finally, a more detailed flame model takes in account a flame reaction rate profile (Figure 24). The reaction rate profile is a greatly peaked function and with a characteristic thickness $\delta_r \ll \delta_d$ ($\delta_d = \delta_p + \delta_r$). The diffusing thickness can be expressed as:

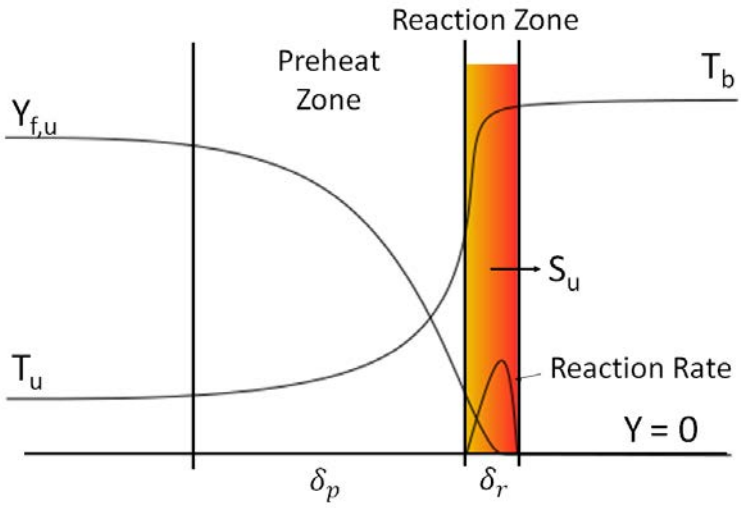

Figure 24. Multi-zone one dimensional planar flame

$$\delta_d = \frac{\lambda_u}{\rho_u C_p}\frac{1}{S_{u,L}} = \frac{\mathfrak{D}}{S_{u,L}} \quad \text{Eq 4}$$

Where $\mathfrak{D}$ is the thermal diffusivity, λ_u is the thermal conductivity and C_p is the heat capacity at constant pressure. A flame thickness estimation can be obtained from the temperature profile as follows:

$$\delta_f = \frac{T_{ad} - T_u}{\max(\frac{\partial T}{\partial x})} \quad \text{Eq 5}$$

The flame velocity can be obtained for laminar one-dimensional premixed flame solving the conservation equations of mass, species and energy:

$$\frac{\partial(\rho u)}{\partial x} = 0 \quad \text{Eq 6}$$

$$\frac{\partial}{\partial x}(\rho(u + V_i)Y_i) = \dot{\omega}_i \quad \text{Eq 7}$$

$$\rho C_p u\frac{dT}{dx} = -\dot{\omega}_i\left[\sum_{i=1}^{Ns}\left[h_{f,i}^0 + C_{p,i}T\right]\right] + \frac{\partial}{\partial x}\left(\lambda\frac{\partial T}{\partial x}\right) - \frac{\partial T}{\partial x}(\rho\sum_{i=1}^{Ns}C_{p,i}Y_iV_i) \quad \text{Eq 8}$$

Where $\dot{\omega}_i$ is the reaction rate, λ the thermal conductivity, C_p the heat capacity of the mixture and V_i the diffusion flux. The conservation equation establishes:

$$\rho u = constant = \rho_u u_u$$

So we have:

$$f^0 = \rho u = \rho_u u_u = \rho_b u_b$$

Where ρ_u and ρ_b are the density of unburnt and burnt gases respectively. This equation demonstrates that the mass flux f^0 is the fundamental parameter describing the flame propagation rate. From $f^0 = \rho u$, an unburnt laminar flame speed $s_u = S_{u,L} = f^0/\rho_u$ at the upstream boundary of the transport zone can be defined, and that is different from the burnt downstream laminar flame speed $s_b = S_s = f^0/\rho_b$.

For complex chemical reactions, numerical solution of the conservation equation is necessary to obtain the flame velocity and the temperature profile of the flame (Poinsot and Veynante, 2005). Nevertheless, analytical solutions of the premixed flame problem have been proposed. For instance, Zeldovich, Frank-Kamentskii and von Karman (ZFK) establish an asymptotic analytical model for high activation energy and based on non-dimensional values. In this model, the system is assumed isobaric, stationary and it is assumed that the reaction follows the Arrhenius law (Varea, 2013). Nevertheless, a detailed solution requires computational solution of the differential equations.

1.4.2. Flame stretch

Planar flames cannot be obtained on experimental configurations and real applications impose a stretched and curved flame. For example, the Bunsen flame cone possesses a curvature that is maximum at the flame tip. Depending on the magnitude and spatial distribution of the unburnt mixture velocity, the flame may have different shapes. Assuming a conical flame, the laminar velocity at the surface of the flame may be related to the velocity of the flow (v) at the exit of the mixing chamber by measuring the cone angle α and decomposing the velocity.

$$S_u^L = v\ sin\alpha$$

However, at the tip of the Bunsen flame, the laminar burning velocity is equal to v. This implies that the laminar burning velocity cannot be regarded as an intrinsic mixture property unless a normalization is done with respect to the flame shape. This velocity increase at the center of the flame for a conical Bunsen flame is due to the flame stretch (Dahoe, 2000). On the one hand, if a curved flame is concave with respect to the unburnt mixture, adjacent points on the flame surface move closer together; on the other hand, for a convex flame, the adjacent points will move further apart. Figure 25 shows the flame structure of a stretched flame for a hydrodynamic level and a transport-reaction dominating step. The conductive, diffusive and convective fluxes change for a curved flame compared to a planar flame, and its behavior during the flame propagation depends on the Lewis number.

For a planar flame, if the molecular and the thermal diffusivities are equal (Le = 1), the flame temperature at any point of the flame surface is the same. However, for a concave flame, the temperature and the burning velocity are higher than those of a planar flame due to compression phenomena, the opposite is true for a convex flame.

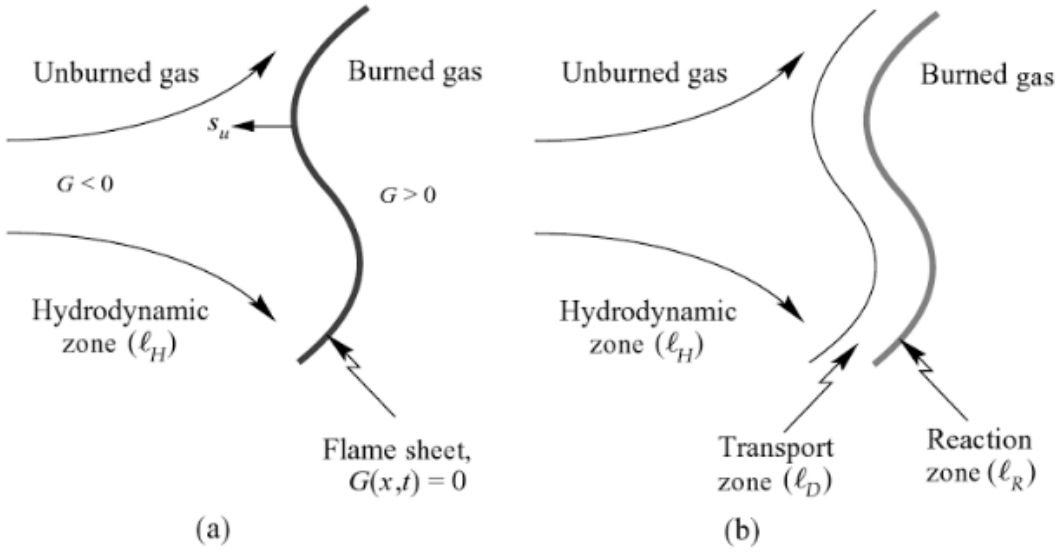

Figure 25. Flame structure of a wrinkled flame a) hydrodynamic level b) transport - reaction level (Law, 2006). G is the surface geometry; l_H, l_D and l_R are the characteristic thickness of the hydrodynamic, diffusive-convective and reaction zone respectively.

In the case of weakly stretched flames, the unstretched laminar burning velocity ($S^0_{u,L}$) can be expressed as:

$$S_{u,L} = \left[1 + \frac{\mathcal{L}}{\mathcal{R}}\right] S^0_{u,L} \qquad \text{Eq 9}$$

Where $\mathcal{L}$ is the Markstein length and $\mathcal{R}$ is the radius of curvature of the flame. The Markstein length is a constant of the mixture that represents the flame thickness and indicates the sensitivity of the laminar velocity to shape modifications (Markstein, 1964). In addition to this relation, the Williams-Clavin equation describes the response of the burning velocity to flame changes (Clavin, 1985):

$$M_k = \frac{\mathcal{L}}{\delta^0_L} = \frac{1}{\gamma}\ln\left(\frac{1}{1-\gamma}\right) + \frac{Ze(Le-1)(1-\gamma)}{2\gamma}\int_0^{\gamma/(1-\gamma)} \frac{\ln(1+x)}{x}\,dx$$

In this equation M_k is the Markstein number, δ^0_L is the thickness of an unstretched laminar flame, Ze is the Zeldovich number $Ze = (E_a/RT_f^2)(T_f - T_u)$, $\gamma = (T_f - T_u)$, T_f is the flame temperature and T_u is the temperature of the unburnt mixture. However, for flames subjected to a high stretching, these equations are not valid and two different Markstein lengths have to be defined: $\mathcal{L}_s$ for the flow induced strain and $\mathcal{L}_c$ for the curvature. The stretch rate (k) is defined as:

$$k = \frac{1}{A}\frac{dA}{dt} \qquad \text{Eq 10}$$

k consist of the contribution of a strain rate k_s and a curvature contribution k_c. A schematic representation of the flame strain and curvature is represented in Figure 26, where the normal and tangential straining are represented on the flame as a thin sheet, moving at S_f and surrounded the

fresh gases at a velocity u (Varea, 2013). Clavin (1985) demonstrates that the laminar burning velocity at each point of the flame can be related to the stretch rate as follows:

$$S_{u,L}^{0} - S_{u,L} = \mathcal{L}\left(\frac{1}{A}\frac{dA}{dt}\right) + O(\epsilon^2) \qquad \text{Eq 11}$$

As the stretch is the contribution of different parameters, the expression $\mathcal{L}$ is a linear combination of the effects of curvature and strain, each having its Markstein length. By this means, the equation is rewritten as:

$$S_{u,L}^{0} - S_{u,L} = (\mathcal{L}_s k_s + \mathcal{L}_c k_c) + O(\epsilon^2) \qquad \text{Eq 12}$$

A positive value of the Markstein length induces that the burning velocity decreases when the stretch increase, generating a stable flame. Conversely, if the Markstein length is negative, an unstable flame is obtained because the burning velocity increases with the flame stretch (Dahoe, 2000)

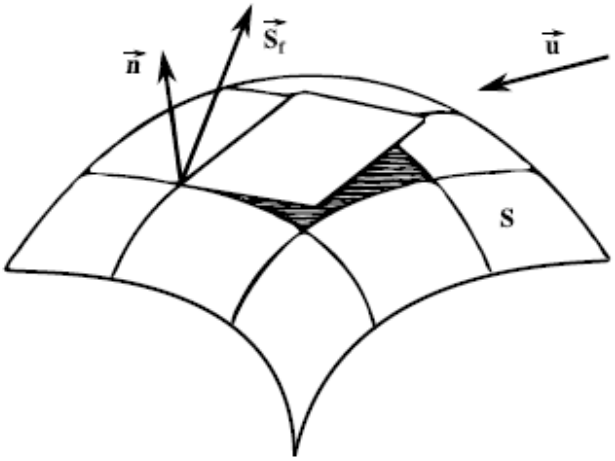

Figure 26. Schematic flame surface submitted to strain and curvature (Varea, 2013).

1.4.3. Expanding spherical flames

Previously, the flame stretching concept had been exemplified in a Bunsen burner in order to highlight the importance of the strain and curvature in the flame velocity estimation. Nevertheless, the burning velocity is estimated in this work assuming a spherical propagation of the flame before the interaction with the internal walls of the vessel (e.g. as in the flame propagation tube in Chapter 3). Under constant pressure conditions, the flame radius evolution is measured and the spatial velocity is estimated (Law, 2006; Varea, 2013):

$$S_s = \frac{dR_f}{dt} \qquad \text{Eq 13}$$

It is assumed that the flame is almost not affected by the ignition energy. Due to the partial confinement of the vessel, the stretched flame velocity can be estimated taking in account the thermal expansion of the gases, which can be obtained using the density ratio (Law, 2006; Varea, 2013):

$$S_l = \frac{\rho_b}{\rho_u} S_s \quad \text{Eq 14}$$

The flame surface for the spherical and flame and the stretch rate reads:

$$A = 4\pi R_f^2 \quad \text{Eq 15}$$

$$k = \frac{2}{R_f} \frac{dR_f}{dt} \quad \text{Eq 16}$$

A linear relation between stretched velocity S_l and k was proposed by Markstein (1964) in order to estimate the unstretched burning velocity:

$$S_l = \mathcal{L}k + S_l^0 \quad \text{Eq 17}$$

1.4.4. Turbulent combustion

The interaction between combustion and turbulence work both ways: the initial turbulence changes the combustion and the combustion modifies the turbulent flow. The effect of turbulence on combustion includes fluctuating characteristics in heat and mass transfer, and particularly in chemical reactions (Skjold, 2003). In addition, the turbulent flow is directly related to the dust deagglomeration and modifications on the PSD over the time. Those effects on the combustion modify the burning velocity and its characterization is necessary. As it was highlighted in section 1.1.2, two types of turbulence must be defined, the 'cold turbulence' associated to the initial turbulence of the flow before the ignition and the 'hot turbulence' related to the turbulent flow generated by the explosion.

The turbulent velocity has been defined, by analogy to the laminar velocity, as the max flux per unit area of the turbulent flame divided by the unburnt density $S_{u,T} = \dot{m}/\rho_u$. The turbulence generates wrinkles on the surface, changing the flame thickness and increasing the flame front area, which results in a higher propagation velocity. The instantaneous flame surfaces generated on the front are known as laminar flamelets (Dahoe, 2000). If the flame structure remains unchanged without changes but the flame surface increases due to the turbulence, a simple relation between the laminar and turbulent velocities has been proposed as a ratio between flame surfaces:

$$\frac{S_{u,T}}{S_{u,L}} = \frac{A_L}{A_T} \quad \text{Eq 18}$$

Some relations have been proposed for the estimation of the ratio between the laminar wrinkled surface and the turbulent flame surface. For instance, Damköhler suggested a direct relation between the turbulent velocity and the root-mean square velocity of the system v_{rms}, which describes the 'cold' turbulence of the system (Law, 2006):

$$\frac{S_{u,T}}{S_{u,L}} = 1 + \frac{v_{rms}}{S_{u,L}} \quad \text{Eq 19}$$

This relation implies that for a high turbulent system where v_{rms}>>S_L, the turbulent velocity does not depend on the chemical kinetics, and the turbulent velocity become independent from the laminar burning velocity. Schelkin proposes another approximation suggesting that the turbulence generates conical bulges in the laminar flame and the increase on the surface can be proportional to the average conical surface divided by the total surface of the front flame (Dahoe, 2000):

$$\frac{S_{u,T}}{S_{u,L}} = \sqrt{1 + \left(\frac{2v_{rms}}{S_{u,L}}\right)^2} \qquad \text{Eq 20}$$

This relation is in accordance with the Damköhler hypothesis, because the turbulent burning becomes independent from the laminar burning velocity when $S_{u,L}$ is negligible with respect to the root-mean-square velocity (v_{rms}).

Karlovitz et al. (1951) proposed several relations taking in account the effect of the scale of turbulence (different approximation for a turbulent eddy) on the turbulent burning velocity assuming an addition of a turbulent diffusion (S_u^t) on the laminar burning velocity:

$$S_{u,T} = S_{u,L} + S_u^t \qquad \text{Eq 21}$$

Table 4 shows the relations between the turbulent and the laminar burning velocities at different turbulent scales. These relations suggest that at high turbulent systems the turbulent flame velocity depends on the laminar burning velocity, and the Damköhler hypothesis is not true for these systems (Dahoe, 2000, p. 200).

Table 4. Proposed relations between the turbulent burning velocity and the laminar burning velocity at different turbulent scales (Dahoe, 2000).

Large Scale	***Intermediate scale***	***Small scale***
$\frac{S_{u,T}}{S_{u,L}} = 1 + \sqrt{2}\left(\frac{v_{rms}}{S_{u,L}}\right)^{\frac{1}{2}}$	$\frac{S_{u,T}}{S_{u,L}} = 1 + \sqrt{\frac{5}{12}}\frac{v_{rms}}{S_{u,L}}$	$\frac{S_{u,T}}{S_{u,L}} = 1 + \frac{v_{rms}}{S_{u,L}}$

Due to the difference in the relations proposed by Damköhler and Karlovitz, a general relationship has been proposed:

$$\frac{S_{u,T}}{S_{u,L}} = 1 + C\left(\frac{v_{rms}}{S_{u,L}}\right)^n \qquad \text{Eq 22}$$

With this equation, a relation between the turbulence velocity and the laminar burning velocity can be determined from experimental data. For a number of gaseous fuels (e.g. propane, acetylene, ethylene) it appears that a wide range of turbulent velocities can be correlated with a single set of constants (Dahoe, 2000). . However, further research must be performed on the correlation of turbulent velocities of dust and hybrid mixtures, due to the non-negligible thickness, the considerably heat radiation transfer and the possible perturbation on the flame surface.

1.4.5. Laminar flame velocity measurements

The burning velocity had been found as the fundamental measure, together with the flame thickness, of the combustion processes. With these parameters, an estimation of the mass burning velocity can be achieved, and the derivation of the pressure evolution can be obtained in order to estimate the explosion violence in industrial applications. Due to this reasons, the experimental determination of the burning velocity of gases, dust and hybrid mixtures has been performed in the last years.

The measure of the burning velocity has been a challenge because of the influence that of the experimental setup and of the reaction conditions (i.e. initial turbulence, obstacles, fuel concentration, particle distribution diameter, oxygen concentration) on the measured value. In an ideal premixed and stationary system, the burning velocity is a physicochemical constant for a given combustible mixture (Andrews and Bradley, 1972a). By this means, further experimental procedures have been proposed in order to measure the burning velocity for gas flames, reducing the effect of variables other than the mixture concentration. The experimental procedures are divided in stationary and non-stationary methods, as follows:

A. Stationary Flames

The stationary flame methods are based on the stabilization of the flame with an inlet unburnt gases velocity, which equals the burning velocity of the mixture in steady state conditions. Different types of burners have been developed to the determination of the flame velocity (Andrews and Bradley, 1972a):

a. **Open circular tube and nozzle method:** The conical flame (Bunsen burners) was widely used for the determination of the burning velocity. The gas velocity normal to the flame can be estimated or measured, and in addition, it is assumed that the premixed gases flow into the flame without air entrainment and without heat losses (Andrews and Bradley, 1972a).

b. **Flat flame burner methods:** The major difficulty with the use of conical flames is the identification of the flame surface. Because of this, flat flame burners have been implemented, where the flow rate is adjusted in order to produce a flat flame which is normal to the flow stream direction. This give a well-defined surface area of the flame, which if it is divided into the volumetric flow rate yields to the laminar burning velocity (Law, 2006). This method had been widely used in order to determine the burning velocity of gases and different configurations had been developed:

- **Heat flux burner:** In this method, a flat flame adiabatic burner is used to study measure the burning velocity (de Goey et al., 1993). The apparatus consist of a burner plate mounted on a plenum chamber. The burner head is a perforated plat which is used to stabilize the flame. The circumference of the plate is heated with a thermostatic fluid at a temperature above the temperature of the unburnt gases (Dirrenberger et al., 2011). If the unburned gas velocity is lower than the adiabatic flame velocity, the sum of heat loss and heat gain is greater than zero, meaning that the center of the plate is hotter than the periphery. In the contrary case, the unburned gas velocity is higher than the adabatic burning velocity, the periphery is hotter than the center of the plate. Therefore, when the temperature over the plate is the same, it means that no heat is lost or gained, and the flame is adiabatic with respect to the burner. By modifying the gas inlet, it is possible to

find the flow rate that cancel the net heat flux, which is the adiabatic flame burning velocity (Dirrenberger et al., 2011; Serinyel et al., 2013)

- **Counterflow flames:** A stagnation flow configuration is obtained by two counterflowing jets with the same chemical composition (Egolfopoulos et al., 2014). By this means, two steady laminar flames are established, obtaining a near adiabatic system due to the symmetry of the flames (Figure 27). The only heat loss is the inherent thermal radiation. The flame stretch must quantified and extracted of the measurement.

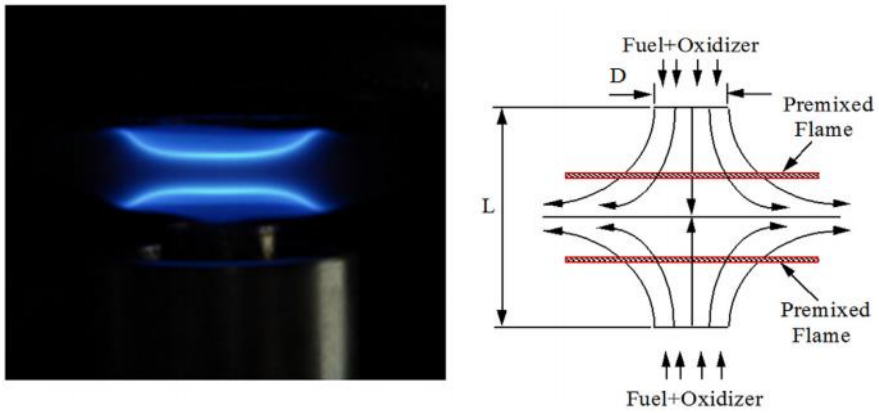

Figure 27. Counterflow flame configuration. (Egolfopoulos et al., 2014).

c. **Slot burner methods:** This method uses a long and rectangular nozzle with a constant velocity profile, which generates a flat-sided inverted "V" flame, which has the advantage that any flame curvature effect is eliminated (Andrews and Bradley, 1972a).

d. Direct measurement of unburnt gas velocity: This method involves the direct measure of the velocity of the unburnt gases of the flame by particle tracking, micro-pitot tube probes and hot wire anemometry (Andrews and Bradley, 1972a).

e. Measurement of flame thrust: The burning velocity is estimated by the experimental measure of the pressure drop across the flame. Applying the momentum equation for a one-dimensional flow without expansion parallel to the flame front, the pressure drop is expressed as (Andrews and Bradley, 1972a):

$$\Delta P = \rho_u S_u^2 \left(\frac{\rho_u}{\rho_b} - 1\right)$$

B. Non-stationary flames

a. Spherical expanding flames: In this method, the explosive mixture is ignited at the center of the containing reservoir and the spatial velocity of the flame front is measured. Close to the ignition point, the high curvature generate low-burning velocities, but at a remote point from the ignition point the flame could be approximate to a planar plane (Andrews and Bradley, 1972a). For these methods, different approaches had been developed, in which an additional measurement is needed to the burning velocity estimation. An example of this method is the determination of the burning velocity using spherical explosion vessel and the measurement of the rate of pressure rise after explosion (Dahoe, 2000; Dahoe et al., 2001, 2002; Varea et al., 2015).

b. **Tube method:** The combustible mixture is ignited at one end of a partially open tube and the flame development toward the other end is studied. The front flame is identified at each point of the tube, and the burning velocity is estimated from the spatial velocity by the mass conservation equation of the unburnt gas. This method has been validated to measure gas burning velocities at quiescent conditions (Andrews and Bradley, 1972a, 1972b), however, this methods had been almost abandoned for gas mixtures, due to the fast wall interactions, the aerodynamic stretch of the flame and the compression of gases generated by the possible pressure and temperature changes. This methods had been used for high turbulent or heterogeneous, as for the case of dust and hybrid mixture explosions (Cuervo, 2015; Di Benedetto et al., 2011).

The stationary flames methods have been preferred to measure the laminar burning velocity, due to the control of the laminar conditions and flame stretch. In addition, the measure of the velocity is easily achieved measuring the gas velocity or the pressure drop. However, some disadvantages are presented in this type of methods, for example, in the burner method, the adiabatic conditions are not assured in this set-up and in addition, the estimation of the flame surface is a difficult to estimate, generating possible errors in the determination of the burning velocity. Regarding the non-stationary methods, the implementation of this methods could be easier to achieve compared to the stationary flame methods, however, the measure of the laminar turbulent in transitory conditions is very challenging due to the turbulent flow and the high stretching present in the flame. Moreover, the possible interaction between the flame and the walls of the experimental vessel may generate additional incertitude to the measure.

1.4.6. Dust and hybrid mixture flame velocity measurements

Flammable gaseous mixtures have been widely studied and different methods of measuring flame velocity have been also developed (Andrews and Bradley, 1972a). Nevertheless, there is still a need for continued research on powder and hybrid mixture explosions and flame propagation (Dahoe, 2000). An overview of some methods applied for the measurement of dust and hybrid mixture explosions is presented in this section:

A. Stabilized flames

The dust flame velocity has been studied by igniting a fluidized powder on a burner, stabilizing the flame with the gas flow. Dahoe et al. (2002) measured the burning velocity of fluidized cornstarch/microbeads in air (i.e. as tracer particle for the Doppler anemometry method). A laser Doppler anemometry method was selected to measure the flow velocity at various locations inside the flame. The laminar burning velocity seems very sensitive to the flame shape on the burner, obtaining velocities of almost the double for parabolic flames compared to planar shape. Dahoe et al. (2002) had found laminar burning velocities between 15 and 30 $cm.s^{-1}$ for cornstarch/air explosion at different dust concentrations. In addition, the authors suggest that the stretch correction of the laminar burning velocity of dust explosion is crucial compared to gas mixtures explosion because the Markstein length of cornstarch flames (around 11 mm) is much larger than reported values of methane – air mixtures (0.1 – 0.2 mm).

Soo et al. (2013) had designed a burner to measure the burning velocity of a stable flame of aluminum/methane/air mixture. An initial high velocity jet of gas is created by flowing premixed methane-air through a concentrically slot, dispersing the dust pushed by a piston flow (Figure 28). The turbulent flow is laminarized by a conical diffuser and the mixture pass through the nozzle, where the mixture is ignited. A transition on the rate of aluminum oxidation was found for a dust

concentration between 140 – 220 $g.m^{-3}$. At stoichiometric conditions, laminar burning velocities between 30 and 35 $cm.s^{-1}$ are obtained for aluminum/methane/air mixtures.

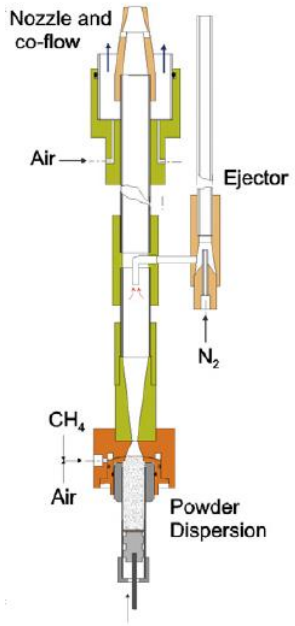

Figure 28. Hybrid flame burner for aluminum/methane/air mixtures for the measure of stabilized flame velocity (Soo et al., 2013).

B. Tube method

Due to the difficulties generating a stable flame of dust with a homogeneous concentration, some studies focus on the determination of the burning velocity of a moving flame inside a cylindrical tube or a square duct. Furthermore, the flame being at turbulent conditions and stretched, an extrapolation must be done in order to obtain the unstretched burning velocities (Andrews and Bradley, 1972b, 1972a).. This method has been validated for gas mixtures, but further experience is necessary for dust and hybrid mixtures

For instance, Proust (2006a, 2006b) measure the burning velocity of sulfur/air and lycopodium/air in a 1.5 m tube provided with a suspension generator and a hot wire as the ignition system. The author estimated he obtained a low turbulent system, and the laminar velocity was directly estimated. The derived laminar velocity was respectively between 10 and 25 $cm.s^{-1}$ and 30 to 50 $cm.s^{-1}$ for sulfur and lycopodium dust, respectively

In the LRGP, a vertical flame propagation tube of 1 meter with square section 7 x 7 cm has been used for the determination of the burning velocity of dust, gas-solid and solid-solid hybrid mixtures (Cuervo, 2015; D'Amico et al., 2016; Di Benedetto et al., 2011; Khalili et al., 2012). A detailed description of this equipment will be developed on Chapter 3 for the determination of the unstretched velocity of carbon black nanoparticles/methane/air mixtures.

C. Explosion vessels

Several studies have been made in order to measure of the burning velocity of hybrid mixtures aluminum/methane/air mixtures in explosion vessels. For instance, Sikes et al. (2016) uses a constant-volume cylindrical explosion vessel with optical access to record Schlieren images using a Z-type system. The explosion vessel can support 15 atm of initial pressure, and the evolution of

this variable is monitored with piezoelectric transducers. The gas mixture is used to disperse directly the nano-aluminum powder placed on U-pipe before the explosion vessel (Lowry et al., 2011; Sikes et al., 2016). The suspended mass of aluminum nanoparticles was estimated by laser extinction method based on the Beer-Lambert's law, and then, for each hybrid mixture the laminar burning velocity was calculated using spherical expanding flame method. In this experiment, a steady decrease in the laminar flame speed is generated when the suspended mass increase up to 20 mg. This trend leads to the conclusion that the suspended aluminium have a measurable effect on the flame speed (i.e. a decrease of 5-7% is evidenced) as a result of particle heating, instabilities of the flame and a possible Al reaction (Sikes et al., 2016).

D. Summary of dust burning velocities

Even if the experimental conditions for the laminar flame velocity are considerably different and a normalization of the measure is not yet performed, Table 5 summarizes some of the measured values of dust flame velocity:

Table 5. Laminar burning velocity of some dust explosions (Silvestrini et al., 2008)

Dust	Concentration ($g.m^{-3}$)	Burning velocity ($cm.s^{-1}$)	Method/Reference
Lycopodium	60 – 175	41	Cylindrical tube (British Materials Handling Board, 1995)
Lycopodium	200	26	Bunsen burner (Krause et al., 1996)
Sulfur (20 µm)	200-300	17 - 25	Tube burner (van der Wel, 1993)
Cornstarch (15 µm)	430 - 800	6 -18	Flat burner (van der Wel, 1993)
Lycopodium (25 – 45 µm)	35-80	47	Square duct (Proust, 1993)t
Cornstarch	260 -380	29	Stabilized flame (Dahoe et al., 2002)
Aluminium (10 µm)	310	55	Cylindrical tube (Goroshin et al., 2005)
Titanium (5 µm)	415	60	Cylindrical tube (Goroshin et al., 2005)
Iron (5 µm)	725	20	Cylindrical tube (Goroshin et al., 2005)

Dust	Concentration ($g.m^{-3}$)	Burning velocity ($cm.s^{-1}$)	Method/Reference
Sulfur (42 µm)	280	23	Square duct (Proust, 2006b)
Aluminium (7 µm)	250-450	33.6	Stabilized burner (Lomba, 2016)
Aluminium (5.6 µm)	300-600	30-39	Counterflow burner (Julien et al., 2017)

Nomenclature

Symbol	Description
A	Flame surface [m^2].
A_L	Laminar flame surface [m^2].
A_T	Turbulent flame surface [m^2].
C_p	Specific heat capacity at constant pressure [$J.kg^{-1}.K^{-1}$].
D	Molecular diffusivity [$m^2.s^{-1}$].
$\mathfrak{D}$	Thermal diffusivity [$m^2.s^{-1}$].
$\left(\frac{dP}{dt}\right)_{max}$	Maximum rate of pressure rise [$bar.s^{-1}$].
f^0	Mass flux
h_f^0	Standard enthalpy of formation [$kJ^2.mol^{-1}$].
I	Thermal radiation intensity [$W.m^{-2}$].
I_b	Black body thermal radiation intensity [$W.m^{-2}$].
k	Stretch rate [s^{-1}].
k_c	Curvature stretch rate [s^{-1}].
k_s	Strain stretch rate [s^{-1}].
K_a	Absorption coefficient [cm^{-1}].
K_s	Scattering coefficient [cm^{-1}].
$\mathcal{L}$	Markstein length [cm].
$\mathcal{L}_c$	Curvature Markstein length [cm].
$\mathcal{L}_s$	Strain Markstein length [cm].
Le	Lewis number [-].
LFL	Lowe Flammable Limit [-].
Mk	Markstein number [-].
MEC	Minimum Explosive concentration [-]
MIE	Minimum Ignition Energy [-]
MIT	Minimum Ignition Temperature [-].
MOC	Minimum Oxygen Concentration [-].
P_{max}	Maximum overpressure [bar].
PSD	Particle Size Distribution [-].
$\mathcal{R}$	Radius of curvature of the flame [cm].

S_s	Spatial velocity [cm s^{-1}].
S_u	Burning velocity [cm s^{-1}].
$S_{u,L}$	Laminar Burning velocity [cm s^{-1}].
$S_{u,T}$	Turbulent Burning velocity [cm s^{-1}].
$S_{u,L}^0$	Unstretched laminar Burning velocity [cm s^{-1}].
S_u^0	Unstretched burning velocity [cm s^{-1}].
S_u^t	Turbulent diffusion. [cm s^{-1}]
T	Temperature [K].
T_{ad}	Adiabatic temperature [K].
T_b	Burnt gas temperature [K].
T_f	Flame temperature [K].
T_u	Unburnt gas temperature. [K].
t_v	Ignition delay time [s].
u	Velocity [m s^{-1}]
u_b	Burnt gas velocity [cm s^{-1}]
u_u	Unburnt gas velocity [cm s^{-1}]
v	Stoichiometric coefficient [-]
v_{rms}	Root-mean-square velocity [m s^{-1}]
V	Volume [m^3]
V_i	Diffusion velocity [m s^{-1}]
Y	Mass fraction [-].
Y_b, $Y_{f,b}$	Burnt gas mass fraction [-]
Y_u, $Y_{f,u}$	Unburnt gas mass fraction [-].
W	Molecular Weight [g.mol^{-1}]
Ze	Zeldovich number [-].

Greek letters	Description
α	Cone angle of Bunsen flame [-].
δ_d	Diffusing thickness [mm]
δ_p	Pre-heat zone thickness [mm]
δ_r	Reaction zone thickness [mm]
δ_f	Flame thickness [mm]
γ	Expansion factor [-].

λ	Thermal conductivity **[**W.m^{-1}.K^{-1}**].**
ρ	Density **[**kg.m^{-3}**]**
ρ_b	Burnt gas density **[**kg.m^{-3}**]**
ρ_u	Unburnt gas density **[**kg.m^{-3}**]**
Ω	Solid angle [-]
θ	Reduced Temperature [-]
φ	Reduced gas fraction [-]
ΔP	Pressure drop [Pa]
τ_r	Reaction time [s]
$\dot{\tau}_r$	Reduced reaction time [-]
$\dot{\omega}_i$	Reaction rate **[**mol.m^{-3}s^{-1}**]**
$\dot{\omega}_{i,r}$	Reduced reaction time [-]

References

Abbasi, T., Abbasi, S.A., 2007. Dust explosions–Cases, causes, consequences, and control. J. Hazard. Mater. 140, 7–44.

Addai, E.K., Gabel, D., Kamal, M., Krause, U., 2016. Minimum ignition energy of hybrid mixtures of combustible dusts and gases. Process Saf. Environ. Prot. 102, 503–512.

Addai, E.K., Gabel, D., Krause, U., 2015. Lower explosion limit of hybrid mixtures of burnable gas and dust. J. Loss Prev. Process Ind. 36, 497–504.

Ajrash, M.J., Zanganeh, J., Moghtaderi, B., 2016a. Effects of ignition energy on fire and explosion characteristics of dilute hybrid fuel in ventilation air methane. J. Loss Prev. Process Ind. 40, 207–216.

Ajrash, M.J., Zanganeh, J., Moghtaderi, B., 2016b. Methane-coal dust hybrid fuel explosion properties in a large scale cylindrical explosion chamber. J. Loss Prev. Process Ind. 40, 317–328.

Amyotte, P., Lindsay, M., Domaratzki, R., Marchand, N., Di Benedetto, A., Russo, P., 2009. Prevention and mitigation of dust and hybrid mixture explosions. Process Saf. Prog.

Amyotte, P.R., 2014. Some myths and realities about dust explosions. Process Saf. Environ. Prot. 92, 292–299

Amyotte, P.R., Eckhoff, R.K., 2010. Dust explosion causation, prevention and mitigation: An overview. J. Chem. Health Saf. 17, 15–28.

Andrews, G.E., Bradley, D., 1972a. Determination of burning velocities: A critical review. Combust. Flame 18, 133–153.

Andrews, G.E., Bradley, D., 1972b. The burning velocity of methane-air mixtures. Combust. Flame 19, 275–288.

ASTM E1491 - 06, 2012. Standard Test Method for Minimum Autoignition Temperature of Dust Clouds. Annu. Book Fo ASTM Stand.

ASTM E1515-14, 2014. Standard Test for Minimum Explosible Concentration of Combustible Dust. Annu. Book Fo ASTM Stand.

ASTM E2019 − 03, 2007. Standard Test Method for Minimum Ignition Energy of a Dust Cloud in Air. Annu. Book ASTM Stand.

ASTM E2931 − 13, 2013. Standard Test Method for Limiting Oxygen (Oxidant) Concentration of Combustible Dust Clouds. Annu. Book ASTM Stand.

Beckstaed, M.W., 2002. A summary of aluminum combustion. Intern Aerodyn Solid Rocket Propuls.

Bidabadi, M., Shakibi, A., Rahbari, A., 2011. The radiation and heat loss effects on the premixed flame propagation through lycopodium dust particles. J. Taiwan Inst. Chem. Eng. 42, 180–185.

Bidabadi, M., Zadsirjan, S., Mostafavi, S.A., 2013. Radiation heat transfer in transient dust cloud flame propagation. J. Loss Prev. Process Ind. 862–868.

Boilard, S.P., Amyotte, P.R., Khan, F.I., Dastidar, A.G., Eckhoff, R.K., 2013. Explosibility of micron- and nano-size titanium powders. J. Loss Prev. Process Ind. 26, 1646–1654.

Bouillard, J., Vignes, A., Dufaud, O., Perrin, L., Thomas, D., 2010. Ignition and explosion risks of nanopowders. J. Hazard. Mater. 181, 873–880.

Bouillard, J., Vignes, A., Dufaud, O., Perrin, L., Thomas, D., 2009. Explosion risks from nanomaterials. J. Phys. Conf. Ser. 170, 012032.

British Materials Handling Board, 1995. Dust explosions, protecting people, equipment, buildings and environment.

BS EN 14034-1, 2004. Determination of explosion characteristics of dust clouds - Part 1: Determination of the maximum explosion pressure Pmax of dust clouds.

Cao, W., Gao, W., Liang, J., Xu, S., Pan, F., 2014. Flame-propagation behavior and a dynamic model for the thermal-radiation effects in coal-dust explosions. J. Loss Prev. Process Ind. 29, 65–71.

Cashdollar, K.L., 2000. Overview of dust explosibility characteristics. J. Loss Prev. Process Ind. 13, 183–199.

Chan, M., Chong, S.J., 2016. Dust explosion from coloured powder causing severe burns. ANZ J. Surg. 86, 103–104.

Cheng, M., Mathews, A.L., Chuang, S., Lark, M.E., Hsiao, Y., Ng, C., Chung, K.C., 2016. Management of the Formosa Color Dust Explosion: Lessons Learned from the Treatment of 49 Mass Burn Casualty Patients at Chang Gung Memorial Hospital. Plast. Reconstr. Surg. 137, 1900–1908.

Clavin, P., 1985. Dynamic behavior of premixed flame fronts in laminar and turbulent flows. Prog. Energy Combust. Sci. 11, 1–59.

Cuervo, N., 2015. Influences of turbulence and combustion regimes on explosions of gas- dust hybrid mixture. PhD thesis. Université de Lorraine.

Dahoe, A., 2000. Dust Explosions: a Study of Flame Propagation. PhD thesis. Delft University

Dahoe, A.E., Cant, R.S., Pegg, M.J., Scarlett, B., 2001. On the transient flow in the 20-liter explosion sphere. J. Loss Prev. Process Ind. 14, 475–487.

Dahoe, A.E., Hanjalic, K., Scarlett, B., 2002. Determination of the laminar burning velocity and the Markstein length of powder–air flames. Powder Technol., Special issue i in Honour of Prof Jimbo 122, 222–238.

D'Amico, M., Dufaud, O., Latché, J.-C., Trélat, S., Perrin, L., 2016. Predicting Graphite/Metals Explosion Severity: from Experimentation to Modelling. Chem. Eng. Trans. 415–420.

de Goey, L.P.H., van Maaren, A., Quax, R.M., 1993. Stabilization of Adiabatic Premixed Laminar Flames on a Flat Flame Burner. Combust. Sci. Technol. 92, 201–207.

Demesoukas, S., Brequigny, P., Caillol, C., Halter, F., Mounaïm-Rousselle, C., 2016. 0D modeling aspects of flame stretch in spark ignition engines and comparison with experimental results. Appl. Energy 179, 401–412.

Denkevits, A., 2007. Explosibility of hydrogen–graphite dust hybrid mixtures. J. Loss Prev. Process Ind. 20, 698–707.

Di Benedetto, A., Garcia-Agreda, A., Dufaud, O., Khalili, I., Sanchirico, R., Cuervo, N., Perrin, L., Russo, P., 2011. Flame propagation of dust and gas-air mixtures in a tube. Proc. 7th Mediterr. Combust. Symp. Chia Laguna Cagliari Sard. Italy.

Di Benedetto, A., Russo, P., Amyotte, P., Marchand, N., 2010. Modelling the effect of particle size on dust explosions. Chem. Eng. Sci. 65, 772–779.

Dirrenberger, P., Le Gall, H., Bounaceur, R., Herbinet, O., Glaude, P.-A., Konnov, A., Battin-Leclerc, F., 2011. Measurements of Laminar Flame Velocity for Components of Natural Gas. Energy Fuels 25, 3875–3884.

Droujko, J., Julien, P., Soo, M., Goroshin, S., Bergthorson, J.M., Frost, D.L., Glumac, N., 2016. The role of radiative preheating on flame propagation in aluminium dust clouds. Proc. 11th Int. Symp. Hazards Prev. Mitig. Ind. Explos. 435–448.

Dufaud, O., Perrin, L., Traoré, M., 2008. Dust/vapour explosions: Hybrid behaviours? J. Loss Prev. Process Ind. 21, 481–484.

Dufaud, O., Perrin, L., Traore, M., Chazelet, S., Thomas, D., 2009. Explosions of vapour/dust hybrid mixtures: A particular class. Powder Technol. 190, 269–273.

Dufaud, O., Vignes, A., Henry, F., Perrin, L., Bouillard, J., 2011. Ignition and explosion of nanopowders: something new under the dust. J. Phys. Conf. Ser. 304, 012076.

Eckhoff, R.K., 2013. Influence of dispersibility and coagulation on the dust explosion risk presented by powders consisting of nm-particles. Powder Technol. 239, 223–230.

Eckhoff, R.K., 2012. Does the dust explosion risk increase when moving from μm-particle powders to powders of nm-particles? J. Loss Prev. Process Ind. 25, 448–459.

Eckhoff, R.K., 2011. Are enhanced dust explosion hazards to be foreseen in production, processing and handling of powders consisting of nano-size particles? J. Phys. Conf. Ser. 304, 012075.

Eckhoff, R.K., 2006. Differences and similarities of gas and dust explosions: A critical evaluation of the European "ATEX" directives in relation to dusts. J. Loss Prev. Process Ind. 19, 553–560.

Eckhoff, R.K., 2004. Partial inerting—an additional degree of freedom in dust explosion protection. J. Loss Prev. Process Ind. 17, 187–193.

Eckhoff, R.K., 2003. Dust explosions in the process industries, 3rd ed. ed. Gulf Professional Pub, Amsterdam ; Boston.

Eggersdorfer, M.L., Pratsinis, S.E., 2014. Agglomerates and aggregates of nanoparticles made in the gas phase. Adv. Powder Technol. 25, 71–90.

Egolfopoulos, F.N., Hansen, N., Ju, Y., Kohse-Höinghaus, K., Law, C.K., Qi, F., 2014. Advances and challenges in laminar flame experiments and implications for combustion chemistry. Prog. Energy Combust. Sci. 43, 36–67.

European Comission, 2011. Commission recommendation on the definition of nanomaterial. Off. J. Eur. Union.

Fumagalli, A., Derudi, M., Rota, R., Copelli, S., 2016. Estimation of the deflagration index KSt for dust explosions: A review. J. Loss Prev. Process Ind. 44, 311–322.

Garcia-Agreda, A., Di Benedetto, A., Russo, P., Salzano, E., Sanchirico, R., 2011. Dust/gas mixtures explosion regimes. Powder Technol. 205, 81–86.

Goroshin, S., Mamen, J., Lee, J.H.S., Sacksteder, K., 2005. Ground-based and microgravity study of flame quenching distance in metal dust suspensions. Proc. ICDERS.

Haghiri, A., Bidabadi, M., 2011. Dynamic behavior of particles across flame propagation through micro-iron dust cloud with thermal radiation effect. Fuel 90, 2413–2421.

Haghiri, A., Bidabadi, M., 2010. Modeling of laminar flame propagation through organic dust cloud with thermal radiation effect. Int. J. Therm. Sci. 49, 1446–1456.

Henry, F., 2013. Thermomécanique des systèmes nanodispersés : application au cas de l'agglomération de nanoparticules. PhD thesis. Université de Lorraine.

Hoet, P.H., Brüske-Hohlfeld, I., Salata, O.V., 2004. Nanoparticles–known and unknown health risks. J. Nanobiotechnology 2, 12.

IEC 1241-2-3, 1994. Electrical apparatus for use in the presence of combustible dust - Test methods -Section 3: Method for determining minimum ignition energy of dust/air mixtures. Int. Electrotech. Comm.

ISO 6184-1, 1985. Explosion protection systems - Part 1: Determination of explosion indices of combustible dust in air. Int. Stand. Organ. Geneva.

Jiang, B., Lin, B., Shi, S., Zhu, C., Li, W., 2011. Explosive characteristics of nanometer and micrometer aluminum-powder. Min. Sci. Technol. China 21, 661–666.

Jiang, J., Liu, Y., Mannan, M.S., 2014. A correlation of the lower flammability limit for hybrid mixtures. J. Loss Prev. Process Ind. 32, 120–126.

Jiang, J., Liu, Y., Mashuga, C.V., Mannan, M.S., 2015. Validation of a new formula for predicting the lower flammability limit of hybrid mixtures. J. Loss Prev. Process Ind. 35, 52–58.

Julien, P., Whiteley, S., Soo, M., Goroshin, S., Frost, D.L., Bergthorson, J.M., 2017. Flame speed measurements in aluminum suspensions using a counterflow burner. Proc. Combust. Inst. 36, 2291–2298.

Karlovitz, B., Denniston, D.W., Wells, F.E., 1951. Investigation of turbulent flames. J. Chem. Phys. 19, 541.

Khalili, I., 2012. Sensibilité, sévérité et spécificités des explosions de mélanges hybrides gaz/vapeurs/poussières. PhD thesis. Université de Lorraine.

Khalili, I., Dufaud, O., Poupeau, M., Cuervo-Rodriguez, N., Perrin, L., 2012. Ignition sensitivity of gas–vapor/dust hybrid mixtures. Powder Technol. 217, 199–206.

Kosinski, P., Nyheim, R., Asokan, V., Skjold, T., 2013. Explosions of carbon black and propane hybrid mixtures. J. Loss Prev. Process Ind. 26, 45–51

Krause, U., Kasch, T., Gebauer, B., 1996. Velocity and concentration effects on the laminar burning velocity of dust–air mixtures. Proc. Seventh Int. Colloq. Dust Explos.

Kuhlbusch, T.A., Asbach, C., Fissan, H., Göhler, D., Stintz, M., 2011. Nanoparticle exposure at nanotechnology workplaces: a review. Part. Fibre Toxicol. 8, 22.

KUHNER Safety, 2015. 20-L Apparatus [WWW Document]. Safetykuhnercomenproductapparatusessafety-Test.-Devicesid-20--Appar.

Laurent, A., 2003. Sécurité des procédés chimiques. Connaissances de base et méthodes d'analyse de risques. TEC & DOC.

Law, C.K., 2006. Combustion Physics. Cambridge University Press.

Liu, Y., Sun, J., Chen, D., 2007. Flame propagation in hybrid mixture of coal dust and methane. J. Loss Prev. Process Ind. 20, 691–697.

Lomba, R., 2016. Utilisation de la combustion métallique dans les machines thermiques. PhD thesis. Université d'Orleans.

Lowry, W., de Vries, J., Krejci, M., Petersen, E., Serinyel, Z., Metcalfe, W., Curran, H., Bourque, G., 2011. Laminar Flame Speed Measurements and Modeling of Pure Alkanes and Alkane Blends at Elevated Pressures. J. Eng. Gas Turbines Power 133, 091501.

Mannan, S., Lees, F.P. (Eds.), 2005. Lee's loss prevention in the process industries: hazard identification, assessment, and control, 3rd ed. ed. Elsevier Butterworth-Heinemann, Amsterdam ; Boston.

Markstein, G.H., 1964. Non-steady flame propagation. Pergamon Press, Oxford.

Mittal, M., 2014. Explosion characteristics of micron- and nano-size magnesium powders. J. Loss Prev. Process Ind. 27, 55–64.

Murillo, C., 2016. Experimental and numerical approaches to particles dispersion in a turbulent flow: application to dusts explosion. Université de Lorraine.

NF EN 14034-3, 2011. Détermination des caractéristiques d'explosion des nuages de poussière - Partie 3 : détermination de la limite inférieure d'explosivité LIE des nuages de poussière.

Oberdörster, G., Oberdörster, E., Oberdörster, J., 2005. Nanotoxicology: An Emerging Discipline Evolving from Studies of Ultrafine Particles. Environ. Health Perspect. 113, 823–839.

Pilão, R., Ramalho, E., Pinho, C., 2006. Explosibility of cork dust in methane/air mixtures. J. Loss Prev. Process Ind. 19, 17–23.

Poinsot, T., Veynante, D., 2005. Theoretical and numerical combustion. RT Edwards, Inc.

Pritchard, D.K., 2004. Literature review: explosion hazards associated with nanopowders. Health and Safety Laboratory.

Proust, C., 2006a. A few fundamental aspects about ignition and flame propagation in dust clouds. J. Loss Prev. Process Ind. 19, 104–120.

Proust, C., 2006b. Flame propagation and combustion in some dust-air mixtures. J. Loss Prev. Process Ind. 19, 89–100.

Proust, C., 1993. Experimental determination of the maximum flame temperatures and of the laminar burning velocities for some combustible dust–air mixtures. Int. Colloq. Dust Explos.

Proust, C., Ben Moussa, R., Guessasma, M., Saleh, K., Fortin, J., 2017. Thermal radiation in dust flame propagation. J. Loss Prev. Process Ind.

Prugh, R.W., 2008. The relationship between flash point and LFL with application to hybrid mixtures. Process Saf. Prog. 27, 156–163.

Rockwell, S.R., Rangwala, A.S., 2013. Modeling of dust air flames. Fire Saf. J. 59, 22–29.

Serinyel, Z., Herbinet, O., Frottier, O., Dirrenberger, P., Warth, V., Glaude, P.A., Battin-Leclerc, F., 2013. An experimental and modeling study of the low- and high-temperature oxidation of cyclohexane. Combust. Flame 160, 2319–2332.

Sikes, T., Mannan, M.S., Petersen, E.L., 2016. Laminar flame speeds of nano-aluminum/methane hybrid mixtures. Combust. Flame 166, 284–294.

Silvestrini, M., Genova, B., Leon Trujillo, F.J., 2008. Correlations for flame speed and explosion overpressure of dust clouds inside industrial enclosures. J. Loss Prev. Process Ind. 21, 374–392.

Skjold, T., 2003. Selected aspects of turbulence and combustion in 20-Litre explosion vessel. University of Bergen, Norway.

Soo, M., Julien, P., Goroshin, S., Bergthorson, J.M., Frost, D.L., 2013. Stabilized flames in hybrid aluminum-methane-air mixtures. Proc. Combust. Inst. 34, 2213–2220.

Stark, W.J., Stoessel, P.R., Wohlleben, W., Hafner, A., 2015. Industrial applications of nanoparticles. Chem Soc Rev 44, 5793–5805.

Stern, S.T., McNeil, S.E., 2007. Nanotechnology Safety Concerns Revisited. Toxicol. Sci. 101, 4–21.

Tamanini, F., 1998. The role of turbulence in dust explosions. J. Loss Prev. Process Ind. 11, 1–10.

Tamanini, F., 1990. Turbulence effects on dust explosion venting. PlantOperations Prog. 9, 52–60.

van der Wel, P., 1993. Ignition and propagation of dust explosions. Thesis Delft Univ. Press.

Varea, E., 2013. Experimental analysis of laminar spherically expanding flames. INSA de Rouen.

Varea, E., Beeckmann, J., Pitsch, H., Chen, Z., Renou, B., 2015. Determination of burning velocities from spherically expanding H2/air flames. Proc. Combust. Inst. 35, 711–719.

Vignes, A., Dufaud, O., Perrin, L., Thomas, D., Bouillard, J., Janès, A., Vallières, C., 2009. Thermal ignition and self-heating of carbon nanotubes: From thermokinetic study to process safety. Chem. Eng. Sci. 64, 4210–4221.

Wengeler, R., Nirschl, H., 2007. Turbulent hydrodynamic stress induced dispersion and fragmentation of nanoscale agglomerates. J. Colloid Interface Sci. 306, 262–273.

Worsfold, S.M., Amyotte, P.R., Khan, F.I., Dastidar, A.G., Eckhoff, R.K., 2012. Review of the Explosibility of Nontraditional Dusts. Ind. Eng. Chem. Res. 51, 7651–7655.

CHAPTER 2: Effect of nanoparticles dispersion on the explosion severity parameters

2.1. Introduction

Hybrid mixture explosions are a growing concern in various types of industries despite the recent efforts to prevent such events. For instance, during incomplete combustions or nano-size carbon black generation, atmospheres of carbonaceous nanopowders and combustible gases are encountered. In addition to the characterization of their explosive properties, it is essential to understand that such hybrid mixtures can exhibit specific behaviors, especially an increased explosivity even at low powder content (see Chapter 1.3) (Dufaud et al., 2009; Garcia-Agreda et al., 2011; Khalili et al., 2012). The modification of the initial turbulence level due to the presence of powders could be presented as one of these causes (for larger particles and agglomerates) as well as the contribution of the combustible dust to the oxidation reactions and to radiative phenomenon. Nanoparticles of carbon black can be regarded as initial soot or soot-nuclei in the system, which also allows studying the influence of such particles on gas explosions.

This chapter aims to document the influence of nanoparticles dispersion in the explosion severity of hybrid gas/solid mixtures, in order to understand the complex heat transfer, and the possible effects of dispersed nano-carbon particles (such as soot nuclei) in the combustion reaction. This case is specifically encountered during gases combustion with high fuel equivalent ratio. The influence of the nanoparticles on the flame propagation properties is also analyzed and detailed in the study of the burning velocity of these mixtures (see Chapter 3).

First, the experimental characterization of the dust bulk properties and its dispersion properties will be presented. Then the turbulent flows developed in the experimental set-ups (flame propagation tube, 20L sphere) will be characterized by Particle Image Velocimetry (PIV).

Second, the study of the effect of carbon black nanoparticles on the explosion severity parameters measured on a 20-L sphere will be analyzed. The influence of the turbulence level, dust concentration, gas concentration and elementary particle diameter will also be addressed. In addition, the burnt gases are quantified by micro gas chromatography (μ-GC) in order to analyze the possible influence of carbon black presence on the chemical reaction. Moreover, the explosion severity results for carbon black nanoparticles and methane/air mixtures will be compared to inert alumina nanoparticles/methane/air mixture, aiming to isolate the possible chemical contribution from the turbulence and heat radiation effect on the explosions.

2.2. Dust characterization

2.2.1. Particles properties

In this study, both Corax N550 and Printex XE2 (provided by Orion) were chosen as carbon black nanoparticles. In addition, alumina AP-D 0.05 (Struers) was chosen as inert dust. The shape and size difference between the powders are shown on the Scanning Electron Microscopy images (Figure 29).

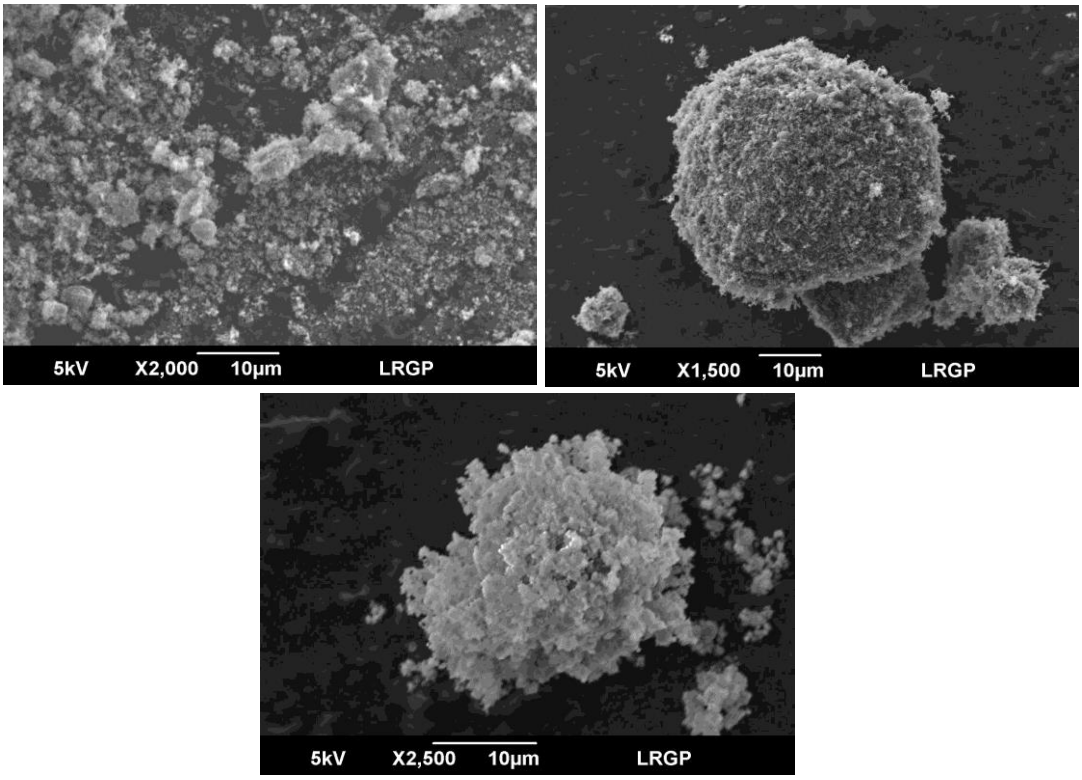

Figure 29. Scanning Electron Microscopy images: a) Printex XE2 b) Corax N550 and c) Alumina AP-D

The characterization of the powders, including the volume mean particle diameter d_{50}, the BET (Brunauer-Emmett-Teller method) specific surface and the equivalent BET diameter, are reported in Table 6. It should be highlighted that the particle size distributions (PSD) were determined using different analytical procedures and that they varied greatly as a function of the dispersion modes as the particle-particle interactions are different as a function of the continuous medium. As a consequence, it clearly appears that the characterization of the PSD of the powders should be carried out, if possible, under the same or similar dispersion conditions than those encountered during the explosion tests.

The particle size distribution is determined using laser diffraction granulometer HELOS Vario (Sympatec^{TM}), which is composed of laser emission and detection systems (33 channels). The incident beam is generated by a 5 mW Helium-Neon source and detectors measuring range are located between 0.5 and 175 µm. Dry samples were dispersed by sedimentation or by an air pulse, as it is the case for the flammability tests in the explosion tube or for explosion under standard conditions (Figure 30). The influence of an air pulse (4 bars) on the deagglomeration of the powders has been tested by using a 40 cm vertical dispersion tube with a 7 cm x 7 cm cross section and glass walls. This set-up has the same cross section as the flame propagation tube and a sufficient height to ensure the powder dispersion – it should be highlighted that in a 1 m long tube, the powder does not fully fill the tube at the moment of the ignition. At the bottom of the tube, a mushroom nozzle, similar to that used in a modified Hartmann tube, is connected. PSD of dry powders can be determined with a 2000 Hz frequency, however, in this chapter, only the mean values, i.e. PSD integrated over the whole dispersion process, will be presented (Figure 31). Test of wet samples were performed in isopropanol using the Mastersizer 2000 S (Malvern Instruments), which is composed of a He-Ne laser (wavelength of 633 nm).

Table 6. Main characteristics of carbon blacks and alumina powders

Powders	BET specific surface area ($m^2.g^{-1}$) (Bouillard et al., 2010)	BET diameter (nm) (Bouillard et al., 2010)	d_{50} Isopropanol (µm)	d_{50} dry sedim. (µm)	d_{50} dry pressure (µm)
Printex XE2	950	3	10	66	6
Corax N550	40	75	15	24	13
Alumina AP-D	84	20	2	69	25

Figure 30. Left: Laser diffraction granulometer Helos Vario (Sympatec, 2017) ; Right: Example of PSD measurement during a dust dispersion in the 20L sphere (D'Amico et al., 2016)

It clearly appears that Printex XE2, alumina AP-D and to a lesser extent Corax N550 are nanopowders, which tends to be greatly agglomerated. The primary nanoparticle size, which is close to the BET diameter -if porosity is neglected- is 2 to 4 orders of magnitude lower than the agglomerate size observed in a dust cloud during sedimentation. For dust explosion studies, the surface/volume ratio is an important parameter due to the air/fuel surface contact area. Hence, alumina AP-D 0.05 was chosen because both its BET specific surface area and its Sauter diameter in dispersed phase are of the same order of magnitude as the Corax N550.

Focusing on the carbon black nanoparticles, if they are both arranged on agglomerates of similar micrometric size, the Printex XE2 has a lower primary particle diameter, which can have an influence on the cloud stability, on the powder reactivity and on the heat transfers.

The dust fragmentation phenomenon has been detected on the PSD measurement during the dispersion of agglomerates in standard test conditions, as evidenced in Table 6. Furthermore, the particle size distribution differences between samples dispersed bye sedimentation and by dispersion (Figure 31) shows that fragmentation is present when the sample is dispersed at turbulent conditions, i.e. an increase in the differential volume distribution is obtained for particles below 40 and 10 µm for alumina and Printex XE2 dust respectively, when the particle is dispersed by a pulse

air of 4 bars. However, due to technical limitations, it was no possible to characterize the PSD below 1 µm approximately. At present, it is technically impossible to characterize a transient aerosol whose PSD is widespread (both over nanometric and micrometric range).

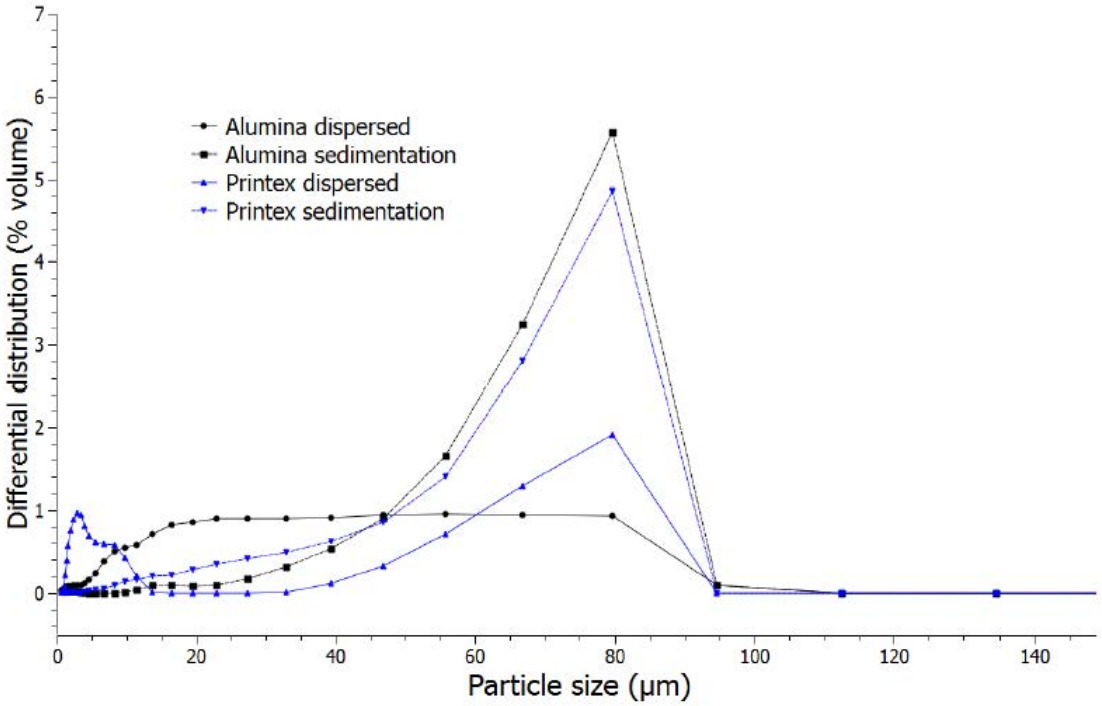

Figure 31. Particle size distributions of alumina and Printex XE2 as a function of the dispersion system: by sedimentation or dispersed by an air pulse.

Figure 32 shows the PSD evolution after dispersion by an air pulse of a Corax N550 sample. It can be observed that the particle size distribution change over the time, due mostly to the particle-particle interactions during the dust suspension. For a particle size below 15 µm, the volumetric fraction distribution increase for the first milliseconds due to dust fragmentation and after 0.8 s, the re-agglomeration of the dust should explain the rise of the volumetric distribution. In addition, for particle size greater than 50 µm, the volumetric distribution decrease after 1.8 s, which is mainly caused by the dust sedimentation.

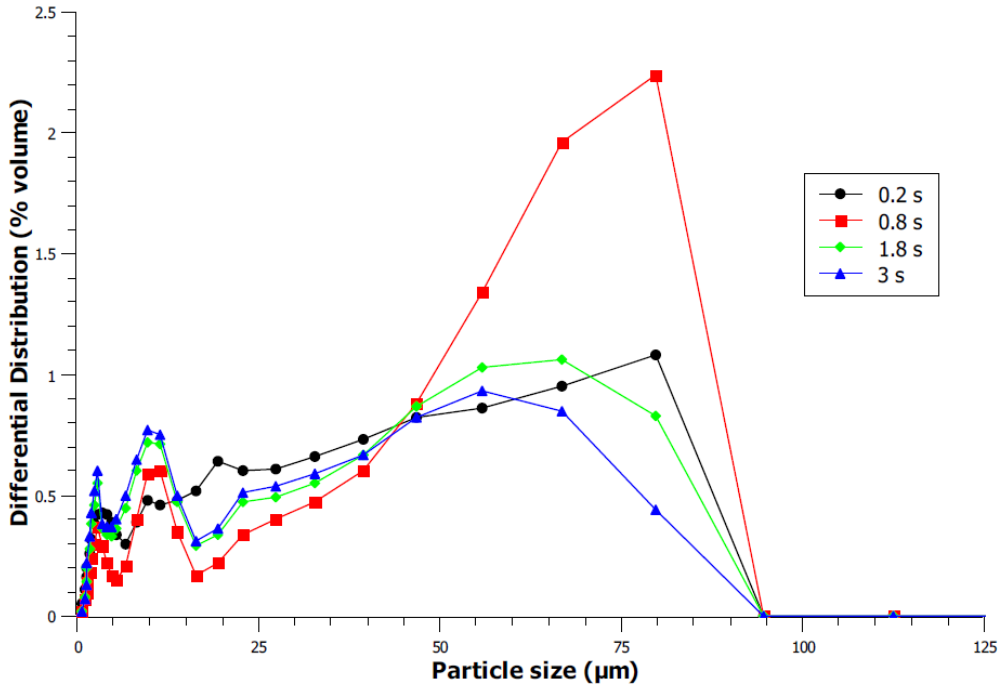

Figure 32. Particle size distributions evolution of Corax N550 at different times after a pulse air dispersion.

Due to the fast re-agglomeration and dust sedimentation, dispersion tests have been made for Printex XE2 and Corax N550 in order to analyze the stability of a dust cloud sometime after the injection. Different scales, from few seconds to minutes where investigated. To accomplish this, the mobility particle size was measured at different times after the powder injection by sequentially using a Differential Mobility Analyzer (Electrostatic Classifier – TSI 3080) and an Ultrafine Condensation Particle Counter (UCPC – TSI 3776). The Differential Mobility Analyzer (DMA) separates by size for measurements of particle size distribution. The poly disperse sample enters through a radiative bipolar charger, generating a bipolar equilibrium charge level on the particles. Then, the particles are separated according to their electrical mobility, which is inversely related to the particle diameter. An electrical field inside influences the flow trajectory of the charged particles (TSI Instruments, 2009). In addition, the particles are counted by the Ultrafine Condensation Particle Counter (UCPC). In this equipment, the sample is drawn with an alcohol through a heater saturator, where the alcohol is vaporized and flows through the sample stream. Then, the vaporized alcohol and the dust sample pass into a condenser, where the vapor becomes supersaturated. Particles present in the flow serve as condensation nuclei, and when condensation begins, the particles larger than the threshold diameter grows quickly into droplets and are counted easily. Even the smallest particles grow into droplets for optical detection (TSI Instruments, 2006). The simultaneous particle differentiation and counting allows measuring the particle size distribution (Figure 33).

Twenty seconds after the dispersion, the estimated mean mobility diameters of the Printex XE2 and the Corax N550 were 245 nm and 346 nm, with a total concentration of 2.1×10^5 and 2.4×10^5 particles.cm^{-3}, respectively (Table 7). The DMA - UCPC results must be analyzed carefully because the particle size distribution analysis takes two minutes, time in which agglomeration and sedimentation phenomena occur. However, the results obtained show that, even 3 minutes after the dispersion, the total concentration of dust is not negligible and the mean mobility diameter does

not change with respect to the first measurement (i.e. carried out 20 seconds after the dispersion). It should be added that, due to the sampling process, a depression would be generated inside the reservoir, so a dilution with air is necessary to continue with the DMA-UCPC tests, which may explain the significant reduction of the total concentration of particles, in addition to the dust sedimentation phenomenon. These results suggest that the agglomeration phenomenon, whatever initial turbulence conditions, is limited because of the low concentration of dispersed dust (i.e. the test were performed at dust concentration of 6 $g.m^{-3}$). As a consequence, it has been indirectly demonstrated that a stable dust cloud of agglomerates is generated and is still present at the ignition delay times of 60 and 120 milliseconds studied in this work.

Table 7. Carbon black mean mobility diameter and total concentration after dispersion

Nanopowders	Time after dispersion (s)	Mean Mobility Diameter (nm)	Concentration (particles.cm^{-3})	Ambiance Concentration (particles.cm^{-3})
Printex XE2	20	245	$2.1x10^5$	$6.3x10^3$
	190	241	$1.5x10^5$	
Corax N550	20	346	$2.4x10^5$	
	180	350	$1.6x10^5$	

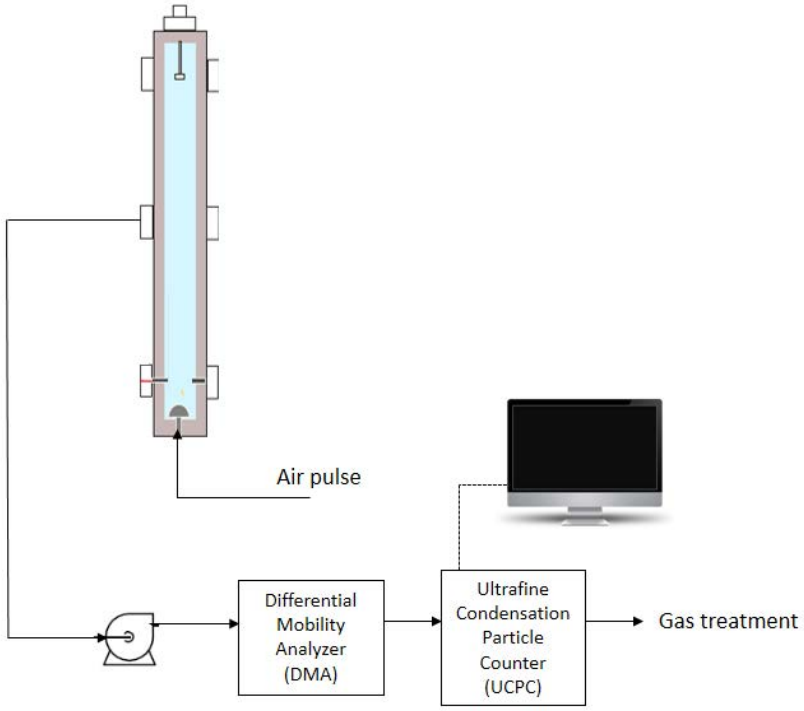

Figure 33. Schematic of dispersion test.

2.2.2. Characterization of the initial turbulence level by Particle Image Velocimetry (PIV)

The homogeneity of the dust particles after dispersion and the turbulence level of the mixture at the moment of the ignition will influence considerably the violence of the explosion. As a consequence, an accurate determination of the turbulence properties of the system is indispensable to assure the reproducibility and the scaling of the experimental results in laboratory set-ups (Tamanini, 1990, 1998). As it has been explained in section 1.1.2, the initial turbulence related to the dust dispersion is linked to the ignition delay time between dust introduction in the device and ignition, i.e. at higher ignition delay times the turbulence of the gas flow is lower. Moreover, non-intrusive methods have been developed to estimate parameters describing the turbulence of the gas flow or particles at different ignition delay times (Cuervo, 2015; Dahoe, 2000; Dahoe et al., 2001, 2002; D'Amico et al., 2016; Murillo, 2016). For instance, the Particle Image Velocimetry has been previously used in the LRGP laboratory to determine the particles mean velocity and the root-mean-square velocity of the dust dispersion, studying the gas-particle interaction and analyzing the effects of the injection pressure or nozzle on the turbulence parameters (Cuervo, 2015; Murillo, 2016). In this work, the initial turbulence level of the gas flow in the propagation tube and 20-L explosion sphere have been investigated with the exact conditions of the explosion severity sphere and the flame propagation tube of the study.

The Particle Image Velocimetry consists in the determination of the flow or particles velocity by the detection of their position thanks to the light scattering by the solid illuminated with a laser sheet. Recording a considerable quantity of images, the measurement of the displacement of the particles Δx at a given time interval Δt permits the velocity estimation (Brossard et al., 2009; Pedersen et al., 2003; Thielicke, 2014). The flow patterns of a gas inside a particular geometry or around an obstacle have been studied in the past years, using tracer particles and assuming they move with the local flow velocity. For the analysis of the digital PIV recording, the evaluation region is divided into "interrogation areas", where the local displacement vector of tracer particles between two illuminations is determined for each interrogation area by means of statistical methods (Raffel et al., 2013). It is also assumed that tracer particles within one interrogation area moves homogeneously between the two illuminations.

Figure 34 shows the PIV experimental set-up for the determination of the flow velocity in the propagation flame tube (left) and the 20-L explosion sphere. The Particle Image Velocimetry experimental set-up is composed of:

1. An **experimental vessel** in which the flow pattern is studied. Hence, the 20L sphere was modified by Murillo (2016) in order to have visual access for the recording of the tracer movement, and to allow illuminate the particles with a parallel laser beam. Measurement was performed at the height of the electrodes, with an area of analysis of 7x7.5 cm^2 with a layer thickness corresponding to the thickness of the laser light sheet, i.e. 0.25 mm.
2. A **continuous wave laser** allows the illumination of a plane with a parallel sheet (to the recording device) with a constant high energy and with pulsations around 5-10 ns. For this experimental set-up a Neodym-Yttrium-Aluminum-Garnet (Nd:YAG) whose laser beam has a wavelength of 532 nm has been chosen. This type of diode solid state laser is very compact and highly efficient (Thielicke, 2014).

Table 8. Continuous wave lase characteristics (Murillo, 2016).

Parameter	Specification
Wavelength	532 nm ± 1 nm
Output power	>2000 mW
Operating mode	Continuous wave
Beam diameter at the aperture	~3.0 mm
Mains supply	100-240VAC
	3A max, 50-60 Hz

3. **Tracer particles**: In the PIV method, the tracer particles are used to study the behavior of the gas flow or the behavior of particles with similar properties to the combustible dust. Indeed, the dispersion of dust particles may generate changes in the turbulence of the fluid depending on the diameter of the dust. Crowe (2000) affirmed that small particle attenuate the gas flow turbulence since large particles tend to increase it. However, this influence is determined by the ratio of the turbulence length scale and the particle diameter; hence nanometric dusts do not represent significant variations in macroscopic turbulent flows (Murillo, 2016). It is then assumed in this work that the carbon black and alumina nanoparticles used in the explosion test will follow the gas flow field and that the interactions solid-gas and solid-solid are negligible. For this reason, the characterization of the initial turbulence of the system consists of the determination of the gas flow velocity properties using glass microbeads as tracers (with a D_{50} mean particle diameter of 35 µm).
4. A **high-speed video camera** (Phantom V91) was used to record videos of the tracer particles dispersion from 5,000 to 6000 frames per second. The laser intensity and the video camera exposure were set to obtain the suitable contrast of the scattered light.

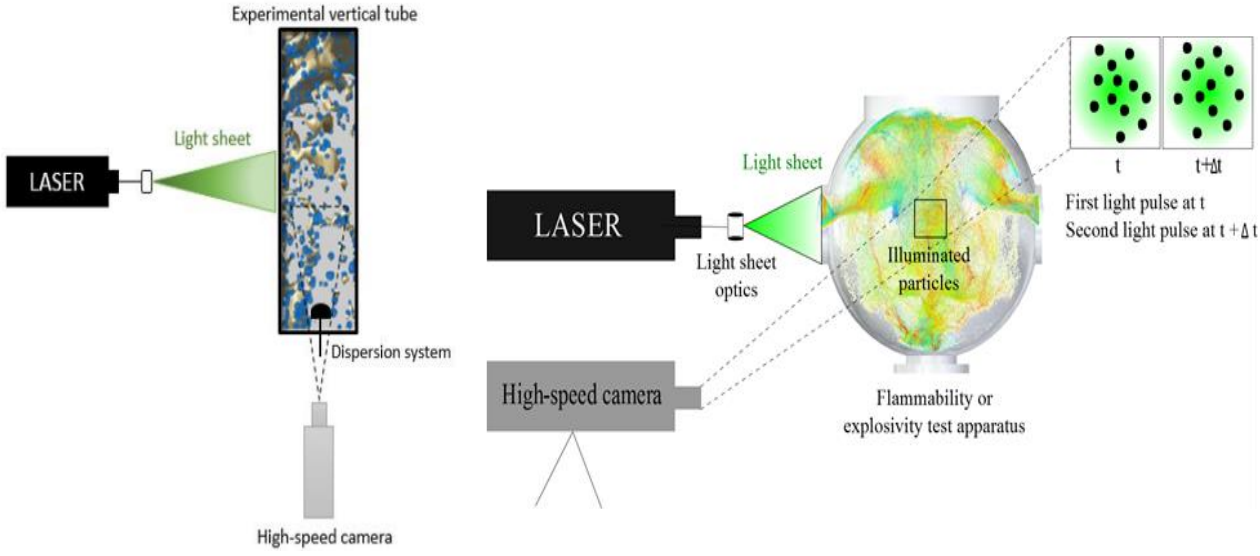

Figure 34. Experimental arrangements for a digital particle image velocimetry analysis for the propagation tube - right and for the 20L explosion sphere – left (Murillo, 2016)

2.2.2.1. Methodology

First of all, the recorded videos are analyzed and the visual identification of the particles is improved using the numerical filters of Phantom Camera software (Cine Viewer) and VirtualDub software. Due to the high turbulence and velocity of the particles after the first milliseconds of dispersion, the gain and brightness (i.e. image processing parameters to which describe the apparent sensitivity to light) are modified to enhance the contrast of the particles, and in some cases a Laplacian 5x5 filter was necessary to differentiate the solid particles.

PIVLAB 1.35 (Thielicke, 2014) was used to perform the image preconditioning, interpolation algorithms, smoothing methods and data validation. Some studies have shown the good agreement of the analyses on PIVLAB with other measurement techniques (Tebianian et al., 2015). The evaluation of the images is made by "interrogation areas", in which statistical methods are used to determine the most likely displacement of the group of particles. The Direct Cross-Correlation (DCC) and Discrete Fourier Transform (DFT) approaches are available in the software to determine the flow pattern of tracer particles. Murillo (2016) obtained similar trends for the two numerical methods on the velocity fluctuations of starch dust on a 20-L sphere.

Figure 35 shows the illuminated dust at different times after dispersion of the glass microbeads glass and the velocity field estimation using PIVLAB in the propagation tube. As a result, the mean velocity and the velocity fluctuations are determined at different times after dispersion. These parameters are used to estimate the horizontal (u_i') and vertical (v_i') velocity fluctuation and the root-mean square velocity (v_{rms}):

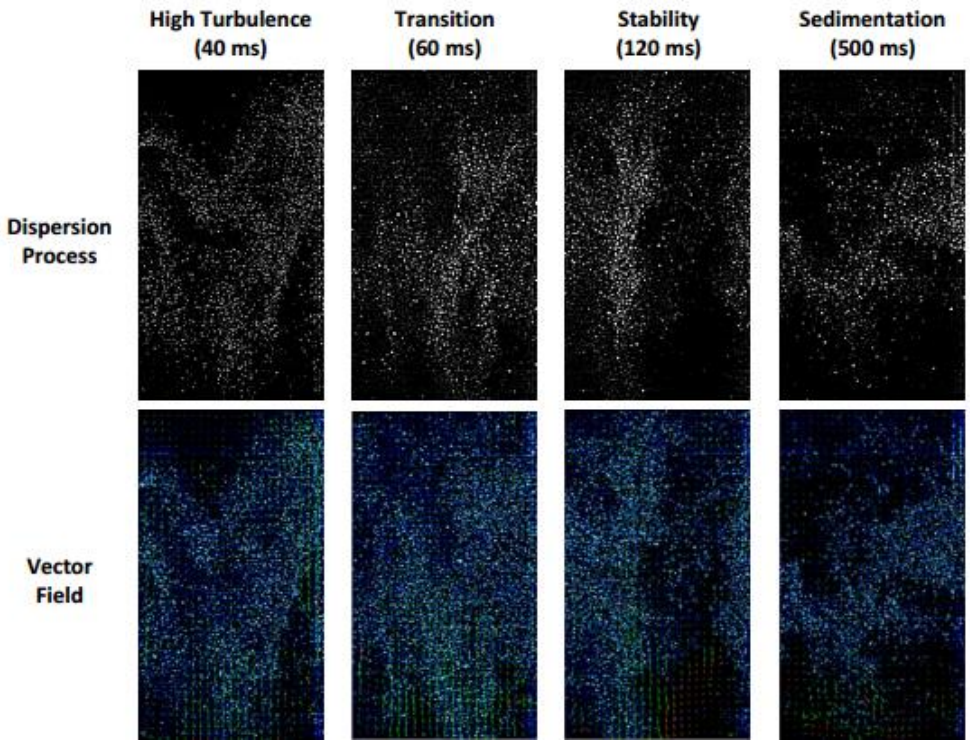

Figure 35. Velocity field estimation using PIVLAB in the propagation tube.

$$u_i' = u - \bar{u} \qquad \text{Eq 23}$$

$$v_i' = v - \bar{v} \quad \text{Eq 24}$$

$$v_{rms} = \sqrt{\frac{1}{N}\sum (u_i')^2 + \frac{1}{N}\sum (v_i')^2} \quad \text{Eq 25}$$

Where N is the number of particles detected for the velocity estimation.

2.2.2.2. Initial Turbulence Characterization

The turbulence level has been analyzed in the propagation tube at different pressure of the initial pulse used to generate the dust dispersion. Figure 36 shows the root-mean-square velocity of the flow field for dispersion pressures between 3 and 5.5 bars. Similar results have been obtained by Murillo (2016), who obtained a high turbulence for times of dispersion between 0 and 40 ms, followed by a transition period when all the dust has been discharged in the vessel and the velocity fluctuations start to decrease. Then, around 120 ms a stable zone is reached, during which the root-mean-square velocity does not considerably change, until a sedimentation stage is reached.

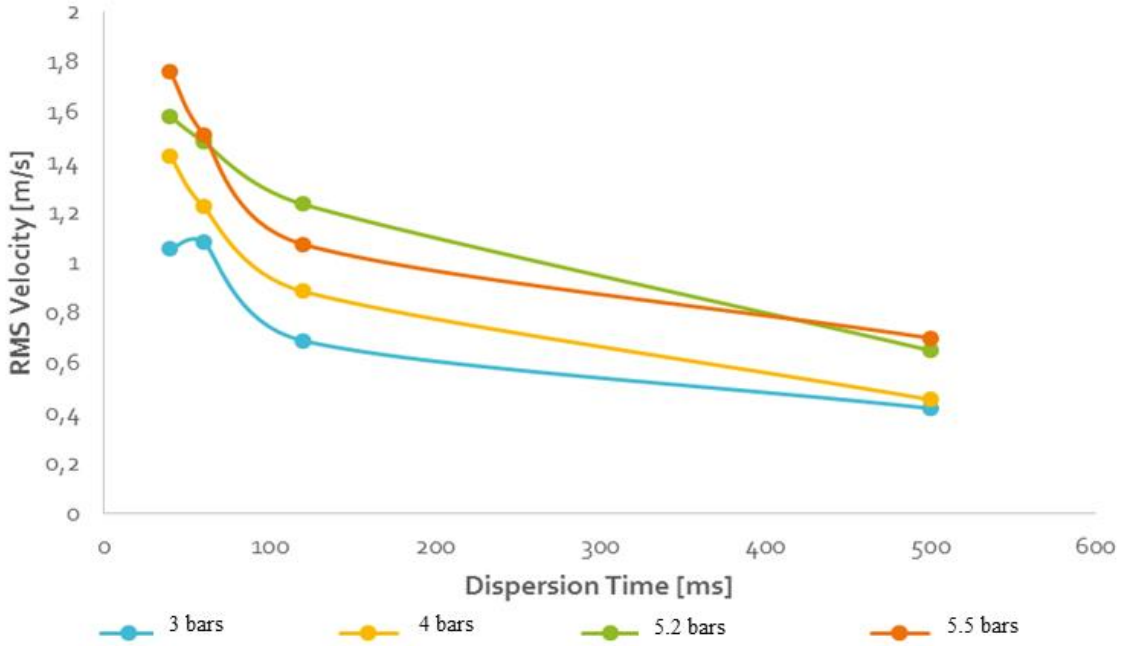

Figure 36. Root-mean-square velocities of the fluid flow in the propagation tube

The results of the root-mean-square velocity obtained for different experimental conditions in the flame propagation tube and in the 20-L sphere are listed on Table 9. The characterization of the turbulence in the 20L sphere has been performed at a dust dispersion pressure of 21 bara and with the standard rebound nozzle. The results are in good agreement with those presented by Dahoe (2000), i.e. root-mean-square (RMS) velocity fluctuations of approximately 3 and 0.9 at 60 and 120 ms respectively. The instability, transition and stable stages of the root-mean-square velocity established by Murillo (2016) have been also observe in the experimental characterization in this study, i.e. the ignition delay time of 60 and 120 ms are located in the transition zone, where the turbulence decrease considerably over the time. The ignition delay time of 500 ms is located on the

stability zone, where the turbulence reaches and stable value. Due to the low velocity, the sedimentation of micrometric particles have been evidenced at this stage, however, the dispersion stability test had shown the presence of suspended nanoparticles that may have an influence on the explosion parameters that will be analyzed in the following section.

Table 9. Root-mean-square velocity v_{rms} measured for the 20-L sphere and the flame propagation tube using Particle Image Velocimetry (PIV)

Ignition delay time - t_v (ms)	v_{rms} $(m.s^{-1})$ **20 L – sphere (20 bar canister pressure)**	v_{rms} $(m.s^{-1})$ **Flame propagation tube (5 bar canister pressure)**
0	0	0
60	5.8	1.6
120	1.6	1.4
500	0.5	0.9

2.3. Explosion severity parameters

2.3.1. 20L sphere test

A. Brief test description

The explosivity parameters of carbon blacks/methane/air mixtures were determined following the standard procedure indicated by the ASTM E1226-12a (ASTM E1226-12a, 2012), with a slight modification to test a hybrid mixture explosion (i.e. gas insertion inside the explosion vessel, which will be described later on). First, the powder sample was placed in the 0.6 L container connected to the sphere (dust reservoir). Then, the chemical ignitors of an equivalent energy are located at the center of the 20-L sphere. Generally, carbonaceous nanopowders exhibit minimum ignition energies (MIE) greater than 100 J (Turkevich et al., 2015; Vignes, 2008) whereas the MIE of methane is 0.3 mJ. Even if the MIE of methane is very low, the addition of carbon black will increase the MIE of the mixtures. Hence, the ignition energy was chosen to ignite the mixtures, without igniting the powder directly. As a consequence, the 20L sphere tests were performed with igniters delivering an energy of 100 J, which is the lowest energy that can be supplied using chemical igniters (Sobbe). A permanent spark could have been used, but the ignition delay time is more easily defined using chemical igniters. Afterwards, it must be verified that both the explosion vessel and the dust reservoir, are correctly closed before the test. The sphere is vacuumed to approximately 0.3 bars and the gas is inserted in order to reach the desired concentration (e.g. from 0.3 to 0.38 barsa to reach 8%vol.). Then, additional air is injected in order to obtain a local pressure of 0.4 barsa before the powder dispersion under 21 bara. This pressure was chosen in order to reach atmospheric pressure when adding dust entrained by the pressurized air pulse in the sphere before the ignition.

The dust sample is dispersed through a standard rebound nozzle and the ignition source is activated after a specific delay. If an ignition occurs, the evolution of the pressure over the time is recorded by two piezoelectric sensors (Figure 37). The maximum explosion pressure (P_m) is identified by

the maximum peak of the profile, whereas the maximum rate of pressure rise (dP/dt_m) is defined by the maximum slope of the curve P vs t.

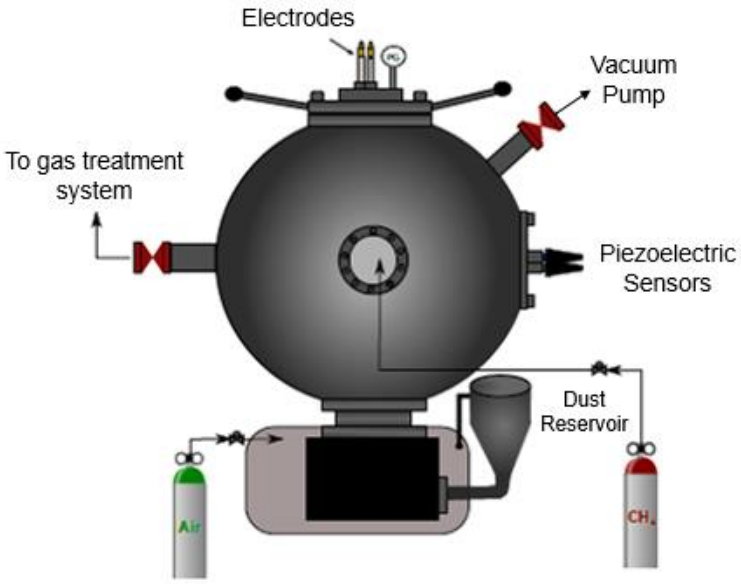

Figure 37. Schematic for explosion severity test of hybrid mixtures.

In order to study the influence of an initial concentration of soot in a methane/air mixture, low concentrations of carbon blacks were chosen. With regard to the scale precision, the lowest concentration of carbon black was set at 0.5 $g.m^{-3}$. Tests were also performed at 2.5 $g.m^{-3}$, which is still far below 60 $g.m^{-3}$, the minimum explosive concentration of such powders (Table 10). The influence of the initial turbulence was characterized by varying the ignition delay tv, i.e. time between the beginning of the air pulse and the ignition. The explosion tests were carried out at three ignition delays, which are related to the root-mean-square velocity, as it was discussed in Table 9. Due to the low settling velocity of nanoparticles, a quiescent case was also considered. It corresponds to the insertion of dust directly inside the explosion vessel (i.e. without dispersion by pulse of air.) and then, the ignition is performed after insertion of the methane and air (the explosion is performed at 1 bar).

Table 10. Explosion tests performed on the 20-L sphere.

Ignition delay time - tv (ms)	**Powder Concentration (g.m-3)**		
	0	**0.5**	**2.5**
0	**Gas Concentration (%v.):**		
60	5.5 - 7 - 8 - 9 - 12		
120			

B. Explosion tests results

Methane explosions:

At first, tests were performed on pure methane at different concentrations and turbulence levels (Figure 38). CEA software was also used to determine the maximum explosion pressure at

thermochemical equilibrium based on the minimization of the Gibbs energy (Gordon and McBride, 1994; Torrado et al., 2016). A considerable difference is observed between the maximum explosion over pressure obtained by the CEA software (dash line in Figure 38) and the experimental results, which evidence that a considerable energy loss is present in the system and methane explosions are not performed under adiabatic conditions. Furthermore, as it was expected, the maximum explosion violence is obtained for stoichiometric methane/air mixture and it is higher for turbulent mixtures than for quiescent ones. Nevertheless, there is no notable difference between the maximum overpressure mixtures with velocity fluctuations of 1.6 $m.s^{-1}$ and 5.8 $m.s^{-1}$. On the contrary, the maximum rate of pressure rise is considerably augmented for the highest initial turbulence level. This trend shows that the maximum pressure is a thermodynamic property, rather than the maximum rate of pressure rise, which has a strong kinetic component (Eckhoff, 2003).

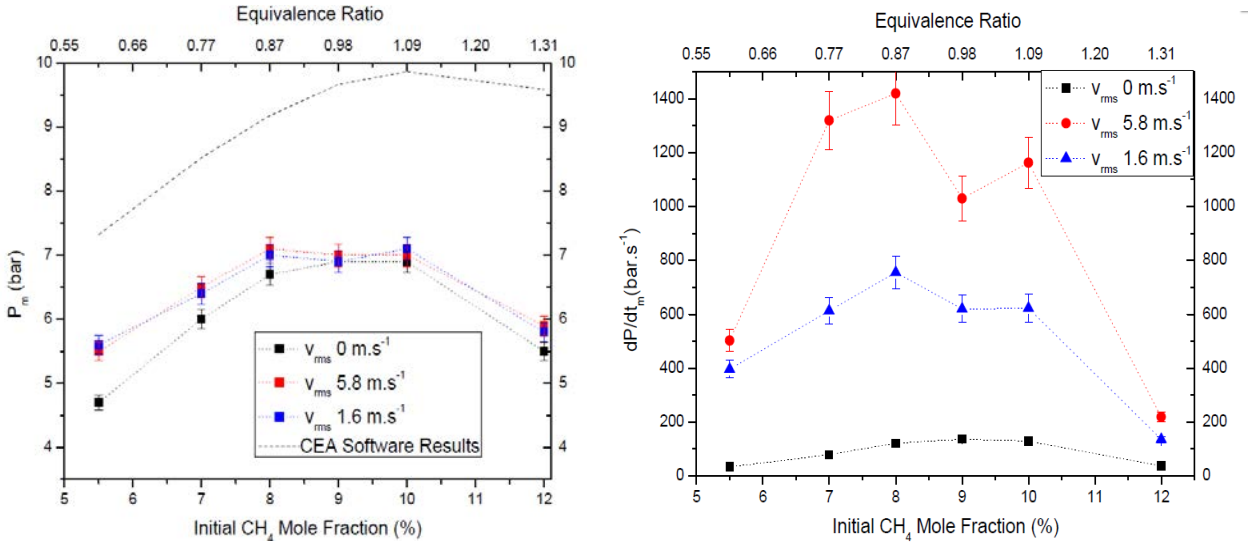

Figure 38. Influence of turbulence level on the maximum overpressure – P_m (left) and on the maximum rate of pressure rise – dP/dt_m (right) for Methane/Air mixtures.

Printex XE2/methane/air and Corax N550/methane/air explosions:

The same experiments were carried out with the adjuction of 0.5 $g.m^{-3}$ Printex XE2 (Figure 39). By comparing Figure 38 and Figure 39, it appears that the insertion of carbon blacks at low concentrations does not modify significantly the maximum explosion pressure, whatever the initial turbulence level. Although, a slight difference is evidenced for lean methane mixture, obtaining different values of the maximum overpressure depending on the turbulent level. Such behavior is consistent with the thermodynamic equilibrium calculated by CEA because the ratio carbon black/methane is very low and the global fuel equivalent ratio is nearly unmodified by the addition. However, Figure 39 right shows modifications of the maximum rate of pressure rise when 0.5 $g.m^{-3}$ Corax N550 are added in the initial mixture, but the trends depend on the initial turbulence level. First, for an initial intermediate turbulence level (1.6 $m.s^{-1}$), dP/dt_m of fuel rich mixtures slightly decreases down to 25% when carbon black is added and remains unchanged for lean and stoichiometric mixtures. In contrast, a reduction of around 15% on the maximum rate of pressure rise is evidenced for stoichiometric mixtures at the highest turbulence level studied on this work, and a considerable reduction of 50% is also presented for fuel rich concentration. The previous results suggest that carbon black particles insertion modifies the explosion kinetics, especially for

methane-rich mixture and high initial turbulence levels (effect that will be discussed later on in this chapter).

Analogous tests were carried out with 0.5 $g.m^{-3}$ Corax N550 dispersed in methane/air mixture (Figure 40 - left). Comparing to results displayed in Figure 39 – left, the observed trends for Printex XE2 are rather similar to Corax N550. Nevertheless, two main differences are observed for the highest turbulence level of 5.8 $m.s^{-1}$ (equivalent to tv 60 ms) that should be analyzed depending on the methane concentration. First of all, the reduction on the maximum rate of pressure rise when carbon black nanoparticles are added is less perceptible for Corax N550 than Printex XE2 under **lean fuel mixture conditions**. This behavior can be explained by considering previous studies highlighting the impact of the fragmentation phenomenon during the dust dispersion (Bagaria et al., 2016; Eckhoff, 2009; Murillo et al., 2013a, 2013b, 2015). As seen in Table 6, the agglomerates of Printex are composed of elementary particles having a diameter lower than those of Corax N550 (BET diameter of 3 nm for Printex compared to 75 nm for Corax). As a consequence, the total surface of the reaction is considerably higher for Printex XE2 if particle de-agglomeration takes place and its effect, for instance on radiative heat transfer, could be greater than the impact of the same weight of Corax N550. Bagaria et al. (2016) have evidenced partial agglomerate break when the dust pass the nozzle and total de-agglomeration when it is dispersed out of the nozzle. In their study, they have found de-agglomeration of carbon nano-fibers that modifies the ignition sensitivity and explosion severity, however, the particle breakage depends on the initial dust concentration and will change along the dispersion process, leading to a very complex phenomenon. At lower turbulence, shear forces are less efficient and fragmentation is less perceptible. The differences observed between the two kinds of carbon blacks are probably related to the characteristics of their agglomerates more than to those of the nanoparticles. The experimental characterization of the nanoparticle dust over the time is necessary for demonstrate the fragmentation and subsequent dispersion characteristics of each type of carbon black, however, the actual experimental set-ups are not adapted for the measurement of the fragmentation state of dust over the time.

A second difference is evidenced for **stoichiometric methane and rich mixture conditions** comparing Figure 39 and Figure 40. In these conditions the maximum rate of pressure rise seems to undergo a more important reduction when Corax N550 is added to the system than when Printex nanoparticles are incorporated on the initial mixture. The reasons why insertion of carbon black nanoparticles of a given particle size has a different effect for lean and rich mixtures are unclear. However, it appears that the insertion of carbon particles at different particle sizes has an effect on the reaction yield. The influence of the fuel equivalent ratio on the explosion violence in hybrid mixtures suggests that, in addition to the possible effects of nanoparticles on the surface of the flame and the heat radiation contribution of emissive particles, the oxidation of the initial carbon black concentration and the soot nucleation on the solid surface may play a role on the explosion severity. The gas chromatography and flame velocity tests will be analyzed in next sections 2.4.1 and 3.4 respectively, in order to elucidate the possible effect of the chemical reaction and of the thermal radiation.

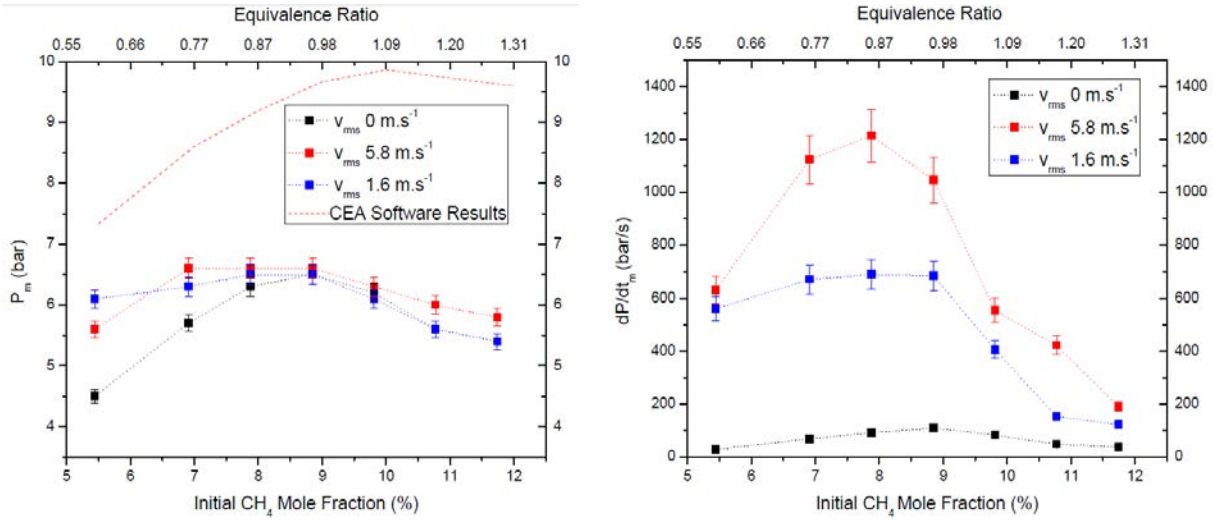

Figure 39. Influence of turbulence level on the maximum overpressure – P_m (left) and on the maximum rate of pressure rise – dP/dt_m (right) for a 0.5 g.m^{-3} Printex XE2/Methane/Air mixture.

Influence of carbon black initial concentration:

The maximum explosion overpressure and the maximum rate of pressure rise are also affected when the initial concentration of carbon nanoparticles increases in the system. As the latter parameter is more sensitive to the variation dP/dt_m, we will focus on it. In Figure 40, the maximum rate of pressure rise decreases when the carbon black content is increased from 0.5 g.m^{-3} to 2.5 g.m^{-3}, especially for high turbulence levels. For instance, for lean fuel-air mixtures at 5.4 %v. of CH_4, such increase of the carbon black content induces a decrease of 45 to 50 % of the maximum rate of pressure rise, i.e. from 750 bar.s^{-1} to nearly 400 bar.s^{-1} at 5.8 m.s^{-1}. This behavior seems to be independent from the fuel equivalence ratio, but for rich fuel mixtures the decrease is less significant e.g. around 5% for 10 %v. of CH_4 at 1.6 m.s^{-1} initial turbulence level.

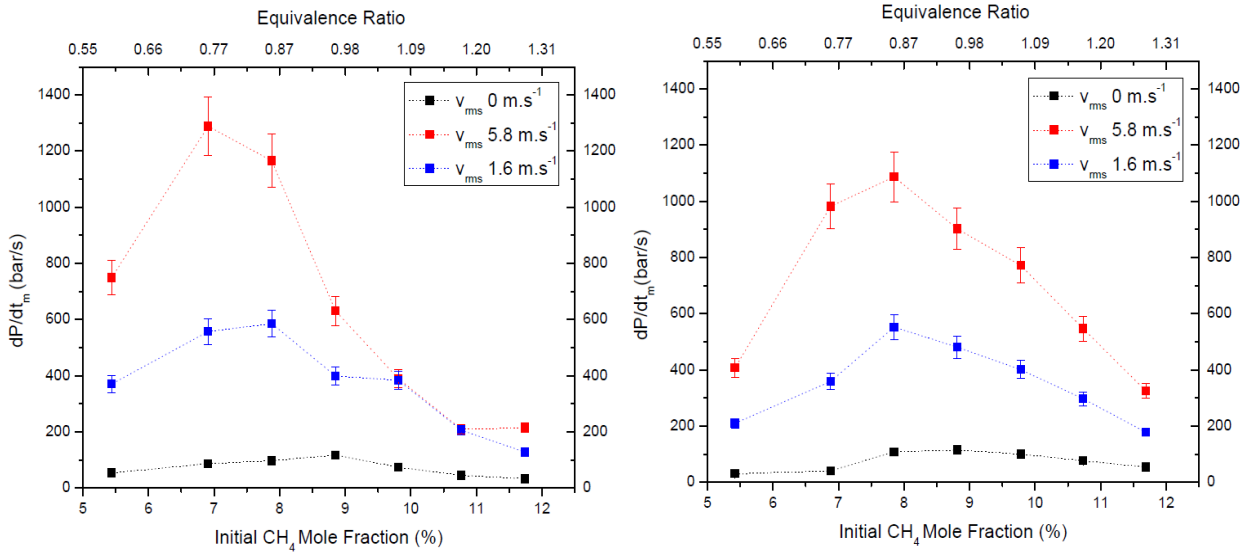

Figure 40. Impact of the turbulence level on the maximum rate of pressure rise – dP/dt_m for 0.5 g.m^{-3} (left) and 2.5 g.m^{-3} (right) CoraxN550/Methane/Air mixtures.

Result at quiescent conditions:

The influence of carbon black insertion on methane/air explosion at quiescent conditions are not easily represented on the precedents figures due to the great differences in the severity results compared with high turbulent sysems. Nevertheless, Figure 41 represents the influence of the concentration of carbon black nanoparticles on the explosivity of Corax N550/Methane/Air mixtures for an initially quiescent system (v_{rms} = 0 $m.s^{-1}$). The maximum overpressure seems to increase for lean mixtures by the addition of 0.5 $g.m^{-3}$ carbon black nanoparticles but decreases for stoichiometric and rich mixtures. However, when the concentration of Corax N550 rises to 2.5 $g.m^{-3}$, the severity of the explosion diminishes for all the concentrations studied in this work (compared to methane/air explosion results). The same trends can be observed on Figure 41 (right) for the maximum rate of pressure rise. Once again, it demonstrates that both the concentration, but also the turbulence play an important role on the dust dispersion and, by consequence, on the flame propagation and on the explosion severity. This point will be addressed in the next chapter.

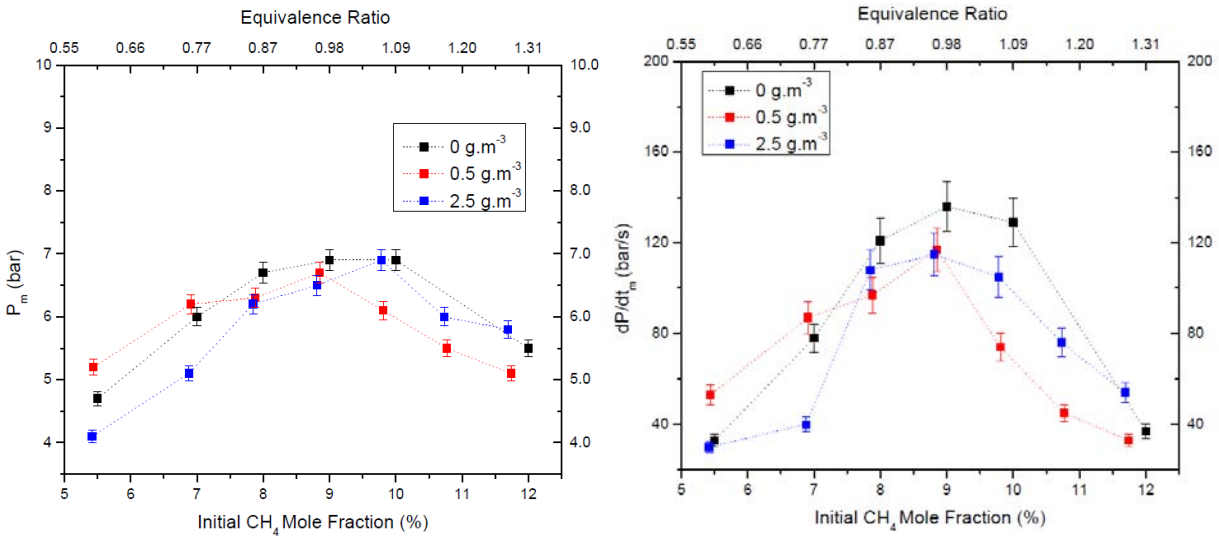

Figure 41. Influence of carbon black concentration on the maximum overpressure - P_m (left) and on the maximum rate of pressure rise - dP/dt_m (right) for a Corax N550/Methane/Air mixture under quiescent conditions.

It must be remembered that the explosion tests at quiescent conditions are performed without the 20 bars air pulse, instead, the dust is placed inside the sphere, it will be entrained the entering gas mixture and it is ignited at an ignition delay time t_v of 0 ms. The results observed at Figure 41 shows that the carbon black nanoparticles are easily suspended and very stable when, dispersed. Similar results have been obtained for Printex XE2/methane/air mixtures at quiescent conditions, with the slight difference that a positive effect of 2.5$g.m^{-3}$ insertion at lean methane conditions Figure 42. These results show that the risk of a gas explosion may be increased when low concentrations of carbon black nanoparticles are present in the mixtures, even in the absence of high turbulence to guarantee the total dispersion of a nano-dust cloud. Nevertheless, the real dispersed concentration of carbon black nanoparticles and the posterior re-agglomeration of the suspended particles are unknown, very complex to measure and may explain the low reproducibility and differences between the type of carbon black nanoparticles (Figure 41 and Figure 42).

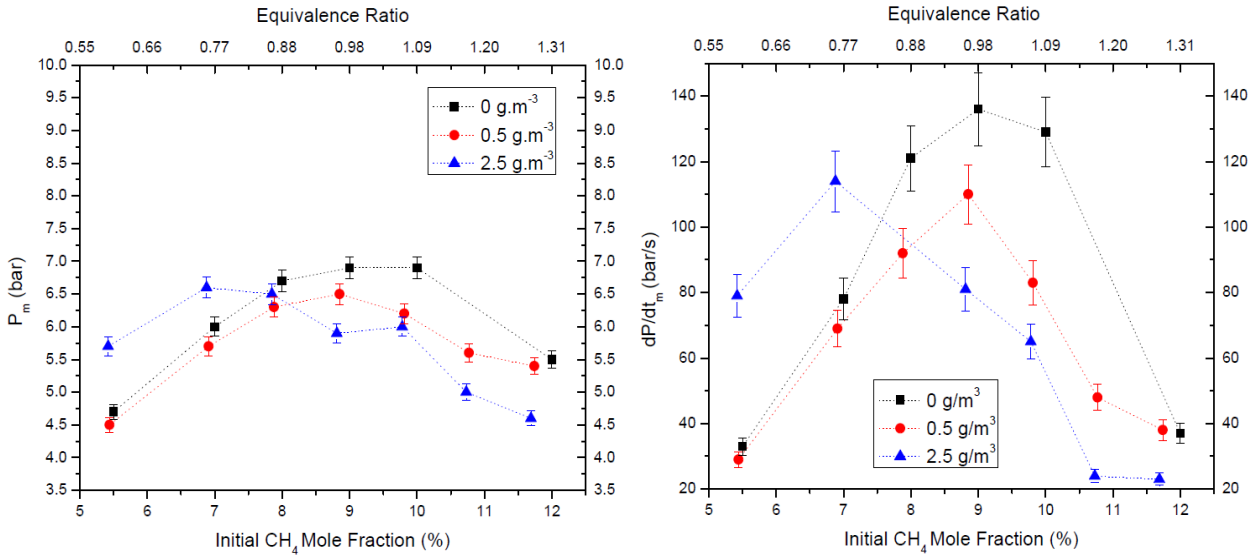

Figure 42. Influence of the carbon black concentration on the maximum overpressure - P_m (left) and on the maximum rate of pressure rise - dP/dt_m (right) for a Printex XE2/Methane/Air mixture under quiescent conditions.

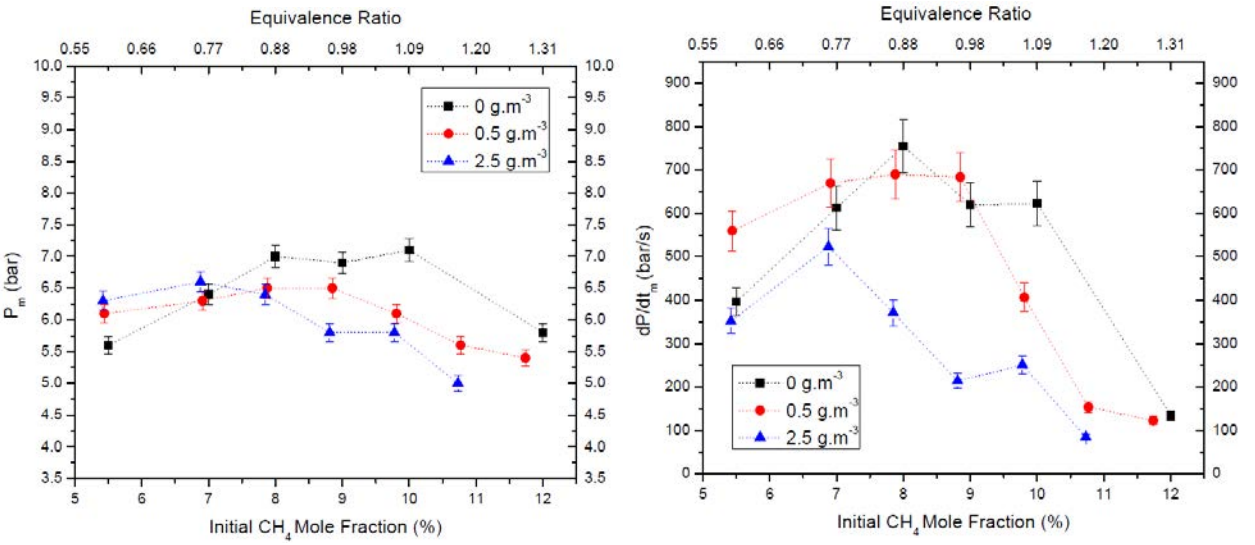

Figure 43. Influence of the carbon black concentration on the maximum overpressure – P_m (left) and on the maximum rate of pressure rise – dP/dt_m (right) for a Printex XE2/Methane/Air at an initial turbulence level u' = 1.6 $m.s^{-1}$.

Influence of initial turbulence level:

Moreover, the same trends on the maximum overpressure and maximum rate of pressure rise have been found at higher initial turbulence level, as observed in Figure 43. The influence of the dispersion of nanoparticles agglomerates on methane/air gas explosions depends on the fuel equivalent ratio φ. In lean mixtures, dust dispersion may generate a deformation of the flame surface, causing an acceleration of the flame and an increase in the explosion severity. However, for fuel rich mixtures, heat radiation transfer appears to offset the effect of particles or agglomerates on the surface of the flame, attenuating the severity of the explosion.

An increase of the dust concentration obviously leads to an increase of the solid surface area, which can play a role on radiative transfers, oxidation reaction, but also on surface radical recombination reactions (Chen and Xu, 2015). In order to verify the hypothesis that a modification of the carbon black surface area can influence the explosion severity, the same solid surface area increase is obtained by using carbonaceous particles with a smaller primary particle size (Table 6). Indeed, Figure 44 - right shows that the addition of Printex XE2 does not lead to the same promotion of P_m for lean fuel mixtures as observed in Figure 44 - left. Moreover, such overpressure increase is never observed for Printex XE2, neither for lean nor for rich mixtures.

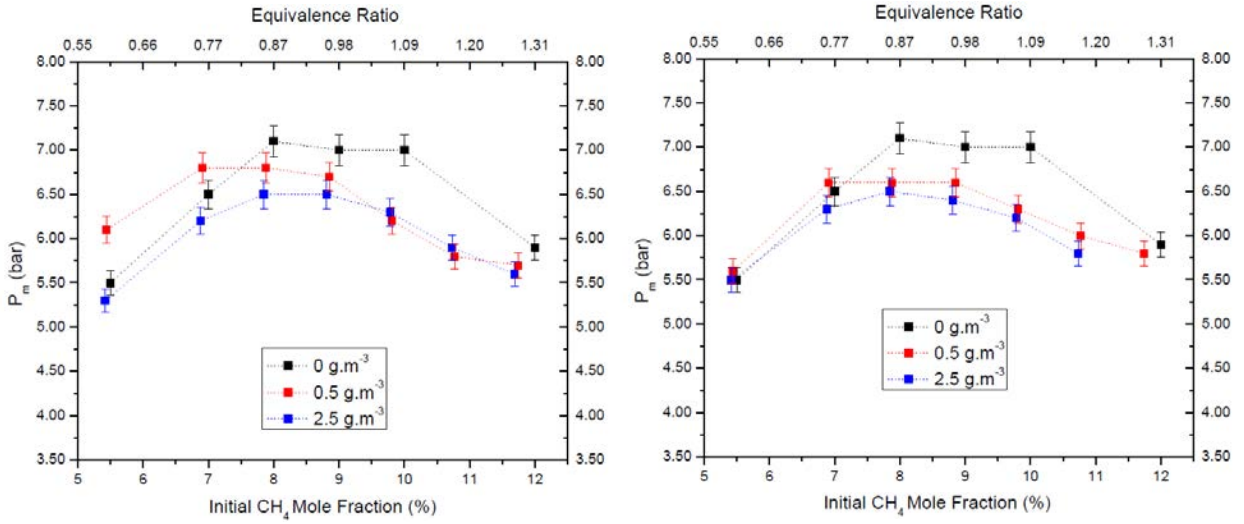

Figure 44. Influence of carbon black concentration on the maximum overpressure for a) Corax N550/Methane/air mixtures and b) Printex XE2/Methane/air mixtures at an initial turbulence level v_{rms} = 5.8 m.s^{-1}.

The explosion severity of methane/nanoparticles mixtures is strongly affected by the initial turbulence level, as shown in Figure 39. The maximum explosion overpressure tends to increase as the turbulence level is higher, but for mixtures near the stoichiometric concentration, the influence is minimal. For a lean fuel mixture, a turbulence level v_{rms}= 5.8 m.s^{-1} produces a slightly lower P_m compared to v_{rms} = 1.6 m.s^{-1}. This effect, observed through numerous experiments, may be due to premature extinction of the flame because of the high level of turbulence in the system. Eckhoff (2003) established that high turbulence may destabilize the flame propagation, generating higher heat losses due to forced convection and it can even generate turbulent quenching of the flame. In addition, for rich fuel mixture of Printex XE2 and methane, ignition was recorded under quiescent conditions and at v_{rms} = 1.6 m.s^{-1} for 12 %v. CH_4, whereas no ignition was obtained for high turbulence levels. Turbulent quenching generated by the "cold" initial turbulence and the explosion itself may explain this difference observed at shorter ignition delay times (Kosinski et al., 2013).

In addition, the maximum rate of pressure rise is considerably enhanced by the transfer properties and thus by the turbulence level of the system, as shown in Figure 39 - right. The effect of turbulence on the maximum rate of pressure rise is significant (almost one order of magnitude) at a high level of turbulence and near stoichiometry (Russo and Di Benedetto, 2007). Eventually, it should be underlined that the reproducibility is also greatly affected by the turbulence. As the carbon black concentration increases, the level of initial turbulence has a negative effect on the gas

explosivity for rich mixtures, which is not observed in the case for a quiescent system. As previously discussed, this phenomenon can be explained because higher turbulence levels may create a powder fragmentation and deagglomeration (Murillo et al, 2013), raising the heat transfer surface. Then, a high level of initial turbulence for these mixtures increases the heat loss by radiation, strongly modifies the flame profile and, as a consequence, reduces the severity of the explosion.

In summary, the dispersion of nanoparticles modifies the explosion severity of methane/air explosion even at low concentrations and low turbulence level. However, the influence of the explosion severity is complex and depends of different parameters (as the initial turbulence, methane concentration and dust concentration). The main hypothesis that may explain the influence of dispersed nanoparticles on methane/air explosion severity are: 1) a chemical contribution of the carbon black nanoparticles, 2) modifications on the radiative heat transfer, 3) modifications of the flame surface and possible perturbations on the propagations and 4) the possible contribution of the suspended carbon black as soot nuclei products. In order to test the first hypotheses, two approaches had been implemented. At first, the combustion gases after the explosion have been studied by µ-gas chromatography. Secondly, the carbon black hybrid mixture explosion results had been compared with the explosion severity of inert alumina hybrid mixture explosions.

2.4. Chemical contribution evaluation

2.4.1. Reaction product analysis

The explosion severity tests previously discussed have shown that the insertion of a low concentration of carbon black modifies the explosion violence of the mixture. Seeing that this insertion could have an effect on the deformation of the propagating flame, on the radiative heat transfer and on the chemical reaction, alternative methods in order to understand the preponderant phenomenon should be implemented. After the explosion test, burnt gases were taken without dilution in a gas sample bag and then analyzed by micro gas chromatography Varian 490 Micro GC (Agilent Technologies). The 490 MGC is equipped with four independent channels/columns, in which the combustion products (CO, CO_2, N_2, H_2, H_2O, CH_4, and O2) will be separated and quantified (Figure 45).

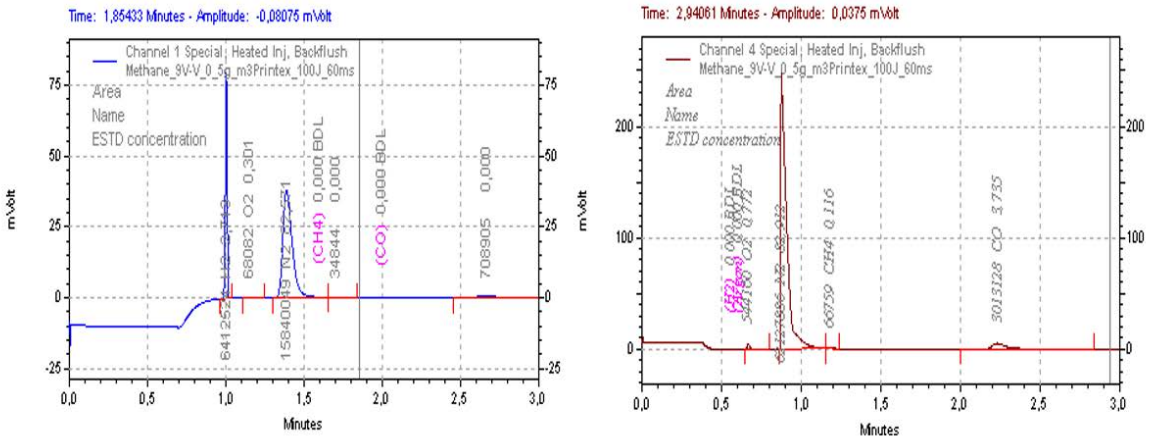

Figure 45. Volumetric measure of combustion products using µ-gas chromatography

Figure 46 and Figure 47 present the CO_2 volume fraction and the CO/CO_2 ratio in the burnt gases for a gas mixture and a hybrid mixture explosion, respectively. Under quiescent conditions, the maximum CO_2 volume fraction is obtained for stoichiometric conditions. The presence of an initial turbulence seems to increase the conversion of CO to CO_2 in lean mixtures, but this conversion decreases for rich mixtures. Nevertheless, the turbulence level does not have an influence on the conversion of CO to CO_2 for the gas mixtures. This result agrees with that analyzed in Figure 38, in which it is observed that the same maximum explosion pressure is obtained for different levels of initial turbulence. Therefore, changes in the initial turbulence level appear to have no significant effect on the reaction yield of pure gas combustion. If the effect of the initial turbulence level on the explosion kinetics is clearly visible on Figure 38 and Figure 39 – right, its specific impact on the combustion chemistry is shown in Figure 46 through the evolution of the CO_2 and CO content in the burnt gases. It should be highlighted that, if the carbon dioxide concentration tends to reach a maximum before decreasing, a shift towards the highest equivalence ratios is noticeable for quiescent conditions (with a maximum near stoichiometry). It implies that an increase of the intensity of velocity fluctuations up to 1 $m.s^{-1}$ improves the combustion for lean mixtures having a fuel equivalence ratio (FER, φ) lower than 0.8, but tends to decrease the CO_2/CO ratio for richer mixtures. This reflects a more important heterogeneity of the initial combustible cloud at high turbulence, leading to local φ higher or lower than unity even if the global φ is 1. As a consequence, CO is less oxidized under such conditions (Figure 47 – right). It can be noticed that the oxidation of CO to CO_2 drops off as soon as φ exceeds unity, whatever the turbulence level.

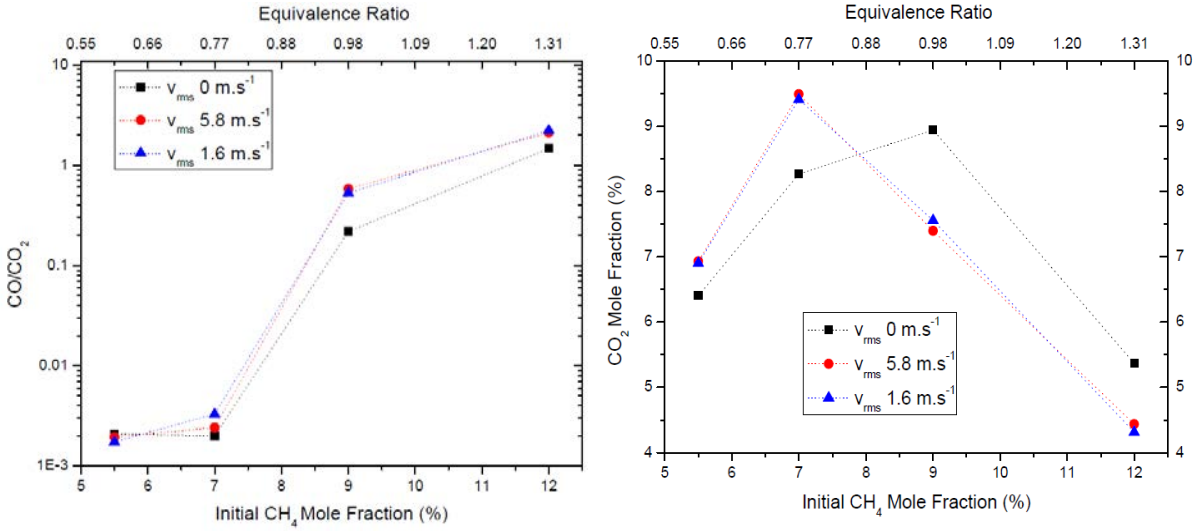

Figure 46. Influence of the turbulence level on the final CO/CO_2 ratio (left) and on the final CO_2 molar fraction (right) for a Methane/Air mixture.

Comparing the explosion severity for Printex XE2/Methane/Air mixture at different initial turbulence levels (Figure 43 and Figure 44), it appears that the maximum rate of pressure rise is greatly increased at high turbulence levels, evidencing a close relationship between the turbulence level and the combustion reaction (Bradley et al., 2017; Cuervo, 2015). The influence of the turbulence level and combustion interactions on the explosion severity of this type of complex mixtures should be studied to design the appropriate prevention or protection devices. The micro gas-chromatography results suggest that there is a relation between the final CO_2 mole fraction and the maximum rate of pressure rise, in which the highest value of $(dP/dt)_{max}$ is obtained when the maximum conversion of CO to CO_2 is reached (Figure 48). In addition, the ratio CO to CO_2 is

directly related to the temperature, which rise when the temperature increase. Therefore, conditions that promote the chemical reaction of oxidation of CO, as a higher initial turbulence level, will generate a higher release of chemical energy and, consequently, an increase on the maximum rate of pressure rise. Similar results were obtained regarding the influence of the carbon black dispersion on the maximum rate of pressure rise (Figure 44 - right), where the higher explosion severity was obtained when the maximum concentration of CO_2 was produced (Figure 49).

The presence of a carbon black cloud seems to modify the combustion reaction, even if the amount of solid fuel is negligible with respect to the methane volume fraction (i.e. the studied concentrations of 0.5 and 2.5 $g.m^{-3}$ represents a molar concentration of 0.1% and 0.5% respectively). Figure 49 shows the influence of the Printex XE2 initial concentration on the CO_2 and CO molar fraction for hybrid mixtures explosions under quiescent conditions. The explosion severity seems to increase due to the presence of dispersed agglomerates, phenomena that appears to promote the conversion of CO_2 for lean fuel mixtures. In addition, this conversion rate decreases for a fuel equivalent ratio higher than 0.8. The CO production seems to increase for lean mixtures when 2.5 $g.m^{-3}$ of Printex is added to the system, outcome that is not observed when using Corax N550 dust. First, this result shows again that both powders have high stability when dispersed and influence the methane/air gas explosion. However, such impact on the explosion becomes more important for powders with a higher specific surface. This result can be also evidenced analyzing the final hydrogen concentration measured for gas and hybrid mixtures (Table 11). For instance, the insertion of Corax N550 seems to have a negligible effect on the final hydrogen concentration, but the addition of Printex N550 seems to increase the final hydrogen concentration. The stable elementary particles and dispersed agglomerates seem to affect the flame surface (observed thanks to flame propagation tests), and, because they undergo oxidation reactions, the concentration of the final gases and the violence of the reaction vary. Secondly, the negative effect on the explosion severity for rich fuel equivalent ratio may be caused by the enhancement of the soot nucleation phenomenon due to primary nuclei when initial carbon particles are added into the combustible mixture.

Table 11. Hydrogen concentration for gas and hybrid mixtures explosions at v_{rms} 1.6$m.s^{-1.}$

Methane molar Concentration (%)	**Hydrogen molar concentration (%)**				
	Methane/air	**Methane/air + 0.5 $g.m^{-3}$ Corax N550**	**Methane/air + 2.5 $g.m^{-3}$ Corax N550**	**Methane/air + 0.5 $g.m^{-3}$ Printex XE2**	**Methane/air + 2.5 $g.m^{-3}$ Printex XE2**
5.5	0	0	0	0	6.4
7	0	0.005	0.01	0	2.7
9	3.09	3.7	2.7	3.5	7.4
11	-	8.73	6.6	9.9	10.28
12	11.7	-	-	-	

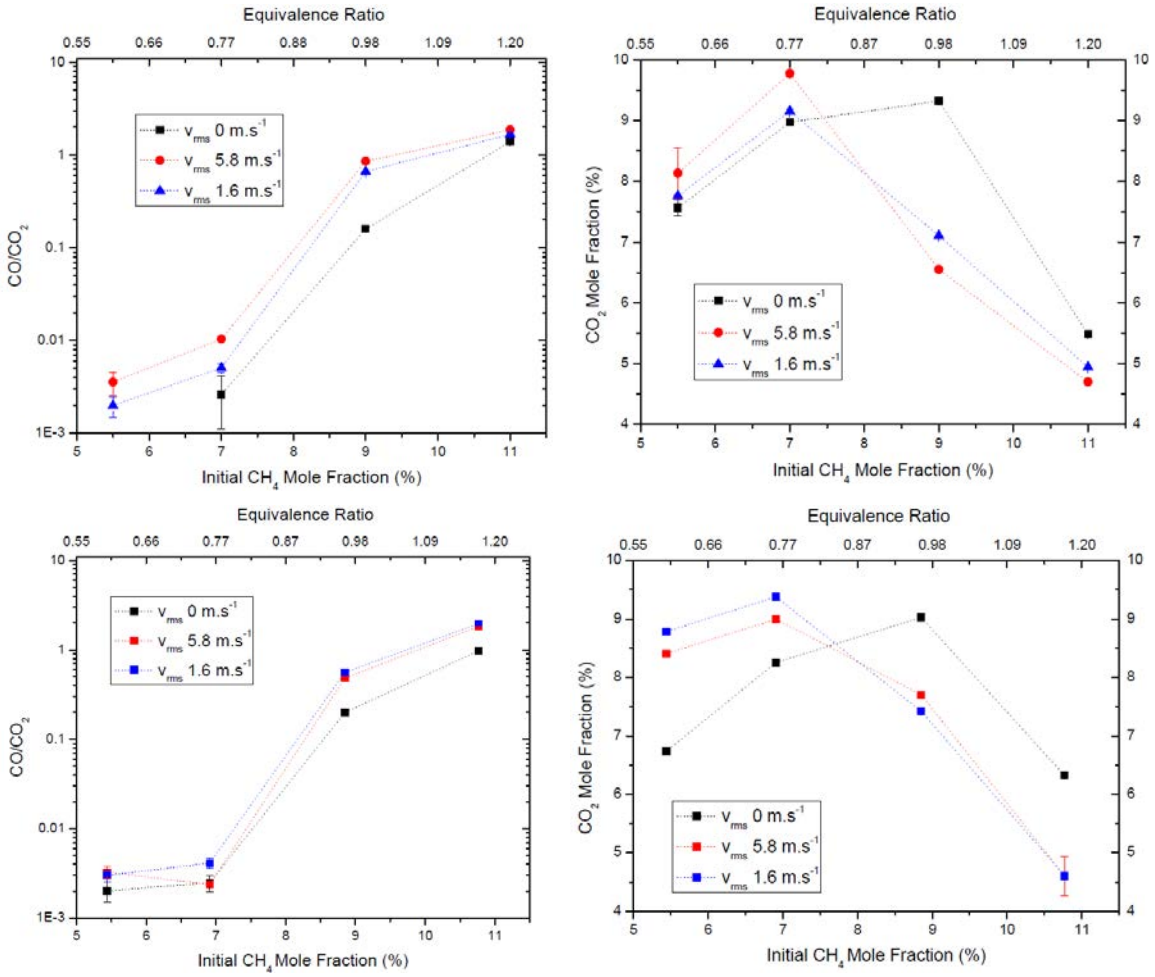

Figure 47. Influence of the turbulence level on the final CO/CO2 ratio and on the final CO_2 molar fraction for a 0.5 g.m^{-3} Corax N550/Methane/Air mixture (up) and 0.5 g.m^{-3} Printex XE2/Methane/Air (down).

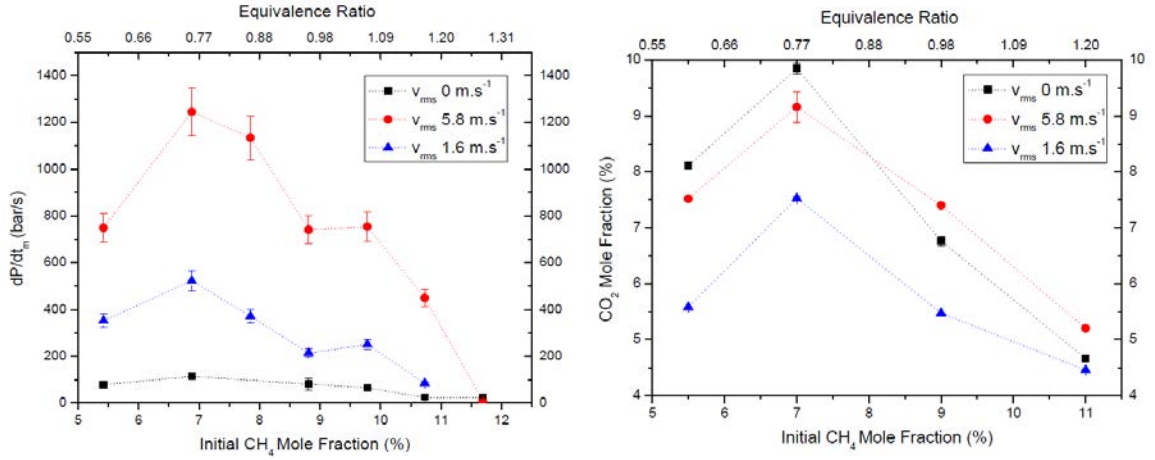

Figure 48. Influence of the turbulence level on the maximum rate of pressure rise - dP/dt_m (left) and on the final CO_2 molar fraction (right) for a 2.5 g.m-3 Printex XE2/Methane/Air mixture.

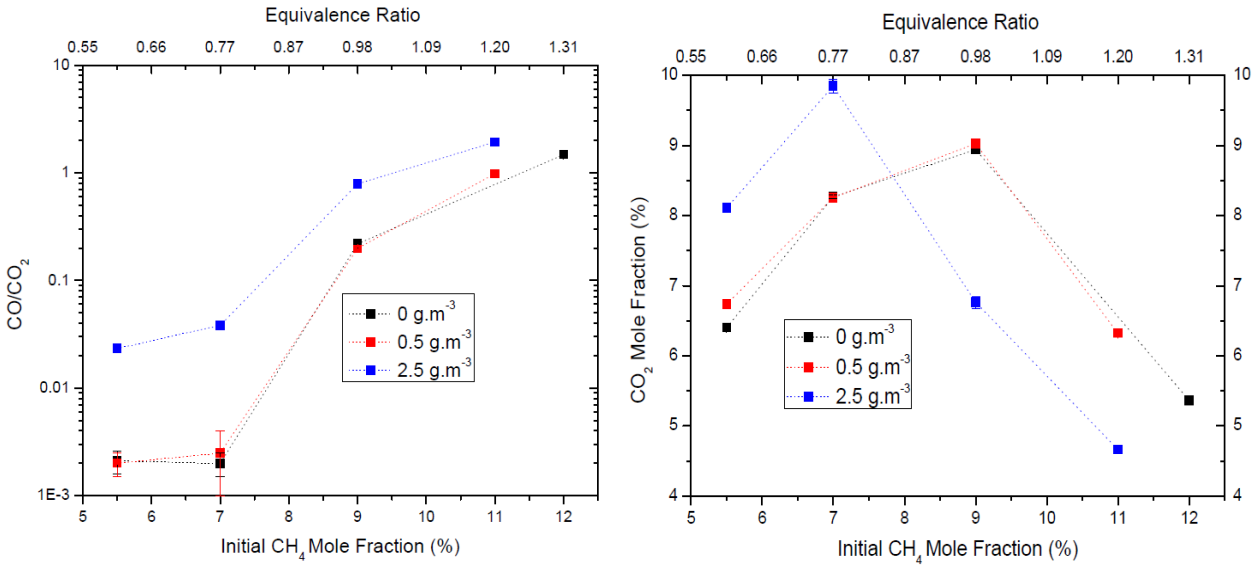

Figure 49. Influence of carbon black level on the final CO/CO_2 ratio (left) and on the final CO_2 molar fraction (right) for Printex XE2/Methane/Air mixture under quiescent conditions.

2.4.2 Effect of inert particle insertion

In order to test the hypothesis of a chemical contribution of the carbon blacks to the gas combustion reaction, explosion severity tests have been carried out with inert AP-D alumina particles instead of carbon blacks. As already written, AP-D 0.05 alumina has been chosen in order to obtain a comparable total surface area developed by the particles (i.e. it should be remembered that the specific surface of AP-D alumina and Corax N550 are 84 and 40 $m^2.g^{-1}$ respectively) at the moment of the explosion as the one of Corax N550/methane/air mixtures (Torrado et al., 2017). It should be stressed that, by changing the nature of the powder, both reactivity and radiative heat transfer can be affected. The latter point will be developed on Chapter 3.

Figure 50 shows the influence of alumina concentration on the explosion severity of methane/air explosions at an initial turbulence level of v_{rms} = 5.8 $m.s^{-1}$. Similarly to the behavior observed for carbon black hybrid mixtures, the influence of the dispersed particles also depends on the equivalence fuel ratio φ. As it was evidenced for carbon black particles, the explosion severity of the methane/air mixture seems to increase for fuel lean mixtures ($\varphi < 1$) when nanoparticles are added. At 7% methane, the insertion of alumina leads to an overpressure increase from 6.5 to 7.5 bars, which is considered as significant in view of the error bars (Figure 50 - right). A similar trend is observed for the maximum rate of pressure rise; however, it is only observable for low alumina concentrations (Figure 50 - left).

Therefore, the inert properties of the alumina suggest that the increase of the explosion severity at fuel lean mixture may not be caused by changes in the chemical combustion reaction, but by other factors as the deformation/stretching of the flame surface due to the dispersion of nanoparticles or the modification of heat transfers (especially radiation). Regarding the stoichiometric and rich mixtures, no significant effect can be seen on the explosion severity when alumina nanoparticles are dispersed in the gas/air cloud before the explosion (e.g. 995 and 1055 $bar.s^{-1}$ for gas and the alumina hybrid mixture respectively at 9%v. of CH_4).

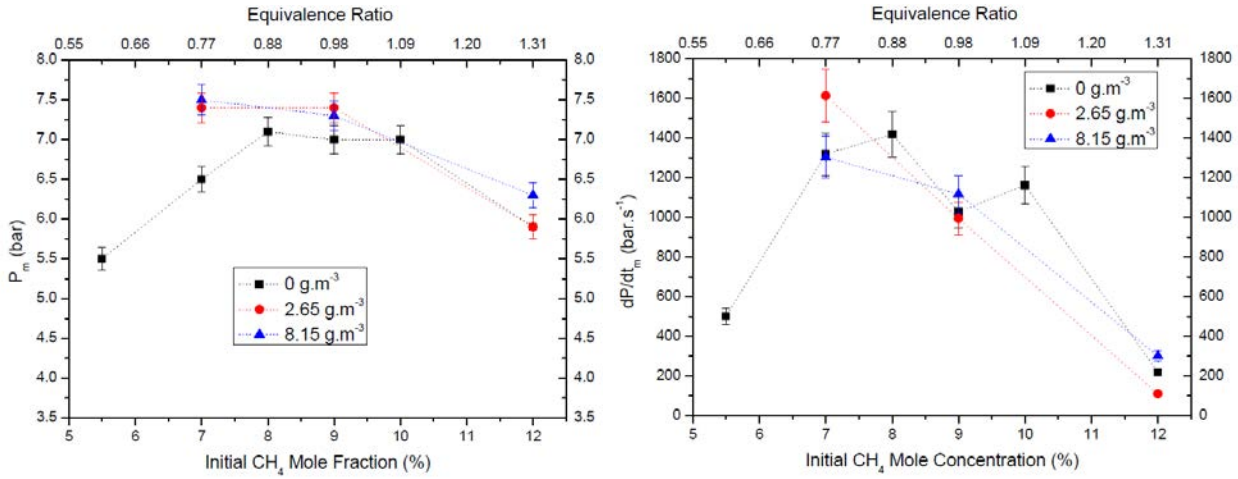

Figure 50. Influence of alumina concentration on the maximum explosion overpressure P_m (right) and on the maximum rate of pressure rise dP/dt_m (left) for alumina/methane/air mixture at an initial turbulence level v_{rms} = 5.8 m.s^{-1}.

Figure 51 compares the explosion severity parameters for methane/air, APD alumina/methane/air and Corax N550/methane/air mixtures, at the same initial turbulence level and dust concentration, i.e. 5.8 m.s^{-1} and 2.5 g.m^{-3} respectively. A different effect on the maximum overpressure of methane explosions is observed when inert particles are dispersed compared to carbon black nanoparticles.

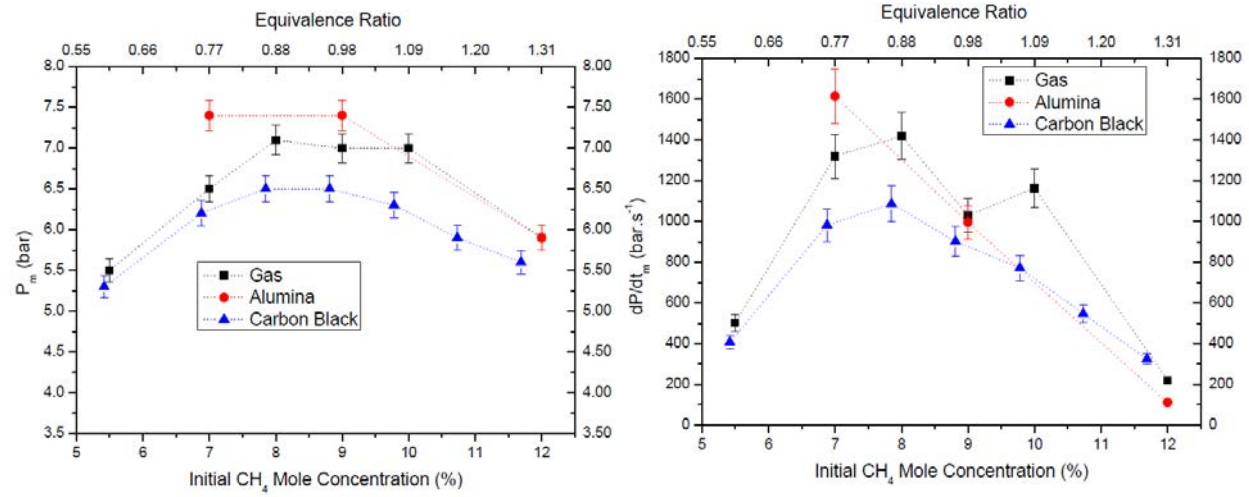

Figure 51. Maximum overpressure (right) and maximum rate of pressure rise (left) for alumina/methane/air, Corax N550/methane/air mixtures and methane at an initial turbulence level v_{rms} = 5.8 m.s^{-1} and 2.5 g.m^{-3} dust concentration.

When 2.5 g.m^{-3} alumina dust are added to lean methane/air mixtures, the maximum overpressure is increased by 15% compared to the methane/air mixture and by 20% compared to Corax N550/methane/mixture. As previously discussed, this trend cannot be caused by a change in the fuel equivalent ratio or in the chemical reaction, as the alumina is an inert compound. It should also be underlined that the influence of powder insertion is more pronounced near the explosivity limits: at 5.5%v. for instance (Figure 42 and Figure 43). The experimental reproducibility is greatly affected by the insertion of nanoparticles. Indeed, some extinction phenomena have been observed

near the explosivity limits, especially at high turbulence levels, which confirms the previous results (see section 2.3.1 – Influence of initial turbulence level) (Kosinski et al., 2013)

For stoichiometric and rich mixtures, very close values of the maximum overpressure were obtained for alumina hybrid mixtures and pure gas. For the case of Corax N550 at 2.5 g.m^{-3}, a diminution of both the maximum overpressure and the maximum rate of pressure rise is observed compared to pure methane and to alumina/methane hybrid mixture. It should be reminded that a slight increase of the severity parameters was obtained when 0.5 g.m^{-3} Corax N550 were dispersed (Figure 39), once again, this positive influence is offset at 2.5 g.m^{-3}, probably due to radiative heat transfers. This point will be discussed later in chapter 3. Moreover, a similar trend has been obtained for Printex XE2/methane/air mixtures at the same initial turbulence level, as has been represented in Figure 44.

The explosion of alumina/methane/air mixture was also carried out at a lower initial turbulence level, here v_{rms} = 1.6 m.s^{-1}, as presented in Figure 52. The initial turbulence level does not generate changes in the trend of the explosion severity of alumina/methane/air mixtures. However, it should be stressed that the initial turbulence level has a considerable effect on the P_m and dP/dt_m variables for carbon black/methane hybrid mixtures. For example, at 7% methane, the addition of 2.65 g.m^{-3} leads to an explosion severity defined by the following combination of maximum explosion pressure and maximum rate of pressure rise (7.4 bars; 1615 bars.s^{-1}) for v_{rms} = 4.5 m.s^{-1}, whereas these parameters greatly decrease when v_{rms} = 2.3 m.s^{-1} (6.9 bars; 770 bars.s^{-1}). The initial turbulence can impact the flame kernel stretching, but also the particle size distribution. Indeed, the fragmentation of the dust increases along with turbulence level (Murillo, 2016; Torrado et al., 2016). For both turbulence levels (v_{rms} = 1.6 m.s^{-1} and v_{rms} = 5.8 m.s^{-1}), similar behavior of the explosion severity parameters for alumina/methane mixtures suggests a noticeable influence of the deagglomeration phenomenon. Nevertheless, contrary to the trends observed for highly loaded suspensions at high turbulence level (Figure 50), the explosivity variations seem to be more pronounced, or at least less mitigated, when the powder concentration reaches 8 g.m^{-3}. For an initial turbulence v_{rms} = 1.6 m.s^{-1}, dust sedimentation is already perceptible and the dust concentration near the ignition zone decreases, which can be an explanation to the observed shift.

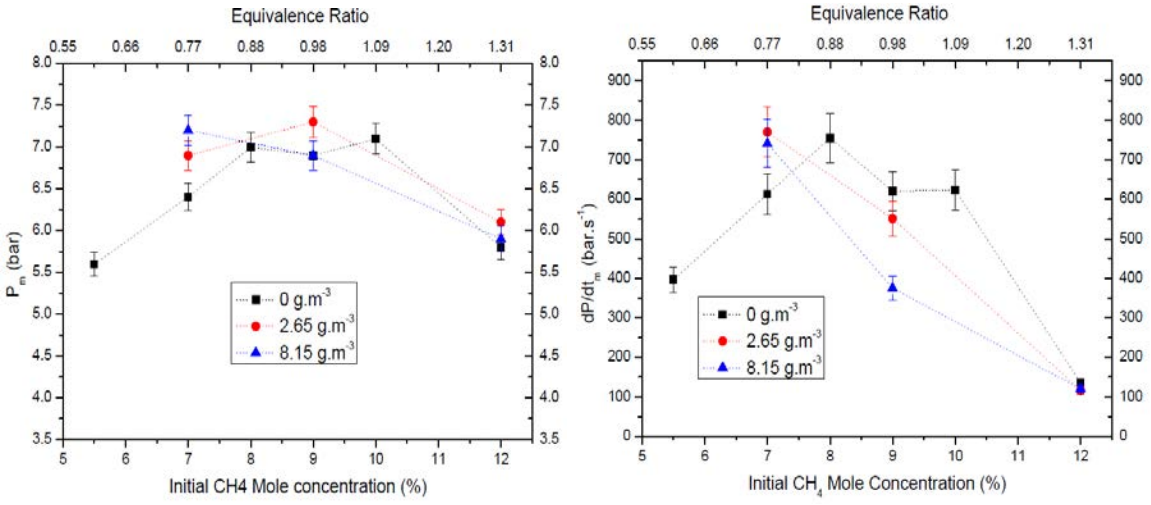

Figure 52. Influence of alumina concentration on the maximum overpressure (right) and maximum rate of pressure rise (left) of alumina/methane/air mixture at an initial turbulence level v_{rms} = 1.6 m.s^{-1}

These results suggest that, at low initial methane concentration, the dispersed nanoparticles and their agglomerates may modify the flame surface thereby producing the acceleration of the flame. Such hypothesis will be tested by studying the flame propagation in a semi-confined tube (Chapter 3).

2.5. Radiative heat transfer contribution

Nevertheless, the flame stretch is probably not the only cause and previous experiments have also shown that the radiative heat exchange is apparently modified by the presence of nanopowders (Torrado et al., 2016). Figure 53 shows the influence of carbon black nanoparticles on the radiative heat transfer in methane/air explosions. An increase on the heat radiation transfer is obtained when 6 $g.m^{-3}$ of Printex EX2 are added into the system. The alumina emissivity being lower than that of carbon (0.07 for alumina compared to 0.97 for carbon particles), the negative impact of the particles radiation, observed for instance in Figure 44 for rich mixtures, is probably less perceptible on the maximum overpressure compared to carbon black hybrid mixtures. The explosivity decrease observed for carbon blacks/methane/air mixtures in Figure 50 could also be related to an increase of the heat radiation transfer. This assertion will be verified with flame propagation tests (Chapter 3).

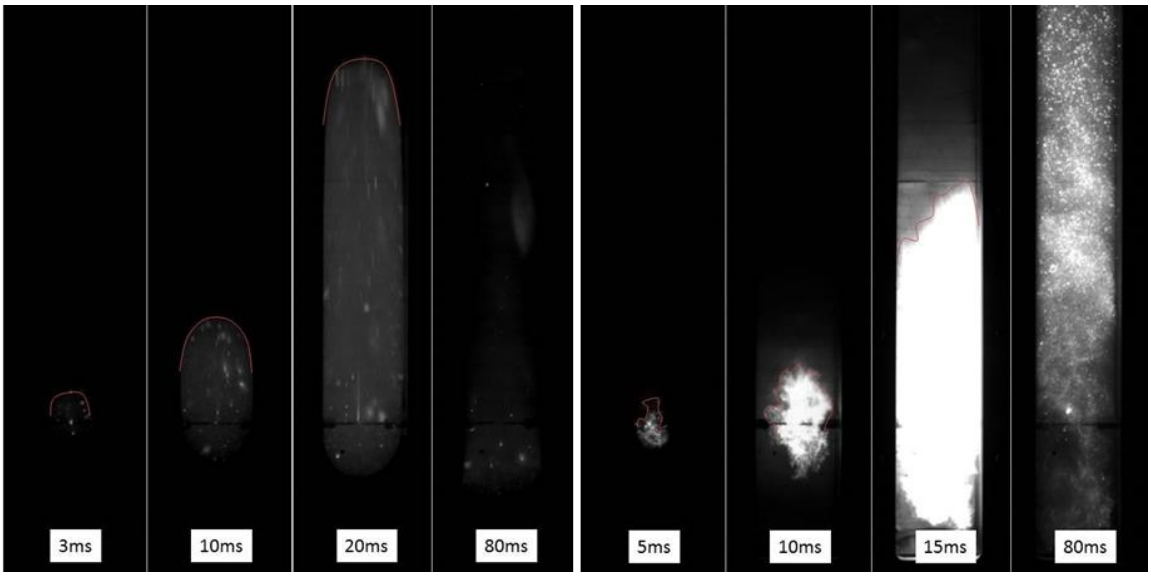

Figure 53. Flame front propagation for a 12%v. CH_4/air explosion at an ignition delay of 60ms (left) and flame front propagation for 30mg of Printex XE2 dispersed in a 12%v. CH_4/air explosion at tv 60ms (right).

Finally, it should be reminded that such particle insertion may enhance radical recombination reactions (Rubtsov, 2016), as it is the case for solid flame retardants, or also improve the condensation process of soot produced by the combustion reaction, changing the overall rate of the reaction.

2.6. Summary of the effect of different parameters

The main influences of the dust concentration, initial turbulence level and particle diameter on the explosion severity of carbon black/methane/air mixtures are summarized in Table 12.

Table 12. Influence of different parameters on the hybrid mixture explosion and gas chromatography results

Parameter	Explosion Severity (P_m, dP/dt_m)	µ-gas chromatography
Carbon black concentration	A slightly increase on the P_m is observed for fuel lean mixture when carbon black are inserted in the system. However, the maximum overpressure decrease for stoichiometric and fuel rich mixtures. When carbon black are added into the system, a considerable reduction is observed on dP/dt_m especially for fuel rich mixtures. When 2.5 $g.m^{-3}$ are added to the combustible mixture, the reduction on the explosion severity is observed whatever the initial CH_4 concentration.	It was not possible to establish a clear trend on the volumetric fraction of burnt gas species when carbon black concentration was augmented. However for Printex XE2, the volumetric CO and H2 fraction of the burnt gases seems to increase when the concentration is increased in the initial system.
Turbulence level	It has a considerable effect on the maximum rate of pressure rise. The influence highlighted when carbon black are added into the reactive mixture seems to be increased at higher turbulence levels. For hybrid mixtures, the explosion severity parameter are modified by the presence of carbon black nanoparticles even at low initial turbulence levels.	When the initial turbulence level increase, the CO/CO_2 seems to increase for fuel lean mixtures.
Particle diameter	The modification on the P_m and dP/dt_m are greater for Printex XE2 than for Corax N550.	

2.7. Conclusions

In this chapter, the influence of low concentrations of carbon black nanoparticles on the explosion severity parameters of methane/air explosions has been studied. The high stability of the nanoparticles dispersion let to study the explosion severity of the hybrid mixture at low turbulence level, in order to isolate the effect of the turbulence/reaction interactions on the explosion violence. The cloud of carbon black nanopowder remains highly stable some minutes after the dispersion, with a constant mean mobility diameter. The dust cloud formed after dispersion, notably composed of agglomerates, has a mean diameter of 240 nm and 370 nm for Printex XE2 and Corax N550 respectively.

The results obtained show that, even when adding carbon blacks at low concentration (well below the minimum explosive concentration), the heat transfer phenomena and the combustion reaction can be modified. The explosion severity tests and the burnt gas characterization suggest that:

a) The explosion severity of methane/air mixture increases when low concentrations of carbon black nanoparticles are present in the system for lean mixtures, even at quiescent conditions. In addition, at stoichiometric and fuel rich mixtures, the presence of carbon black nanoparticles generates a negative effect on the explosion severity. This trend seems to be independent of the turbulence levels studied on this work.
b) The addition of alumina particles generates similar trend of the explosion severity parameters dP/dt_m and P_m: these parameters increase when low concentrations of carbon black and alumina nanoparticles are injected on the methane/air mixtures at fuel lean mixtures conditions. Such tests also reveal that the turbulence level has a greater influence on the explosion severity parameters of carbon black hybrid mixtures compared to alumina hybrid mixtures.
c) The addition of carbon black particles for fuel lean mixtures seems to promote the oxidation of CO, which will generate a higher release of chemical energy and, consequently, an increase in the maximum rate of pressure rise. The presence of carbon blacks (or as a consequence, soot) has effects on gas explosion severity which can vary as a function of the turbulence level. Such influence can lead to explosion quenching and has to be further studied in order to design appropriate prevention or protection devices as well as to propose intrinsic safety measures.
d) The specific surface area of the dispersed particles has a great influence on the explosion severity of carbon black/ methane/ air mixtures. At high turbulence levels, the deagglomeration effects on heat transfer and flame surface are amplified for powders with higher specific surface.

In addition to applications in the field of risk assessment of hybrid mixtures explosion, this study can bring new insight into the impact of soot formation on gas combustion, due to the similarities between the carbon black nanoparticles and soot particles. By this means, the modifications on the explosion severity at specific methane concentration could be explained because of the presence of particles that may play the role of soot-nuclei.

The origins of these specificities of these hybrid mixtures explosions can notably be explained by the chemical contribution of the particles, the impact of the powders on the radiation transfers, their influence on the flame stretching and/or the fact that they can act as solid kernel for soot nucleation. The similarities on the trends between the explosion severity parameters of alumina and hybrid mixture explosions suggest that the chemical contribution of the carbon particles is negligible, and

the influence of the radiation heat transfer, flame deformation and soot nucleation seems to be higher. In the next chapter, the influence on the radiative heat transfer will be evidenced and the flame surface modifications will be analyzed.

2.8. Conclusions (Français)

Dans ce chapitre, l'influence de l'ajout de faibles concentrations de nanoparticules de noir de carbone sur les paramètres de sévérité des explosions de méthane/air a été étudiée. La forte stabilité après dispersion des nanoparticules permet d'étudier la sévérité de l'explosion d'un mélange hybride à faible turbulence initiale, afin d'isoler l'effet des interactions turbulence / réaction sur la violence des explosions. En effet, le nuage de noir de carbone nanométrique reste très stable quelques minutes après la dispersion, avec un diamètre de mobilité moyen constant. Composés de particules primaires et d'agglomérats fins, ces nuages possèdent des diamètres moyens de 240 nm et 370 nm pour Printex XE2 et Corax N550 respectivement.

Les résultats obtenus montrent que, même en ajoutant des noirs de carbone à faible concentration (bien en dessous de la concentration minimale d'explosivité), les phénomènes de transfert de chaleur et de réaction de combustion peuvent être modifiés. Les tests de sévérité de l'explosion menés en sphère de 20 L et l'analyse chimique des gaz brûlés par chromatographie suggèrent que :

a) La sévérité de l'explosion du mélange méthane/air augmente lorsque de faibles concentrations de nanoparticules de noir de carbone sont présentes dans le système pour des mélanges pauvres en méthane, même à faible turbulence initiale. De plus, pour des mélanges stœchiométriques et riches en méthane, la présence de nanoparticules de noir de carbone diminue la sévérité de l'explosion. Cette tendance semble être indépendante des niveaux de turbulences étudiés sur ce travail.
b) L'addition de particules d'alumine génère une tendance similaire vis-à-vis des paramètres de sévérité d'explosion $(dP/dt)_m$ et P_m : ils augmentent lorsque de faibles concentrations de nanoparticules de noir de carbone et d'alumine sont injectées sur les mélanges de méthane/air dans des conditions de mélange pauvre en carburant. Les tests révèlent également que le niveau de turbulence a une plus grande influence sur les paramètres de sévérité de l'explosion des mélanges hybrides méthane/noir de carbone noir que sur ceux des mélanges méthane/alumine.
c) Pour les mélanges pauvres en méthane, l'insertion de particules de noir de carbone semble favoriser l'oxydation du CO, ce qui génère une libération plus élevée d'énergie chimique et, par conséquent, une augmentation de la vitesse de montée en pression. La présence de noir de carbone (ou le cas échéant, de suies) a des effets sur la gravité de l'explosion du gaz qui peuvent varier en fonction du niveau de turbulence. Cette influence peut notamment entraîner des phénomènes d'extinction de l'explosion (lors des phases de croissance du noyau de flamme) et doit être étudiée plus en détail afin de concevoir des dispositifs de prévention ou de protection appropriés.
d) La surface spécifique des particules dispersées a une grande influence sur la sévérité de l'explosion des mélanges de noir de carbone/méthane/air. À des niveaux élevés de turbulence, les effets de désagglomération sur le transfert de chaleur et sur la surface de la flamme sont amplifiés pour les poudres qui présentent alors une surface spécifique globale supérieure.

En plus des applications dans le domaine de l'évaluation des risques de l'explosion des mélanges hybrides, cette étude peut apporter un nouveau regard sur l'impact de la formation de suie sur la combustion de gaz, en raison des similitudes entre les nanoparticules de noir de carbone et les particules de suie. De ce fait, les modifications observées de la sévérité de l'explosion pour une

concentration spécifique de méthane pourraient être expliquées notamment par la présence de particules pouvant contribuer à la condensation de suies.

Au final, les origines des spécificités des explosions de mélanges hybrides peuvent notamment être expliquées par la contribution chimique des particules, l'impact des poudres sur les transferts radiatifs, leur influence sur l'étirement de la flamme et/ou le fait qu'elles peuvent contribuer à la condensation de suies.

Les similitudes entre les tendances observées sur les paramètres de sévérité pour des mélanges hybrides contenant de l'alumine et ceux contenant du noir de carbone suggèrent que la contribution chimique des particules de carbone est négligeable et que les influences du transfert de chaleur par rayonnement, de la déformation de la flamme et de la nucléation des suies semblent être plus élevée.

Dans le chapitre suivant, l'influence de l’ajout de poussières sur les transferts de chaleur radiatif sera mise en évidence et les modifications de la surface de la flamme seront analysées.

Nomenclature

Symbol	Description
BET	Brunauer, Emmett et Teller method
DMA	Differential Mobility Analyzer
$\frac{dP}{dt}$	Rate of pressure rise [Pa.s^{-1}].
m_u	Unburnt gases mass [kg].
m_{u_0}	Initial unburnt gases mass [kg].
P	Pressure [Pa].
P_e	Explosion Pressure [Pa].
P_0	Initial Pressure [Pa].
PIV	Particle Image Velocimetry.
PSD	Particle Size Distribution.
r_f	Flame radius [m].
R_{vessel}	Vessel radius [m].
S_e	Burnt gas expansion velocity [m.s^{-1}].
S_n	Velocity due to unburnt reaction gases [m.s^{-1}].
S_u	Burning velocity [m.s^{-1}].
UCPC	Ultrafine Condensation Particle Counter
u	Horizontal component of the flow velocity [m.s^{-1}].
v	Vertical component of the flow velocity [m.s^{-1}].
u'	Horizontal component of the velocity fluctuations [m.s^{-1}].
v'	Vertical component of the velocity fluctuations [m.s^{-1}].
v_{rms}	Root-mean-square velocity [m.s^{-1}].
Greek letters	Description
γ	Heat capacity ratio of the gas [-].
φ	Fuel Equivalence Ratio [-].
ρ_u	Unburnt gas density **[**kg.m^{-3}**]**

References

Agilent Technologies, 2017. Agilent 490 Micro Gas-Chromatography apparatus. Httpwwwagilentcomen-Usproductsgas-Chromatogr.-Syst.-Micro-Gc.

ASTM E1226-12a, 2012. Standard Test Method for Pressure and Rate of Pressure Rise for Combustible Dusts. Annu. Book ASTM Stand. 1–11.

Bagaria, P., Zhang, J., Yang, E., Dastidar, A., Mashuga, C., 2016. Effect of dust dispersion on particle integrity and explosion hazards. J. Loss Prev. Process Ind. 44, 424–432.

Bauffman, J., Cox, K., 2008. Measurement of laminar burning velocity of methane-air mixtures using a slot and Bunsen burner (Major qualifying project). Worcester Polytechnic Institute, Worcester, United States.

Bouillard, J., Vignes, A., Dufaud, O., Perrin, L., Thomas, D., 2010. Ignition and explosion risks of nanopowders. J. Hazard. Mater. 181, 873–880.

Bradley, D., Lawes, M., Mumby, R., 2017. Burning velocity and Markstein length blending laws for methane/air and hydrogen/air blends. Fuel 187, 268–275.

Brossard, C., Monnier, J.C., Barricau, P., Le Sant, Y., Champagnat, F., Le besnerais, G., 2009. Principles and Applications of Particle Image Velocimetry. J. AerospaceLab 1–11.

Cloney, C.T., Ripley, R.C., Amyotte, P.R., Khan, F.I., 2013. Quantifying the effect of strong ignition sources on particle preconditioning and distribution in the 20-L chamber. J. Loss Prev. Process Ind. 26, 1574–1582.

Crowe, C., 2000. On models for turbulence modulation in fluid–particle flows. Int. J. Multiph. Flow 26, 719–727.

Cuervo, N., 2015. Influences of turbulence and combustion regimes on explosions of gas- dust hybrid mixture. Université de Lorraine.

Dahoe, A., 2000. Dust Explosions: a Study of Flame Propagation.

Dahoe, A.E., Cant, R.S., Pegg, M.J., Scarlett, B., 2001. On the transient flow in the 20-liter explosion sphere. J. Loss Prev. Process Ind. 14, 475–487.

Dahoe, A.E., Hanjalic, K., Scarlett, B., 2002. Determination of the laminar burning velocity and the Markstein length of powder–air flames. Powder Technol., Special issue i in Honour of Prof Jimbo 122, 222–238.

Dahoe, A.E., Zevenbergen, J.F., Verheijen, P.J.T., Lemkowitz, S.M., Scarlett, B., 1996. Dust explosions in spherical vessels: prediction of the pressure evolution and determination of the burning velocity and flame thickness.

D'Amico, M., Dufaud, O., Latché, J.-C., Trélat, S., Perrin, L., 2016. Parametric study of the explosivity of graphite-metals mixtures. J. Loss Prev. Process Ind. 43, 714–720.

Dirrenberger, P., Le Gall, H., Bounaceur, R., Herbinet, O., Glaude, P.-A., Konnov, A., Battin-Leclerc, F., 2011. Measurements of Laminar Flame Velocity for Components of Natural Gas. Energy Fuels 25, 3875–3884.

Dufaud, O., Perrin, L., Traore, M., Chazelet, S., Thomas, D., 2009. Explosions of vapour/dust hybrid mixtures: A particular class. Powder Technol. 190, 269–273.

Eckhoff, R.K., 2012. Does the dust explosion risk increase when moving from μm-particle powders to powders of nm-particles? J. Loss Prev. Process Ind. 25, 448–459.

Eckhoff, R.K., 2009. Understanding dust explosions. The role of powder science and technology. J. Loss Prev. Process Ind. 22, 105–116.

Eckhoff, R.K., 2003. Dust explosions in the process industries, 3rd ed. ed. Gulf Professional Pub, Amsterdam ; Boston.

Garcia-Agreda, A., Di Benedetto, A., Russo, P., Salzano, E., Sanchirico, R., 2011. Dust/gas mixtures explosion regimes. Powder Technol. 205, 81–86.

Gordon, S., McBride, B., 1994. Computer program for calculation of complex chemical equilibrium and applications. NASA Ref. Publ. 1311.

Khalili, I., Dufaud, O., Poupeau, M., Cuervo-Rodriguez, N., Perrin, L., 2012. Ignition sensitivity of gas–vapor/dust hybrid mixtures. Powder Technol. 217, 199–206.

Kosinski, P., Nyheim, R., Asokan, V., Skjold, T., 2013. Explosions of carbon black and propane hybrid mixtures. J. Loss Prev. Process Ind. 26, 45–51.

Murillo, C., 2016. Experimental and numerical approaches to particles dispersion in a turbulent flow: application to dusts explosion. Université de Lorraine.

Murillo, C., Bardin-Monnier, N., Muñoz, F., Dufaud, O., 2015. Application of CFD on the sensitivity analyses of some parameters of the modified Hartmann tube. J. Loss Prev. Process Ind. 36, 296–307.

Murillo, C., Dufaud, O., Bardin-Monnier, N., López, O., Munoz, F., Perrin, L., 2013a. Dust explosions: CFD modeling as a tool to characterize the relevant parameters of the dust dispersion. Chem. Eng. Sci. 104, 103–116.

Murillo, C., Dufaud, O., López, O., Perrin, L., Vignes, A., Muñoz, F., 2013b. CFD modelling of nanoparticles dispersion in a dust explosion apparatus. Chem. Eng. Trans. 889–894.

Pedersen, N., Larsen, P.S., Jacobsen, C.B., 2003. Flow in a Centrifugal Pump Impeller at Design and Off-Design Conditions—Part I: Particle Image Velocimetry (PIV) and Laser Doppler Velocimetry (LDV) Measurements. J. Fluids Eng. 125, 61.

Proust, C., 2006. Flame propagation and combustion in some dust-air mixtures. J. Loss Prev. Process Ind. 19, 89–100

Raffel, M., Willert, C.E., Wereley, S., Kompenhans, J., 2013. Particle image velocimetry: a practical guide. Springer.

Rubtsov, N.M., 2016. The Modes of Gaseous Combustion, Heat and Mass Transfer. Springer International Publishing, Cham.

Russo, P., Di Benedetto, A., 2007. The effect of turbulence on the theoretical evaluation of dust explosions severity. Chem. Eng. Trans. 11, 83–988.

Shy, S.S., Lin, W.J., Wei, J.C., 2000. An experimental correlation of turbulent burning velocities for premixed turbulent methane-air combustion. Proc. R. Soc. Math. Phys. Eng. Sci. 456, 1997–2019.

Skjold, T., 2003. Selected aspects of turbulence and combustion in 20-Litre explosion vessel. University of Bergen, Norway.

SYMPA TEC, 2017. Particle size analysis with laser diffraction HELOS. http://www.sympatec.com/EN/LaserDiffraction/HELOS.html.

Tamanini, F., 1998. The role of turbulence in dust explosions. J. Loss Prev. Process Ind. 11, 1–10.

Tamanini, F., 1990. Turbulence effects on dust explosion venting. PlantOperations Prog. 9, 52–60.

Tebianian, S., Dubrawski, K., Ellis, N., Cocco, R.A., Hays, R., Reddy Karri, S.B., Leadbeater, T.W., Parker, D.J., Chaouki, J., Jafari, R., Garcia-Trinanes, P., Seville, J.P.K., Grace, J.R., 2015. Investigation of particle velocity in FCC gas-fluidized beds based on different measurement techniques. Chem. Eng. Sci. 127, 310–322.

Thielicke, W., 2014. The Flapping Flight of Birds Analysis and Application (PhD Thesis). University of Groningen.

Torrado, D., Buitrago, V., Glaude, P.-A., Dufaud, O., 2017. Explosions of methane/air/nanoparticles mixtures: Comparison between carbon black and inert particles. Process Saf. Environ. Prot.

Torrado, D., Cuervo, N., Pacault, S., Dufour, A., Glaude, P.-A., Murillo, C., Dufaud, O., 2016. Explosions of gas/carbon black nanoparticles mixtures: An approach to assess the role of soot formation. Chem. Eng. Trans. 48, 379–384.

TSI Instruments, 2009. Electrostatic Classifier Series 3080 - Operation and Service Manual.

TSI Instruments, 2006. Ultrafine Condensation Particle Counter Model 3776 - Operation and Service Manual.

Turkevich, L.A., Dastidar, A.G., Hachmeister, Z., Lim, M., 2015. Potential explosion hazard of carbonaceous nanoparticles: Explosion parameters of selected materials. J. Hazard. Mater. 295, 97–103.

Vignes, A., 2008. Evaluation de l'inflammabilité et de l'explosivité des nanopoudres : une demarche essentiell pour la maîtrise des risques. Institut National Polytechnique de Lorraine.

CHAPTER 3: Study of the burning velocity of nanoparticles/methane/air hybrid mixtures

3.1. Introduction

The prediction of the explosion severity of hybrid mixture is an essential step for the protection device sizing on industrial applications, for which the cubic root law is usually applied to estimate the $K_{g/st}$ parameter and then the relief area. However, the cubic root law is invalid for some specific cases and may generate considerable errors on the design of the protection devices, especially when the radiative transfers are important (e.g. metallic powders). For this reason, models using the mass burning velocity during the explosion can be implemented to assess the dust/hybrid mixtures explosivity instead of the cubic law. Moreover, the laminar burning velocity and the flame thickness are fundamental measures of the combustion process and these variables are essential inputs in order to successfully model the mass burning rate of mixtures (Dahoe et al., 2002). In this chapter, the experimental determination of the burning velocity of methane/air, carbon black/methane/air and alumina/methane/air mixtures is developed. In addition, the influence of nanoparticles concentration and of the initial turbulence level on the burning velocity is also analyzed.

In the previous chapter, the influence of carbon black nanoparticles on the maximum overpressure and maximum rate of pressure rise of methane/air explosions were analyzed. It was found that the explosion severity of methane/air mixture increases when low concentrations of carbon black nanoparticles are present in the system for lean mixtures, but decreases for stoichiometric and fuel rich mixtures. The modifications of the explosion severity can be associated with changes on the chemical contribution of the nanoparticles or a contribution of the particles to soot nucleation, changes on the radiative behavior and modifications on the flame stretch and thickness. The first causes have been developed in the previous chapter. The influence of turbulence/combustion interactions will be developed now by analyzing the potential modifications on the flame surface, stretch and radiative heat transfer, which was not possible using the standard 20 L explosion sphere.

3.2. Flame propagation study: methodology

3.2.1 Experimental set-up

In order to measure the flame propagation velocity, the explosions of methane/carbon black/air mixtures are generated in a vertical 1m long tube with a cross section area of 7 × 7 cm connected to a gas mixing system (Figure 54). The tube is made of two opposite glass walls and two opposite stainless steel walls (Cuervo, 2015; Di Benedetto et al., 2011). The bottom of the tube is closed, while the top is partially open using a pressure relief valve, which opens at 1.15 atm in order to assure a constant pressure. At the closed bottom, a mushroom-shaped nozzle (similar to that used in standard test methods, i.e. the modified Hartman tube) is placed to disperse the carbon black dust homogeneously. The term “homogeneously” has to be discussed as a spatial homogeneity of a dust cloud is rather difficult to obtain and maintain for a hundred milliseconds with this kind of dispersion system. PIV measurements (Chapter 2), observations and CFD simulations (Murillo et al., 2013) have demonstrated that if a suitable dispersion can be obtained, it can, of course, never be considered as an ideal dispersion of equidistant particles in a gas cloud.

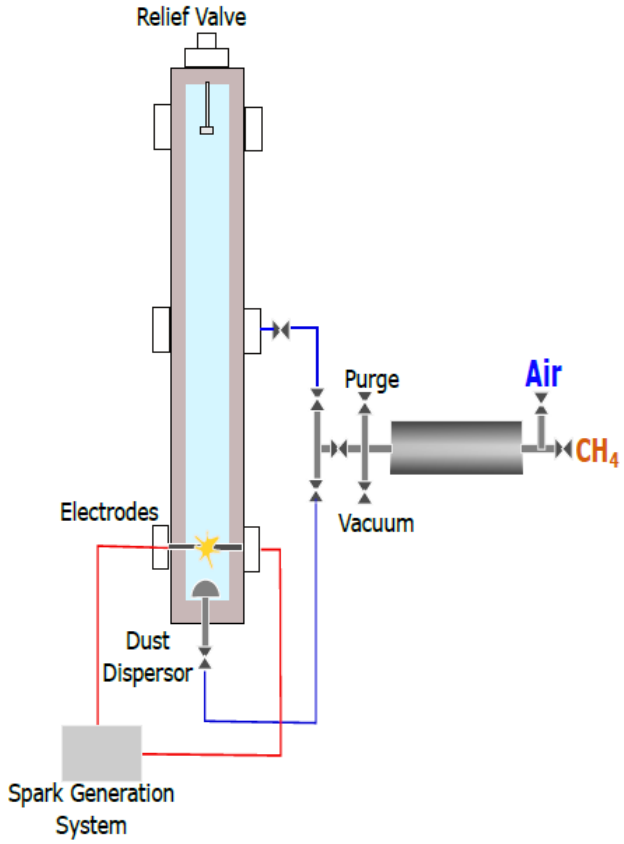

Figure 54. Experimental set-up for the measurement of flame propagation of hybrid mixtures.

The pressure in the tube at the moment of the ignition is the atmospheric pressure. Electrodes are located at 12.5 cm from the bottom of the tube. However, as previously said, the addition of carbon black nanoparticles tends to increase the MIE of the mixture. The ignition energy was chosen considering the minimal energy at which a stoichiometric and turbulent gas mixture (standard ignition delay tv of 120 ms) does not lead to flame quenching. For ignition energies of 1, 3 and 5 J, the fuel mixture had not been systematically ignited. Moreover, for too high ignition energies, overdriving phenomenon will occur and can modify the flame propagation. In order to be consistent with the tests performed in the 20 L sphere, an ignition energy of 100 J could have been chosen. However, the use of a chemical igniter of 100 J in the tube generates a blinding flash which hinders the observation of the flame kernel. The use of a permanent spark, generated by a KSEP 320 system (Kühner AG - 15 kV / 15 mA, i.e. 225 W), implies that the energy is proportional to the spark duration. A 100 J spark, if technically possible, will then last 444 ms, which is too long to consider that the mixture between the two electrodes will not change. As a consequence, an ignition energy of 10 J has been chosen.

The gas mixing system consists of a 50 mL vessel equipped with valves that allow a manual control of the gas pressure. The gas mixtures are injected in two different positions in the tube to ensure homogeneity of the gas concentration across the tube (proven during this study by gas chromatography measurements by using a Varian 490 MGC). A first injection of the gas is made at a 0.50 m height, and then the 5.2 bar gas mixture is used to generate the dust dispersion at the bottom of the tube. The initial turbulence level is studied by changing the ignition delay time (tv) between the beginning of the dispersion and the ignition. The root-mean-square (rms) velocity was

estimated using the Particle Image Velocimetry (PIV) with glass microbeads glass as tracer particles (Section 2.2.2). The obtained values of the v_{rms} were 1.6, 1.4 and 0.9 m.s^{-1} at ignition delay times of 60, 120 and 500 ms respectively. A Phantom V91 high-speed video camera is used to record videos of the flame propagation from 1,000 to 4,000 frames per second.

3.2.2 Calculation of burning velocity of unstretched flames

The flame burning velocity S_u can be calculated from the spatial velocity S_s of the flame and the relation between the front flame surface A_f and the surface of the cross section of tube A (Andrews and Bradley, 1972a; Bradley et al., 2017):

$$S_u = S_s \frac{A}{A_f} \quad \text{Eq 26}$$

Due to the partial confinement of the tube (closed bottom), this velocity should also be corrected considering the thermal expansion factor α which is the ratio between the temperatures of the hot burnt gases generated by the combustion reaction and the initial cold gases ($\alpha \approx \frac{\rho_u}{\rho_b} = \frac{T_b}{T_u}$). The CEA software is used to determine the adiabatic temperature at equilibrium conditions of the reaction mixture (Gordon and McBride, 1994).

$$S_u = \frac{S_s}{\alpha} \frac{A}{A_f} \quad \text{Eq 27}$$

This model assumes that the unburnt gas density, spatial velocity, and burning velocity are independent of the cross-section area of the tube (Andrews and Bradley, 1972a; Cuervo et al., 2017). In addition, the model is valid if the thickness of the flame is negligible in comparison with the curvature of the flame. The burning velocity depends on the initial concentration of the mixture, the pressure, the temperature and the turbulence. The latter is very important for the dust/gas hybrid mixture to generate the solid dispersion, which is not the case for pure gases. The flame stretching can be quantified through the factor K, called Karlovitz's factor. It will take into account both the influence of the turbulence of the flame surface and the contribution of the flame curvature. The flame stretching factor is calculated as (Law, 2006; Varea, 2013):

$$K = \frac{1}{A_f} \frac{dA_f}{dt} \quad \text{Eq 28}$$

A linear relation between S_u and K was proposed for gas mixtures by Markstein (1964) and then by Clavin (1985):

$$S_u = -LK + S_u^0 \quad \text{Eq 29}$$

where L is the Markstein length and S_u^0 is the unstretched flame velocity. A positive value of the Markstein length induces that the burning velocity decreases when the stretch increase, generating a stable flame. Conversely, if the Markstein length is negative, an unstable flame is obtained because the burning velocity increases with the flame stretch (Dahoe, 2000).

Even though other measurement techniques, notably flat flame static techniques (Andrews and Bradley, 1972a; Dirrenberger et al., 2014), have been developed to determine laminar flame velocity of gases accurately, these techniques are difficult to apply to mixtures involving dispersed solids. Therefore, the flame propagation tube allows estimating the laminar flame velocity for these mixtures despite the turbulence of the system and the interactions of the flame with the tube walls. The previous relationships were developed for homogeneous mixtures in the tube at low initial turbulence, that also means that we will have to take into account the influence of the "cold turbulence" (i.e. turbulence of the initial cloud). Contrary to micro-powder, nano-powder / gas hybrid systems can generate explosions even at low levels of initial turbulence, and thus a homogeneous mixture can be assumed to implement these relationships. Although this relation was established for gas mixtures, it will be used for hybrid mixtures (only for gas-driven systems) assuming a homogeneous solid/gas mixture across the propagation tube (Cuervo, 2015). Further discussion on the validity of this relationship for hybrid mixture explosion will be given in section 3.3.1.A.

3.2.3 Video analysis

In order to estimate the flame propagation characteristics (S_u, S_u^0, K, S_s, A_f), a model has been developed in Matlab's Simulink using the Vision toolbox (Cuervo, 2015). This model analyzes the videos of the flame propagation in the system and extracts the front flame profile at each frame in the video. In a previous stage, the video has been edited in VirtualDub software in order to enhance the flame detection, adding numerical color filters. The Simulink model can then separate each color channel from the RGB image and analyze it separately. Firstly, the background is estimating analyzing the first 50 frames before the electrical spark. Then, the flame is isolated as the difference between the background and the frames after the ignition. In order to increase the flame detection precision, the moving object is detected on the three primary colors and compared to the background (Figure 55).

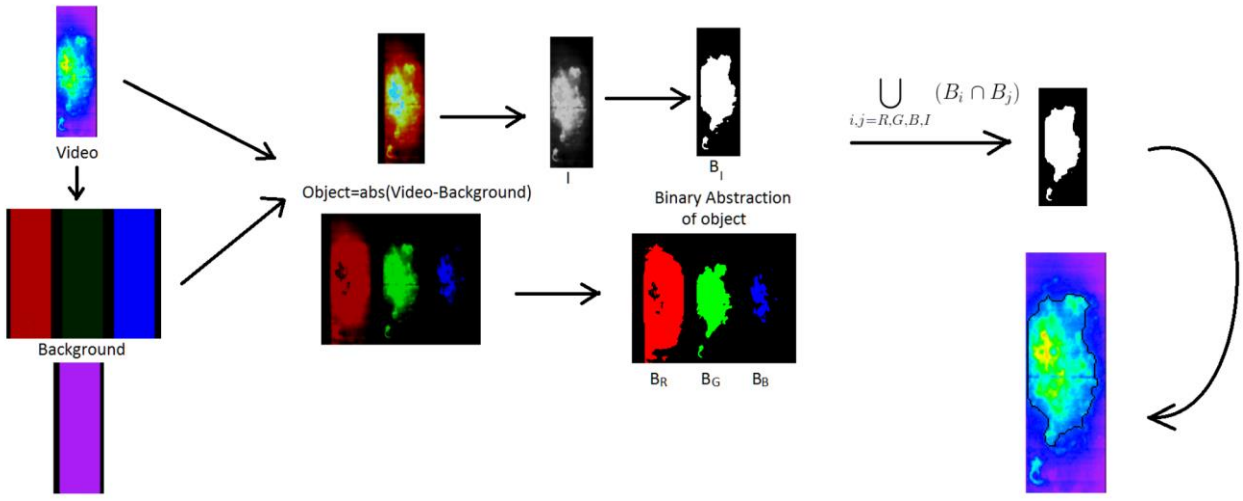

Figure 55. Example of the video analysis using the Matlab - Simulink model (Cuervo, 2015).

The moving flame can now be detected and the flame profile estimated as shown in Figure 56. With the position of the flame z, the estimated cross-section area. A_s and the estimated flame surface A_f for different points in time t, the spatial velocity S_s, the burning velocity S_u and the

stretching K can be calculated. Then, the method previously explained in section 3.2.2 can be developed.

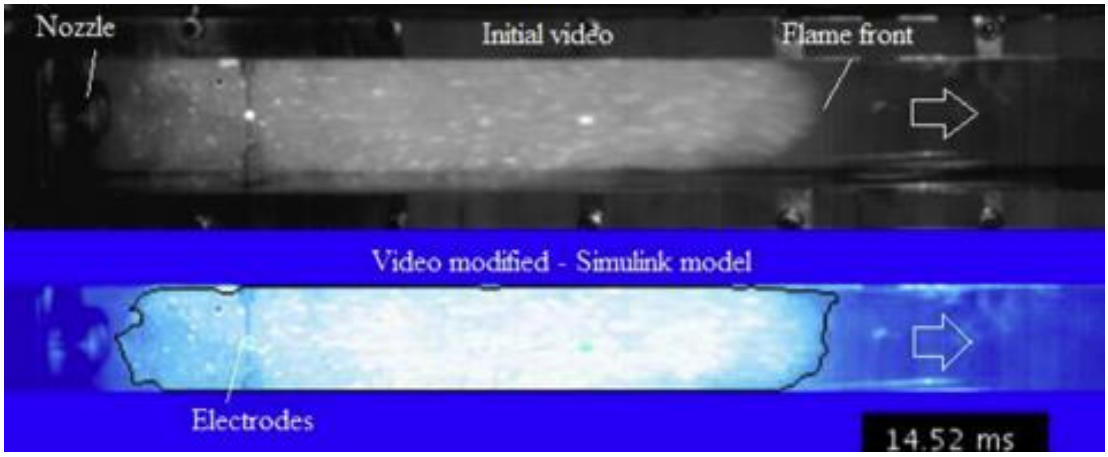

Figure 56. Moving flame detection by the Matlab's Simulink model for 10.5% Methane/30 mg Corax N550. Flame propagating the left to right on the image (upward direction).

3.3. Flame propagation measurements

3.3.1. Carbon black/methane/air mixtures

A. Analysis of flame propagation phenomena

It clearly appears that the explosions performed are quite sensitive to the gas and solid concentration, and to the initial turbulence of the system. The initial turbulence of the dust/gas cloud has also an impact on the flame turbulence/combustion interactions. After the ignition spark, an initial stretched flame is generated that initially seems to move in the vertical direction. For low initial turbulence, a spherical propagation takes place after some milliseconds (Figure 57 - left), until the moment when the flame interacts with the walls. The duration of the semispherical development depends on the mixture concentration and turbulence level. For instance, for a 10.5% methane/30 mg Corax N550 mixture at v_{rms} = 0.9 m.s^{-1}, the semispherical propagation duration is around 3 ms. Regarding the high initial turbulence cases (Figure 57 - right), spherical propagation is not always evidenced; however, the flame is intensively stretched (sometimes leading to quenching) and touches the wall more rapidly. Once the flame interacts with the one of the walls, it becomes parabolic and its surface increases, causing in turn a modification - often an increase - in the flame speed.

Besides the role of the turbulence, the initial presence of dispersed nanoparticles modifies the surface of the flame. For pure methane, the front flame seems well defined, continuous and appears rather smooth, as it is usually reported for a gaseous mixture (Proust, 2006). However, for hybrid mixtures, the flame profile is not uniform and irregularities appear when the flame reaches dispersed particles or aggregates. The estimation of the flame surface and its behavior with respect to time becomes particularly difficult to measure for these mixtures. Aggregates or agglomerates reached by the flame induce a wrinkled flame and generate flamelets in the surface (see Chapter 1.1.2). Moreover, the initial presence of carbon nanoparticles increases flame luminosity in the visible range due to the radiative heat transfer. Additionally, the initial turbulence in the system appears to have an influence on the deagglomeration of the nanoparticles and thus on the heat exchange by radiation, generating a flame brightness gradient, which sometimes makes the flame

front detection more uneasy. The deagglomeration phenomenon due to the dispersion have a low reproducibility at the same initial turbulence level. Due to these difficulties of getting a precise estimation of the flame surface, uncertainties on the combustion velocity are unavoidable.

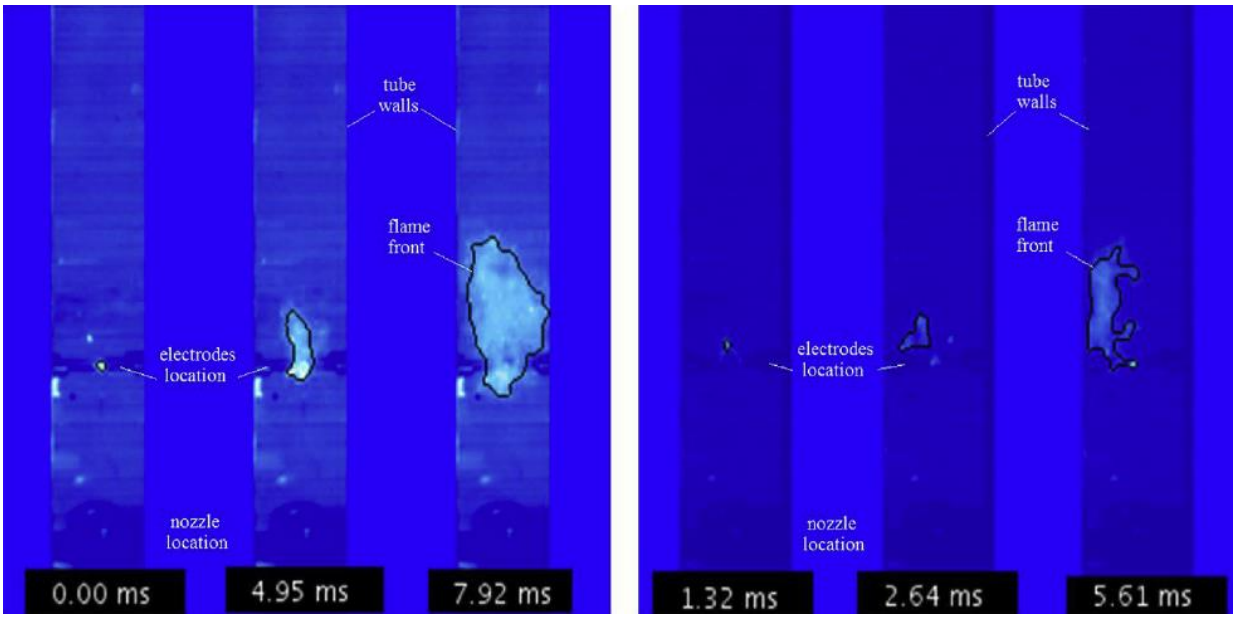

Figure 57. Flame propagation of 10.5% methane/30 mg Corax N550 mixture at v_{rms} = 0.9 m.s^{-1}(left) and 12% methane/30 mg Corax N550 mixture at v_{rms} = 1.4 m.s^{-1} (right).

The method developed by Andrews and Bradley (1972) allows to estimate the combustion velocity of a moving turbulent mixture, but its assumptions and limitations must be considered in order to analyze possible deviations from the reality of the phenomena. In order to estimate S_u, the model assumes a constant density of unburnt gases with respect to the tube cross-section surface which is difficult to guarantee, especially for highly turbulent systems. Additionally, the model assumes that the increase in temperature is due to an adiabatic compression of the unburnt gases, which represents a deviation from the actual compression of the gases. Moreover, the thermal expansion correction of the flame velocity is performed from the beginning of the ignition until the end of the propagation. This correction can generate a deviation in the S_u value because the thermal expansion of the gases has less influence in the first moments of the flame kernel growth than when the flame covers the entire tube cross-section. In the light of the above, the application of the linear relationship expression (Eq. 29) to gas/solid mixtures is still questionable and has to be validated (see section 3.2.2).

B. Spatial velocity of methane/Air mixture explosion

In order to validate the flame tube propagation method using the Matlab Simulink model and the relationships previously described (see section 3), measures of the flame velocity of methane/air mixtures has been performed at different initial turbulence levels (Figure 58). The spatial velocity of the flame increases during the flame propagation and seems to be sensitive to the initial turbulence level. For a quiescent system, the flame spatial velocity seems to increase constantly over the time for the flame kernel propagation but its slope increases after 5 milliseconds of propagation, probably because of the indirect interaction with the tube walls. Moreover, for a fuel rich mixture, the flame spatial velocity increases from 133 cm/s to 439 cm/s (before 5 ms after the ignition) when the initial turbulence of the system is augmented. However, the flame spatial

velocity of the flame kernel propagation appears to have similar behavior of the two turbulence levels analyzed in this work (0-5 ms of propagation). After this first propagation, the flame spatial velocity of the mixture is higher for a system with an ignition delay of 120 ms compared to an ignition delay of 60 ms (Figure 58). This trend could be explained because the flame appears to be strongly destabilized by the turbulent vortices presented at a very high initial turbulence level (tv=60 ms). It seems that the destabilization of the spherical flame propagation by the turbulent flow generates a considerable reduction in the spatial flame velocity. The determination of the unstretched burning velocity thanks to Eq.29 will be developed in the following paragraphs. The detection of the flame profile for methane-air mixtures during the first instants of the propagation is very difficult to obtain without physical filters and an adequate optical methodology. The development of the flame kernel growth will be analyzed in section 3.4 using Schlieren images. The spatial flame velocity has been also studied for stoichiometric mixtures at different turbulence levels (See Appendix A). The spatial flame velocity present similar behavior whatever the turbulence for different methane concentrations.

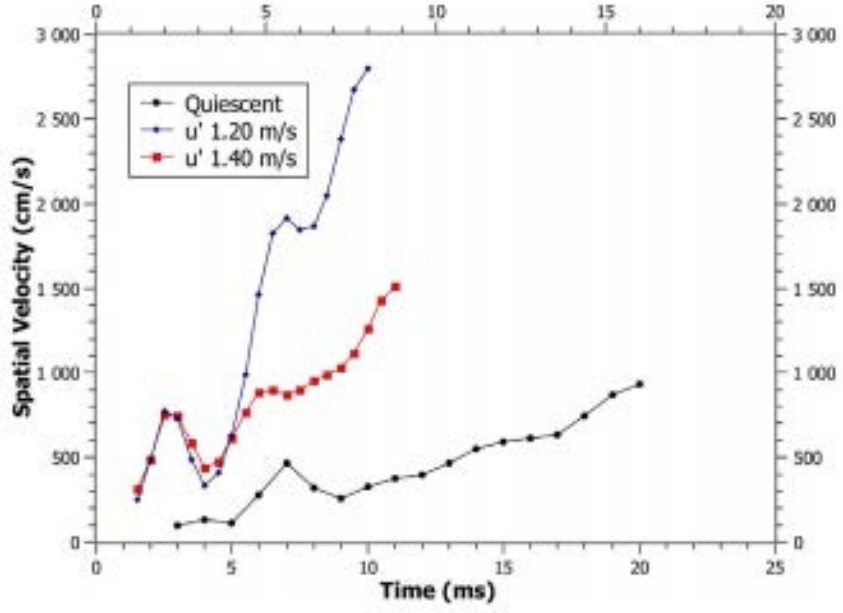

Figure 58. Spatial velocity of 12% Methane/air explosion at different initial turbulence level (related to an ignition delay tv).

C. Spatial Velocity of Carbon Black/Methane/Air Mixture Explosions

Before analyzing the influence of the initial concentration of carbon black nanoparticles on the burning velocity (this influence will be analyzed later on in section 3.3.1.D), reproducibility tests have been performed. Figure 59 shows the behavior of the spatial flame speed versus time for mixtures at different initial turbulence conditions. Repeatable results were obtained for explosions performed at a low initial turbulence (Figure 59 - up). Moreover, several experiments at the same turbulence (Appendix A) have shown a good reproducibility during the whole propagation except for the first two milliseconds of the explosion. This result is in agreement with the experiments reported by Cuervo (2017), obtaining a variability of approximately ± 3 cm.s^{-1} whatever the initial turbulence level. Regarding explosions with high initial turbulence (Figure 59 - down), the space velocity seems to have a similar trend with respect to time, and, however, a time lag is sometimes

observed. This behavior can be related to the presence of a continuous spark whose energy is proportional to its duration: due to the movement of the combustible cloud and its potential heterogeneity, ignition is sometimes obtained for a few milliseconds less/more for each replicate. Moreover, the small size of the initial flame kernel makes it perfect detection difficult. Thus, for some mixtures the flame profile detection is very difficult to identify, generating inaccurate estimations of the position and flame velocity. Such time lag does not change the slope of the spatial velocity and thus the flame's acceleration.

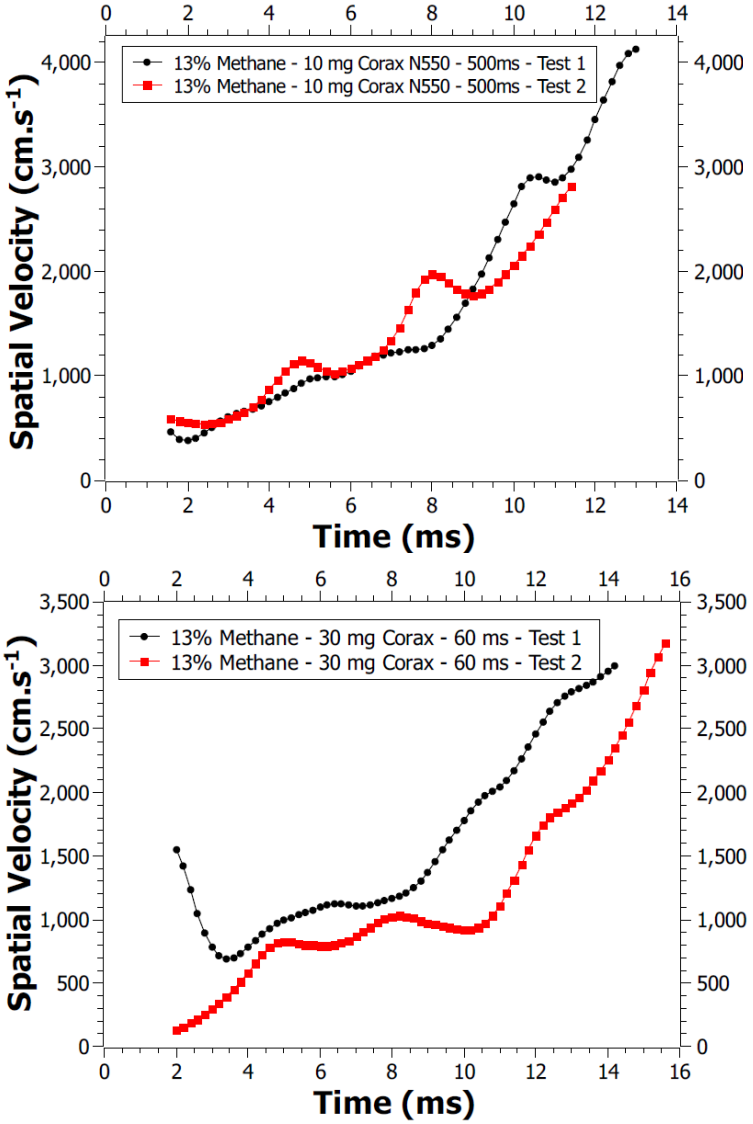

Figure 59. Spatial velocity of two different tests for a mixture of 13% Methane and 10 mg of Corax N550, at v_{rms} = 0.9 m.s^{-1} (Up) and a mixture of 13% Methane and 30 mg of Corax N550, ignition delay at v_{rms} = 1.4 m.s^{-1} (Down).

Figure 60 shows the behavior of the space velocity with respect to time for a hybrid explosion 10.5% molar concentration of methane/30 mg Corax N550 at an ignition delay time of 500 milliseconds. It can be seen that the flame speed globally tends to increase with time, with slope changes at specific points of the propagation. These inflection points are associated to considerable

changes on the flame deformation or physical interactions of the flame with the tube walls. The identification and understanding of these points is essential to ensure the validity of such analysis. The first two inflection points of the flame spatial velocity (Figure 60A) can be associated with the interaction of the flame with the glass walls of the tube, which do not allow a visual detection. The space velocity of the flame has a third inflection point at 5.6 ms when the flame stretching leads to a semi-spherical profile of the flame. Finally, the flame speed is affected by the presence of the stainless-steel walls, touching the left wall of the tube at 7.92 ms after ignition and the right wall 1.62 ms later. The aim of this work is not to analyze the flame/wall interaction but to focus on the flame propagation itself. As a consequence, only the pseudo-spherical development of the flame has been considered, and the parabolic flame propagation after the wall interaction has not been analyzed in this study. It should be reminded that the flame propagation tests are performed in an existing equipment, which its small cross-section limits the study of the kernel growth.

D. From the Flame Spatial Velocity to an unstretched Flame Velocity

As previously discussed, Markstein (1964) proposed a linear relationship between the burning combustion of the flame and its deformation (Eq. 29). Figure 60B shows its application to the test described above. It has been found that each interaction point between the flame and a tube wall, or drastically changes in the deformation of the flame (inflection points) generates a drastic change in the slope of the graph S_u-K. Some of the interactions of the flame with the tube that generates a change in the deformation can be visually identified and their effect on the burning rate can be realized. It should be reminded that such slope modifications express a change in the flame stability. Figure 60 shows that a positive Markstein length is obtained when an initial stretched flame starts a pseudo-spherical propagation, change that seems to stabilize the flame. On the other side, the interaction of the flame with the left wall at 7.92 ms produces a negative Markstein length that destabilizes the flame. Finally, the burning velocity values during the propagation are observed on the Figure 60, which lies between 5 and 25 $cm.s^{-1}$.

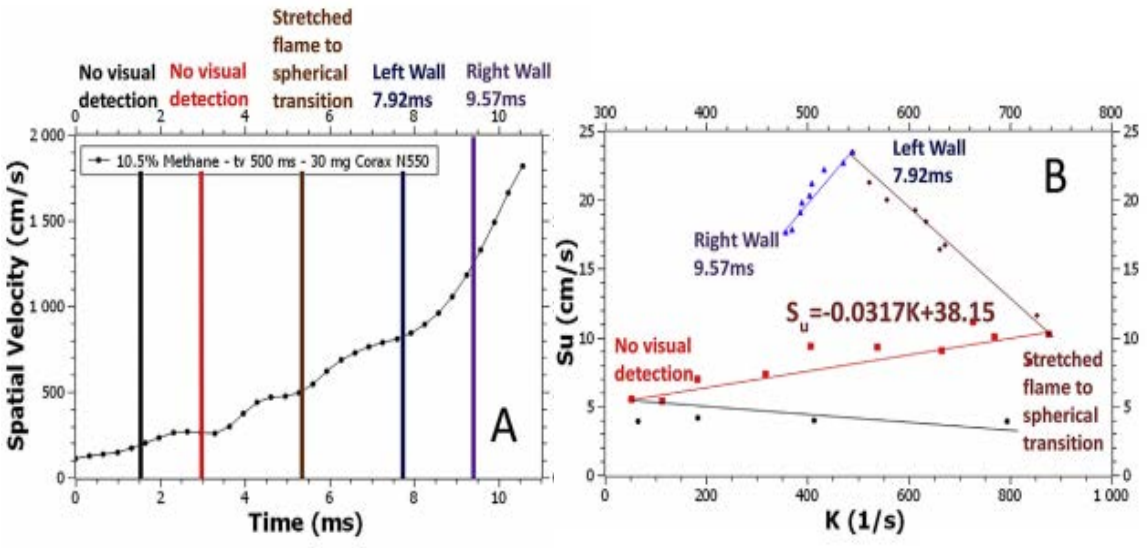

Figure 60.Spatial velocity behavior (A) and burning velocity - stretching relation (B) of 10.5% Methane/30 mg Corax N550 explosion at ignition delay 500 ms.

The flame propagation was evaluated for methane/nanoparticles Corax N550 mixtures at different gas concentrations. The chemical reaction seems to be greatly modified by the turbulence level at

different gas concentrations. In the case of a mixture of 10 mg Corax N550/methane at low initial turbulence (500 ms ignition delay), the flame speed is maximum under stoichiometric conditions (Figure 61 - Up), obtained at 9% molar concentration of methane (Fuel Equivalence Ratio, $\varphi = 1$). For the explosion of hybrid mixture at 8.5 % and 10.5% methane concentration, the spatial velocity seems to have similar trends, however a time lag is observed. This result suggests that the initial concentration of gas generates a difference in the ignition of the mixture, but appears to have no influence on the subsequent propagation of the flame. For the case of a rich mixture the initial concentration appears to have an effect on both the ignition of the mixture and the flame propagation, during which the slope of the curve is significantly smaller compared to mixtures near stoichiometry. Regarding an initial turbulent system (Figure 61 - Down), the gas concentration does not influence the flame propagation during the flame kernel growth, as shwon by the similar values of the spatial velocity. However, after 4 ms, the flame spatial velocity is different for the three gas concentration, which seems higher for rich mixtures. Furthermore, a larger initial turbulence of the system appears to accelerate the pseudo-spherical flame propagation at the same gas concentration, because the flame spatial velocity could be duplicated at high turbulent systems. The previous results agree with the severity results in the 20 L sphere, which suggests considerable modifications of the severity parameters when the Fuel Equivalence Ratio (FER) and the initial turbulence level were modified in the system (see Chapter 2).

Figure 62 shows the influence of the initial concentration of nanoparticles on the spatial velocity of the flame, for a 12% methane/Corax N550 mixture at high initial turbulence (up) and a 8.5% methane/Corax N550 mixture at low initial turbulence (down). The flame spatial velocity tends to decrease when the dust concentration increases in the initial mixture (Figure 62 - Up). However, the slope of the spatial velocity curves is not modified, which means that the presence of more dispersed nano-dust does not change significantly the flame acceleration. This result suggests that the nanoparticles seem to decrease the kinetics of the flame kernel growth but there is no modification on the posterior flame propagation. These trends could be explained regarding the changes in the radiative heat exchanges and the possible effect of the nanoparticles deagglomeration on this phenomenon. Similar results were obtained at lower initial turbulence (Figure 62 - Down), suggesting that the spatial velocity diminution does not just depend on the initial turbulence of the system.

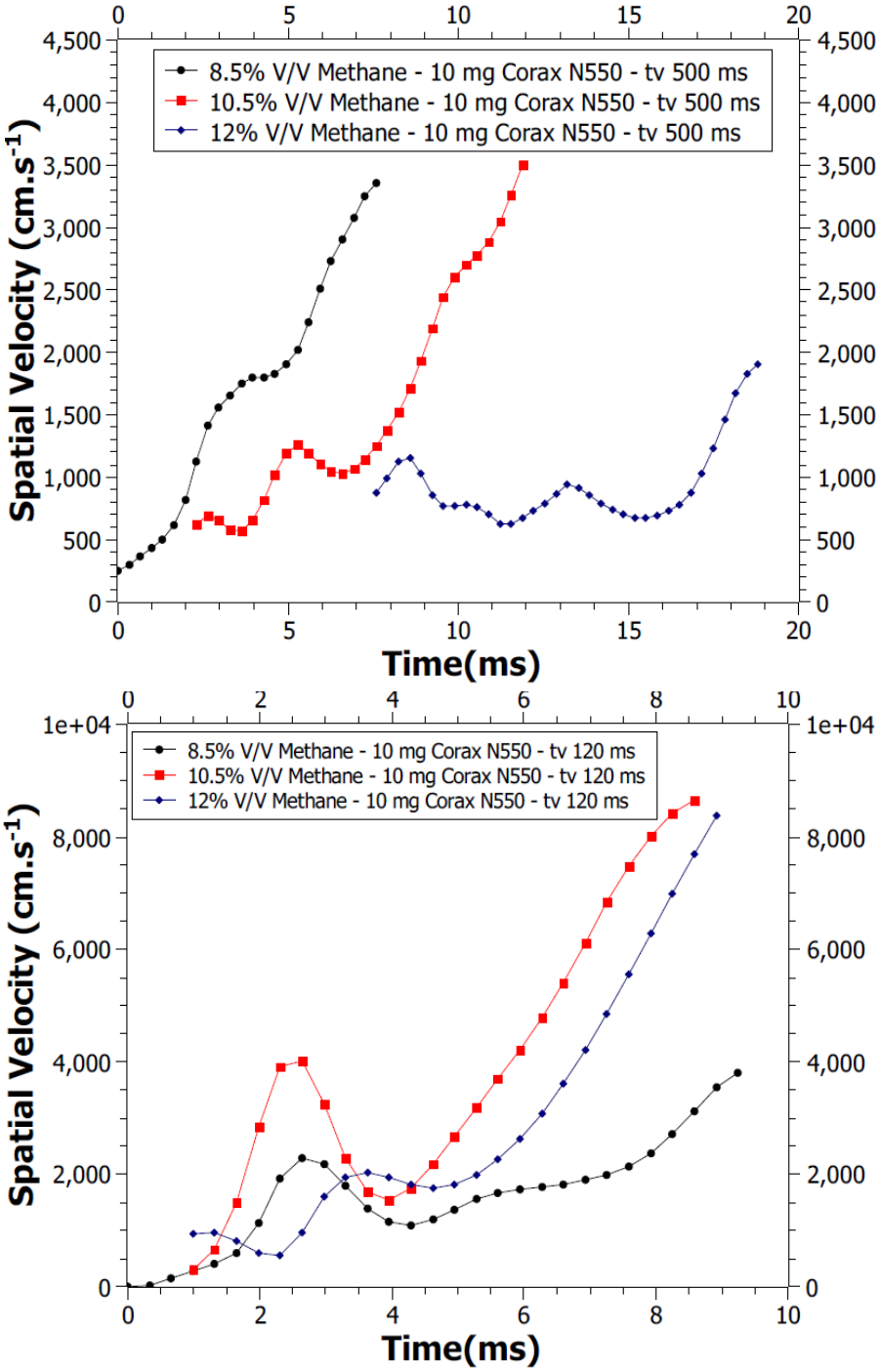

Figure 61. Influence of the gas concentration on the flame spatial velocity for a Methane/10 mg Corax N550 mixture at v_{rms} = 0.9 m.s^{-1} (Up) and at v_{rms} = 1.4 m.s^{-1} (Down)

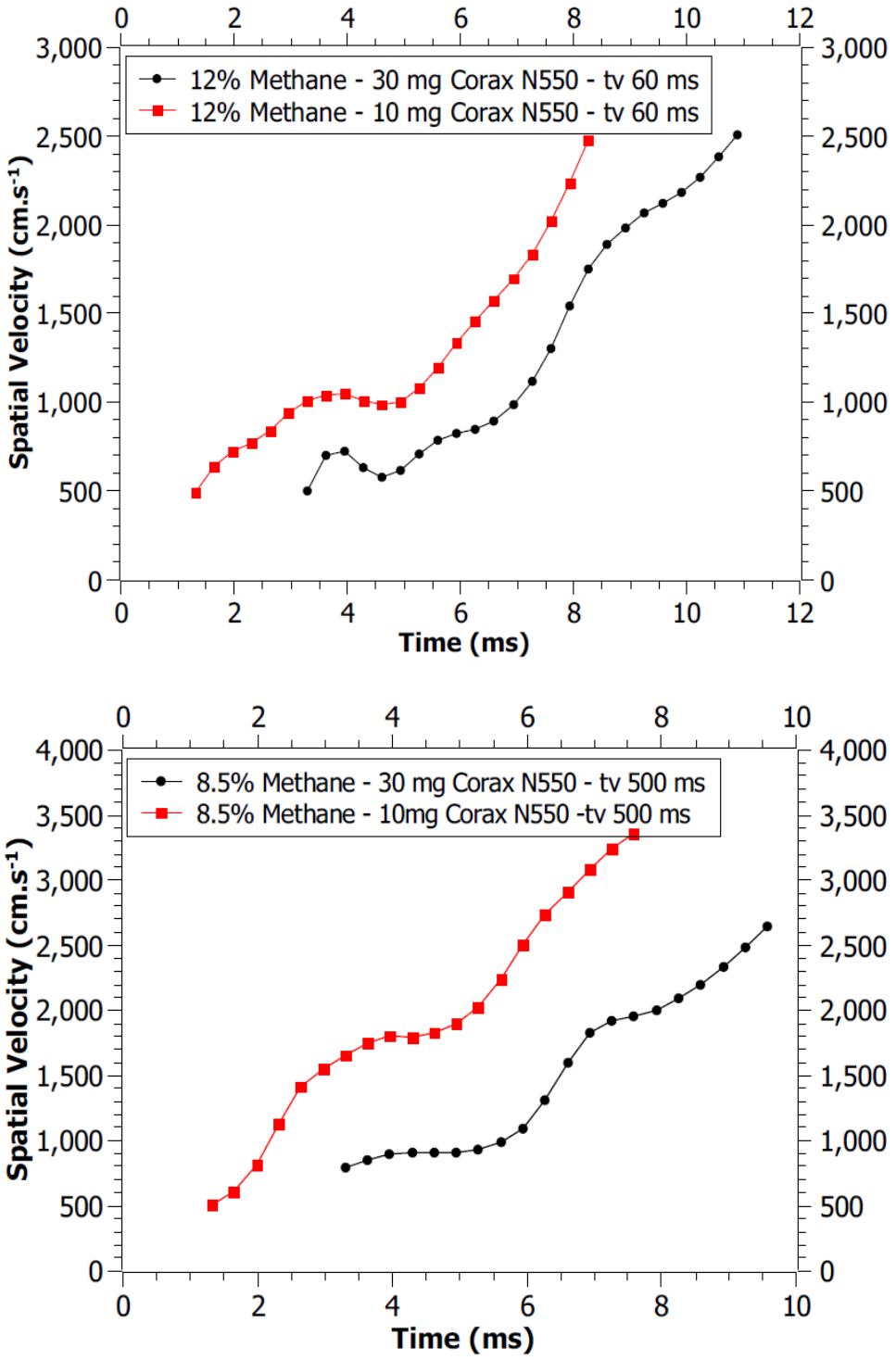

Figure 62. Influence of the nanoparticle concentration on the flame spatial velocity for a Methane/10 mg of Corax N550 at tv=60ms (Up) and at tv=500 ms (Down).

The unstretched flame velocity is estimated for the pseudo-spherical propagation of the flame for methane/air and methane/Corax N550/air explosions using the linear relation between the burning flame velocity and the Karlovitz factor (Eq. 29). Figure 63 shows the burning velocity-stretch factor relation of a 12% methane/air flame propagating under initial quiescent conditions. Negative values of the Markstein length have been initially obtained until the development of pseudo-spherical flame propagation. Then, positive values of the Markstein flame were obtained, showing stable flame propagation. The unstretched flame propagation velocity is 27.4 cm/s for 12% methane/air mixture (φ = 1.3) under quiescent conditions, which is lower than the literature values for stoichiometric mixtures between 34 and 38 $cm.s^{-1}$ (Dirrenberger et al., 2011; Proust, 2006). This discrepancy is explained by the incomplete combustion of the rich mixture. Similar results, i.e. burning velocities ranging between 24 and 29 $cm.s^{-1}$ for 1.3 fuel equivalent ratio, have been obtained by Buffman et al.(2008) and Dirrenberger el al. (2011).

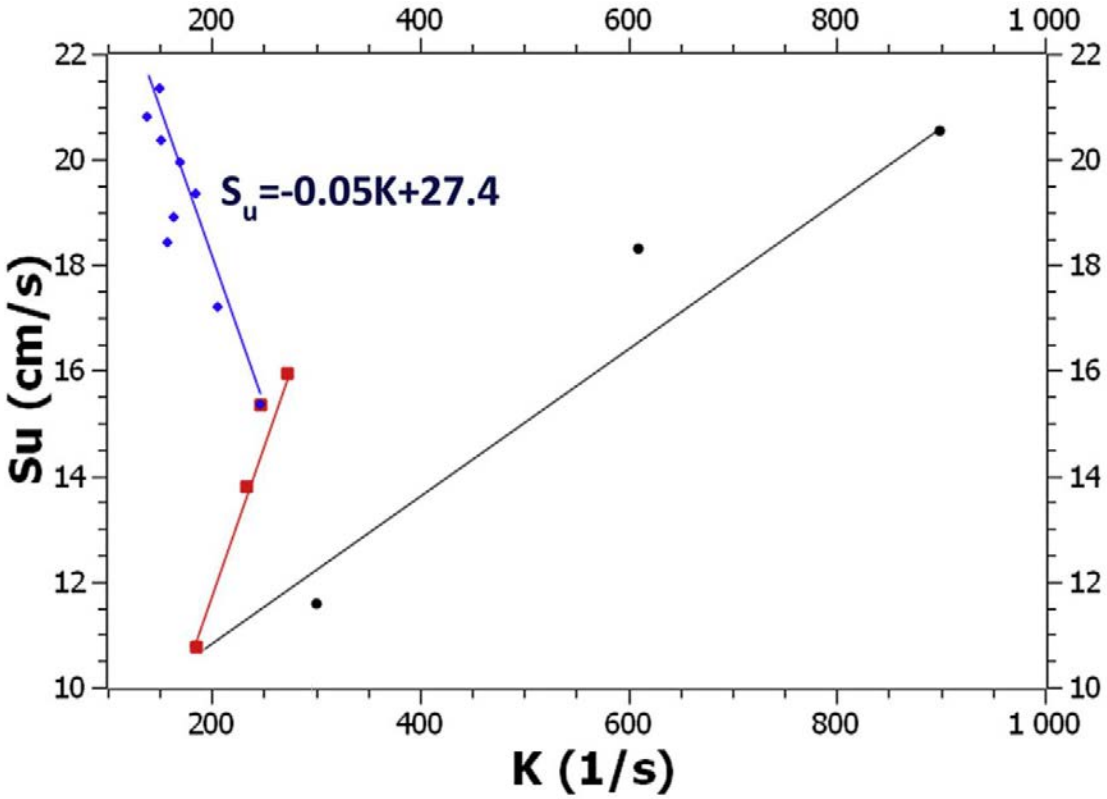

Figure 63. Burning velocity – stretching relation of 12% Methane quiescent conditions

The unstretched burning velocity for 10 mg Corax N550/10.5% methane mixtures are presented in Figure 64 at two different initial turbulence levels. The unstretched burning velocity of this mixture at an ignition delay of 500 ms (Figure 64A) diminishes from 52 to 38 $cm.s^{-1}$ when the initial turbulence level is augmented at an ignition delay of 60 ms (under the conditions of Figure 60B). This trend shows a good agreement with the behavior encountered for the spatial velocity, which may be reduced because the modifications on the radiative heat transfer when the nanoparticles concentration is augmented on the system. These differences on the radiative heat transfer will be easily evidenced in the Schlieren images presented below (section 3.4). Although the spatial velocity seems increased when the initial turbulence level augments, the S_u^0 behavior suggests that the turbulence increases the flame surface, which diminishes the burning velocity (Eq.28).

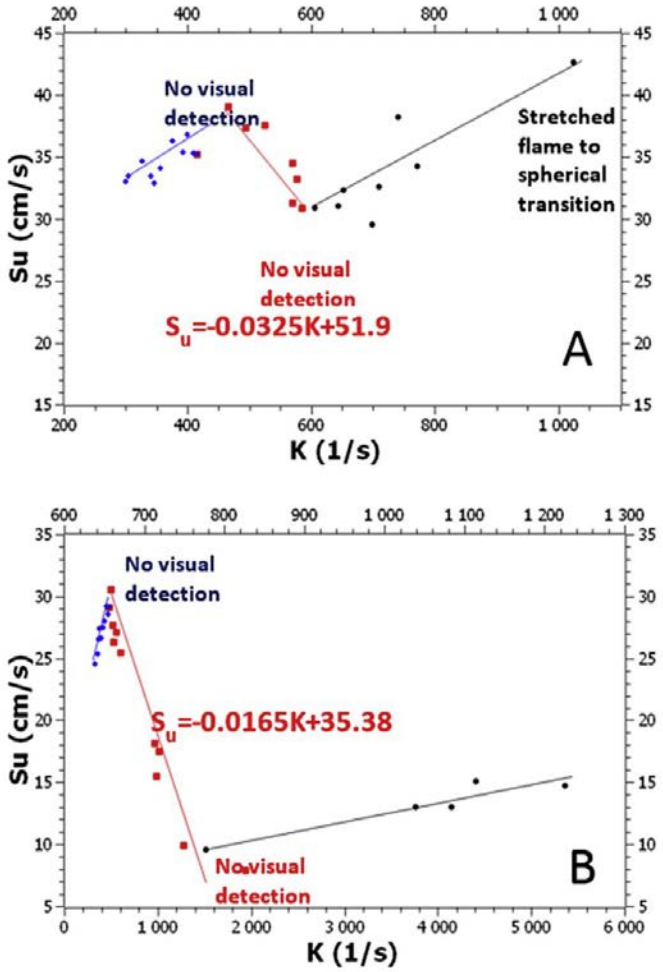

Figure 64. Burning velocity – stretching relation of 10.5% methane/10 mg Corax N550/ explosion at 500 ms ignition delay (A) and 10.5% methane/10 mg Corax N550/ explosion at 60 ms ignition delay (B).

Table 13 summarizes the results obtained for the unstretched burning velocity at three gas concentrations, two concentrations of carbon black nanoparticles and three initial turbulence levels. A clear evolution of the unstretched flame velocity with the gas concentrations is not obtained for neither gas nor hybrid mixtures. In addition, for almost all the gas concentrations, the unstretched flame velocity is higher an at intermediate turbulence level (v_{rms} = 1.4 m.s^{-1}/t_v = 120 ms). At the highest turbulence level studied in this work (v_{rms} = 1.6 m.s^{-1}/t_v = 60 ms), the unstretched velocity decreases in comparison to low turbulence levels (v_{rms} = 0.9 m.s^{-1}/t_v = 500 ms), which suggests that the flame is greatly destabilized by the turbulent flow. Regarding the influence of dust concentration, at t_v = 500 ms, the unstretched flame velocity seems to increase for fuel lean mixtures but decrease for stoichiometric and fuel rich mixtures. For high turbulent systems, it was not possible to establish a clear trend. More experiences should be performed in order to determine if the same evolutions are obtained or the variability of the tube method does not allow to generate clear conclusions.

Table 13. Unstretched burning velocity for gas and hybrid mixtures estimated deduced from the experiments

Ignition delay time t_v (ms)	**Root-Mean-Square velocity ($m.s^{-1}$)**	**Methane $S_u^0(cm.s^{-1})$**			**Corax $S_u^0(cm.s^{-1})$**							
					10 mg				**30 mg**			
		8.5%	**9%**	**12%**	**8.5%**	**9%**	**10.5%**	**12%**	**8.5%**	**9%**	**10.5%**	**12%**
60	1.6	37	48	30	21	29	35	21	33	18	34	53
120	1.4	71	33	77	80	66	113	38	31	91	44	38
500	0.9	24	29	33	50	49	52	14	60	37	38	6

3.3.2. Alumina/methane/air mixtures

The chemical contribution of carbon black nanoparticles in the explosion severity had been tested comparing the results with hybrid mixtures explosions with inert AP-D alumina particles. The maximum overpressure and maximum rate of pressure rise results suggest that the dispersion of inert nanoparticles produce modifications on the explosion severity parameters (see Chapter 2.4.2), which may be related to perturbations in the flame surface and a possible contribution of the radiative heat transfer. In order to analyze the influence of dispersed nanoparticles on the flame stretching and burning velocity, the explosion of AP-D alumina/methane/air hybrid mixtures had been performed in the flame propagation tube.

Influence of the powder chemical nature

The flame spatial velocity of methane/air, alumina/methane/air and carbon black/methane/air mixtures at an initial turbulence v_{rms} = 1.4 $m.s^{-1}$ (i.e. ignition delay time tv = 120 ms) for two powders concentrations is presented in Figure 65 (tests performed at 9%v. methane). As previously mentioned, the flame detection of the first two milliseconds of the flame kernel growth is very difficult because of the high instabilities created by the initial turbulence and of the low luminosity of the flame kernel (Figure 65). For this reason, the flame velocities are analyzed from 2 or 3 ms to until approximately 10 ms, moment at which the flame interacts with one of the tube walls.

A similarevolution of the spatial velocity for the gas and hybrid mixtures is evidenced; nevertheless, a greater initial velocity is obtained for the methane/air mixture. This result could be explained by two different phenomena: a) the flame moves upwards from the spark ignition zone and a stretched flame is generated (fast transition between a semispherical propagation and a semiparabolic propagation (Cuervo, 2015); b) a fast displacement of the ignition point is generated because of the high initial turbulence. The presence of dispersed particles in the mixtures appears to decrease the initial ignition velocity and impacts the subsequent flame propagation (Figure 65a). The flame kernel stretching is increased by the presence of particles, which limits the flame acceleration but also affects the experimental reproducibility when the tests are performed close to the flammability limits.

After 6 milliseconds, the flame spatial velocity of methane/air mixtures decreases by 40% when 2.5 $g\text{-}m^{-3}$ of Corax N550 are dispersed in the tube, probably as a result of the radiative heat transfer as shown in paragraph 3.3.3. Furthermore, when comparing the flame propagation of the hybrid mixtures explosion of alumina and carbon black nanoparticles, the dispersed dust seems to modify the initial ignition of the mixture, but the similarities in the slope of the flame spatial velocity of both mixtures suggest that the subsequent propagation is not significantly affected by the nature of the dispersed particles.

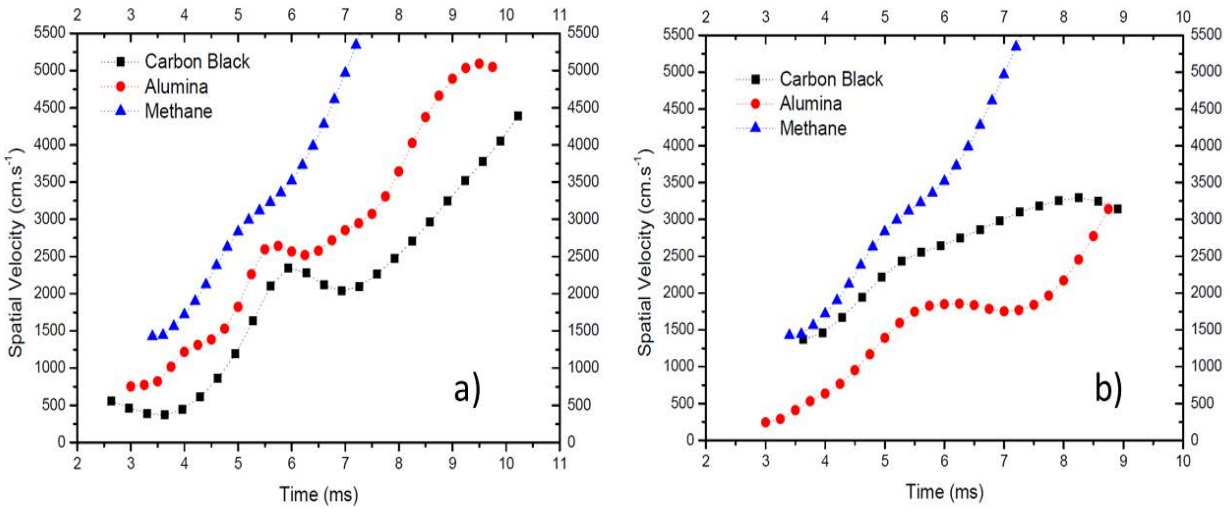

Figure 65. Flame spatial velocity of methane/air, AP-D/methane/air and Corax N550/methane/air for a) 2.5 g.m^{-3} and b) 6 g.m^{-3} dust concentration. Initial turbulence level vrms = 1.4 m.s^{-1} and 9% methane molar concentration.

When the dust concentration is augmented from 2 g.m^{-3} to 6 g.m^{-3}, a different behavior is obtained (Figure 65b). A higher carbon black concentration induces a higher initial flame velocity but a reduction of the flame acceleration compared to the gas and AP-D alumina/gas mixtures. The flame spatial velocity of AP-D alumina/methane/air mixtures appears to be lower than the one of mixtures with the same concentration of carbon blacks. Nevertheless, it is more accurate to consider that the initial expansion rate of flame kernel is lower for alumina than for carbon blacks mixtures. Once again, the nature of the particle presence has not only an effect on the global reaction kinetics (combustible powder or inert one), but can also affect other phenomena as the heat transfer or it can promote nucleation of combustion products.

Influence of the initial turbulence

The flame propagation of gas and hybrid mixture explosions have been also analyzed for a very low initial turbulence of v_{rms} = 0.9 m.s^{-1} as shown in Figure 66. The flame velocity of methane/air mixture is slightly but not significantly enhanced by the initial turbulence of the explosive atmosphere. Regarding the hybrid mixtures, the results show that the AP-D alumina and carbon black nanoparticles are still dispersed 500 ms after the dispersion, generating a considerable reduction in the flame velocity. This result is consistent with our previous experiments carried out by using DMA and UCPC and showing that nanopowders are still present in the tube even after a few seconds (section 2.2.1 - Chapter 2).

Figure 13a shows that the insertion of dust nanoparticles decreases the flame acceleration mostly until 6 ms, compared to gas mixture explosion. When the carbon black concentration is increased to 6 g.m^{-3}, the flame spatial velocity decreases by 30% for low turbulence systems. However, non-significant changes on the flame velocity are observed when the same AP-D alumina concentration is added (Figure 66b). The similarities on the spatial velocity of AP-D and Corax N550 hybrid mixtures at 6 g.m^{-3} suggest that the modifications on the flame propagation are likely to be caused by surface and thermal heat transfer rather chemical modifications of the system. Such assertion has to be verified by taking the flame stretching into account.

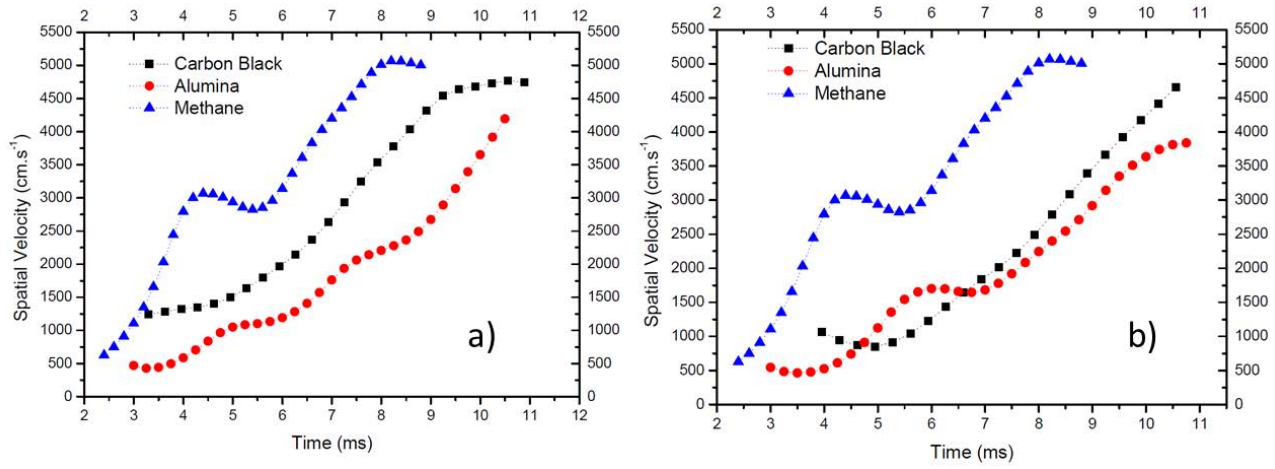

Figure 66. Flame spatial velocity of methane/air, AP-D/methane/air and Corax N550/methane/air for a) 2.5 g.m^{-3} and b) 6 g.m^{-3} dust concentration. Initial turbulence level v_{rms} = 0.9 m.s^{-1} and 9% methane molar concentration.

Unstretched flame velocity of alumina/methane/air mixtures

The unstretched flame velocity S_u^0 is estimated for the semi-spherical flame propagation for methane/air, Corax N550/methane/air and AP-D alumina/methane/air using the linear relation between the burning velocity and the Karlovitz factor, as presented in Eq 29. The estimated values of the unstretched burning velocity, at initial turbulence levels vrms = 1.4 m.s^{-1} and vrms = 0.9 m.s^{-1}, are presented on Table 14. The unstretched flame velocity of methane/air mixture at stoichiometric conditions are 29.8 and 33.4 cm.s-1 for initial turbulence level of vrms = 0.9 m.s^{-1} and vrms = 1.4 m.s^{-1} respectively. The estimated value at turbulent conditions is close to burning flame velocity values reported on the literature, between 34 and 38 cm.s^{-1}, for methane/air mixture at stoichiometric conditions (Andrews and Bradley, 1972b; Bradley et al., 2017; Dirrenberger et al., 2011). The unstretched flame velocity seems to slightly decrease 10% when the mixture is ignited at low turbulent conditions for gas explosion. It should be stressed that the dispersion mode of the gas (by an air pulse) is not the usual condition used to determine the laminar burning velocity of pure gas.

Regarding the hybrid mixture explosion, the measured burning velocities changes when low concentrations of dust are injected in the system. In the case of carbon blacks, higher unstretched burning velocity of Corax N550/methane/air mixtures are obtained compared to methane/air mixtures. The flame front of the carbon black hybrid mixtures is greatly destabilized by the presence of dispersed particles and agglomerates, generating an stretched/wrinkled flame (Torrado et al., 2016). A different behavior of the burning velocity of Corax N550/methane/air mixture had been found for the two turbulent levels studied on this work. As expected, this evolution shows that the unstretched flame velocity still depends on the initial properties of the explosive atmosphere and is not only dependent on its chemical composition. This trend could then be explained because, at higher turbulent levels, the deagglomeration phenomenon is augmented, increasing the surface of the reaction zone and the burning velocity, but also because of potential spatial heterogeneity in the initial dust cloud (Murillo, 2016).

Table 14. Unstretched burning velocity for gas and hybrid mixtures estimated deduced from the experiments

Ignition delay time – t_v (ms)	**Methane**	**Corax** $S_u^0(cm.s^{-1})$		**Alumina** $S_u^0(cm.s^{-1})$	
	$S_u^0(cm.s^{-1})$	**10 mg**	**30 mg**	**10 mg**	**30 mg**
120	33.4	66.7	91.1	28.8	39.3
500	29.8	49.2	37.2	36.3	87.2

The unstretched burning velocity estimated for AP-D alumina/methane/air mixtures are considerable higher than those obtained for gas mixture explosions. The previous results and specifically the fact that flames with similar spatial velocities can exhibit different unstretched burning velocities, suggest that the presence of solid particles such as alumina modifies the flame surface during the propagation.

The previous results do not allows to quantify the chemical reaction contribution of the carbon black nanoparticles dispersed in the system. Nevertheless, the insertion of inert particles shows considerable modifications of the flame propagation due to perturbations on the flame surface. In consequence, it is not possible to eliminate the contribution of the chemical reaction, and instead, the results shows that the influence of dispersed nanoparticles should be due to the interaction of different contributions (chemical reaction, radiative transfer and modifications on the flame surface). In addition, the flame propagation results should be analyzed with caution, because even if the total dust concentrations had been chosen to have a comparable total surface of carbon black and alumina particles, considerable differences in the deagglomerations and dispersion of the particles can be obtained. Further experiments must be implemented in order to have a more information about the concentration and particle size distribution of both dust clouds after dispersion. Finally, in addition to the surface flame modifications, the presence of nanoparticles generate modification on the radiative heat transfer and it will be analyzed in the following section.

3.3.3 Influence of the radiative transfers

Table 14 also shows a considerable difference between the alumina and carbon black hybrid mixtures unstretched burning velocities. It tends to prove that the heat transfer (radiation) and chemical kinetics modifications (radical recombination on a solid surface, for instance) due to the presence of particles influence the flame burning velocity. Such assumption on the influence of the radiative transfer on the flame propagation has already been validated (see section 2.5, Chapter 2) and is illustrated by the Figure 67. In the visible spectrum, the addition of particles has an impact both on the flame speed and on its radiation. For carbon blacks/methane/air mixtures (Figure 67b), the radiation is more intense than for alumina/methane/air (Figure 67c), the latter mixture exhibiting itself a brighter flame than pure methane/air flames (Figure 67a). As previously mentioned, the difference between alumina and carbon blacks optical properties can notably explain this observation (i.e. the emissivity of alumina is 0.07, compared to 0.97 for carbon particles). Moreover, the luminosity of carbon blacks/methane/air flames and the presence of ‘bright points’ (especially Figure 67b and c) are characteristic of carbon formation and light emission from hot soot particles (Rubtsov, 2016). In fuel-rich flames, soot is generated from highly

unsaturated molecules through polycyclic aromatic hydrocarbons, before a condensation phase (Griffith and Barnard, 1995). The presence of nanoparticles in the unburnt gases can affect this peculiar step, i.e. the transformation from a molecular to a particulate system. Once again, it appears that the soot nucleation and the radiation transfer are strongly correlated and that decoupling the effects of these phenomena on the flame propagation is challenging.

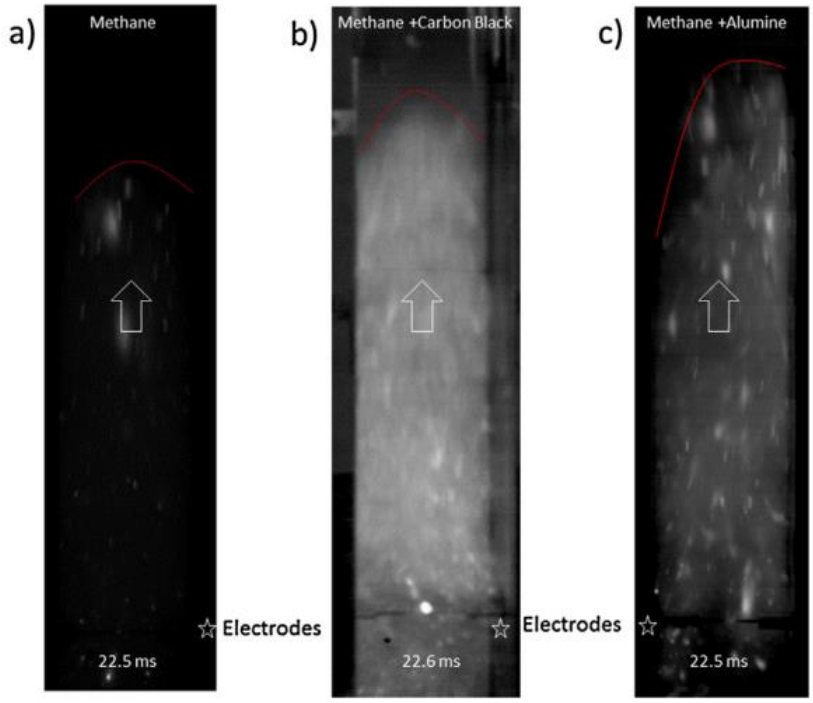

Figure 67. Visualization of flame propagation at an initial turbulence level of 1.4 $m.s^{-1}$ for a) a 9%v. methane/air explosion, b) for 10 mg Corax N550 dispersed in a 9%v. methane/air mixture explosion, and c) for 13 mg APD-Alumina dispersed in a 9%v. methane/air.

3.4. Burning velocity from severity tests

As it has been highlighted in the section 1.4, the cubic-law extrapolation (Eq 1) could be inaccurate to scale-up laboratory results to plant size equipment, generating oversizing or under sizing of the protection equipment. While the cube root-law uses a single instant of the rate of pressure rise, balance integration models take in account the entire pressure evolution during explosion. In addition, since their derivation is based on fundamental relationships between the pressure development and the mass burning rate at any instant, the effect of all external parameters on the transient combustion process is included in the model. It has been proposed to use the mass burning rate in balance models, which requires the burning velocity and the flame thickness as fundamental parameters. In the following paragraphs the thin flame model for the estimation of the burning velocity from the explosion severity results on closed explosion vessels is described (Dahoe, 2000; Dahoe et al., 1996). This model is related to the cubic law and it has been chosen because the burning velocity is estimated in an explosion sphere from the rate of pressure rise and the mass burning rate.

3.4.1. Thin flame propagation model

During the explosion, the content of the vessel is divided in two different spherical regions, an inner region composed of completely burnt gases and the outer region consisting of the fresh gases. Both regions are separated by a thin interface (flame front) characterized by its position r_f .The flame front moves with a velocity S_f equals to the sum between the velocity of the expansion of the burnt mixture S_e, the velocity due to the reaction of unburnt gas molecules into the burnt mixture and the burning velocity S_u (Figure 68). Hence, the flame reaches the unburnt mixture with the burning velocity S_u, which describes the mass burning consumption and heat production of the fresh gases S_n (Dahoe et al., 1996). Dahoe (2000) proposed a model relating the burning velocity to the pressure and mass burning rate evolution, taking into account the hypothesis presented in Table 15.

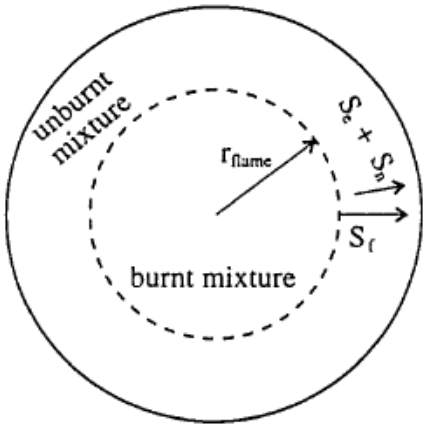

Figure 68. Model for a moving flame on a closed vessel assuming an infinitely thin flame thickness (Dahoe et al., 1996).

Table 15. Hypothesis of the thin flame model (Dahoe, 2000).

#	**Hypotheses**
1	The burnt and unburnt gases follow the ideal gas state equation.
2	Specific heats of both gases are the same, and it does not change during the explosion.
3	The reaction is described by an irreversible global reaction rate
4	The gas compression is assumed adiabatic.
5	The ignition source is located at the center of the vessel, and it does not generate overdriving (Cloney et al., 2013).
6	The burning velocity does not change during the explosion.

The mass fraction of the unburnt gases could be related to the fractional pressure rise as follows:

$$\frac{m_u}{m_{u_0}} = \frac{P_e - P}{P_e - P_0} \qquad \text{Eq 30}$$

A differentiation of this equation with respect to the time leads to:

$$\frac{dP}{dt} = -\frac{P_e - P_0}{m_{u_0}}\frac{dm_u}{dt} \quad \text{Eq 31}$$

The unburnt mixture enters the combustion wave with a velocity equals to minus the burning velocity, the mass burning rate is calculated as (Dahoe, 2000):

$$\frac{dm_u}{dt} = -4\pi r_f^2 \rho_u S_u \quad \text{Eq 32}$$

By combining Eq 31 and 32, we obtain:

$$\frac{dP}{dt} = 4\pi \frac{P_e - P_0}{m_{u_0}} r_f^2 \rho_u S_u \quad \text{Eq 33}$$

Dahoe (2000) estimated the radius of the flame estimating the difference between the volume of the vessel and the volume of the unburnt gases. By this means, r_f is expressed as:

$$r_f = R\left[1 - \left(\frac{P_0}{P}\right)^{\frac{1}{\gamma}} \frac{P_e - P}{P_e - P_0}\right]^{\frac{1}{3}} \quad \text{Eq 34}$$

Finally, substituting the flame location on the rate of pressure rise equation, a complete relation between the rate of pressure rise and the burning velocity is obtained:

$$\frac{dP}{dt} = \frac{3(P_e - P_0)}{R_{vessel}}\left[1 - \left(\frac{P_0}{P}\right)^{\frac{1}{\gamma}} \frac{P_e - P}{P_e - P_0}\right]^{\frac{2}{3}} \left(\frac{P}{P_0}\right)^{\frac{1}{\gamma}} S_u \quad \text{Eq 35}$$

We will use this equation (Eq. 35) in order to estimate the burning velocity from the experimental values of the maximum rate of pressure rise and maximum overpressure obtained in the explosion severity test for gas and hybrid mixtures (see section 2.3).

3.4.2. Burning Velocity Results

The burning velocities of methane-air and nano-carbon black/methane/air hybrid mixtures from explosion severity tests presented on section 2.3.2 are estimated using the thin-flame model postulated by Dahoe (2000). Figure 69 shows the influence of the gas concentration and the concentration of nanoparticles for methane/ Corax N550/air mixtures (A) and methane/ Printex XE2/ air (B) mixtures. The burning velocity for a stoichiometric mixture methane/ air is about 32 $cm.s^{-1}$, which is close to the reported value for such mixtures (Bauffman and Cox, 2008; Dirrenberger et al., 2011; Proust, 2006). A similar order of magnitude of the burning velocity had been obtained for methane/air mixtures under quiescent conditions by using the flame propagation tube method (see section 3.3). In addition, the burning velocity of methane/air mixtures present a maximum value at the stoichiometric concentration and decrease considerably for $\varphi \neq 1$.

Regarding hybrid mixtures, an effect of the insertion of carbon black particles on the burning velocity is evidenced even for quiescent conditions. Figure 69 shows that the flame rate increases

for fuel lean mixture when an initial concentration of carbon black is added to the system e.g. 33% increase when 0.5 $g.m^{-3}$ of Corax N550 is added to the system for of 5.5% v. CH_4. Moreover, the particle size seems to have a significant effect on the burning velocity, since this variable presents a higher increase when 2.5 gm^{-3} of Printex XE2 are inserted in the system (i.e. 30 $m.s^{-1}$ compared to 15 $m.s^{-1}$ and 16 $m.s^{-1}$ for Corax N550/methane/air and methane/air mixtures respectively). Hence, this result agrees with the trends obtained for the explosion severity parameters, where the phenomena of fragmentation and dispersion seem to have a significant influence on the explosion violence. It should be reminded that the possible influences of dispersed nanoparticles in the explosion severity could be a chemical contribution to the reaction, heat transfer modifications between burnt/unburnt mixtures, modifications on the flame surface and a contribution as soot nuclei particles. The dispersion and fragmentation phenomena have a considerable effect on this contributions (Eckhoff, 2012; Murillo, 2016).On the contrary, the flame velocity seems to decrease considerably for carbon black hybrid mixtures compared to pure gas systems. For instance, at a methane concentration of 10% v. the burning velocity decrease around 45% when 2.5 $g.m^{-3}$ are added to the explosive mixture.

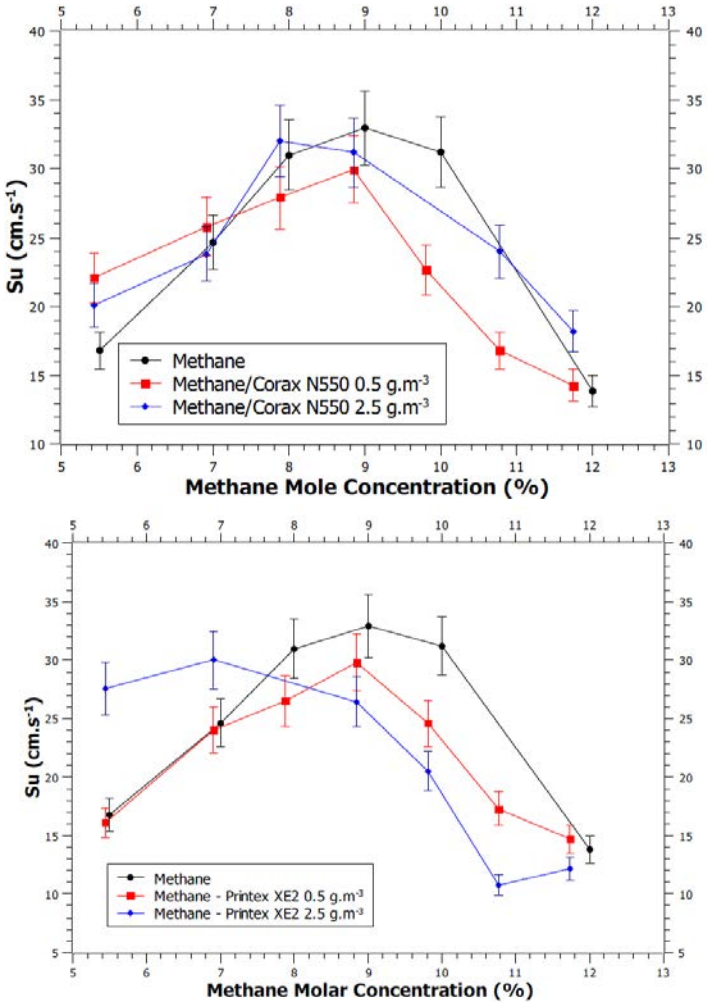

Figure 69. Burning velocity calculated by the thin flame model for Methane/Corax N550/Air (Up) and Methane/Printex XE2/Air (Down) for an initially quiescent system.

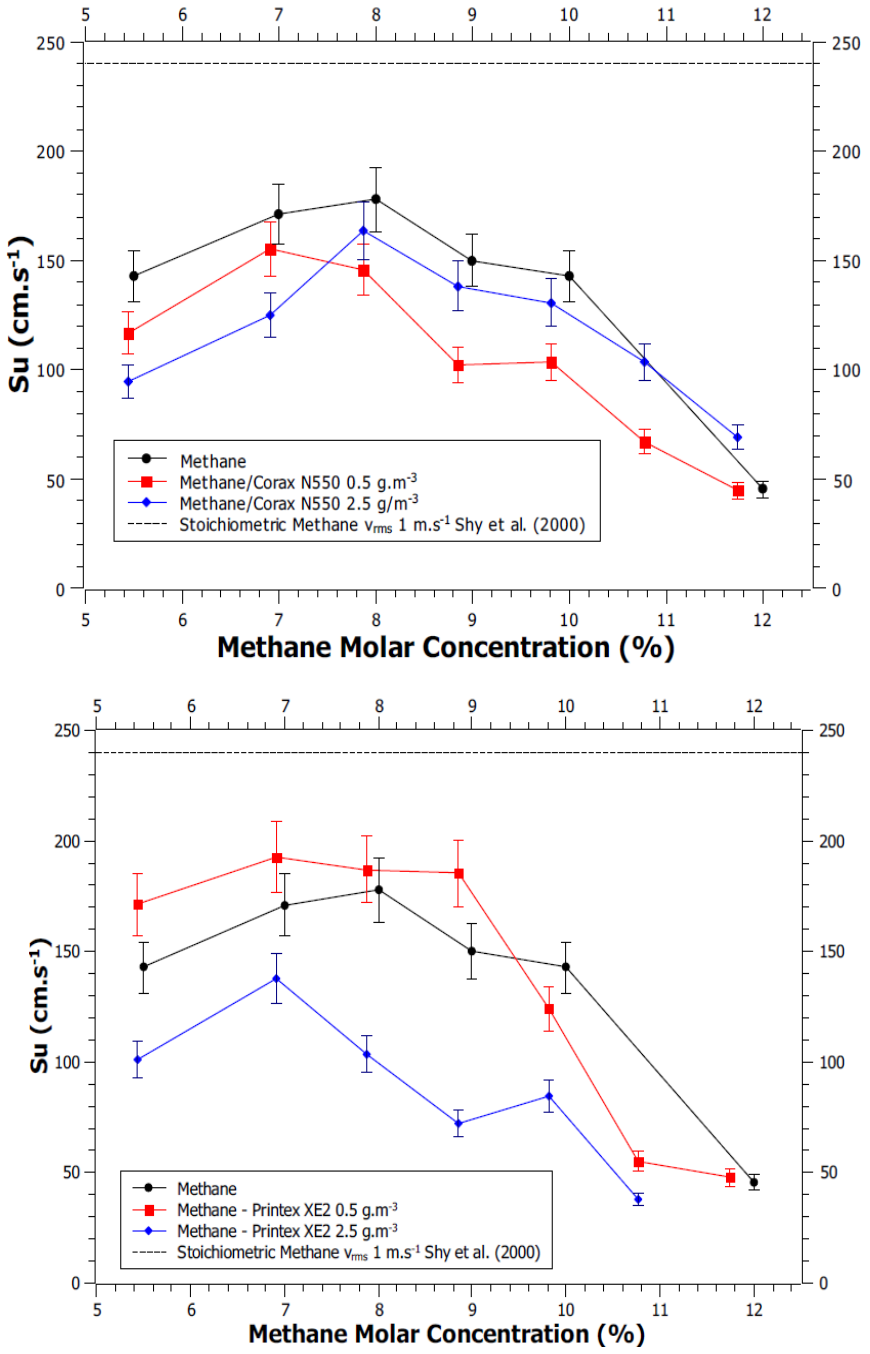

Figure 70. Burning velocity calculated by the thin flame model for Methane/ Printex XE2 /Air (Up) and Methane/Corax N550/Air (Down) for at an initial turbulence level u' = 1.6 $m.s^{-1}$

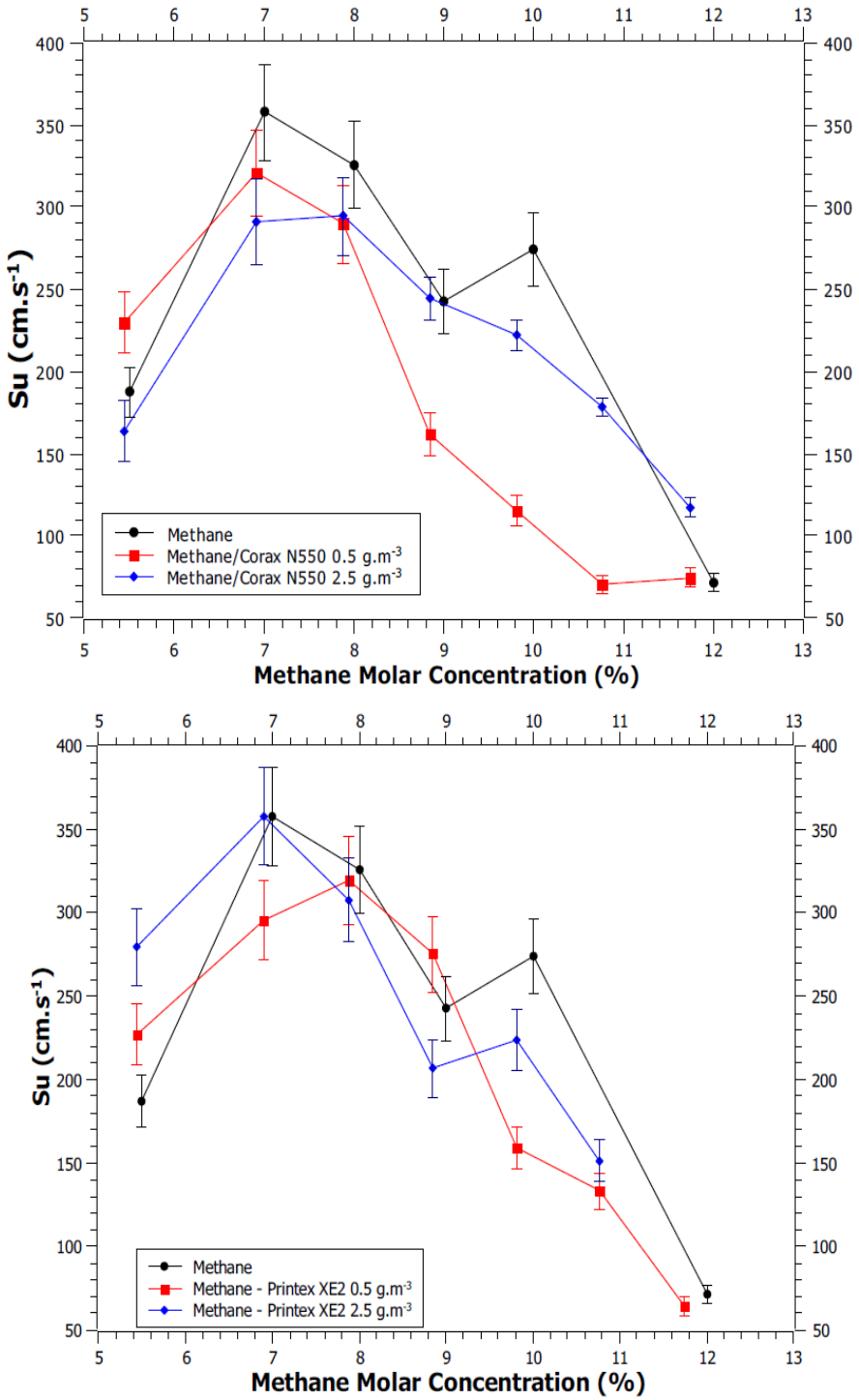

Figure 71. Burning velocity calculated by the thin flame model for Methane/ Printex XE2 /Air (Up) and Methane/Corax N550/Air (Down) for at an initial turbulence level v_{rms} = 5.8 m.s^{-1}

The estimation of the burning velocities (by Eq. 35) for the hybrid mixtures Printex XE2/methane/air and Corax N550/methane/air at an initial turbulence level of u' = 1.6 m.s^{-1} are presented on Figure 70. However, it should be underlined that this relationship may underestimate the burning velocity, because the flame thickness is often not negligible at high pressure and for

systems involving dispersed dust clouds. Likewise, as highlighted on Table 15, this model suppose a perfect spherical propagation of the front flame, which may be actually altered because of the interactions of the flame with the internal elements of the sphere, and, because of inertial effects created by the dispersion. Shy et al. (2000) reported a flame velocity of methane/air at stoichiometric concentrations of approximately 2.4 $m.s^{-1}$ at an initial turbulence of velocity fluctuation v_{rms}= 1.6 $m.s^{-1}$, which is higher than our estimated value of 1.74 $m.s^{-1}$. The addition of 0.5 $g.m^{-3}$ of Printex XE2 generates an increase of 20% on the burning velocity for fuel lean mixtures compared to gas mixtures, while a decrease is noticeable for fuel rich mixtures. These results suggest that the influence of the insertion of carbon black nanoparticles on the burning velocity is independent of the turbulence level, which increase compared to the burning velocity of methane/air mixtures whatever the initial turbulence of the system (Figure 70 and Figure 71).

In addition, the burning velocity is considerably reduced when the carbon black concentration is augmented to 2.5 $g.m^{-3}$, even if the maximal overpressure seems to be enhanced with the presence of a Printex XE2 dust cloud (Figure 43). Similarly, the presence of a dust cloud of Corax N550 generates a decrease of the burning velocity with respect to gas explosions. The previous behavior could be explained by two possible phenomena. On one hand, the increase of the radiative heat transfer caused by the dispersed dust may generate heat losses on the propagating flame front and will be enhanced by a higher turbulence level. On the other hand, the cloud dust may generate changes on the flame surface, generating local flamelet regimes (Dahoe et al., 2002; Skjold, 2003) and reducing the overall flame velocity, which has been observed on the flame propagation effects.

Additionally, the calculated burning velocities within the 20L sphere data can be underestimated due to the model hypotheses (Table 15). Firstly, the flame is assumed to be infinity thin, which may be acceptable for gas explosions but for the case of hybrid mixtures the flame thickness may not be negligible. The insertion of nanoparticles modifies the flame surface, generate local perturbation and may increase the thickness of the flame. Secondly, this model takes in account a global reaction rate, which it has been demonstrated that for gas and solid mixtures, simultaneous reactions are present and the generation of combustion radicals plays an important role on the flame velocity and explosion severity (the influence of semi-global kinetic mechanism will be analyzed in Chapter 4). Moreover, the burning velocity changes considerably during the propagation due to the interactions with the internal walls of the vessel and due to the high initial turbulence of the system, generating another deviation from the hypotheses of the model. Finally, in Figure 38 shows a considerable difference between an adiabatic system and the experimental results, showing that the assumption of an adiabatic system is not accurate. The insertion of carbon black modifies the heat transfer between the flame and he unburnt gases, which are not taken in account in the model and may generate a considerable deviation in the results.

3.5. Flame detection using Schlieren Images

As it was previously shown, both influences of radiation and turbulence/combustion interactions have to be quantified in order to study the flame propagation of carbon black/methane/air hybrid mixtures. However, both phenomena are interconnected and the presence of radiation sometimes hinders greatly the identification of the flame profile. It appears that interferometry is a technique which can help us in order to identify the flame front using the difference of densities between the burnt and unburnt gases, and thus limiting the impact of radiation. In other words, the flame surface estimation could be greatly enhanced if a correct identification of the flame front is performed.

3.5.1 Brief description of Schlieren method

Optical methods, as the interferometry, Schlieren and shadowgraph, intended to measure changes in the media exploiting the modifications on the refractive index with the media density. The density depends on the temperature and components concentration that will generate heterogeneities on the refractive index and as a consequence, will bring pieces of information on the heat and mass transfer phenomena (Panigrahi and Muralidhar, 2012; Settles, 2001). The refractive index is defined as:

$$\eta = \frac{c_0}{c}$$

where η is the refractive index, c_0 is the light velocity in vacuum and c is the light velocity in the transparent media. The index value must respect the condition: $\eta \geq 1$.

Optical imaging techniques are used to identify changes in the media that are not directly visible, working in the visible range of the electromagnetic spectra (λ = 400 – 700 nm).If two monochromatic waves originated from a single light source and having a phase difference ϕ are represented by:

$$E_1 = A\ sin\left(\frac{2\pi}{\lambda}(ct - x)\right)$$

$$E_2 = A\ sin\left(\frac{2\pi}{\lambda}(ct - x) + \phi\right)$$

Optical measurements are based on the information contained between the difference of phases, which is created by the density field (difference between the test beam and the source beam). These measurements are only possible if the phase difference is stable and independent of the time (a coherent source) (Panigrahi and Muralidhar, 2012; Settles, 2001)**.** The superposition of two light beams with uniform intensity gives:

$$E_1 + E_2 = 2A\ cos\frac{\phi}{2}.\sin\left(\frac{2\pi}{\lambda}(ct - x) + \frac{\phi}{2}\right)$$

The superposition of two light beams with uniform intensity but with a phase difference, results in interference consisting of alternatively dark (destructive interference) and bright regions (constructive interference). The method bases on these interferences are known as Interferometry methods, e.g. Schlieren and shadowgraph techniques. Schlieren is based on the light beam deflection but not displacement, while shadowgraph is focused on the shadow of the object, which implies a displacement and deflection of the image. Because of this, quantitative analysis of shadowgraph images could become tedious and the Schlieren method is preferred (Panigrahi and Muralidhar, 2012). A Schlieren image is an optical image generated by a lens (or mirror) conjugate to the object of study, in order to identify changes in the refractive index of the media. For these reasons, Schlieren technique has been implemented in the flame propagation tube.

Different types of configurations are possible in order to obtain optical Schlieren images, but typical Schlieren systems are composed of:

- **Light source**: A punctual light source with an overall dimension of few millimeters (~2 mm) with high luminosity intensity and a constant emissivity, according to sensitivity and the desired range of wavelengths (Settles, 2001). The appropriate light source should be

monochromatic, intense, directional and coherent. Some examples of light sources are incandescent lamps, compact-arc lamps, laser and light-emitting diodes (LED). In this work, a Xe arc lamp 150 W – UV enhanced (Newport) has been used.

- **Concave mirror or lens**: The mirrors or lenses are used to direct, collimate and decollimate the light beam. Depending on the experimental set-ups, the Schlieren image could be obtained using parabolic lenses, two concave mirrors or in the configuration shown in Figure 72, a single mirror. In this work, the single mirror coincident system or "autocollimating" arrangement is implemented. The light source is placed at the same height as the parabolic mirror at a distance equal to the curvature radius (R = 2f, f being the focal length). The diverging beam fills the mirror and return on a coincident path, forming a source image upon the light source (Settles, 2001). In order to obtain a Schlieren analysis sensitive to concentration and thermal gradients, it is recommended to use mirrors with a large focal length (Panigrahi and Muralidhar, 2012). A parabolic mirror (Edmund Optics) of 4.25 inches diameter and a focal length of 45 inches is used in the experimental set-up in this study.

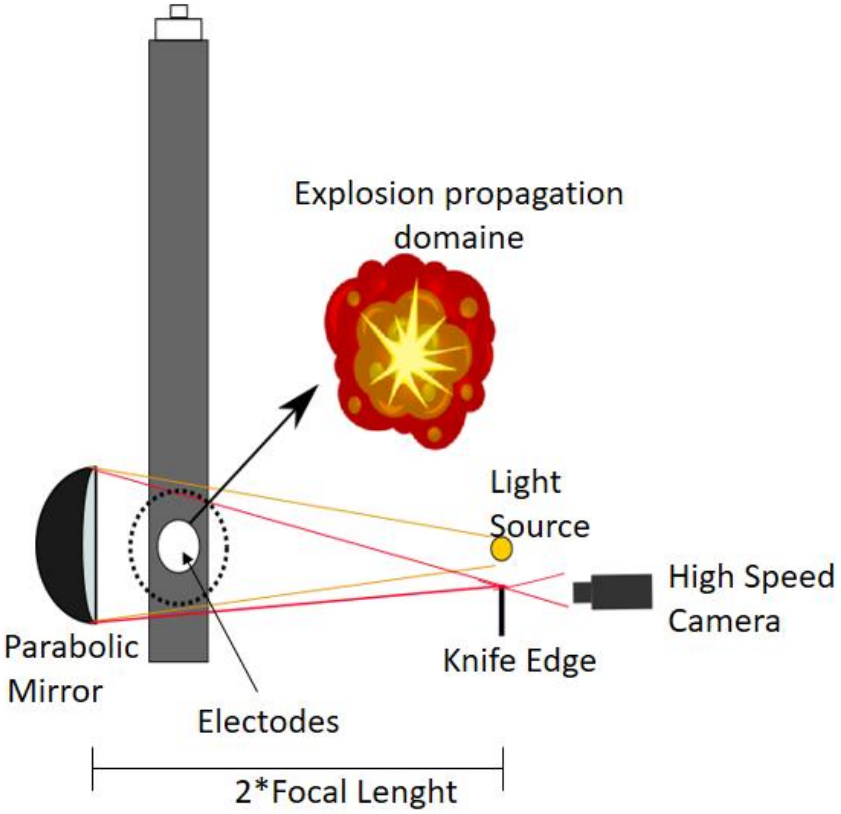

Figure 72. Schema Schlieren set-up.

- **Knife-edge:** It is placed on the focal plane of the concave mirror to cutoff a part of the reflected light. In the absence of any disturbance, the illumination of the image should decrease uniformly (Panigrahi and Muralidhar, 2012). In this study, a single razor blade is used as a Schlieren knife-edge.

The Phantom V91 high-speed video camera used for recording the flame propagation (see section 3.3.1) test is as well used to record Schlieren images. In this section, the flame velocity of gas and hybrid mixtures is analyzed in the flame propagation tube using Schlieren images.

3.5.2 Schlieren images for flame velocity estimation – Brief state of art

This section summarizes some literature studies about explosion mixtures parameters and flame velocity determination using Schlieren visualization of the front flame . Grune et al. (2015) studied the flammability limits and the pressure rise of CO-H_2-H_2O-CO_2-N_2 mixtures in a steel explosion vessel at different pressures and oxidizer concentrations. In order to better understand the effect of the variation of different parameters of the system, the front flame was visualized using Schlieren. However, this method was not used to estimate the flame velocity of the mixtures. With a similar objective, Kuznetsov et al. (2015) implemented the Schlieren imaging method in order to differentiate the burnt gases from the unreacted hydrogen-air mixture at medium scale. In this study, the flame behavior during vented deflagrations was analyzed.

The Minimum Ignition Energy (MIE) of methane-air mixture at an equivalence ratio $\varphi = 0.7$ at different turbulence levels and pressure explosion was studied by Peng et al. (2013). In their work the kernel flame propagation was analyzed at different turbulence levels using the Schlieren method, observing a high flame destabilization and drastic modifications of the flame surface (Figure 73).

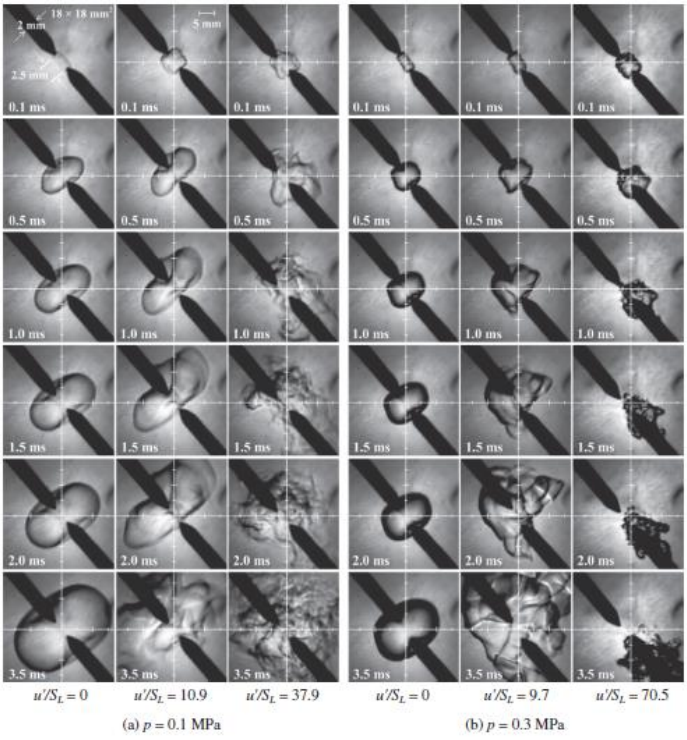

Figure 73. Schlieren time sequential images for spark kernel development at two different pressures and initial turbulence level for methane-air mixture at $\varphi = 0.7$ (Peng et al., 2013)

Some studies focused on the determination of the laminar burning velocity of gas mixtures using Schlieren images for the determination the front flame position and the estimation of the flame surface. For example, Liu et al. (2015) estimated the laminar velocity of spherical flames under quiescent conditions for propane/air mixtures at different equivalence ratio (Figure 74). In their

work, the spatial velocity, flame surface, flame stretch were estimated as presented in section 3.2.2 and the unstretched flame velocity is estimated for the gas mixture explosion. Furthermore, Ilbas et al. (2006) estimated the laminar burning velocity of hydrogen/methane/air explosions in a cylindrical vessel calculating the flame position and the front flame surface from Schlieren images. The Schlieren optical method has been also used for the determination of gas explosion turbulent velocity at high pressures, for reciprocating engines and gas turbines applications (Bradley et al., 2011, 2013).

The Schlieren method has not been very used for the determination of the burning velocity of dust and hybrid mixture explosion, even if these images let to a better estimation of the flame surface and front face determination. In the following section, the determination of the front flame velocity of carbon black nanoparticles/methane/air mixtures, using Schlieren images is presented.

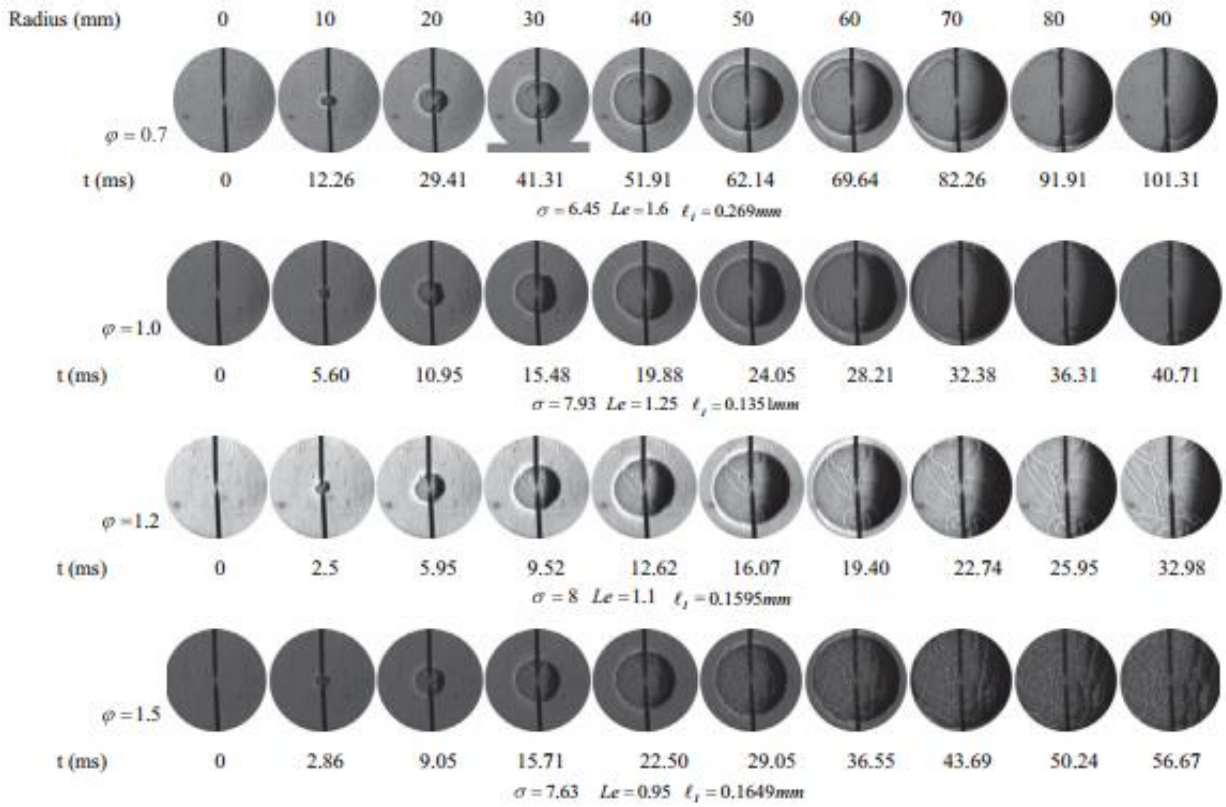

Figure 74. Images sequences of Schlieren at different equivalence ratio (Liu et al., 2015).

3.5.3 Results of flame velocity tests using Schlieren set-up

In the videos used for analysis of the burning velocity of hybrid mixtures, no physical filters were implemented, and only the luminosity of the flame was used for the flame detection. For the flame analysis, some digital filters were added in order to improve the flame detection.

The previous methodology presented three main problems: firstly, the luminosity of the flame kernel was weak in some cases and the estimation of the flame velocity for the first instants was difficult to perform (as evidenced in Figure 58 and Figure 59). Secondly, for carbon black hybrid mixtures, the flame became very bright after some milliseconds of propagation, generating a difficult estimation of the real interface between the burnt and unburnt gases, and consequently an

overestimation of the flame surface. Finally, the flame surface characteristics are lost and the perturbations of the surface are not detectable during the propagation.

To overcome these difficulties, the flame propagation videos of gas and hybrid mixture explosions were recorded using Schlieren experimental set-up (i.e. a point-light source, a parabolic mirror and a knife edge were incorporated to the previous flame propagation set-up as shown in Figure 72). The experiments performed with this set-up are summarized in Table 16.

Table 16. Explosion tests performed on the flame propagation tube using Schlieren set-up.

Ignition delay time	**Powder Concentration ($g.m^{-3}$)**		
- tv (ms)	0	2	6
0	**Gas Concentration (%v.):** 8.5 – 10.5 - 12		
120			
500			

Methane explosions:

Figure 75 shows the front flame propagation of 8.5% v. methane/air explosion under quiescent conditions. A spherical kernel propagation is observed in the first 10 ms of the propagation, after that, the flame acquires an elliptical shape due to the combined effects of the walls and gravity. However, the first observable interaction with the left wall is obtained 20 ms after the ignition. A layer of approximately 40 mm is observed on the left side of the flame (invisible on the right side due to a shadow effect on the Schlieren images), which may have different temperatures and concentration characteristics compared to the burnt gases. This layer could be associated with a preheat zone of the gases present around the flame surface. The thickness of this layer seems to remain constant during the whole propagation phenomena. In addition, the flame seems continuous and smooth during the explosion, with some slight perturbations at the electrodes position.

A similar behavior is observed for a 12% v. methane/air gas explosion under quiescent conditions as presented in Figure 76. A first difference is observed in the kernel flame development (between 0 and 2.8 ms), where a wrinkled flame surface is obtained due to the energy liberated during the ignition. Then, the spherical propagation is observed between 2.8 and 15 milliseconds. The layer associated to a possible preheat zone has a thickness of approximately 55 mm.

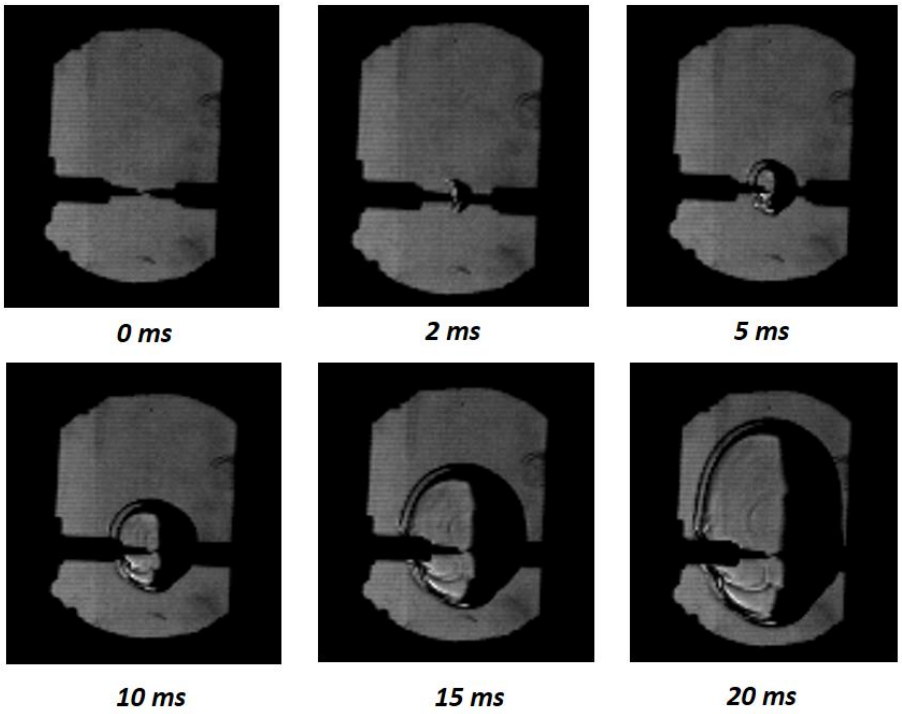

Figure 75. Flame propagation of 8.5% v. Methane/air under quiescent conditions

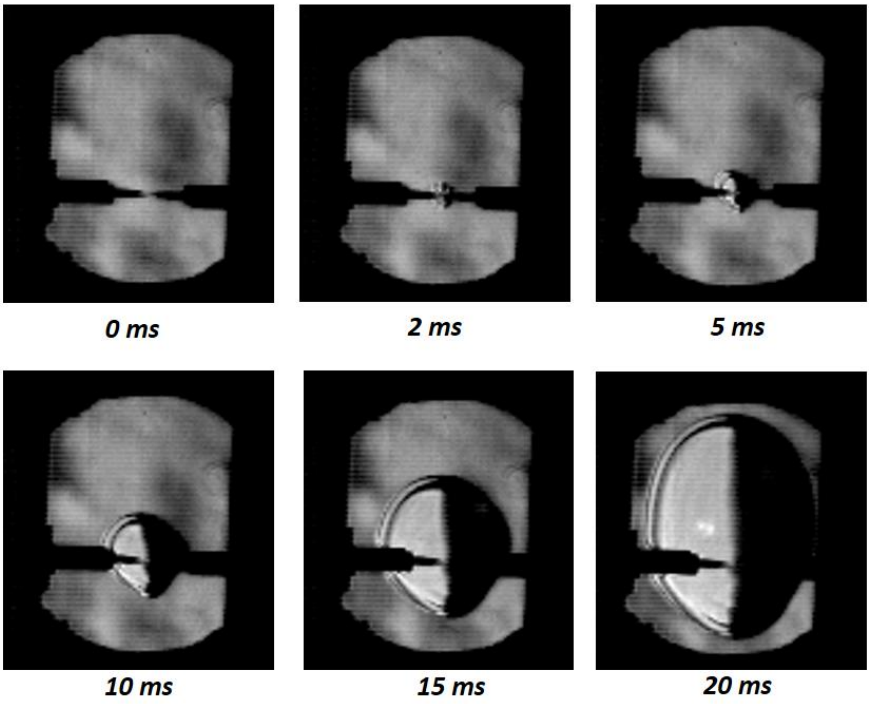

Figure 76. Flame propagation of 12% v. Methane/air under quiescent conditions

Influence of initial turbulence level:

The influence of the turbulence level can also be witnessed with the Schlieren images. Figure 78 shows the front flame propagation of 8.5% v. methane/air mixture at an initial turbulence level of

v_{rms} = 0.9 m.s^{-1}. At this turbulence level, the flame kernel for gas explosions was not very bright and the videos without Schlieren effect were not analyzable (Figure 77). The first instants of the flame propagation observed in the Schlieren images shows the influence of the turbulence on the propagation. By comparison to gas explosions at quiescent conditions (Figure 75), the flame seems to be more stretched and an elliptical flame is obtained as soon as the explosion takes place. Additionally, the flame surface seems to be irregular and much wrinkled due to the "cold" turbulence of the system. The estimation of the flame surface on the propagation tube using the Simulink – Matlab (see section 3.2.2) identifies an irregular flame front but assumes a smooth surface, approximation that may generate an underestimation for turbulent flames as evidenced in Figure 78. The optical and numerical tools available for the analysis of the video do not allow to estimate the turbulent structures of the flame surface. However, the structures formed on the flame surface can be observed from the Schlieren images.

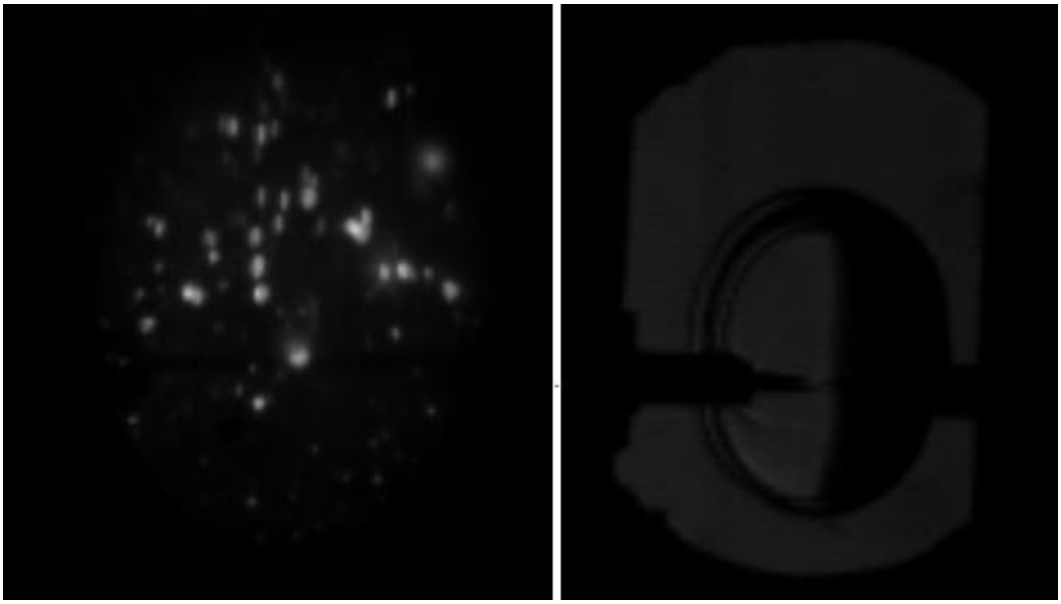

Figure 77. Flame propagation image of a 10.5% methane/air explosion without (right) and with (left) schlieren technique.

Figure 79 presents the flame propagation of 8.5% methane/ air gas mixture for a high initial turbulence level 1.4 m.s^{-1} (associated to 120 ms ignition delay time). As expected, the important turbulence of the gas flow limit the spherical/elliptical propagation and instead, generates an elongated non-continuous flame. As it is observed in Figure 79, the high turbulence seems to deform the flame and to generate a small flame in front of the kernel flame (as observed at 2 and 3.4 ms). Moreover, in comparison to quiescent and low turbulent flames, the brightness of the flame surface is increased, which can represent a higher heat exchange with the unburnt gases induced by the initial turbulence. If the flame surface identification is performed taking advantage of the flame luminosity, an overestimation of the total surface will be obtained.

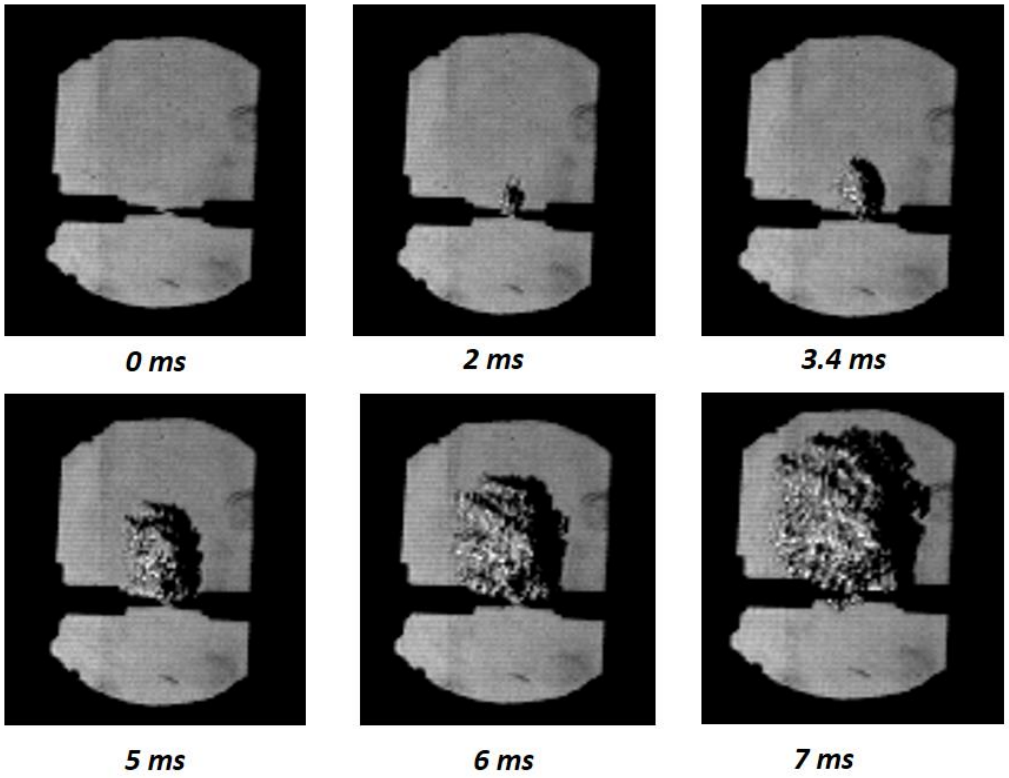

Figure 78. Flame propagation of 8.5% v. Methane/air at v_{rms} = 0.9 m.s^{-1}.

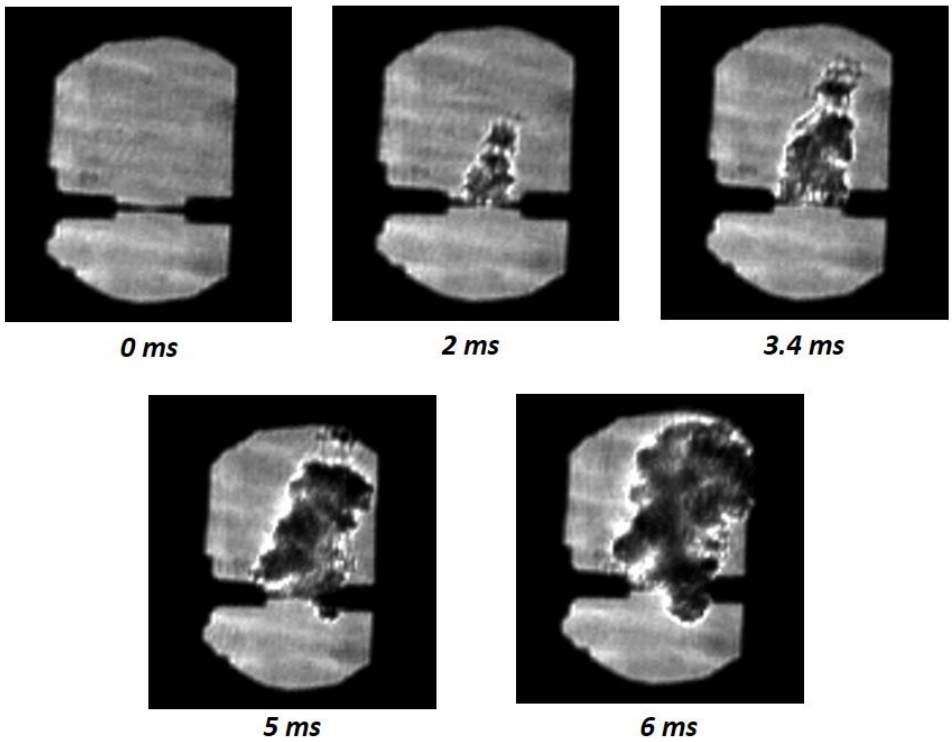

Figure 79. Flame propagation of 8.5% v. Methane/air at v_{rms} = 1.4 m.s^{-1}.

Influence of carbon black initial concentration:

The kernel flame propagation for carbon black/methane/air mixture explosions at an initial turbulent level of $v_{rms} = 0.9$ m.s^{-1} for two different dust concentrations are shown on Figure 80 and Figure 81. The Schlieren image resolution is not as good in hybrid mixtures than in gas mixture explosions. However, the detection of the front flame interface (i.e between the burnt and unburnt gases) is still possible. Moreover, due to the dispersion of carbon black nanoparticles, the flame appears darker and the visualization of the flame surface becomes very difficult to achieve compared to the explosion of gas mixtures at the same initial turbulence level conditions (Figure 78). Regarding the shape of the flame during the propagation, an elongated flame is observed through the first two milliseconds but then, a somewhat spherical flame is obtained until it interacts with the left wall (as for methane/air mixtures).

In addition, the Schlieren images of hybrid mixture explosions evidence that the dispersion of carbon black nanoparticles increases the radiative heat transfer. In Figure 80, a bright layer is observed around the front flame, which seems to be associated with the dispersed nanoparticles which are heated and then burnt before the flame reaches them. Furthermore, the radiative heat transfer is greatly augmented when the carbon black nanoparticle mass increases from 10 to 30 mg due to the fact that the carbon black nanoparticles continue to burn in the burnt gas. This enhanced heat transfer increases the temperature of the unburnt mixture, promoting the reaction in the preheat zone.

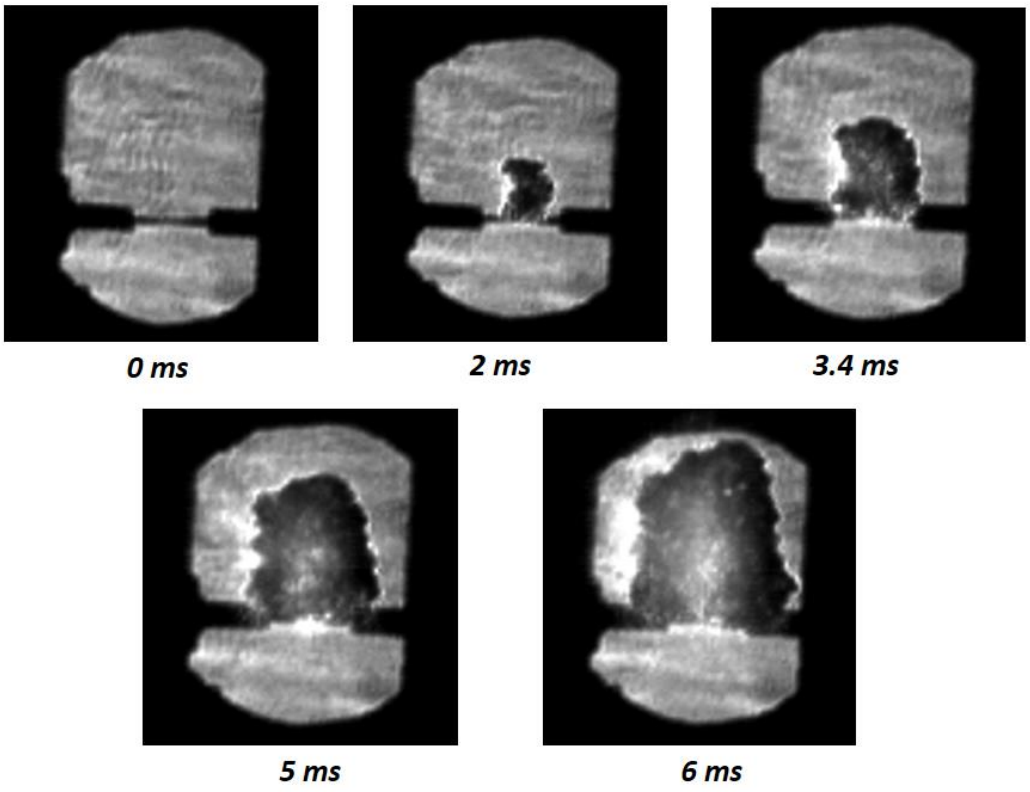

Figure 80. Flame propagation of 8.5% v. Methane/10 mg Corax N550/air at $v_{rms} = 0.9$ m.s^{-1}

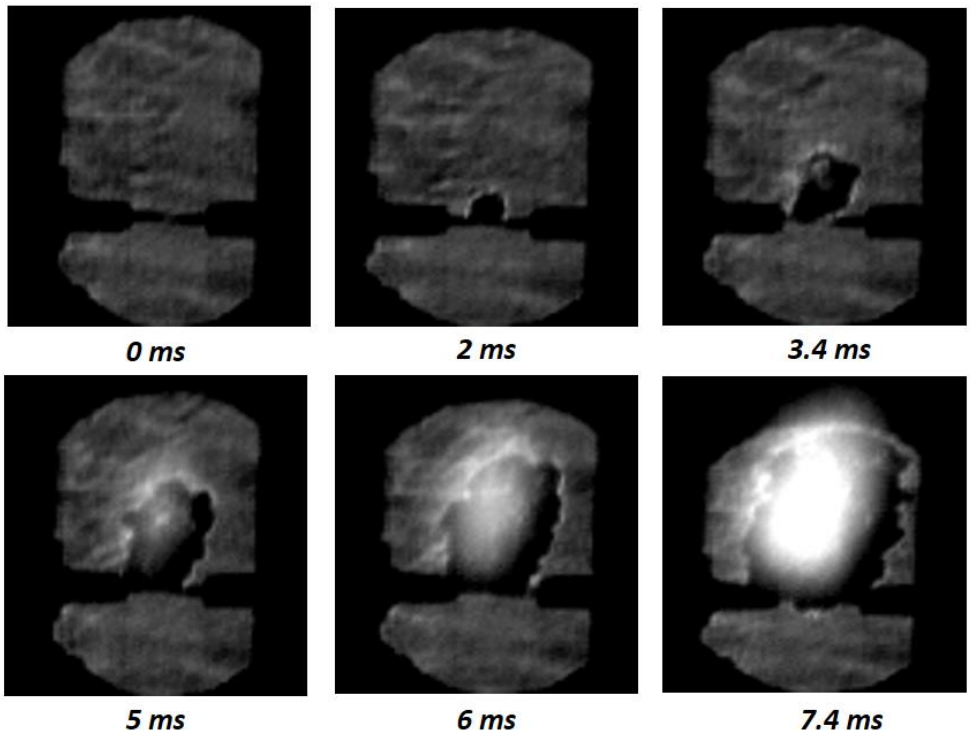

Figure 81. Flame propagation of 8.5% v. Methane/30 mg Corax N550/air at v_{rms} = 0.9 m.s^{-1}.

Unstretched flame velocity estimation:

It should be remembered that the estimation of the position, velocity and surface of the flame kernel was not possible in the analysis performed on the section 3.3 for gas and hybrid mixture explosions (Figure 77). The implantation of the Schlieren technique then brings clear advantages as it allows to analyze the flame velocity and surface at different turbulence conditions. Figure 82 presents the kernel flame position and surface for methane/air explosions at different methane concentrations. The evolution of the position over the time seems to present a constant slope for all the studied concentrations, suggesting a constant spatial velocity during the kernel growth. In addition, as expected, the higher spatial velocity is obtained for the mixture close to the stoichiometric concentration. Moreover, the 10.5% methane/air mixture flame seems to have a higher surface area, which seems to have also a significant change over time. Furthermore, the continuous evolution of the position and surface of the flame is linked to the spherical evolution of the kernel flame growth.

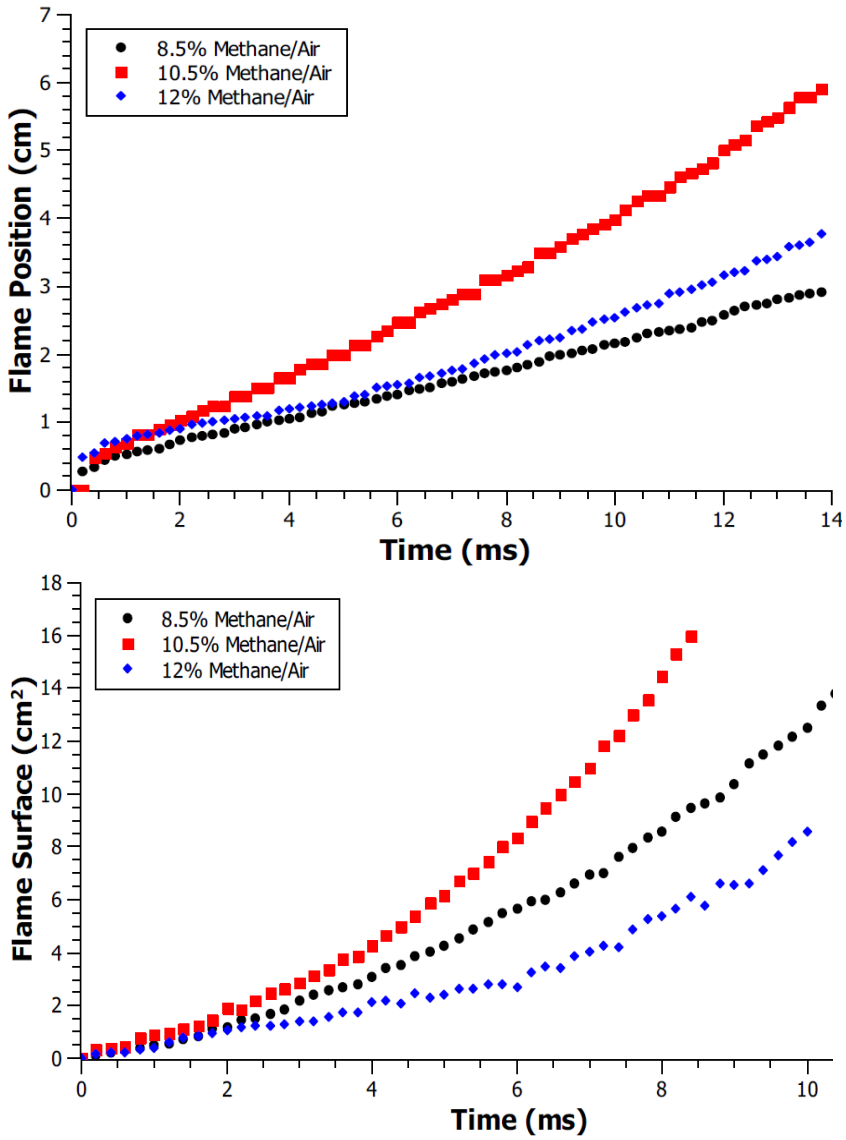

Figure 82. Flame Front position (up) and surface (down) for 8.5% methane/air explosions under quiescent conditions.

The influence of the initial turbulence level on the flame kernel growth for 10.5% methane/air mixture explosions on the position and surface is presented in Figure 83. As previously highlighted, the methane flame under quiescent conditions seems to propagate at a constant velocity, except at the very first moments at which the flame seems to be accelerated by the a possible overdriving (i.e. a strong ignition source generating a flame acceleration) In contrast, when the initial turbulence level increases to v_{rms} = 0.9 m.s^{-1}, the flame spatial velocity seems to increase during the time of the propagation and it is considerably higher than mixtures under quiescent conditions. Nevertheless, for explosions performed under high turbulence conditions, the flame seems to be destabilized by the turbulent flow. This result explains the behavior obtained for the unstretched flame velocity for gas and hybrid mixtures presented in section 3.3. It is also noticed that there is only a few differences on the flame growth under quiescent conditions and on the highest turbulence level studied on this section (i.e. the flame propagation velocity seems to decrease around 10% when the turbulence is increased to a v_{rms} = 1.4 m.s^{-1}).

Regarding the flame surface, even if the flame spatial velocities between a methane/air mixture under quiescent conditions and at an initial high turbulence level (t_v 120 ms) are very similar, significant differences on the flame surface are encountered. As it is observed in Figure 79, the flame is elongated, stretched and wrinkle at v_{rms} 1.4 $m.s^{-1}$ initial turbulence level (c.f. section 1.1.2), producing a higher superficial area of the flame. However, the high turbulence limit the propagation and deform the sphere, obtaining an explosion with similar properties under quiescent conditions. It should be highlighted that the turbulent quenching is found at this turbulent level if the ignition energy is reduced from 10 J to 5 J. On the other hand, the initial turbulence seems to have a positive effect on the flame propagation at the intermediate turbulence level studied in this test (v_{rms} 0.9 $m.s^{-1}$).

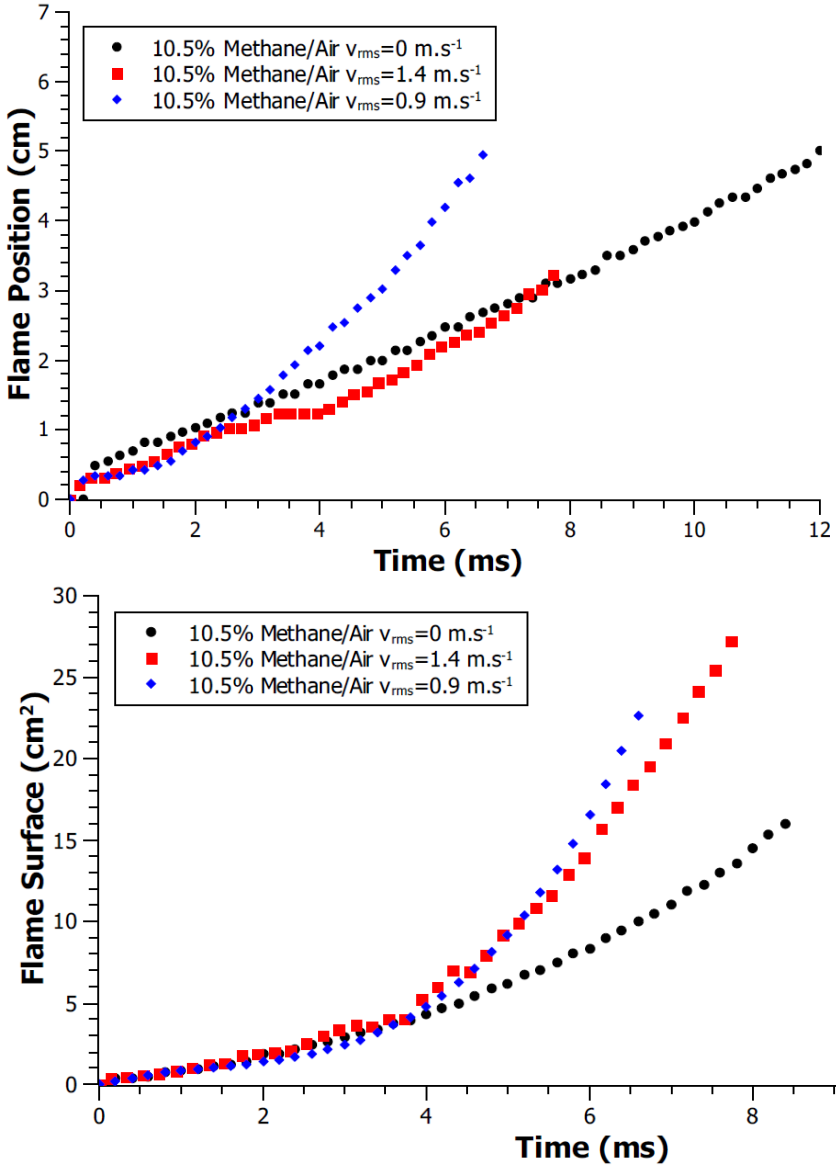

Figure 83. Influence of the turbulence on the front flame position (up) and surface (down) for 10.5% v. methane-air mixture explosions.

The effect of the insertion of carbon black nanoparticles on methane/air mixtures at a high initial turbulence level (v_{rms} =1.4 $m.s^{-1}$) is represented in Figure 84. These results are in agreement with

the previous trends in which the insertion of nanoparticles generate a diminution on the flame propagation velocity (see section 3.3.1.D). For the gas mixture, a high spatial velocity is obtained on the first 2 ms of propagation (942 $cm.s^{-1}$) and then a considerable reduction of the flame spatial velocity is evidenced, approximately 50% (927 to 542 $cm.s^{-1}$). A similar inflection point is found for 30 mg Corax/methane/air hybrid mixtures around 0.5 ms and then the flame propagates at lower spatial velocity compared to gas mixtures (i.e. a reduction around 25% is found when 30 mg of Corax N550 are added to the system). Regarding the flame surface (Figure 84 - down), when 30 mg of carbon black nanoparticles are inserted on the system, a reduction around 23% is evidenced on this variable. It seems that the presence of dispersed solids in the system stops the spherical development of the flame and generates perturbations on the flame surface, explaining the considerable reduction on the flame surface during the propagation.

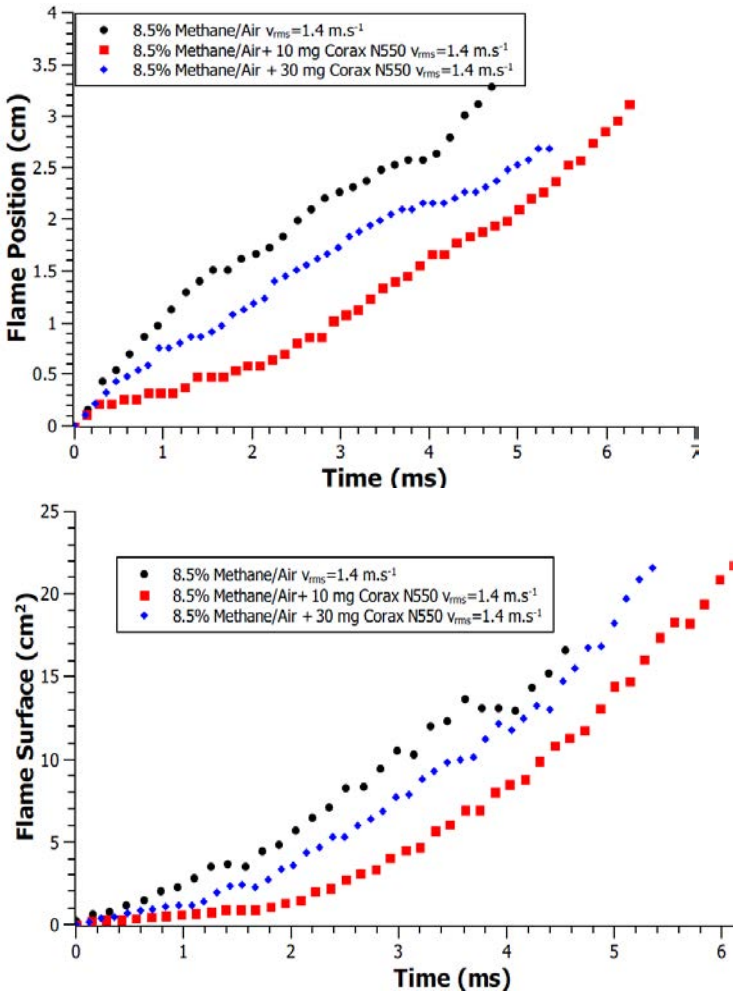

Figure 84. Influence of Corax N550 nanoparticles on the front flame position (up) and surface (down) for 8.5% v. methane-air mixture explosions at v_{rms} = 1.4 $m.s^{-1}$.

Comparing the flame velocity, a lower spatial velocity is obtained for 10 mg Corax N550/methane/air mixture compared to the 30 mg Corax N550 hybrid mixture during the first 2 ms of flame propagation. However, the flame seems to accelerate and an increase of approximately 70% is recorded after two milliseconds of propagation.

Figure 85 presents the influence of carbon black nanoparticles on the flame position and surface at an initial turbulence level of v_{rms} 0.9 m.s^{-1}. Compared to the high turbulence level, a different trend is observed on the flame spatial velocity of gas and hybrid mixture explosions. A slight increase of the spatial velocity is obtained when 10 mg of Corax N550 is added to the methane/air mixture, i.e. from 639 to 535 cm.s^{-1}. However, a considerable reduction is obtained for 30 mg Corax N550/methane/air mixture (approximately 430 cm.s^{-1}: mean spatial velocity). This trend may be explained by the high radiative heat loss observed for the hybrid mixture containing 30 mg of carbon black nanoparticles, as it is observed on Figure 78. Figure 85 – down shows the evolution of the flame surface for different concentrations of carbon black nanoparticles, at which a clear trend this variable is difficult to elucidate. However, for a dust concentration of 10 mg, a considerable modification on the flame surface is observed, due to a higher stretch factor obtained in comparison with gas mixtures during the kernel growth (i.e. after two milliseconds of propagation, a stretch factor of 1042 s^{-1} is calculated for the hybrid mixture 10 mg Corax N550/methane air and 606 s^{-1} for a methane/air mixture). This result suggest that the particles will increase the flame surface and generate an acceleration of the flame. Nevertheless, when the carbon black concentration is increased until 30 mg, even if a slight increase of the flame stretch is evidenced in comparison with gas mixtures, the particles seems to reduce the flame propagation.

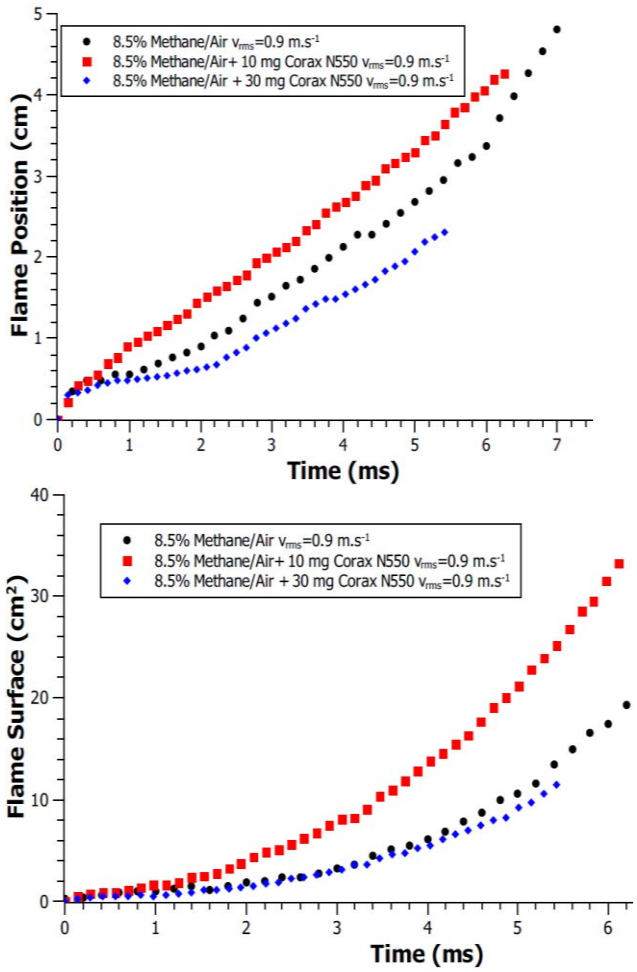

Figure 85. Influence of carbon black nanoparticles on the front flame position (up) and surface (down) for 8.5% v. methane-air mixture explosions at v_{rms} = 0.9 m.s^{-1}.

The linear relation proposed by Markstein (1962) and described on section 3.2.2 was used to estimate the unstretched velocity of gas and hybrid mixtures, as presented in Figure 86 and Figure 87. As previously highlighted, the stability, represented by the sign of Markstein length, changes after the ignition and when the flame interacts with the walls of the tube as observed in the burning velocity versus stretch factor figures. For the mixtures tested in Table 16, different behaviors on the flame stability were obtained. Nevertheless, in almost every case, negative values of Markstein length are obtained during the first milliseconds of the propagation. After the wall interaction, the flame seems to be stabilized and positive values of Markstein length are obtained (Figure 86).

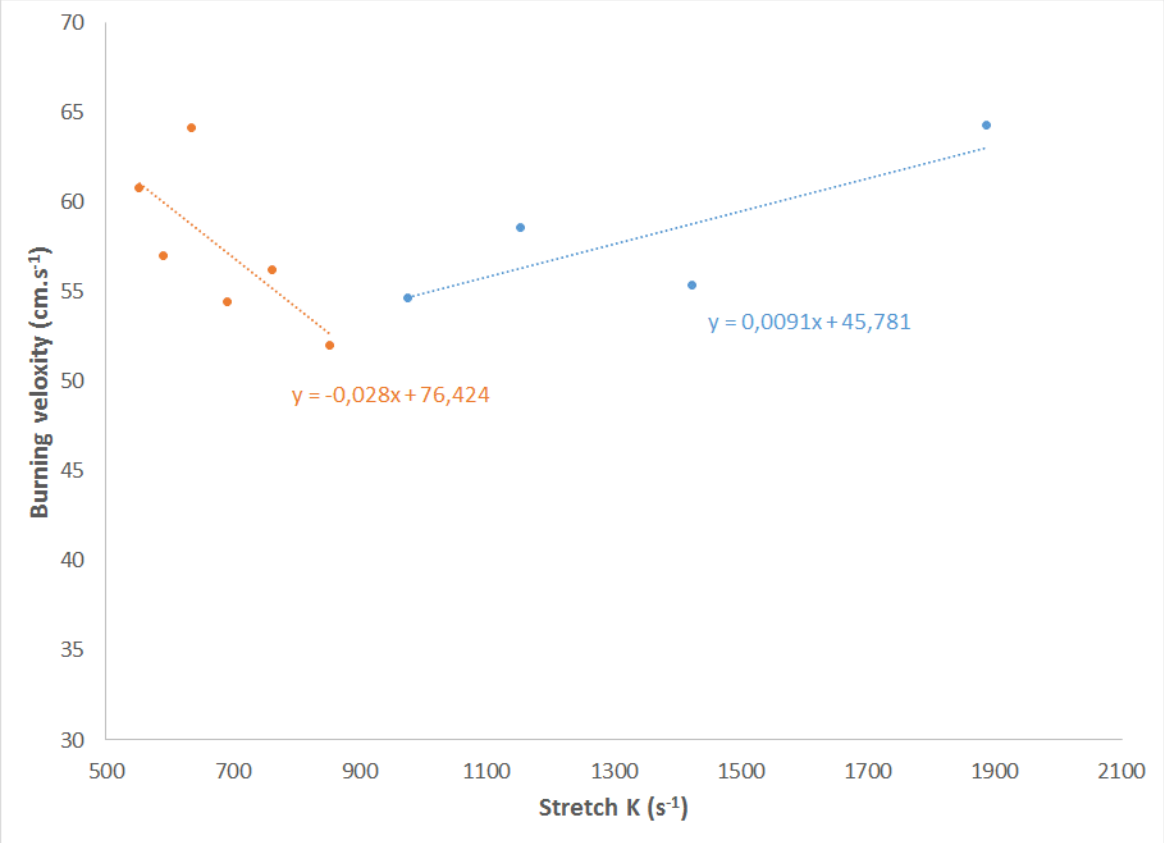

Figure 86. Burning velocity – stretching relation of 10.5% methane/air explosion under quiescent conditions.

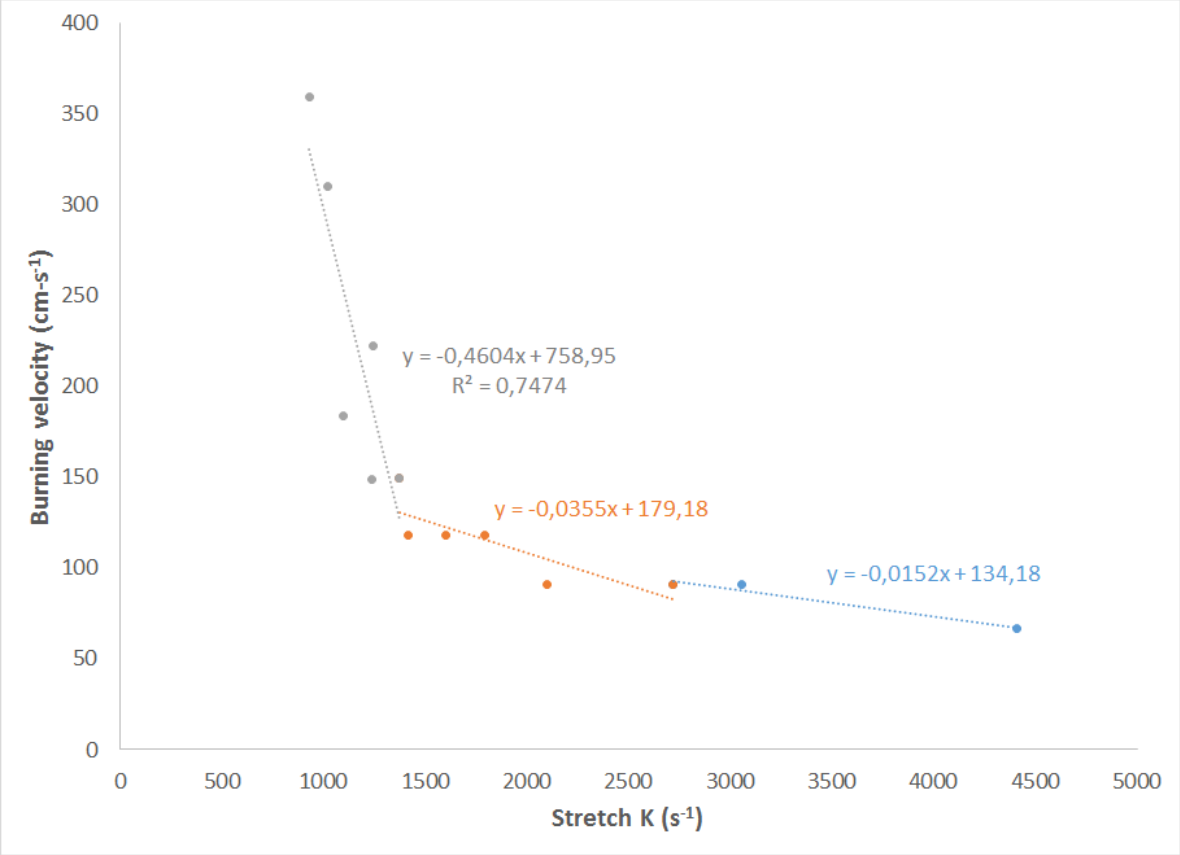

Figure 87. Burning velocity – stretching relation of 10.5% methane/ 30 mg Corax N550/ air explosion at 120 ms ignition delay time.

The burning velocity versus stretching linear relationship is observed in Figure 87 for a 30 mg Corax N550 and 10.5% methane-air mixture. Positive values of the Markstein length are obtained during all the spherical propagation of the flame, which seems to increase during the propagation (i.e. the Markstein length increase from 1.52 to 46 mm after 5 ms of propagation). It should be reminded that the Markstein length can be associated to the flame thickness (Clavin, 1985). Furthermore, this result suggests an augmentation of the flame thickness with the time, which can be modified by dust dispersion. Nevertheless, it seems that the interaction with the walls of the tube does not impact the flame propagation and the flame remains stable during the entire flame development.

Synthesis

Table 17 presents the unstretched flame velocity for methane and carbon black nanoparticles hybrid mixtures. Only for gas mixtures at quiescent conditions, the unstretched burning velocity is the highest at stoichiometric conditions, but it is significantly higher than the values reported in the literature, i.e. 45 $cm.s^{-1}$ in this work compared to 34-38 $cm.s^{-1}$ obtained by Dirrenbeger (2011). For hybrid mixtures it was not possible to establish a relation between the influence of gas concentration and the unstretched flame velocity. A considerable reduction of S_u^0 can be observed when the initial turbulence level is augmented for pure gas mixtures. For instance, for a 10.5% methane/air gas mixture, the unstretched burning velocity decreases from 45.7 to 16.6 $cm.s^{-1}$ when the turbulence level increase for an initial quiescent system to v_{rms} equals to 0.9 $m.s^{-1}$. A high

variability is obtained for turbulent hybrid mixtures. In comparison with the results presented in section 3.3, a difference is observed in the behavior of the velocity when carbon black nanoparticles are added to the mixture. For almost all the gas concentrations reported in Table 17, the unstretched flame velocity seems to increase with the addition of carbon black nanoparticles, for example, a velocity of 44.5 $cm.s^{-1}$ is obtained for a 12% gas mixture, which increases until 73.3 $cm.s^{-1}$ with the addition of 10 mg of Corax N550 and until 134 $cm.s^{-1}$ when 30 mg of carbon blacks are inserted in the system. Nevertheless, the variability seems very high for this method.

Table 17. Unstretched burning velocity for gas and hybrid mixtures estimated by using Eq.29 method using Schlieren images.

Ignition delay time t_v (ms)	**Root-Mean-Square Velocity ($m.s^{-1}$)**	**Methane $S_u^0(cm.s^{-1})$**			**Corax $S_u^0(cm.s^{-1})$**					
					10 mg			**30 mg**		
		8.5%	**10.5%**	**12%**	**8.5%**	**10.5 %**	**12%**	**8.5%**	**10.5 %**	**12%**
0	0	22	45	28	-	-	-	-	-	-
120	1.4	15	18	44	6	19	73	22	112	134
500	0.9	19	16	41	60	21	10	100	30	67

The differences between the unstretched flame velocity estimations obtained recording the flame propagation without physical filters and with the Schlieren set-up shows a high variability in the results. Firstly, some differences on the unstretched flame velocity are related to the difference on the detection of the flame surface, which is improved using Schlieren images: The detection of the flame interface based on the luminosity generate an overestimation of the flame surface or of the position of the flame, and in addition, the irregularities on the surface were not taken into account with such analysis. Secondly, the differences could also be associated to the variability encountered for hybrid mixture at turbulent conditions. The estimated slope of the flame using the Eq. 29 is very sensitive to the position and surface of the flame, so a very small change in this variable will produce a huge difference on the final unstretched velocity. Finally, the difference may be related to the limitations of the flame propagation tube methodology, due to the very fast interactions with the tube walls and the limited time of spherical analysis.

3.6. Conclusions

The flame velocity of methane and carbon black nanoparticles/methane explosion mixture has been calculated in a flame propagating tube using a method validated for pure gases (Andrews and Bradley, 1972a). The estimation of the burning velocity of such mixtures is very difficult compared to static methods applied to pure gases. Nevertheless, this method allows to calculate a first estimation of the burning velocity of hybrid mixtures and allows to identify the flame modifications during the propagation.

The results show that adding low concentrations of nanoparticles (at concentrations far below the minimal explosive concentration), the front flame propagation is modified. It seems that the dispersion of nanoparticles modifies the radiative heat phenomena (heat sink and radiative heat transfer), the flame stretch and the combustion reaction. The previous experimental results suggest that:

a) The reproducibility test shows similar values on the flame spatial velocity at low turbulence levels and similar trends delayed on time for high turbulence systems (i.e. especially for stoichiometric and rich mixtures) due to the variability provided by the initial turbulence intensity.
b) The spatial velocity of hybrid mixtures at low turbulence level is maximum under gas stoichiometric conditions. However, the gas concentration does not have influence on the flame kernel propagation at high initial turbulence conditions.
c) The initial turbulence increases the flame spatial velocity but at the highest turbulence conditions, a reduction on the unstretched flame velocity seems to be obtained.
d) The spatial and burning velocity decrease when the concentration of carbon black nanoparticles is augmented. Similar influence of the nano-dust concentration on the maximum overpressure and maximum rate of pressure rise for carbon black/methane mixture explosions, which confirms the previous results obtained with the 20L sphere.
e) The unstretched burning velocity estimated for AP-D alumina/methane/air mixtures are considerable higher than those obtained for gas mixture explosions. The previous results and specifically the fact that flames with similar spatial velocities can exhibit different unstretched burning velocities, suggest that the presence of solid particles such as alumina modifies the flame surface during the propagation.
f) The insertion of nanoparticles modifies greatly the radiative heat transfer, as it has been observed in the flame propagation videos and Schlieren images. However, this energy has to be quantified in order to better understand the influence of dispersed particles.
g) The burning velocity was estimated by the thin spherical propagation model using the explosion severity tests. For methane/air mixture, the estimated values are very close to the reported values. However, for the hybrid mixtures, the estimated values of the flame velocity could present a deviation from the reality because the model assumes an infinitely thin flame spherical flame. The insertion of nanoparticles may increase the flame thickness and deform the flame, condition at which a perfect spherical flame propagation is unlikely to take place.
h) Schlieren images show a significant change on the flame surface when the initial turbulence level of the system increases, which it is initially smooth and became highly wrinkled at very turbulent conditions.

Considerable differences have been found between the unstretched velocity measured from videos

without physical filters and from videos recorded using the Schlieren images. For both methods, an elevated variability has been obtained, especially at high turbulence levels. As a consequence, it is difficult to establish if the results are related to an influence of a specific phenomenon or they are the result of the randomness of the system. In addition, the very fast interactions of the flame with the walls of the tube generate important perturbations on the flame propagation and it can also increase the variability of the results.

Furthermore, the differences between the two methods of detection of the flame front suggest that the flame surface estimation is a key parameter in the estimation of the unstretched flame velocity. Despite the variability of the results, a considerable improvement on the flame surface is obtained by the Schlieren method. The detection of the flame interface based on the luminosity generates an overestimation of the flame surface.

The linear relation proposed by Markstein (1964) and applied to the flame propagation on the flame propagation tube seems appropriate to obtain an estimation of the burning velocity of hybrid mixtures and allow to study of the influence of different parameters. Moreover, the interaction between the flame and the tube walls can be identified with the burning velocity versus stretch factor graph. However, the fast interaction of the flame with the walls of the tube generate difficulties on the unstretched burning velocity estimation. The development of an experimental set-up with a higher volume allowing the propagation of the flame kernel and reducing the interaction with the walls and electrodes is highly recommended. In addition, further test must be implemented using the Schlieren images in order to try to estimate the flame thickness and the quenching distance with the tube walls. Finally, a temperature measure of the system during the propagation may provide important information in order to better estimate the expansion of the burnt gases and the radiation transfer between the flame and the media (unburnt gases and dispersed particles).

3.7. Conclusions (Français)

Les vitesses de flamme du méthane et des mélanges nanoparticules de noir de carbone/méthane ont été calculées dans un tube de propagation de flamme en utilisant une méthode validée pour les gaz purs (Andrews et Bradley, 1972a). Il faut signaler que l'estimation de la vitesse de combustion de poussières ou de mélanges hybrides par la méthode du tube de propagation est ardue par rapport aux méthodes statiques appliquées aux gaz purs. Néanmoins, cette méthode permet d'estimer la vitesse de combustion de ce type de mélanges et permet d'identifier les modifications de la flamme pendant sa propagation.

Les résultats confirment que l'ajout de faibles concentrations de nanoparticules (à des concentrations très inférieures à la concentration explosive minimale) modifie la propagation de la flamme. Il semble que la dispersion des nanoparticules modifie les phénomènes de transfert de chaleur, l'étirement de la flamme et la réaction de combustion. Les résultats expérimentaux suggèrent plus précisément que :

a) Les tests montrent une bonne reproductibilité pour les vitesses spatiales de flamme à faible turbulence et des tendances similaires retardées dans le temps pour des turbulences élevées (spécialement pour les mélanges stœchiométriques ou riches). Ces décalages seraient liés au caractère stochastique de la turbulence initiale de la dispersion.
b) La vitesse spatiale des mélanges hybrides à faible niveau de turbulence est maximale dans les conditions stœchiométriques du gaz. Cependant, la concentration de gaz n'a pas d'influence sur la propagation du noyau de flamme à des conditions de turbulence initiales élevées.
c) Un accroissement de la turbulence initiale augmente dans un premier temps la vitesse spatiale de la flamme mais au niveau de turbulence le plus élevé de ce travail, une réduction de la vitesse de la flamme non étirée semble être obtenue.
d) La vitesse spatiale et la vitesse de combustion diminuent lorsque la concentration en nanoparticules de noir de carbone augmente. Une influence similaire de la concentration en nanopoudre sur la surpression maximale et la vitesse maximale de montée en pression pour les explosions de mélange de noir de carbone / méthane a été observée, ce qui confirme les résultats précédents obtenus avec la sphère 20L.
e) La vitesse de combustion non étirée estimée pour les mélanges d'alumine / méthane / air est considérablement supérieure à celle obtenue pour les explosions de mélange de gaz. Le fait que les flammes avec des vitesses spatiales similaires peuvent présenter des vitesses de combustion non étirées différentes suggère que la présence de particules solides telles que l'alumine modifie la surface de la flamme pendant la propagation.
f) L'insertion de nanoparticules modifie considérablement le transfert de chaleur radiatif, comme cela a été observé dans les vidéos de propagation de la flamme et les images Schlieren. Cependant, cette énergie rayonnée doit encore être quantifiée afin de mieux comprendre l'influence des particules dispersées.
g) La vitesse de combustion a été estimée par le modèle de propagation sphérique à épaisseur de la flamme mince, en utilisant les tests de sévérité de l'explosion. Pour le mélange méthane/air, les valeurs estimées sont très proches des valeurs reportées dans la littérature. Cependant, pour les mélanges hybrides, les valeurs estimées de la vitesse de la flamme pourraient présenter une déviation de la réalité car le modèle suppose une flamme infiniment fine. Or, l'insertion de nanoparticules peut augmenter l'épaisseur de

la flamme et la déformer, ce qui conduit à des conditions de propagation de flamme non idéales et non adaptées au modèle de flammes minces.

h) Les images Schlieren montrent un changement significatif de la surface de la flamme lorsque le niveau de turbulence initiale du système augmente : la surface qui est initialement lisse, devient très plissée dans des conditions très turbulentes.

Des différences considérables ont été trouvées entre la vitesse non étirée mesurée à partir de vidéos sans filtres physiques et de vidéos enregistrées à l'aide des images Schlieren. Pour les deux méthodes, une variabilité élevée a été obtenue, en particulier à des niveaux élevés de turbulence (faible reproductibilité). En conséquence, il est difficile d'établir si les résultats sont liés à une influence d'un phénomène spécifique ou sont dus au caractère stochastique de la turbulence. En outre, les interactions très rapides de la flamme avec les parois du tube génèrent des perturbations importantes sur la propagation de la flamme et peuvent également augmenter la variabilité des résultats.

Enfin, les différences entre les deux méthodes de détection du front de flamme suggèrent que l'estimation de la surface de la flamme est un paramètre clé dans l'estimation de la vitesse de la flamme non étirée. Malgré la variabilité signalée des résultats, la méthode optique dite de Schlieren permet d'obtenir une amélioration considérable de l’estimation de la surface de flamme. La détection de l'interface de flamme basée sur la luminosité génère une surestimation de la surface de la flamme par rapport à celle basée sur la différence de densité.

Nomenclature

Symbol	Description
A	Tube cross-section [cm^2].
A_f	Front flame surface [cm^2].
f	Focal length [cm].
K	Karlovitz's factor [s^{-1}].
L	Markstein length [cm].
R	Radius of curvature of the spherical mirror [cm].
S_s	Spatial velocity [cm s^{-1}].
S_u	Burning velocity [cm s^{-1}].
S_u^0	Unstretched burning velocity [cm s^{-1}].
Greek letters	Description
α	Thermal expansion correction [-].
γ	Heat capacity ratio of the gas [-].

References

Andrews, G.E., Bradley, D., 1972a. Determination of burning velocities: A critical review. Combust. Flame 18, 133–153.

Andrews, G.E., Bradley, D., 1972b. The burning velocity of methane-air mixtures. Combust. Flame 19, 275–288.

Bauffman, J., Cox, K., 2008. Measurement of laminar burning velocity of methane-air mixtures using a slot and Bunsen burner (Major qualifying project). Worcester Polytechnic Institute, Worcester, United States.

Bradley, D., Lawes, M., Liu, K., Mansour, M.S., 2013. Measurements and correlations of turbulent burning velocities over wide ranges of fuels and elevated pressures. Proc. Combust. Inst. 34, 1519–1526.

Bradley, D., Lawes, M., Mansour, M.S., 2011. Measurement of turbulent burning velocities in implosions at high pressures. Proc. Combust. Inst. 33, 1269–1275.

Bradley, D., Lawes, M., Mumby, R., 2017. Burning velocity and Markstein length blending laws for methane/air and hydrogen/air blends. Fuel 187, 268–275.

Clavin, P., 1985. Dynamic behavior of premixed flame fronts in laminar and turbulent flows. Prog. Energy Combust. Sci. 11, 1–59.

Cloney, C.T., Ripley, R.C., Amyotte, P.R., Khan, F.I., 2013. Quantifying the effect of strong ignition sources on particle preconditioning and distribution in the 20-L chamber. J. Loss Prev. Process Ind. 26, 1574–1582.

Cuervo, N., 2015. Influences of turbulence and combustion regimes on explosions of gas- dust hybrid mixture. Université de Lorraine.

Cuervo, N., Dufaud, O., Perrin, L., 2017. Determination of the burning velocity of gas/dust hybrid mixtures. Process Saf. Environ. Prot. 109, 704–715.

Dahoe, A., 2000. Dust Explosions: a Study of Flame Propagation.

Dahoe, A.E., Hanjalic, K., Scarlett, B., 2002. Determination of the laminar burning velocity and the Markstein length of powder–air flames. Powder Technol., Special issue i in Honour of Prof Jimbo 122, 222–238.

Dahoe, A.E., Zevenbergen, J.F., Verheijen, P.J.T., Lemkowitz, S.M., Scarlett, B., 1996. Dust explosions in spherical vessels: prediction of the pressure evolution and determination of the burning velocity and flame thickness.

Di Benedetto, A., Garcia-Agreda, A., Dufaud, O., Khalili, I., Sanchirico, R., Cuervo, N., Perrin, L., Russo, P., 2011. Flame propagation of dust and gas-air mixtures in a tube. Proc. 7th Mediterr. Combust. Symp. Chia Laguna Cagliari Sard. Italy.

Dirrenberger, P., Glaude, P.A., Bounaceur, R., Le Gall, H., da Cruz, A.P., Konnov, A.A., Battin-Leclerc, F., 2014. Laminar burning velocity of gasolines with addition of ethanol. Fuel 115, 162–169.

Dirrenberger, P., Le Gall, H., Bounaceur, R., Herbinet, O., Glaude, P.-A., Konnov, A., Battin-Leclerc, F., 2011. Measurements of Laminar Flame Velocity for Components of Natural Gas. Energy Fuels 25, 3875–3884.

Eckhoff, R.K., 2012. Does the dust explosion risk increase when moving from μm-particle powders to powders of nm-particles? J. Loss Prev. Process Ind. 25, 448–459.

Gordon, S., McBride, B., 1994. Computer program for calculation of complex chemical equilibrium and applications. NASA Ref. Publ. 1311.

Griffith, J.., Barnard, J.., 1995. Flame and combustion, 3rd ed. ed. Published. London: Blackie Academic & Professional, CRC Press.

Grune, J., Breitung, W., Kuznetsov, M., Yanez, J., Jang, W., Shim, W., 2015. Flammability limits and burning characteristics of CO–H2–H2O–CO2–N2 mixtures at elevated temperatures. Int. J. Hydrog. Energy 40, 9838–9846.

Ilbas, M., Crayford, A., Yilmaz, I., Bowen, P., Syred, N., 2006. Laminar-burning velocities of hydrogen–air and hydrogen–methane–air mixtures: An experimental study. Int. J. Hydrog. Energy 31, 1768–1779.

Kuznetsov, M., Friedrich, A., Stern, G., Kotchourko, N., Jallais, S., L'Hostis, B., 2015. Medium-scale experiments on vented hydrogen deflagration. J. Loss Prev. Process Ind. 36, 416–428

Law, C.K., 2006. Combustion Physics. Cambridge University Press.

Liu, Q., Zhang, Y., Niu, F., Li, L., 2015. Study on the flame propagation and gas explosion in propane/air mixtures. Fuel 140, 677–684.

Markstein, G.H., 1964. Non-steady flame propagation. Pergamon Press, Oxford.

Murillo, C., 2016. Experimental and numerical approaches to particles dispersion in a turbulent flow: application to dusts explosion. Université de Lorraine.

Murillo, C., Dufaud, O., Bardin-Monnier, N., López, O., Munoz, F., Perrin, L., 2013. Dust explosions: CFD modeling as a tool to characterize the relevant parameters of the dust dispersion. Chem. Eng. Sci. 104, 103–116.

Panigrahi, P.K., Muralidhar, K., 2012. Schlieren and Shadowgraph Methods in Heat and Mass Transfer, SpringerBriefs in Applied Sciences and Technology. Springer New York, New York, NY.

Peng, M.-W., Shy, S. (Steven), Shiu, Y.-W., Liu, C.-C., 2013. High pressure ignition kernel development and minimum ignition energy measurements in different regimes of premixed turbulent combustion. Combust. Flame 160, 1755–1766.

Proust, C., 2006. Flame propagation and combustion in some dust-air mixtures. J. Loss Prev. Process Ind. 19, 89–100.

Rubtsov, N.M., 2016. The Modes of Gaseous Combustion, Heat and Mass Transfer. Springer International Publishing, Cham.

Settles, G.S., 2001. Schlieren and Shadowgraph Techniques. Springer Berlin Heidelberg, Berlin, Heidelberg.

Shy, S.S., Lin, W.J., Wei, J.C., 2000. An experimental correlation of turbulent burning velocities for premixed turbulent methane-air combustion. Proc. R. Soc. Math. Phys. Eng. Sci. 456, 1997–2019.

Skjold, T., 2003. Selected aspects of turbulence and combustion in 20-Litre explosion vessel. University of Bergen, Norway.

Torrado, D., Cuervo, N., Pacault, S., Dufour, A., Glaude, P.-A., Murillo, C., Dufaud, O., 2016. Explosions of gas/carbon black nanoparticles mixtures: An approach to assess the role of soot formation. Chem. Eng. Trans. 48, 379–384

Varea, E., 2013. Experimental analysis of laminar spherically expanding flames. INSA de Rouen.

CHAPTER 4: One dimensional model of flame propagation of methane/air/dust hybrid mixture

4.1. Introduction

As explained in previous chapters, the determination of the explosion severity of complex mixtures should be made from intrinsic properties of the system in order to avoid the influence of external parameters, as the vessel volume or the "cold" turbulence. The laminar burning velocity is a mixture's intrinsic property that describes the severity of an explosion andis a necessary input for CFD simulation of the systems (Castellanos et al., 2013; Skjold et al., 2014) and the protection devices dimensioning. The aim of this chapter is to describe and explain a numerical model used to determine the flame velocity of a gas mixture explosion through a two-phase media containing nanoparticles. Firstly, the system properties, the mass and the energy balance equations and the chemical reactions are described. Then, the numerical discretization and algorithm of the simulation are explained. Finally, the results of the simulation and the comparison with the experimental data are presented.

4.2. Model Equations and Hypotheses

4.2.1 1-D Flame System

In chapter 3, the front flame velocity was estimated for hybrid mixture explosions in a square cross-section vertical tube. Due to the complexity of reaction kinetics, of the turbulence and heat transfer in such a real system, the estimation of the flame velocity by a numerical model simulation was developed for a simplified schema of the tube. In this chapter, the flame propagation of gas and hybrid mixtures is analyzed using a 1-D numerical model, taking into account the reaction kinetics, the diffusion of species, the convection and radiative heat transfer. Moreover, the flame propagation in a tube involving two parallel walls is analyzed. The solution is obtained dividing the simulation domain in three different zones (Dahoe, 2000): preheat, reaction and post-flame zones (Figure 88). The numerical model will be developed in one coordinate in the space, and because the influence of the gravity on the flame propagation will not be taken into account, it is indifferent if the propagation of the flame is solved for a vertical or horizontal tube. In addition, the numerical length of the tube should be enough to observe a stable propagation of the flame (i.e. in this model a distance of 5 cm had been chosen because the results shown that an stable propagation is obtained and a longer distance will not contribute to the final solution).

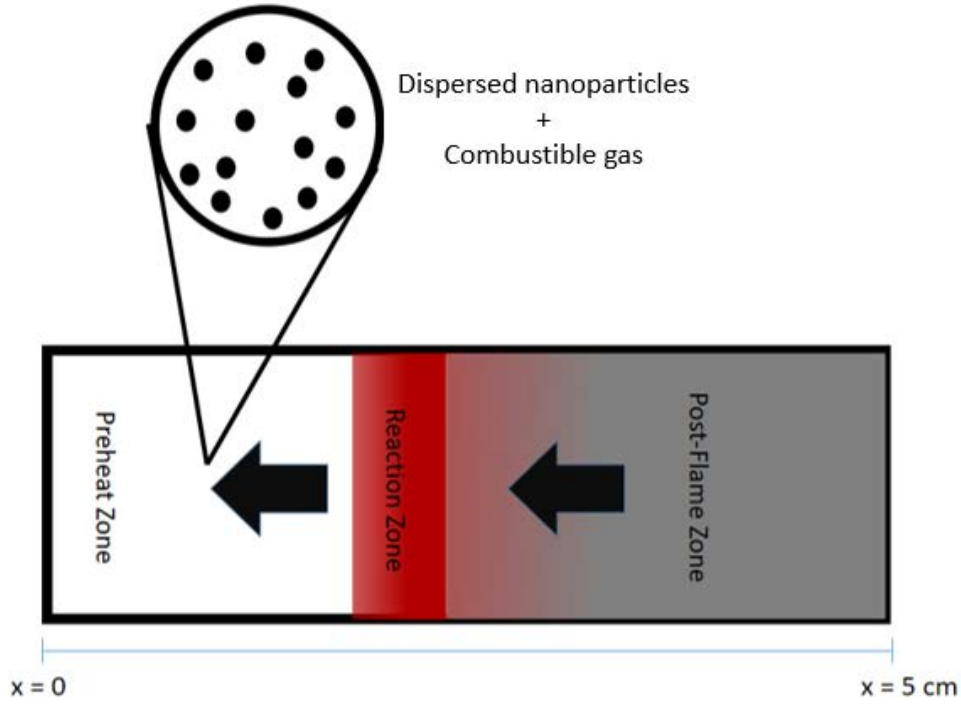

Figure 88. Schematic of the flame zones used on the 1-D numerical model.

The evolution of the 1-D model flame propagation will be analyzed and validated against experimental data for methane-air mixtures. Then, the specific case of hybrid mixtures will be addressed. Firstly, the dispersed dust will be assumed as an inert solid, and only the thermal contribution through the radiative heat transfer will be taken into account. Then, a simultaneous reaction of solid and gas will be analyzed in the model, in order to better understand the probable interactions between heat radiation and combustion reaction present in a hybrid mixture explosion an already observed in the experimental results of this study (see Chapter 2 and 3). In this numerical model, the influence of the initial turbulence is not taken into account.

4.2.2 Mass and Species Balance

The transitory flame properties are determined solving the mass and energy conservation equations (Poinsot and Veynante, 2005).

$$\frac{\partial \rho}{\partial t} + div(\rho u) = 0 \qquad \text{Eq 36}$$

$$\frac{\partial}{\partial t}(\rho y_i) + div(\rho y_i u) + div(j_i) = \dot{\omega}_i \qquad \text{Eq 37}$$

Where ρ, y_i, j_i and u are the mixture density, mass fraction of the i component, the mass diffusion flux and velocity respectively. The mass reaction rate component ($\dot{\omega}_i$) is expressed as:

$$\dot{\omega}_i = W_i \sum_{j=1}^{N_r} v_{i,j} r_j \qquad \text{Eq 38}$$

where W_i is the molecular weight of th compound i. In equation 38, the subscript i represent the specie and j the number of the reaction. The rate of the reaction j is expressed as:

$$r_j = k_j^f \prod \phi^{\varepsilon_{ji}} - k_j^r \prod \phi^{\varepsilon_{ji}}$$

Where k_j is the reaction rate constant, ϕ is the mole concentration and ε_{ji} is the reaction order of the component i in the reaction j. The subscripts f and r define the forward and reverse reaction. The reaction constant k_j are assumed to follows the Arrhenius law and are defined as:

$$k_i = A_i T^{\beta} \exp\left(\frac{-E_i}{RT}\right) \qquad \text{Eq 39}$$

Some studies simplify the combustion reaction of gas and dust flame assuming a global mechanism, in which one reaction describes the consumption of the fuel, oxygen and burnt gases (Bidabadi et al., 2010; Haghiri and Bidabadi, 2011). This assumption allows the simplification of the differential equations, but generating deviations on the final properties of the flame (i.e. temperature, mass fractions and velocity). In this work, the methane-air combustion is assumed to follow a semi-global kinetic mechanism, in order to describe the temperature and final fraction of the components in the burnt gases. A detailed methane combustion mechanism is not implemented because of the numerical complexity demand to solve the differential equations for all the involved species. For this reason, the Jones – Lindstedt (1988) mechanism had been implemented in this work, in which 6 simultaneous reactions are present in the reaction zone, involving 10 chemical species. The reactions describing the generation of radicals H, OH and O are added to the system in order to improve the prediction of the flame temperature (Frassoldati et al., 2009). In addition, the reaction constants for the reverse reaction of the hydrogen oxidation proposed by Andersen et al. (2009) are implemented in the combustion mechanism. The pre-exponential factor, reaction orders and activation energy of the reactions of the Jones-Lindstedt mechanism are listed in Table 18. It should be reminded that the coefficients and reactions order in this semi-global mechanism has been fitted in order to describe experimental results of gas flames. Due to this reason, the coefficients are empirical values and do not have a physical meaning.

Table 18. Reaction mechanism for methane/air reaction (Andersen et al., 2009; Frassoldati et al., 2009; Jones and Lindstedt, 1988).

#	Reaction	A_i[1]	β	$E_i[cal.mol^{-1}$	$\left[\frac{\rho_{A,i}}{W_{A,i}}\right]^{\alpha}\left[\frac{\rho_{B,i}}{W_{B,i}}\right]^{\gamma}$
1	$CH_4 + 0.5O_2 \rightarrow CO + 2H_2$	2.45×10^9	0	3×10^4	$[CH_4]^{0.5}[O_2]^{1.25}$

[1] Reaction 1 $\left[\frac{(m^3)^{0.75}}{mol^{0.75}s}\right]$ Reactions 2, 3 and -3: $\left[\frac{m^3}{mol \cdot s}\right]$. 4: $\left[\frac{(m^3)^{0.75}K}{mol^{0.75}s}\right]$.Reaction -4: $\left[\frac{(m^3)^{0.25}K^{0.88}}{mol^{0.25}s}\right]$. Reaction 5 and 6: $\left[\frac{1}{s}\right]$

#	Reaction	A_i[1]	β	$E_i[cal.mol^{-1}$	$\left[\frac{\rho_{A,i}}{W_{A,i}}\right]^{\alpha}\left[\frac{\rho_{B,i}}{W_{B,i}}\right]^{\gamma}$
2	$CH_4 + H_2O \rightarrow CO + 3H_2$	3×10^5	0	3×10^4	$[CH_4][H_2O]$
3	$CO + H_2O \rightarrow CO_2 + H_2$	2.75×10^6	0	2×10^4	$[CO][H_2O]$
-3	$CO_2 + H_2 \rightarrow CO + H_2O$	9×10^7	0	2.8×10^4	$[CO_2][H_2]$
4	$H_2 + 0.5O_2 \rightarrow H_2O$	1.01×10^{13}	-1	4×10^4	$[H_2]^{0.25}[O_2]^{1.50}$
-4	$H_2O \rightarrow H_2 + 0.5O_2$	2.25×10^{16}	-0.88	9.8×10^4	$[H_2O][H_2]^{-0.75}[O_2]$
5	$O_2 \leftrightarrow 2O^{\cdot}$	1.5×10^9	0	1.13×10^5	$[O_2]$
6	$H_2O \leftrightarrow H^{\cdot} + OH^{\cdot}$	2.3×10^{22}	-3	1.2×10^5	$[H_2O]$

The mass reaction rate implemented for each specie in the conservation equation (Eq 37) is presented on Table 19. The model should take in account the forward and reversible reaction of the radicals $O^{\cdot}, H^{\cdot}$ and $OH^{\cdot}$ In order to obtain a better prediction of the flame temperature. However, the reversible reactions are not taken into account in the present work due to numerical instability problems observed in the hydrogen and oxygen solutions.

Table 19. Mass consumption/generation of species.

Component	Reaction rate
$\boldsymbol{CH_4}$	$\dot{\omega}_{CH_4} = W_{CH_4}[-r_1 - r_2]$
$\boldsymbol{CO}$	$\dot{\omega}_{CO} = W_{CO}[r_1 + r_2 - r_3 + r_{-3}]$
$\boldsymbol{CO_2}$	$\dot{\omega}_{CO_2} = W_{CO_2}[r_3 - r_{-3}]$
$\boldsymbol{O_2}$	$\dot{\omega}_{O_2} = W_{O_2}[-0.5r_1 - 0.5r_4 + 0.5r_{-4} - r_5]$
$\boldsymbol{H_2O}$	$\dot{\omega}_{H_2O} = W_{H_2O}[-r_2 - r_3 + r_{-3} + r_4 - r_{-4} - r_6]$
$\boldsymbol{H_2}$	$\dot{\omega}_{H_2} = W_{H_2}[2r_1 + 3r_2 + r_3 - r_{-3} - r_4 + r_{-4}]$
$\boldsymbol{O^{\cdot}}$	$\dot{\omega}_{O^{\cdot}} = W_{O^{\cdot}} 2r_5$
$\boldsymbol{H^{\cdot}}$	$\dot{\omega}_{H^{\cdot}} = W_{H^{\cdot}} r_6$
$\boldsymbol{OH^{\cdot}}$	$\dot{\omega}_{OH^{\cdot}} = W_{OH^{\cdot}} r_6$
$\boldsymbol{N_2}$	$\dot{\omega}_{N_2^{\cdot}} = 0$

The gas mixture density is estimated assuming ideal gas:

$$\rho = \frac{1}{\frac{RT}{P}\sum\frac{y_i}{W_i}} \quad \text{Eq 40}$$

Mass diffusion fluxes

The general expression for the determination of the diffusion fluxes is presented in the equation 41 (Bird et al., 2007):

$$j_i = -\rho \sum_j D_{i,j} \nabla y_i \quad \text{Eq 41}$$

Due to the computational cost of working with a complete tensor D, an approximation on the estimation of the diffusion coefficient D_i is implemented (Eq 44) and the diffusion flux reads (Poinsot and Veynante, 2005):

$$j_i = -\rho D_i \nabla y_i + y_i J \quad \text{Eq 42}$$

The term $y_i J$ is a correction term added in order to assure the global mass conservation ($\sum_j^{N_s} y_i = 0$)

$$J = \rho \sum_{i=1}^{Nspecies} D_i \nabla y_i \quad \text{Eq 43}$$

The Hirschfelder and Curtiss approximation is implemented in order to calculate the diffusion coefficient of the specie i in the mixture (Poinsot and Veynante, 2005; Solomon, 1955):

$$D_k = \frac{1 - y_i}{\sum_{j \neq i} \frac{x_j}{D_{ji}}} \quad \text{Eq 44}$$

In Table 20, some diffusion coefficients D_{ji} are listed (Haynes, 2012). The mole fraction x_j can be calculated from the mass fraction y_i by using the following relationship:

$$x_i = \frac{W}{W_i} y_i$$

where the mean molecular weight is calculated as follows:

$$W = \sum_{i=1}^{Nspecies} \frac{y_i}{W_i}$$

If the temperature of the system is not in the Table 20, an extrapolation is developed following molecular theory of diffusion in gases (Bird et al., 2007; Gosse, 2012):

$$D_{ij} = 1.858x10^{-7} \frac{[T^3(W_A + W_B)/W_A + W_B]^{1/2}}{P\sigma_{AB}^2 \Omega_{AB}^{(1,1)^*}}$$

Where P is the pressure, σ_{AB} is the characteristic distance and $\Omega_{AB}^{(1,1)^*}$ is the collision integral. Assuming that the collision integrals and the characteristic distance do not depend with the temperature, the diffusion coefficient will change with the temperature with a factor of $\sim T^{3/2}$.

Table 20. Mass diffusion coefficients of the reactive species D_{ij} ($cm^2.s^{-1}$) (Haynes, 2012).

Mixture	293 K	373K	473K	573K	673K
$CH_4 - Air$	0.106	0.321	0.485	0.678	0.899
$CO_2 - Air$	0.160	0.252	0.390	0.549	0.728
$H_2O - Air$	0.242	0.399	0.638	0.873	1.132
$H_2 - Air$	0.672	1.153	1.747	2.444	3.238
$CO - Air$	0.208	0.315	0.473	0.662	0.875
$CH_4 - H_2$	0.782	1.084	1.648	2.311	3.070
$CH_4 - N_2$	0.220	0.317	0.480	0.671	0.890
$CO - CO_2$		0.162	0.250	0.384	
$CO - H_2$	0.772	1.162	1.743	2.423	3.196
$CO - N_2$	0.208	0.231	0.491	0.673	0.878
$CO_2 - H_2$	0.412	0.964	1.47	2.066	2.74
$CO_2 - H_2O$	0.162	0.292	0.496	0.741	1.021
$CO_2 - N_2$	0.160	0.253	0.342	0.553	0.733
$H_2 - N_2$	0.772	1.162	1.743	2.423	3.196
$H_2O - N_2$	0.242	0.399	-	-	-
$N_2 - Air$	0.890	-	-	-	-
$O_2 - Air$	0.214	-	-	-	-

4.2.3 Energy Balance

The energy balance is presented in equation 45, assuming constant pressure and neglecting viscous terms:

$$\sum_{i=1}^{Nspecies} C_{p,i}[\rho y_i \partial_t(T) + \rho y_i u div(T) + j_i div(T)] = -\dot{\omega}_i \left[\sum_{i=1}^{Nspecies} \left[h_{f,i}^0 + C_{p,i} T \right] \right] + div(\lambda \nabla \mathrm{T}) \quad \text{Eq 45}$$

where $C_{p,i}$, $h_{f,i}^0$, λ and T are the specific heat of specie i, the enthalpy of formation of the chemical species, the coefficient of heat conductivity and the temperature respectively. The detailed development of the energy balance from the total energy conservative equation is presented in the Appendix B. The properties of the chemical species used in the numerical model are listed in Table 21 and

Table 22.

Table 21. Molecular weight, standard enthalpy of formation and thermal conductivity of the reactive species (Smith et al., 2004).

Component	$\boldsymbol{W_i\left(\frac{kg}{mol}\right)}$	$\boldsymbol{\Delta H_f^0\left(\frac{J}{mol}\right)}$	$\boldsymbol{\lambda\left(\frac{J}{m \cdot s \cdot K}\right)}$
$\boldsymbol{CH_4}$	$16.04\text{x}10^{-3}$	$-7.24\text{x}10^{4}$	$9.3\text{x}10^{-2}$
$\boldsymbol{CO}$	$28.01\text{x}10^{-3}$	$-1.11\text{x}10^{5}$	$3.91\text{x}10^{-2}$
$\boldsymbol{CO_2}$	$44.01\text{x}10^{-3}$	$-3.94\text{x}10^{5}$	$4.41\text{x}10^{-2}$
$\boldsymbol{O_2}$	$31.99\text{x}10^{-3}$	0	$5.23\text{x}10^{-2}$
$\boldsymbol{H_2O}$	$18.01\text{x}10^{-3}$	$-2.42\text{x}10^{5}$	$4.63\text{x}10^{-2}$
$\boldsymbol{H_2}$	$2.01\text{x}10^{-3}$	0	$32.8\text{x}10^{-2}$
$\boldsymbol{O\cdot}$	$15.99\text{x}10^{-3}$	$2.49\text{x}10^{5}$	0
$\boldsymbol{H\cdot}$	$1.00\text{x}10^{-3}$	$2.18\text{x}10^{5}$	0
$\boldsymbol{OH\cdot}$	$17.01\text{x}10^{-3}$	$3.94\text{x}10^{4}$	0
$\boldsymbol{N_2}$	$28.01\text{x}10^{-3}$	0	$4.53\text{x}10^{-2}$

Table 22. Specific heat of reactive species (Smith et al., 2004).

Component	$Cp_i{}^o\left(\frac{J}{kg\ K}\right)$
CH_4	$(1.072 + 9.08\text{x}10^{-3}T - 2.16\text{x}10^{-3}T^2)\frac{R}{W_{CH_4}}$
CO	$(3.376 + 5.57\text{x}10^{-4}T - 3.10\text{x}10^{3}T^{-2})\frac{R}{W_{CO}}$
CO_2	$(5.457 + 1.05\text{x}10^{-3}T - 1.16\text{x}10^{5}T^{-2})\frac{R}{W_{CO_2}}$
O_2	$(3.639 + 5.06\text{x}10^{-4}T - 2.21\text{x}10^{4}T^{-2})\frac{R}{W_{O_2}}$
H_2O	$(3.47 + 1.47\text{x}10^{-3}T + 1.21\text{x}10^{4}T^{-2})\frac{R}{W_{H_2O}}$
H_2	$(3.249 + 4.22\text{x}10^{-4}T + 8.3\text{x}10^{3}T^{-2})\frac{R}{W_{H_2}}$
$O^{\cdot}$	$2.73\text{x}10^{3}$
$H^{\cdot}$	$20.7\text{x}10^{3}$
$OH^{\cdot}$	$2.31\text{x}10^{3}$
N_2	$(3.28 + 5.93\text{x}10^{-4}T + 4.0\text{x}10^{3}T^{-2})\frac{R}{W_{N_2}}$

4.2.4 Numerical Scheme, Boundary and Initial Conditions

The flame propagation phenomenon is governed by the conservation differential equations of mass, species and energy, which depends on the space and on the time. The calculation of a flame propagation velocity and of the mass fraction profiles across the numerical domain requires a numerical integration of the differential equations. This integration is developed by a numerical method that estimates unknown values of the dependent variable at a finite number of grid points. The differential equations are transformed into algebraic equations by discretization

approximations and a finite number of numerical values for the mass fractions and temperature will be the outcome (Patankar, 1980; Saatdjian, 2009). The finite volume method was chosen and will be developed in the next sections.

4.2.4.1 Finite Volume Discretization

The calculation domain is divided in non-overlapping and well-defined control volumes such that each grid point is surrounded by two control volumes (except for the limit points that will have particular conditions):

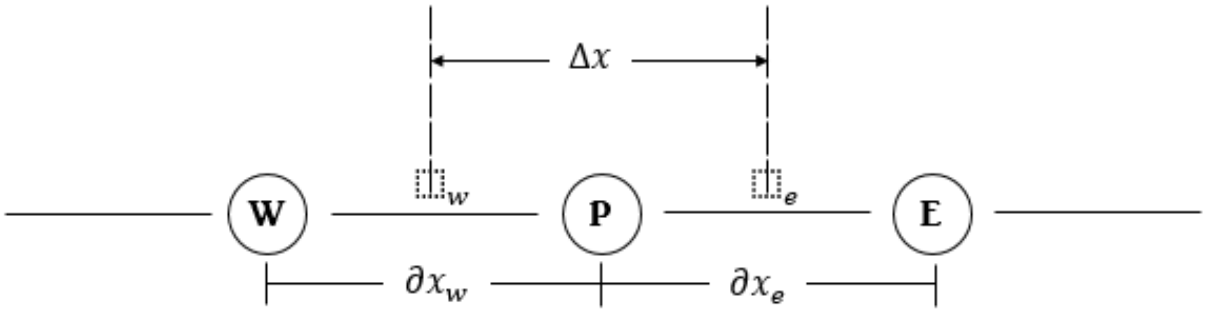

Figure 89. Discretization scheme.

The differential equations are integrated over each control volume. The result is then a system of algebraic equations containing the value of a specific property ϕ for a group of grid points. The obtained discretization equation describes the conservation principle under the grid as the differential equation expresses for the infinitesimal domain. The discretization is detailed for the point P, which has the grid points west (W), east (E) as neighbors and the dash lines represents the boundaries between the control volumes (Figure 89). By this means, the integration of the differential equations could be done in each control volume assuming a linear interpolation function between grid points (Patankar, 1980). For example, the discretization of the diffusion term of a variable ϕ (which could be the temperature or the mass fraction) and a source term S (e.g. the mass reaction rate $\dot{\omega}_i$ for the species conservation equation) is read as

$$\frac{\partial}{\partial x}\left(K\frac{\partial \phi}{\partial x}\right)+S=0 \qquad \text{Eq 46}$$

$$\left(K\frac{d\phi}{dx}\right)_e-\left(K\frac{d\phi}{dx}\right)_w+\int_w^e S dx=0 \qquad \text{Eq 47}$$

$$\frac{K_e(\phi_E-\phi_P)}{\partial x_e}-\frac{K_w(\phi_P-\phi_W)}{\partial x_w}+\bar{S}\Delta x=0 \qquad \text{Eq 48}$$

Where K is the diffusion coefficient (e.g D_i and λ for the species and energy conservation balance respectively). As the number of grid points increases, all the formulations of the interpolation function should give the same solution. Nevertheless, other requirements should be imposed to narrow the discretization to an acceptable formulation. It is not imperative that the distances ∂x_e

and ∂x_w be equal, in fact the use of non-uniform grid points may enhance the computation time of the solution, especially for systems with drastic changes of the solution. For this reason, the grid spacing is greatly related to the way the dependent variable changes in the calculation domain. In this work, a uniform grid discretization is implemented.

4.2.4.2 Properties on the boundary of a control volume

Using the discretization scheme described in the Figure 89, some properties of the mixture must be estimated on the interfaces of the control volumes, for example, the thermal conductivity and the diffusion coefficient. The most common methodology consist in supposing a linear variation of K between the points P and E (applies identically for W and P):

$$K_E = f_e K_e + (1 - f_e) K_P \quad \text{Eq 49}$$

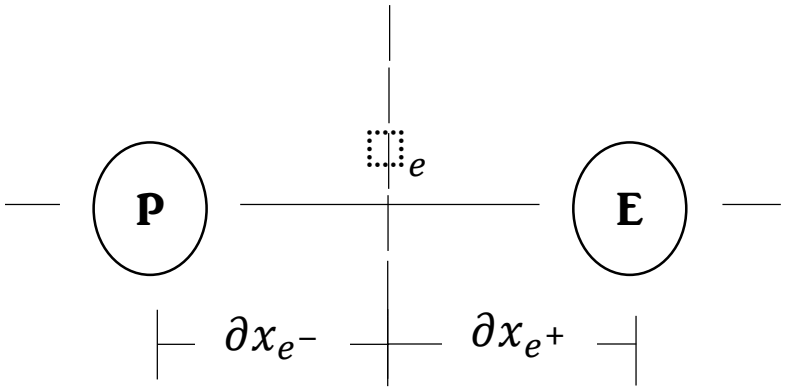

Figure 90. Volume properties between two control volumes.

where the interpolation factor is defined as (Figure 90):

$$f_e = \frac{\partial x_{e^+}}{\partial x_e} \quad \text{Eq 50}$$

When the interface is equidistant from E and P, then:

$$K_e = \frac{2 K_E K_P}{K_P + K_E} \quad \text{Eq 51}$$

4.2.4.3 Convection term

A special attention should be given to the discretization of the convection term in the integration schema: the central difference schema, as that applied for the diffusion term, may produce problems of convergence in the solution (Patankar, 1980; Saatdjian, 2009). The problem of the central difference schema is to assume that the convection flux in the interface is the average value between the neighbor control volumes. For this reason, the upwind scheme was proposed as a solution of this problem since it recognizes that the convective flow will depend on its direction. The value of the property ϕ at an interface is equal to the value of the flux at the grid point in the upwind side of the interface (Patankar, 1980):

and

$$\phi_e = \phi_E \quad if\ (\rho u)_e \gtrless 0 \qquad \text{Eq 53}$$

The value on the interface ϕ_w can be determined in a similar way. The upwind schema has been implemented to the convective term for the discretization of the equations 37 and 45, in order to increase the stability of the numerical integration.

$$\rho u y_i = (\rho u)|_e y_{i,P}((\rho u)_e > 0) + (\rho u)|_e y_{i,E}((\rho u)_e < 0) - (\rho u)|_w y_{i,W}((\rho u)_w > 0) - (\rho u)|_w y_{i,P}((\rho u)_w < 0) \qquad \text{Eq 54}$$

4.2.4.4 Unsteady Problem

The species and energy balance for the flame propagation implies an unsteady problem, which may need a discretization on the time. The volume control method discretization for unsteady problems should be exemplified with the basic equation:

$$\rho \frac{\partial \phi}{\partial t} + \frac{\partial}{\partial x}\left(K \frac{\partial \phi}{\partial x}\right) = 0 \qquad \text{Eq 55}$$

The unsteady problem is limited to find the values of the variable ϕ in all grid points of the numerical domain at time t+Δt (denote as ϕ^{n+1}) using the values of ϕ at the time t (denote as ϕ^n). This could be expressed as the integration problem:

$$\int_t^{t+\Delta t}\int_w^e \rho \frac{\partial \phi}{\partial t} dt dx + \int_w^e \int_t^{t+\Delta t} \frac{\partial}{\partial x}\left(K \frac{\partial \phi}{\partial x}\right) dx dt = 0$$

The values of the variable ϕ at the points E, P and W vary from t to t+Δt. This means that the spatial change of the variable ϕ could be estimated at the point n or n+1, which may change the final values of the variables in the numerical domain. As a consequence, a weighting factor is used to take in account the temporal change of the variables:

$$\rho(\phi_P^{n+1} - \phi_P^n)\Delta x + f\left[\frac{K_e({\phi_E}^{n+1} - {\phi_P}^{n+1})}{\partial x_e} - \frac{K_w({\phi_P}^{n+1} - {\phi_W}^{n+1})}{\partial x_w}\right]\Delta t + (1 - f)\left[\frac{K_e({\phi_E}^{n} - {\phi_P}^{n})}{\partial x_e} - \frac{K_w({\phi_P}^{n} - {\phi_W}^{n})}{\partial x_w}\right]\Delta t = 0$$

Where f is weighing factor between 0 and 1. If f = 0, the discretization leads to an explicit schema, and f = 1, to an implicit schema. The previous discretization allows to reorganize the system of algebraic equations in order to calculate all the property values ϕ^{n+1} at each grid point from the ϕ^n values using a matrix operation.

$$\phi^{n+1} = [A_{n+1}]^{-1} b \phi^n$$

Nevertheless, this resolution is possible only if the discretization of the differential equations results in a linear algebraic system. However, the order of some reactions of the combustion mechanism (Table 18) and the dependence of the reaction rate on the temperature generate a non-linear system. As a consequence, the implementation of a numerical method to solve a group of non-linear

algebraic equations is necessary. In this work, the method of lines has been used to solve the system of partial differential equations.

4.2.4.5 Method of Lines

The Method of Lines (MOL) allows to solve partial differential equations in which only one dimension is discretized (Kahaner et al., 1991; Sarmin and Chudov, 1963; Schiesser, 1991). Therefore, a system of ordinary differential equations is built by discretizing the spatial derivatives and the time variable remains continuous. Then, a numerical method for solving Ordinary Differential Equations (ODE) can be implemented.

In this study, the space derivatives have been discretized using the finite volume method, as previously described, and then, the system of ordinary differential equations has been solved using the integration functions ODE in MATLAB®. The ODE system is solved using a Runge-Kutta (4,5) method, which calculates the ϕ^{n+1} from the immediately preceding time point (Dormand and Prince, 1980; MathWorks, 2017; Shampine et al., 2003). Initially, the ode45 MATLAB® solver was chosen to calculate the temperature and mass fraction in every grid point at each time. However, if the ode45 solver is unable to solve the problem or the solution take too much time, a stiff ode15s solver is implemented. The stiffness problem may be evidenced when the solution of a variable changes drastically at different time scales (MathWorks, 2017).

4.2.4.6 Initial Conditions

In order to solve the system of ordinary differential equations, an initial value of the temperature and mass fractions in all the numerical domain must be defined. Thus, the integration variables for the numerical domain has been defined according to the flame zone. The integration distance L is defined and discretized in an initial amount of control volumes. At first, a number of 60 control volumes has been imposed. This quantity was evaluated by varying the number of control volumes and by choosing the limit number at which the result of the integration does not change. Then, the initial distance of each zone was defined, i.e. the preheat zone was imposed as the 25% of the numerical domain and the reaction zone as a 5% of the total distance (Figure 91). The initial value of the temperature and the mass fraction was defined as follows:

- **Preheat zone**: In this zone, the initial value of the temperature and mass fraction was chosen to describe the initial conditions of the unburnt gases in the laboratory tests. By this means, the mass fractions were defined according to the fuel concentration to be analyzed (Figure 91 shows the condition for a stoichiometric mixture) at an initial temperature of 298 K.
- **Reaction zone**: It was assumed that at the initial time (t = 0), the mass fractions and temperature change linearly in the reaction zone. Therefore, the value of this variables is known if the conditions in the preheat and post-flame zones are defined. This assumption decreases the calculation time and favor the convergence of the numerical simulation if a discontinuity or a drastic change in the solution is present during the integration time.
- **Post-flame zone**: The temperature and the initial mass fractions in this zone are defined according to the values obtained for a laminar and stable flame at equilibrium conditions. For this, the adiabatic temperature and mass fraction of the burnt gases for a steady flame were calculated using PREMIX program (Dirrenberger et al., 2011). This approach is used to initialize the properties values close to the stable solution, in order to reduce the calculation times and to improve the convergence of the program. Table 23 shows the PREMIX results of a steady 1-D flame set as the initial points in the post flame zone.

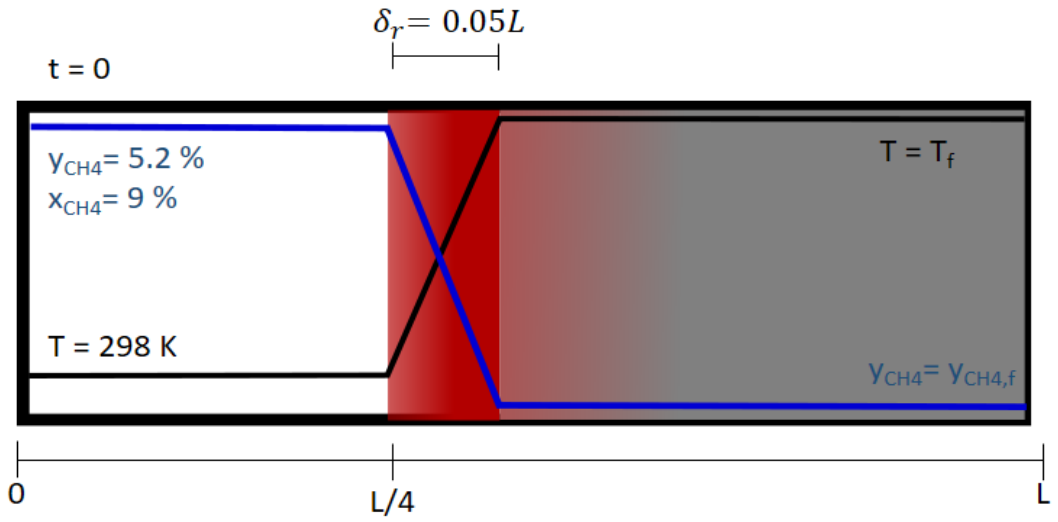

Figure 91. Schema of the initial conditions of the temperature and methane fraction in each zone of the flame.

Table 23. Premix results in the post-flame zone for a 9% methane/air mixture.

	$T(K)$	y_{CH_4}	y_{CO}	y_{CO_2}	y_{O_2}
Properties of 9% Methane mole concentration	2236	$1.2\text{x}10^{-17}$	$7.8\ \text{x}10^{-3}$	$1.3\ \text{x}10^{-1}$	$6.2\ \text{x}10^{-3}$
	y_{H_2O}	y_{H_2}	y_H	y_{OH}	y_O
	$1.2\text{x}10^{-1}$	$2.6\text{x}10^{-4}$	$1.5\text{x}10^{-5}$	$2.0\text{x}10^{-3}$	$1.4\text{x}10^{-4}$

The velocity of the mixture is initially defined null, so only the reactive and diffusion terms are analyzed.

4.2.4.7 Boundary Conditions

In the sections 4.2.4.2 and 4.2.4.3, the discretization of the spatial derivatives have been explained for the internal points of the numerical domain; however, special attention must be paid to the boundary conditions, which could generate code divergence problems (Saatdjian, 2009). For this study, it was assumed that at the x = 0 limit, the mass and thermal flux are null (which means that the initial value of the temperature and mass fraction remain constant during all the integration time):

$$\left.\frac{\partial \phi}{\partial t}\right|_{x=0} = 0 \qquad \text{Eq 56}$$

For the control volume at x = L, the convection, reaction and diffusion terms have been taken in account with a different discretization of the derivative terms. For instance, for the internal control volumes, the spatial derivative in the interface of a control volume P is estimated using the neighbor volumes W and E is shown in the Eq. 48 and 54. However, for the last control volume, the diffusion

and convection terms are estimated using backwards discretization for the derivatives (Burden and Faires, 2010):

$$D\frac{\partial^2\phi}{\partial x^2} = \frac{D(\phi_P - 2\phi_W + \phi_{W-1})}{\partial {x_w}^2} \quad \text{Eq 57}$$

$$\rho u y_i = (\rho u)|_P y_{i,P} - (\rho u)|_w y_{i,W} \quad \text{Eq 58}$$

The reaction term on the boundary distance x = L, the rate of reaction is evaluated taking the properties of mass fractions and temperature in that control volume.

4.2.4.8 Discretized Equations

The spatial derivative of the mass, species and energy partial differential equations have been discretized using the finite volume method and the time derivatives are kept continuous in order to apply the method of lines. Table 24 shows the discretized ordinary differential equations solved in this study.

Table 24. Examples of the ordinary differential equation system

Species Balance

$$\left[\frac{\partial}{\partial t}(\rho y_i)\right]\Delta x = -\left[(\rho u)|_e y_{i,P}((\rho u)_e > 0) + (\rho u)|_e y_{i,E}((\rho u)_e < 0) - (\rho u)|_w y_{i,W}((\rho u)_w > 0) - (\rho u)|_w y_{i,P}((\rho u)_w < 0)\right] + \frac{D_{i,e}(y_E - y_P)}{\partial x_e} - \frac{D_{i,w}(y_P - y_W)}{\partial x_w} + \dot{\omega}_i|_P$$

Energy Balance

$$\left[\frac{\partial T}{\partial t}\right]\Delta x = -Convection(T) + j_i div(T)|_P - \dot{\omega}_{iP}\left[\sum_{i=1}^{Nspecies}\left[h_{f,i}^0 + C_{p,i}T\right]\right]_P + Conduction(T)$$

$$Convection(T) = \frac{\left[(\rho u y_i)|_e T_{i,P}((\rho u)_e > 0) + (\rho u y_i)|_e T_{i,E}((\rho u)_e < 0) - (\rho u y_i)|_w T_{i,W}((\rho u)_w > 0) - (\rho u y_i)|_w T_{i,P}((\rho u)_w < 0)\right]}{\sum C_{p,i}\rho y_i}$$

$$Conduction(T) = \frac{\lambda_{i,e}(T_E - T_P)}{\partial x_e} - \frac{\lambda_{i,w}(T_P - T_W)}{\partial x_w}$$

$$j_i div(T)|_P = \left[\frac{D_{i,e}(y_E - y_P)}{\partial x_e} - \frac{D_{i,w}(y_P - y_W)}{\partial x_w}\right]\frac{(T_E - T_W)}{2\Delta x}$$

.

4.3. Results of Numerical Simulations

4.3.1. Methane/Air Flame

Initially, the system of differential equations previously described was solved in order to study the flame propagation of pure gases, and to estimate the flame velocity. As previously mentioned, the system has been analyzed for a distance between 0 and 5 cm and the integration time studied in this work is of 50 ms. Figure 93 shows the evolution of temperature with respect to time at different positions of the numerical domain for a flame 9% methane/air. The control volumes shown in Figure 93 were chosen to describe the behavior of the temperature in each of the flame zones, i.e. the points at 5 and 2.5 cm are in the post-flame zone, the volumes between 1.22 and 1.45 cm are within the reaction zone and the volume at 0.66 cm is part of the pre-heat zone (i.e. as shown in Figure 92).

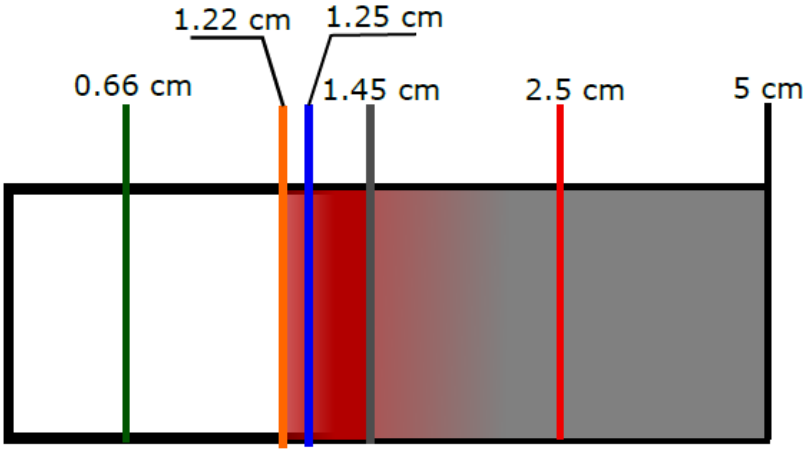

Figure 92. Representation of the control volumes analyzed at each flame zone.

Regarding the post-flame zone, the properties (temperature and mass fractions) were initialized to describe the burnt gas conditions of a flame at equilibrium using PREMIX calculations. A slight decrease of the temperature in this zone can be observed by heat diffusion transport towards the preheat zone. Although, a fast increase in the temperature is observed in the reaction zone after some milliseconds, until reaching to a maximum (e.g. the maximum temperature is reached after 5 ms at 1.22 cm). Then the temperature stabilizes at the conditions of the post-flame zone. Finally, at a distance equal to 0.66 cm (located initially at the middle of preheat zone), the temperature shows a slow increase caused by thermal diffusion, but after approximately 30 ms, the exothermic reaction takes place and a similar trend as observed in the reaction zone is also presented in this zone.

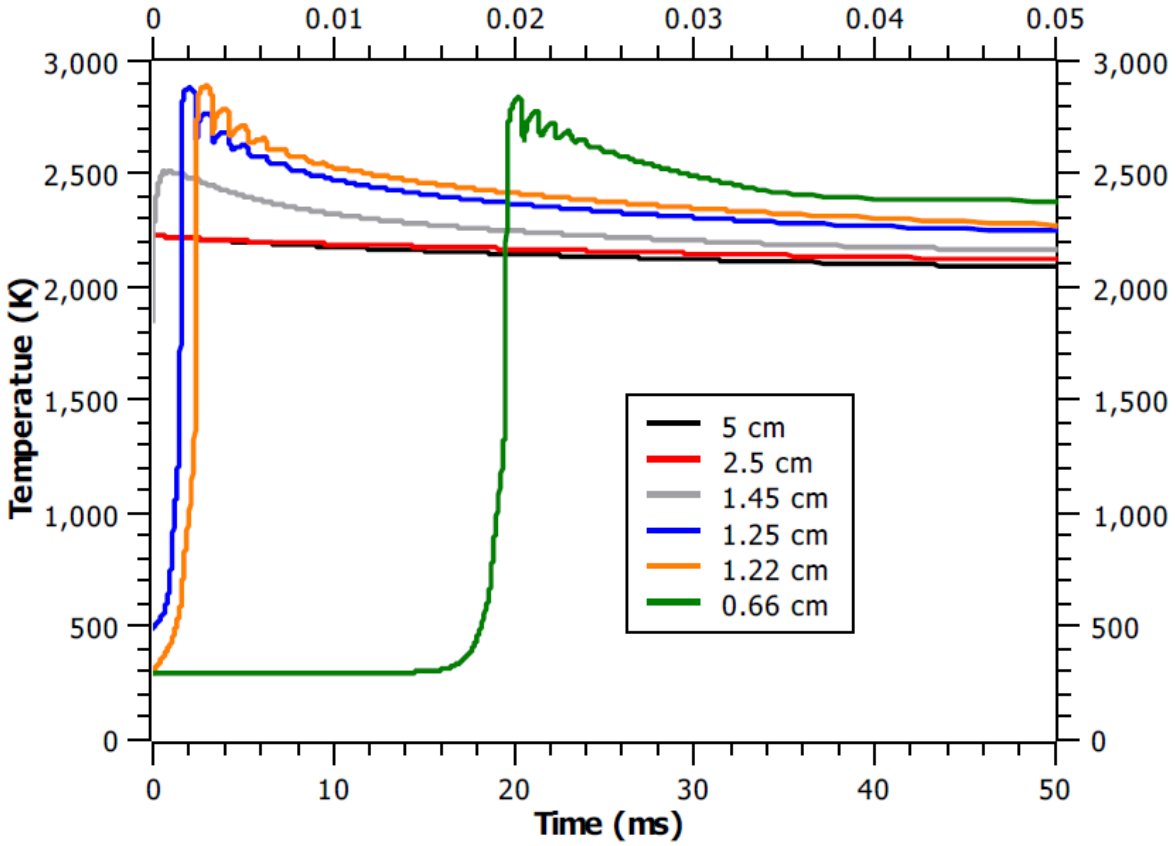

Figure 93. Temperature evolution different control volumes during the evaluation time of 9% methane/air at initial temperature of 298 K in the preheat zone.

The evolution of the reaction products during the integration time, more precisely on the CO and CO_2 mass fractions are shown in Figure 94 and Figure 95. The Jones-Lindstedt chemical combustion mechanism implemented in this study (Table 19) states that methane oxidation reactions generate carbon monoxide and hydrogen, and in a simultaneous reaction, the CO oxidation will produce CO_2. As expected, the CO mass fraction increases rapidly due to the methane combustion until reaching a maximum concentration. Then, the CO oxidation became predominant, generating a considerable reduction of the CO concentration until arriving to a stable final concentration. Correspondingly, a continuous generation of CO_2 is evidenced in Figure 95 until reaching an equilibrium concentration, which is determined by the forward/reverse kinetics constants reported in Table 19. In addition, the carbon monoxide oxidation reaction is very exothermic, explaining why the CO_2 concentration is related to the temperature growth in the system. The numerical results are in good agreement with the micro-gas chromatography, comparison that will be detailed in the following paragraphs.

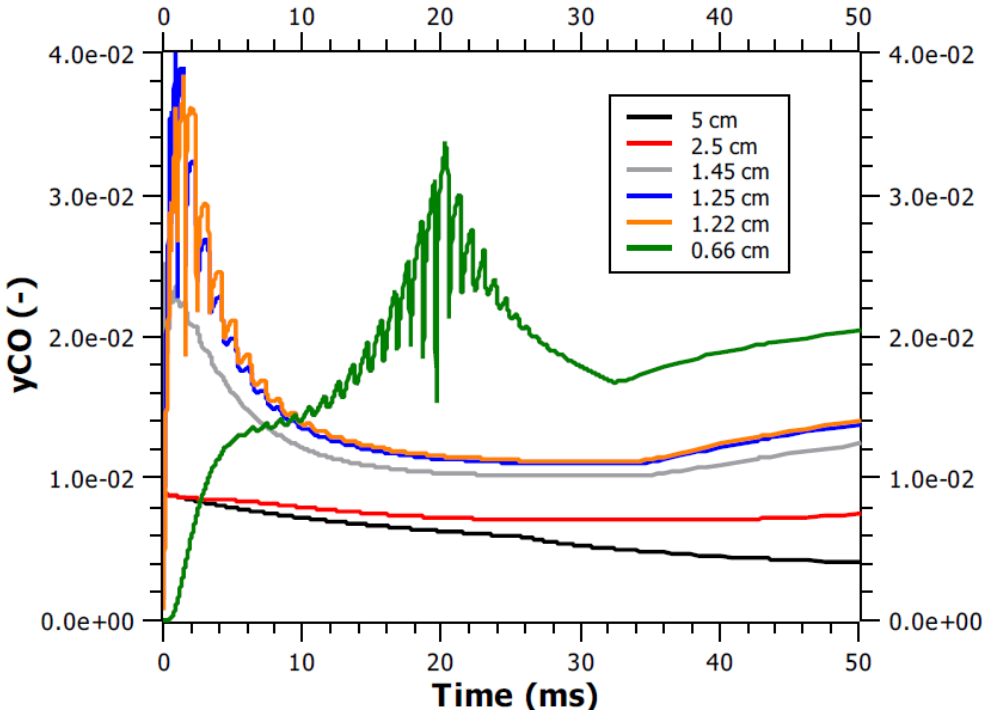

Figure 94. CO evolution at different control volumes of the flame during the evaluation time of 9% methane/air at initial temperature of 298 K in the preheat zone.

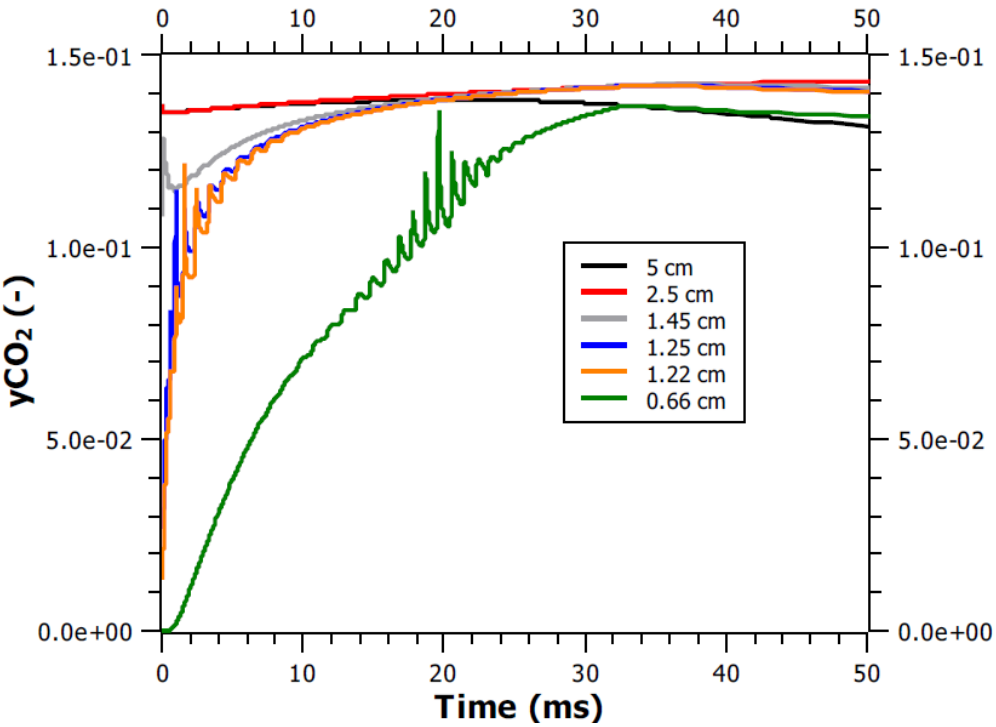

Figure 95. CO_2 evolution at different control volumes of the flame during the evaluation time of 9% methane/air at initial temperature of 298 K in the preheat zone.

The results for the hydrogen mass fraction in a stoichiometric methane/air mixture are observed in Figure 96 at each zone of the flame. In contrast with the results of a stoichiometric flame obtained

by PREMIX, the H_2 mass fraction decreases over time in the post-flame zone until reaching a stable value. These differences can be explained considering the differences in the chemical kinetics used in each model, e.g. PREMIX use detailed mechanism kinetics with an adaptable grid to improve the accuracy of the model. However, a semi-global kinetic mechanism is implemented in this work, in which the reaction of hydrogen is still present in the post-flame zone at the initial conditions defined to solve the system. Concerning the reaction zone (from 1.22 to 1.45 cm in Figure 96), a very fast increase of H_2 mass fraction is evidenced due to methane oxidation, followed by a rapid decrease caused by the reaction with oxygen (reaction 4 in Table 19). Finally, a fast generation of hydrogen is observed in the preheat zone (even before 1 ms), even if the concentration of CO, CO_2 and H_2O are negligible.

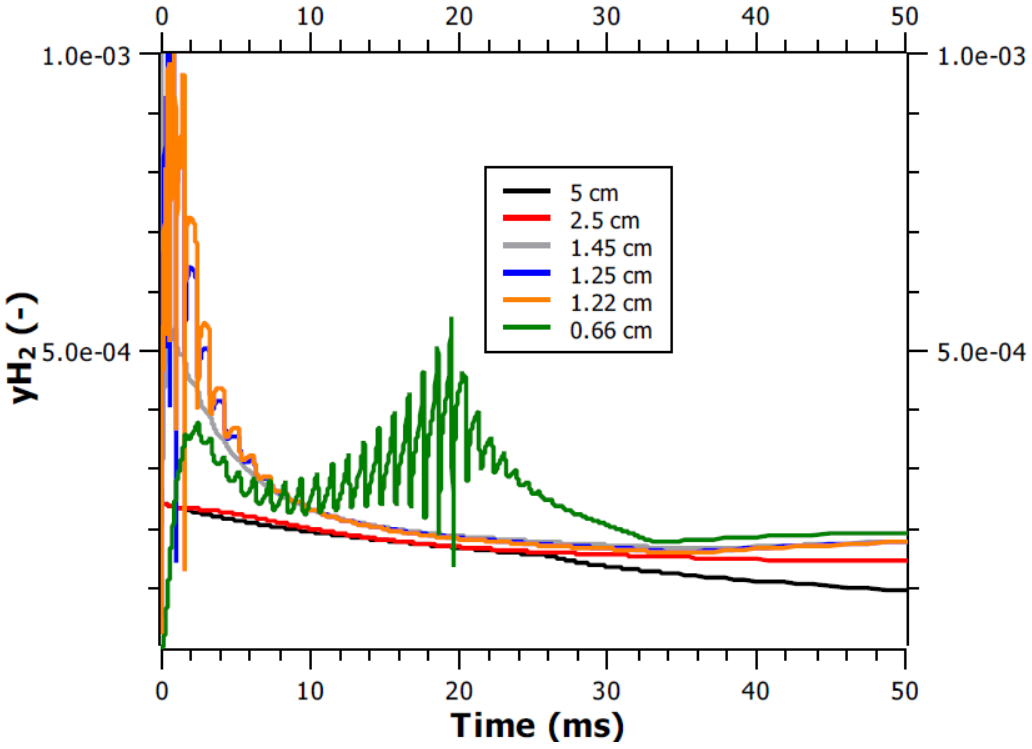

Figure 96. H_2 evolution at different control volumes of the flame during the evaluation time of 9% methane/air at initial temperature of 298 K in the preheat zone.

The numerical simulation results reveal an unrealistic oscillation pattern observed in the mass fraction results, especially for the hydrogen mass fraction. This behavior can be associated with numerical incertitude and numerical diffusion caused by the discretization approximation used to solve the partial differential equations. In addition, the non-linear behavior of the hydrogen reaction rate, i.e. forward and reverse reactions, can lead to numerical difficulties to solve the problems and can produce this behavior. Furthermore, a peculiar attention must be paid to the implementation of global and semi-global reaction mechanism in this type of numerical model, because rate constants (Table 18) have been fitted with the results of the stationary flame. It means that the mechanism has not been developed to describe methane combustion under transitory conditions. In addition, the reaction properties may have no physical meaning: they are established to fit experimental results to a reaction rate equation. These limitations can present another source of error that explains the oscillation found in the numerical results. Nevertheless, it should be added that if such

oscillations are present, they do not lead to a destabilization if the system and they are damped after a few milliseconds.

$$\tau_i = \left.\frac{\rho}{\dot{\omega}_i}\right|_{t=0} \qquad \text{Eq 59}$$

Table 25 presents the initial reaction times for the reactions of the Jones–Linstedt chemical combustion mechanism occurring in the reaction zone (i.e. estimated using the Eq. 59). This result supports the mass fraction trends previously analyzed, where a very fast generation of CO and H_2 will take place (τ_1), followed by the oxidation of carbon monoxide (τ_3). The reaction time for CH_4 oxidation by H_2O (τ_2) is considerably higher than the other reaction times due to the very low concentration at the initial conditions.

Table 25. Initial reaction time at a distance x = 1.35 cm within the reaction zone.

Initial reaction time at x =1.35 cm	$\boldsymbol{\tau_1(s)}$	$\boldsymbol{\tau_2(s)}$	$\boldsymbol{\tau_3(s)}$	$\boldsymbol{\tau_{-3}(s)}$	$\boldsymbol{\tau_4(s)}$	$\boldsymbol{\tau_{-4}(s)}$
	$2.6\text{x}10^{-4}$	4.5	$7.7\ \text{x}10^{-2}$	0.46	$4.83\ \text{x}10^{-3}$	$1.8\ \text{x}10^{5}$

As previously reported, the temperature of each control volume increase over the time due to the heat diffusion transfer and the methane combustion reaction (Figure 93). Figure 97 shows the evolution of the temperature over the space at different times. At first, an increase of the temperature in the reaction zone is observed (between 0 and 1 ms). Then, the temperature of the neighbor control volume in the preheat zone increases, the combustion reaction takes place and the propagation of the reaction zone is evidenced. Therefore, the reaction zone, initially placed from 1.22 to 1.45 cm, moves towards the preheat zone (left direction in Figure 97), which after 30 ms, is located at 0.25 cm. Moreover, at this point, a higher temperature is obtained compared to the values reached in the reaction and post-flame zone. This result is due to the boundary condition of null thermal and mass flux in x = 0, which limit the heat transfer and generates an accumulation of energy in that zone.

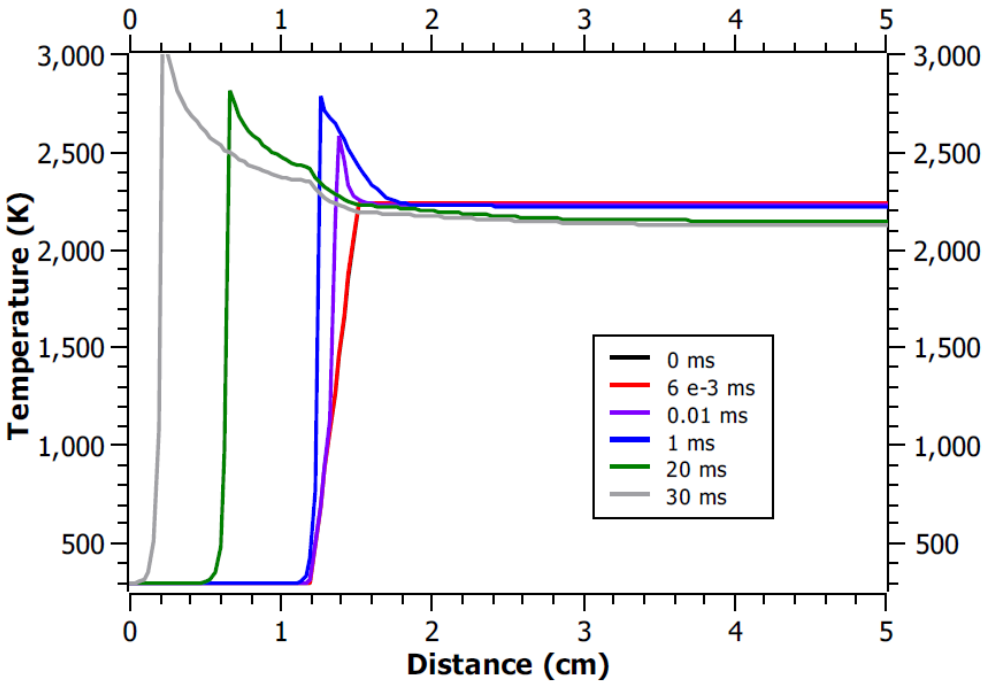

Figure 97. Temperature evolution inside the integration domain at different times, for a 12% methane/air mixture.

In order to analyze the displacement of the reaction zone, the position of the highest temperature, assimilated to the flame front, has been recorded at each integration time. Figure 98 shows the flame position as a function of time for a stoichiometric methane/air mixture (9% vol.). Before 1 ms, an increase of the temperature in the reaction zone is observed, for which a very fast displacement of the maximal temperature is evidenced. Then, a linear displacement of the flame position is observed, which can be represented by a linear regression in Figure 98. In the first place, the constant value of the regression represents the initial position of the flame before the propagation, at 1.38 cm, i.e. it should be reminded that, for initial conditions, the reaction zone was imposed between 1.25 and 1.44 cm. The velocity of displacement of the maximum temperature is represented by the slope of the linear regression, e.g. 34 $cm.s^{-1}$ for a methane/air mixture at stoichiometric conditions in Figure 98. The burning velocity had been defined as the rate of flame propagation relative to the unburnt gases, however, its determination will depend on the definition of flame propagation. The position of the flame can be determined by the drastic modifications on the temperature or combustion radicals. In this work, the flame is defined as the maximum tempertarure obtained in the numerical domain and its displacement is studied in order to calculate the velocity. The latter result is in good agreement with the flame velocity reported experimentally for methane/air mixture, for example, the reported velocity of a stoichiometric methane/air mixture lies between 34 and 38 $cm.s^{-1}$ (Dirrenberger et al., 2011; Proust, 2006). Nevertheless, this result needs to be analyzed with caution. First of all, the production and diffusion of combustion radicals are not described by the semi-global reaction mechanism implemented in this work. As a matter of fact, a deviation from the value reported by detailed mechanisms or experimental data is expected, because the considerably high diffusion of radicals favors the combustion reaction and accelerate the flame. In addition, the radical reaction has a great effect on the final flame temperature. Secondly, it has been assumed that the flame reference point moves with the flame front (as if the reference frame was moving with the flame), so the convection transfer due to the density and

temperature changes is not taken into account, which represents a second source of error. Nevertheless, the values obtained by the 1-D model are comparable with the experimental results reported in the literature and in Chapter 3 of this work (e.g. 33.4 $cm.s^{-1}$ obtained in the flame propagation tube).

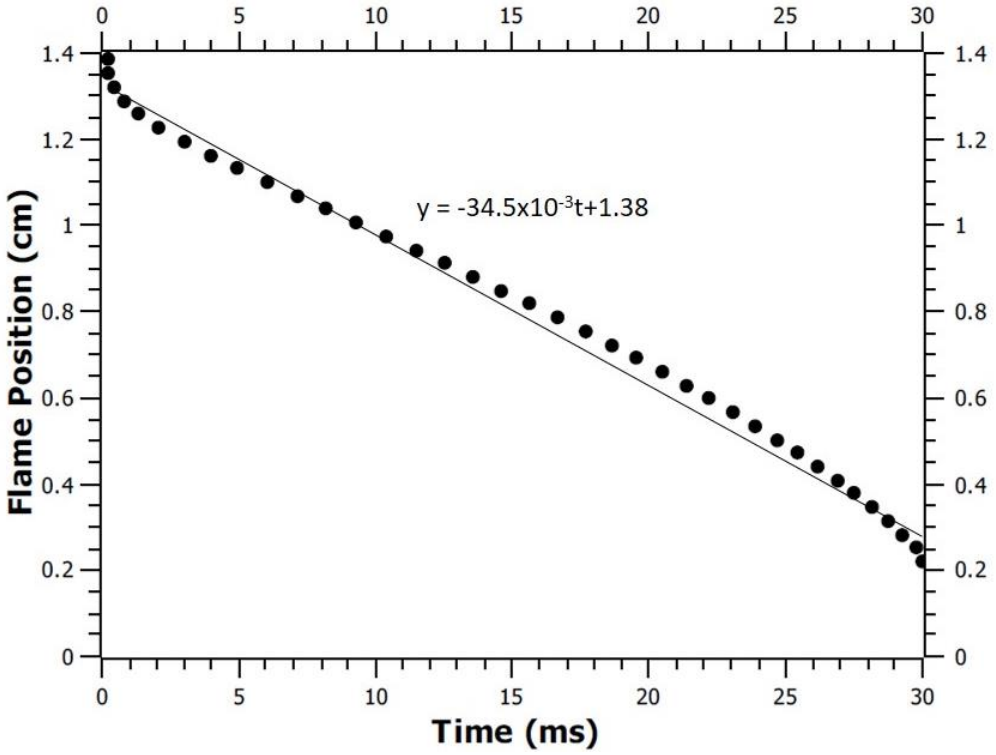

Figure 98. Flame position in the numerical domain over the time for a methane/air stoichiometric mixture

Likewise, the flame propagation model has been used to study the flame propagation and final properties of a rich methane/air mixture, as shown in Figure 99. An unexpected fast increase of the temperature has been evidenced in comparison with stoichiometric methane/air mixtures. A possible reason for this result is related to the very fast reaction of the methane oxidation reaction that will be higher than stoichiometric conditions due to the excess of fuel. Despite the elevated flame temperature obtained in the reaction zone, the front flame propagation velocity and temperature obtained with the model are in agreement with the results reported in the literature, i.e. 32 $cm.s^{-1}$ in this work compared to 30 $cm.s^{-1}$ (Dirrenberger et al., 2011). In addition, this result suggests that the flame propagation phenomena will be limited by the heat and mass diffusion transfer after a very fast combustion reaction, which explains a lower flame propagation compared to a stoichiometric flame mixture.

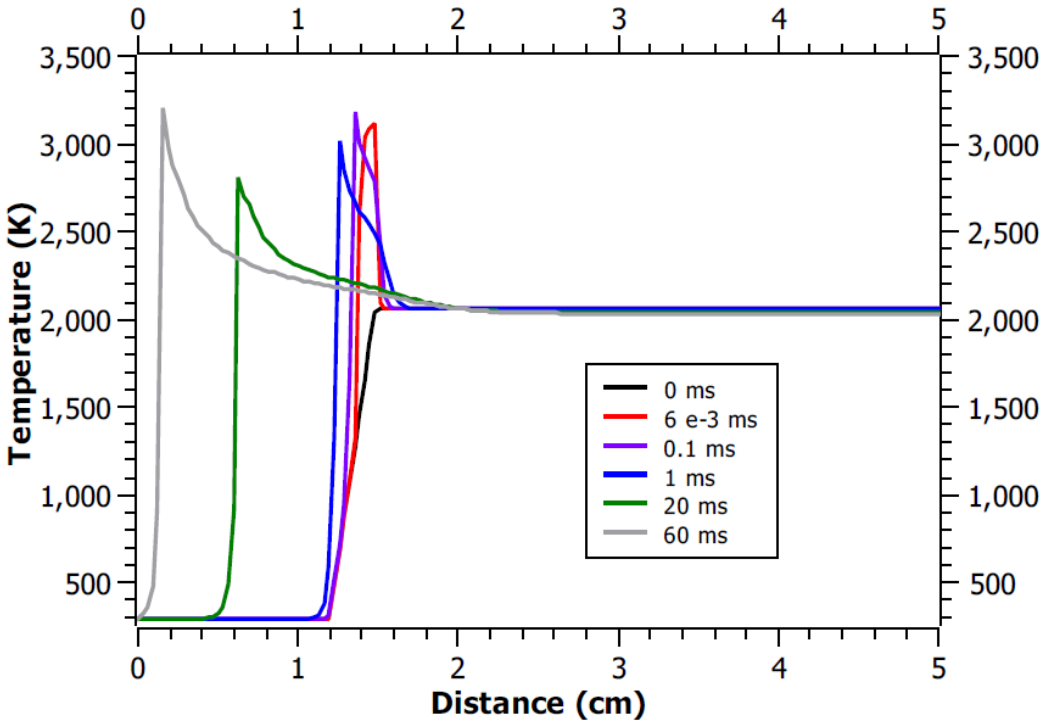

Figure 99. Temperature evolution inside the integration domain at different times, for 12% methane/air mixture

Table 26 presents the temperature, mass fraction and flame propagation velocity (estimated from the displacement of the maximum temperature location – see Figure 97) for three gas mole concentrations. In comparison with the PREMIX stationary flame solution obtained with a detailed kinetic mechanism, the flame temperature calculated by the model of the present study is slightly higher (i.e. a difference of 2% is obtained) for all gas mixtures. However, a coherent result is obtained, where a maximum in temperature and front flame velocity are obtained for conditions close to the stoichiometry. It should be reminded that the aim of the present model is not to reproduce exactly the flame velocity, adiabatic temperature and mass fractions (like it is the case for commercial software such like CHEMKIN). The main objective is rather to obtain a coherent flame propagation model that allows to analyze the influence of dispersed particles on the flame properties. Thus, as the results presented here for gas mixtures are comparable to the PREMIX software and consistent with experimental measurements obtained with μ-gas chromatography (Table 27), we will now consider that the 1-D flame propagation model is validated, even it can be obviously improved.

Table 26. Temperature and mass fraction results of methane/air mixtures at stationary conditions.

Properties	**v.% Methane concentration**		
	8.5%	**9%**	**12%**
***Temperature* (*K*)**	2116	2278	2144

Properties	v.% Methane concentration		
	8.5%	**9%**	**12%**
y_{CH_4}	0	0	0
y_{CO}	0.017	0.014	0.079
y_{CO_2}	0.13	0.14	0.081
y_{O_2}	0.018	$6.7\text{x}10^{-4}$	$2.2\text{x}10^{-6}$
y_{H_2O}	0.074	0.058	0,066
y_{H_2}	$4.24\text{x}10^{-5}$	$1.7\text{x}10^{-4}$	$2.3\text{x}10^{-3}$
y_H	$3.8\text{x}10^{-4}$	$4.9\text{x}10^{-4}$	$4.2\text{x}10^{-4}$
y_{OH}	0.028	0.048	$4.0\text{x}10^{-2}$
y_O	$2.1\text{x}10^{-4}$	$3\text{x}10^{-4}$	$1.4\text{x}10^{-4}$
u_f (cm.s^{-1})	31.7	34.5	32.1

Table 27. Measured mass fraction (µ-Gas Chromatography) of experimental explosion of 9% methane/air mixture under quiescent conditions.

Mass fraction	y_{H_2}	y_{CO}	y_{CO_2}	y_{O_2}
µGC	0.014	$1.5\text{ x}10^{-2}$	$8.9\text{ x}10^{-2}$	$2.5\text{ x}10^{-3}$

Despite the good agreement of the flame model for methane gas mixture at stoichiometric and rich fuel mixtures, the model does not converge for methane concentrations close to the LFL. For instance, for 7% methane/air mixture, stiffness problems had been evidenced and the simulation of the flame propagation is only possible for an integration time below 5 milliseconds. Due to the complex kinetics of the hydrogen oxidation reaction (i.e. non-integer/negative reaction order and dependence on T^{-1}), unstable changes on the hydrogen mass fraction are observed and generates non-singular matrix that impede the ODE resolution. Figure 100 shows the evolution of the hydrogen mass fraction at different control volumes of the numerical domain. It can be evidenced a fast and oscillating change of the H_2, especially for the post-flame due to the high temperature in this zone. After 1 ms, the oscillating behavior seems to decrease, but then, approximately at 5 ms a negative solution of the hydrogen mass fraction is obtained, generating a non-singular matrix.

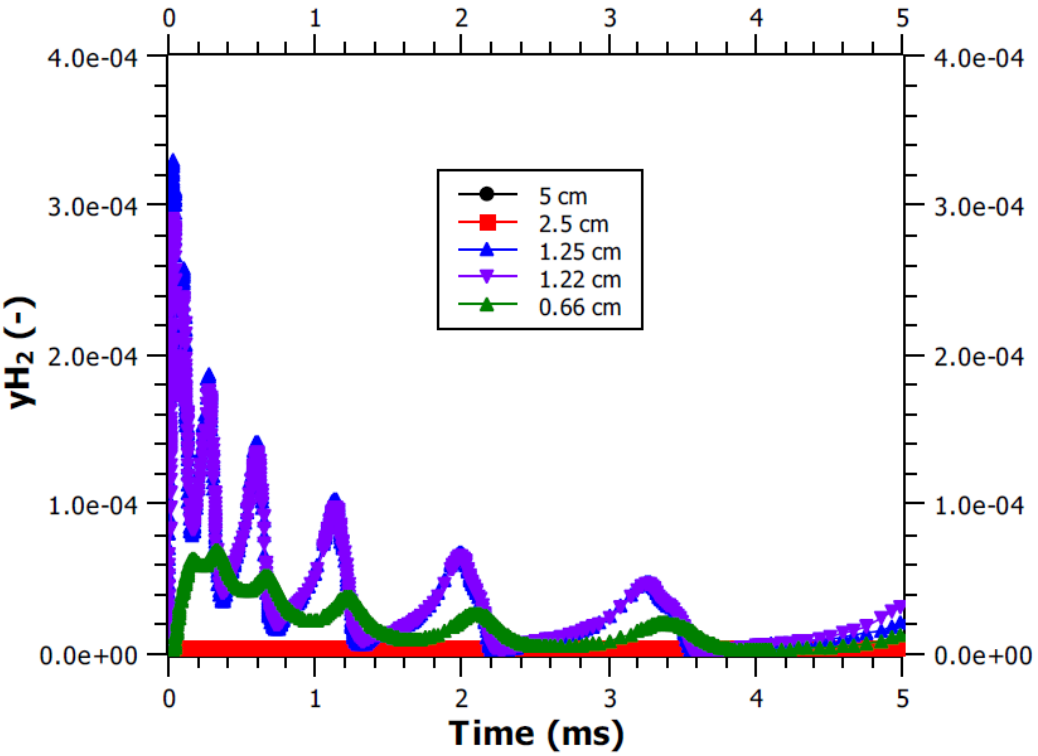

Figure 100. H_2 evolution at different control volumes of the flame during the evaluation time for 7% .molar methane/air mixture.

4.3.2. Hybrid mixture Flame

4.3.2.1 Model of Radiative Heat Transfer

The experimental tests have shown that the dispersion of solid particles generates changes in the explosion severity of methane/ air mixtures, mainly by the variations of the heat transfer and reactivity of the mixture. As a first approach, the effect of the solid particles on the thermal energy transfer will be only analyzed, which means that the modifications on the mean heat capacity of the mixture and the radiative heat transfer will be taken in account (no chemical reaction of the solid). Therefore, the radiative heat transfer is added to the energy balance (Equation 45):

$$\sum_{i=1}^{Nspecies} C_{p,i}[\rho y_i \partial_t(T) + \rho y_i u div(T) + j_i div(T)] = -\dot{\omega}_i \left[\sum_{i=1}^{Nspecies} \left[h_{f,i}^0 + C_{p,i}T\right] \right] + div(\lambda \nabla \mathrm{T}) + Q_{rad}$$

The thermal radiation of a participating media (two-phase media) has been estimated solving the Radiative Transfer Equation (RTE). In this equation, the mixture of gas and nanoparticles is assumed to be gray and to be at thermal equilibriumwithout temperature difference between the gas and the solid particles. The emitted, absorbed and scattered energy is estimated as (Adzerikho, 1987; Haghiri and Bidabadi, 2011, 2010; Meinköhn et al., 2007; Modest, 2013):

$$\frac{dI}{dx} = K_a I + K_s I - K_a I_b - \frac{K_s}{4\pi}\int_{4\pi} I(\Omega)\, P d\Omega \quad \text{Eq 60}$$

where I, I_b, K_a and K_s are the thermal intensity, the thermal intensity of a black body, the absorption coefficient and the scattering coefficient respectively. The first three terms on the right side of the equation 60 represent the absorbed, scattered and the emitted energy. The integral term take in account the scattered energy coming from surrounding particles in all directions. Assuming an homogeneous dispersion of the particles and a similar particle diameter, the absorption and scattering coefficients are estimated as (Modest, 2013):

$$K_a = \frac{\pi {d_p}^2 n_s}{4} Q_{abs} = \frac{3}{2}\frac{\varphi}{\rho_p d_p} Q_{abs} \quad \text{Eq 61}$$

$$K_s = \frac{\pi {d_p}^2 n_s}{4} Q_{sca} = \frac{3}{2}\frac{\varphi}{\rho_p d_p} Q_{sca} \quad \text{Eq 62}$$

It was assumed that the absorption and scattering properties of the media are mainly dependent on the dust characteristics, and the influence of the methane on the radiation properties of the media can be neglected compared to the effect of the solid particles (Thellmann, 2010). In equations 61 and 62, Q_{abs} and Q_{sca} are the absorption and scattering efficiencies, respectively, which depends on the particle's emissivity ε_P if the dispersed particles are mainly diffusely reflecting spheres (Haghiri and Bidabadi, 2010; Modest, 2013):

$$Q_{abs} = \varepsilon_P \quad \text{Eq 63}$$

$$Q_{sca} = 1 - \varepsilon_P \quad \text{Eq 64}$$

An analytical solution of equation 60 has been proposed by Haghiri et al., for each zone separately in order to estimate the heat transport by radiation. The flame zone division makes possible to neglect some terms of the RTE equation (Bidabadi et al., 2013, 2011; Bidabadi and Azad, 2015; Haghiri and Bidabadi, 2010). Firstly, the multi-scattering contribution (integral term in equation 60) is neglected, and the transfer radiation equation becomes an ordinary differential equation. Then, the radiative heat transfer is estimated solving the differential equation at each zone (Haghiri and Bidabadi, 2010).

Preheat zone (Ph): Assuming that only the absorbed radiation intensity flux is stored as internal energy, the heat radiation term is read as (Haghiri and Bidabadi, 2010):

$$Q_{rad,Ph} = K_a I \quad \text{Eq 65}$$

In addition, considering that the media will only absorb and scatter the thermal intensity flux and neglecting the black body emission, the RTE is expressed as:

$$\frac{dI}{dx} = K_t I \quad \text{Eq 66}$$

Relocating the x-axis on the reaction zone, the boundary condition between zones establishes that the intensity (I) at the flame zone (x = 0) will be equal to the flame intensity I_f :

$$Q_{rad,Ph} = K_a I_f \exp(K_t x) \quad \text{Eq 67}$$

Reaction zone (f): In this zone the radiative heat transfer consists of the absorption and black body emission at the flame conditions (Bidabadi and Azad, 2015):

$$Q_{rad,f} = K_a I - K_a I_{bp} \quad \text{Eq 68}$$

In a similar manner than for the preheat zone, the RTE is developed in the flame zone, but without neglecting the black body emission:

$$\frac{dI}{dx} = K_t I - K_a I_{bp} \quad \text{Eq 69}$$

The solution of the differential equation 68 taking the boundary condition in the flame zone is shown in equation 60:

$$I = \frac{K_t I_f \exp(K_t x) - K_a I_{bp} \exp(K_t x) + K_a}{K_t}$$

Evaluated in the flame zone, the radiation term is defined as (Haghiri and Bidabadi, 2010):

$$Q_{rad,f} = -K_a (I_{bp} - I_f) \quad \text{Eq 70}$$

Post flame zone (Pf): The heat radiation term in the post flame zone has the same definition as for the reaction zone (Eq. 68):

$$Q_{rad,Pf} = K_a I - K_a I_{bp} \quad \text{Eq 71}$$

However, the intensity is determined by the boundary conditions between the two zones. Bidabadi and Azad (2015) established that at $x \rightarrow \infty$, the intensity has a finite value , and matching with the reaction zone, the intensity can be expressed as:

$$I = \frac{K_a}{K_t} I_{bp}$$

Replacing in equation 71, the heat radiative transfer in the post-flame zone reads as:

$$Q_{rad} = -\Omega K_a I_{bp} \quad \text{Eq 72}$$

where

$$K_t = K_a + K_s, \quad \Omega = \frac{K_s}{K_a + K_s} \quad \text{Eq 73}$$

$$I_{bp} = \frac{\sigma T_f^4}{\pi}, \quad I_f = \frac{K_a}{K_t} I_{bp} \quad \text{Eq 74}$$

In order to take into account the radiative heat contribution generated by non-transparent media composed by dispersed nanoparticles and a combustible gas, the dust concentration, the mean diameter and the emissivity of the solid must be defined. The mean particle diameter defined from the particle size distribution tests. The emissivity of the particles had been defined from values reported in the literature (Auerkari, 1996; Omega, 2017).

4.3.2.2 Application of the Numerical Model to Hybrid Mixtures: Results

In order to study the influence of a dispersed constant concentration of nanoparticles on the flame propagation velocity, the 1-D model has been solved for a hybrid mixture at 9% molar concentration of methane. Three main hypotheses have been implemented: 1) the concentration of dust is constant over the time and it is homogeneously dispersed in all the integration domain, 2) the carbon black nanoparticles oxidation reaction is negligible in comparison with methane oxidation and 3) nanoparticles have the same diameter, equal to the mean diameter of the dust (Table 28). In Figure 101, the evolution of the temperature at two different positions (initially in the preheat zone) is presented for 6 $g.m^{-3}$ of carbon black added to the methane/air mixtures, for two different particle diameters. The mean agglomerate diameter (10 μm or specific surface of 0.3 $m^2.g^{-1}$) and the elementary particle diameter (measured by BET method - 75 nm or specific surface of 44 $m^2.g^{-1}$) of Corax N550 carbon black (see section 2.2.1) have been tested for the hybrid mixtures. It has been evidenced that the temperature does not change significantly in the flame zone when 6 $g.m^{-3}$ of carbon black particles with a mean particle diameter of 10 μm. To illustrate, the temperature of the preheat zone increases only about 0.5% due to the radiative heat transfer between the participating media and the reaction zone. In fact, this result suggests that, if such concentration of carbon black is dispersed without deagglomeration of the dust after dispersion, the flame propagation would not be modified due to the radiation heat transfer with the dispersed particles. Nevertheless, in reality, very fast deagglomeration/agglomeration phenomena are likely to occur when nanoparticles are dispersed at high turbulence levels (Eckhoff, 2011; Murillo, 2016; Murillo et al., 2013).

In the case of a dispersion of 6 $g.m^{-3}$ carbon black having a particle diameter of 75 nm (case that represent a total deagglomeration of Corax N550 agglomerates and aggregates into a homogeneous dispersion of elementary particles), significant modification of the flame temperature have been evidenced. The flame temperature evolution of two control volumes in the preheat zone, i.e. 0.66 and 0.91 cm, are shown in Figure 101. Initially, the temperature increases linearly due to the radiative heat absorption, i.e. after 5 ms the temperature of the hybrid mixture is increased 200 K. The radiative heat transfer to the preheat zone leads to a faster reaction than for methane/air mixtures and to a greater front flame velocity. In addition, when a total fuel reaction is achieved, the final temperature of the system decreases due to the radiative heat loss toward the unburnt mixture. For example, the final temperature obtained in the post-flame zone for methane/air mixture was 2278K, whereas the final temperature of the system decreases to 2126 K in presence of dispersed particles. These results suggest that the radiative heat transfer due to a dispersion of nanoparticles has a considerable influence on the flame propagation and on the final temperature of a hybrid mixture.

Table 28. Properties of the carbon black particles used in the numerical simulation.

	d_p Elementary Particle	Bulk density ($kg.m^{-3}$)	$Emissivity$	Heat Capacity $\left(\frac{J}{kg\ K}\right)$
Carbon Black	75 nm	1800	0.81	$(1.7 + 7.7\text{x}10^{-4}T - 8.6\text{x}10^{4}T^{-2})\frac{R}{W_C}$
Alumina	20 nm	3950	0.07	880

However, the interpretation of these results must be done taking into account the hypotheses made in the development of the numerical model. Firstly, a homogeneous concentration of the unburnt mixture is very difficult to achieve because of the influence of the inertial forces on the particles dispersion in a hybrid mixture. Secondly, a perfect dispersion of elementary nanoparticles (monodisperse PSD) is a utopic scenario, due to the strong agglomeration forces and to the fast agglomeration between nanoparticles. In addition, the interactions between the dispersed particles and the flame are not taken into account in the model (for example, flame surface modifications/stretching). It is also assumed that the radiative heat transfer takes place at thermal equilibrium, which may be true for the case of nanoparticles, but for larger particles a difference of temperature between the gas and the dispersed solid may be evidenced. Finally, the multi-scattering term in equation 60 has been neglected, which can have an effect on the flame propagation phenomena. Despite the previous hypotheses, the modified numerical model allows the quantification of the thermal radiation contribution and the analysis of the influence of some parameters (as the particle size/specific surface area and particle concentration) on the flame propagation.

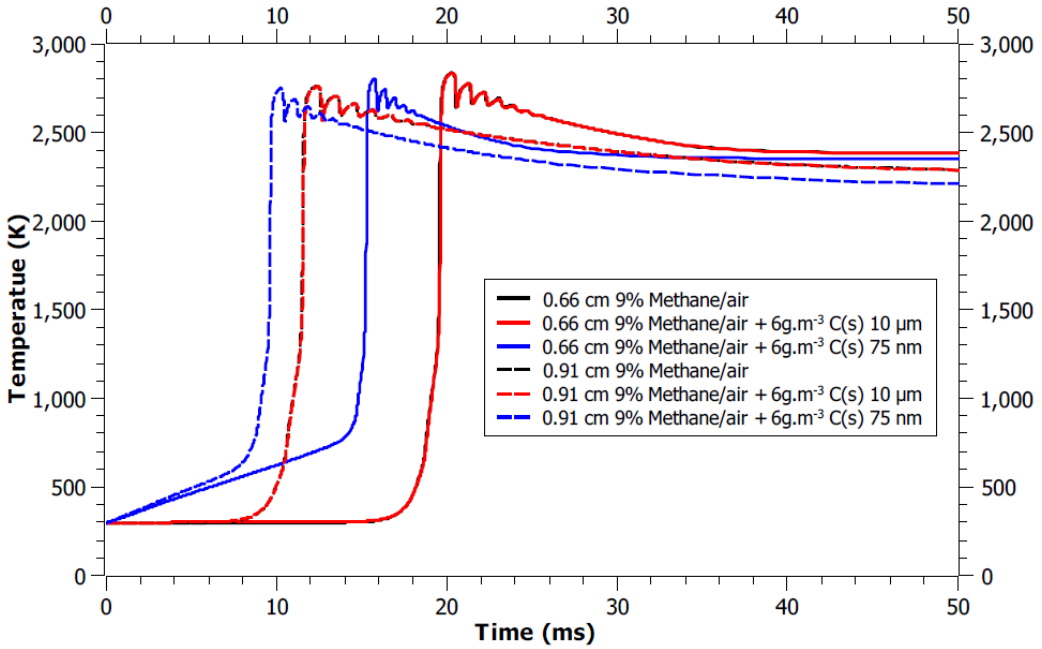

Figure 101. Effect of the particle diameter in the heat radiation transfer on 9% Methane/ 6g.m-3 Carbon black/ air mixtures.

In order to illustrate the important effect of the dispersion of elementary nanoparticles on the radiative heat transfer, the influence of 10 nm carbon black nanoparticles (representing a particle diameter close to the elementary particle diameter of Printex XE2 – 3 nm) on the flame propagation has been analyzed too, as shown in Figure 102. A considerable increase in the flame temperature is observed as well as a faster reaction for carbon black particles with a diameter of 10 nm. This evolution represents an increase of around 450% in terms of flame propagation velocity compared to methane/air gas mixtures.

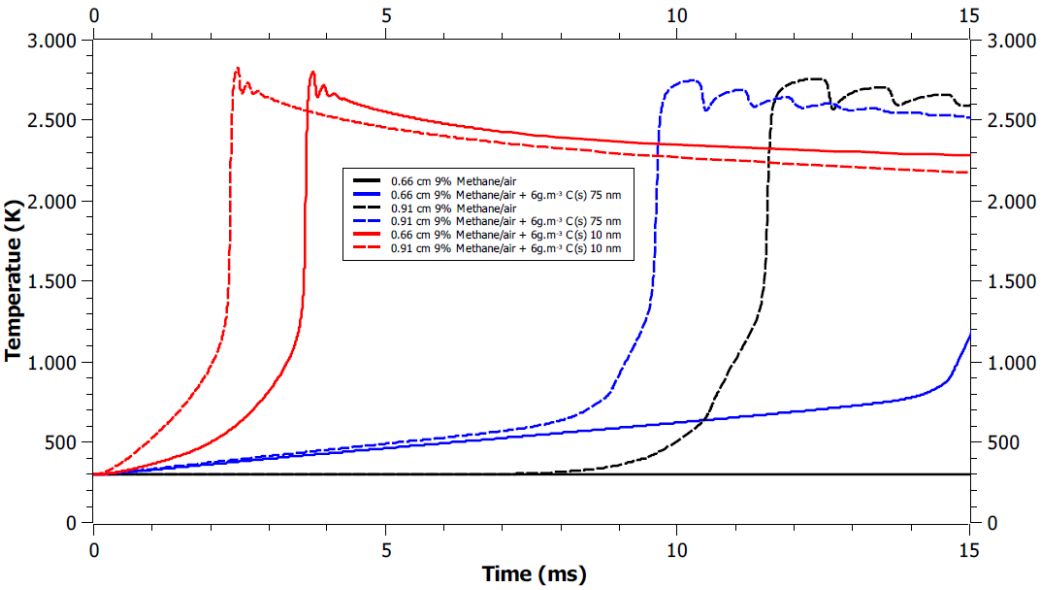

Figure 102. Effect of the particle diameter in the heat radiation transfer on 9% Methane/ 6g.m-3 Carbon black/ air mixtures.

The concentration of 75 nm carbon black nanoparticles on the flame radiation transfer has been also studied. The influence of the dispersion of 2.5 and 6 $g.m^{-3}$ in the reactive mixture is represented in Figure 103. As expected, an increase in the concentration of carbon black nanoparticles generates a rise in the temperature of the preheat zone and reduces the time necessary for the reaction to take place. In order to obtain a reaction at 0.91 cm, methane reaction requires 12 ms, while only 11.8 and 10 ms are necessary if 2.5 and 6 $g.m^{-3}$ are added to the system. This result suggests that the temperature conditions of the preheat zone plays an important role on the flame propagation, due to the acceleration of the reaction and the increases of heat transfer. The final temperature of the burnt gases decreases when the heat radiation emission toward the unburnt mixture increases, as observed in Figure 103.

The flame velocity has been estimated as well for the hybrid mixtures and compared to the case of methane/air mixture (Figure 104). The results obtained for the displacement of the reaction zone shows that a rise of the flame propagation is obtained when the concentration of carbon black is increased in the system. For instance, the flame velocity increases from 34.5 to 36 $cm.s^{-1}$ when 2.5 $g.m^{-3}$ of carbon black (75 nm) are added into the system and it increases up to 41 $cm.s^{-1}$ when 6 $g.m^{-3}$ are inserted. Moreover, the results of the flame propagation model suggest that the linear behavior of the flame velocity obtained for methane/air is not any longer observed for hybrid mixture, as shown in Figure 104. In other words, the flame velocity seems to be accelerated when carbon black nanoparticles are added into the combustible mixture, due to the radiative heat transfer, i.e. the flame acceleration is evidenced after 23 ms and 19 ms for 2.5 and 6 $g.m^{-3}$ carbon black/methane/air mixtures respectively.

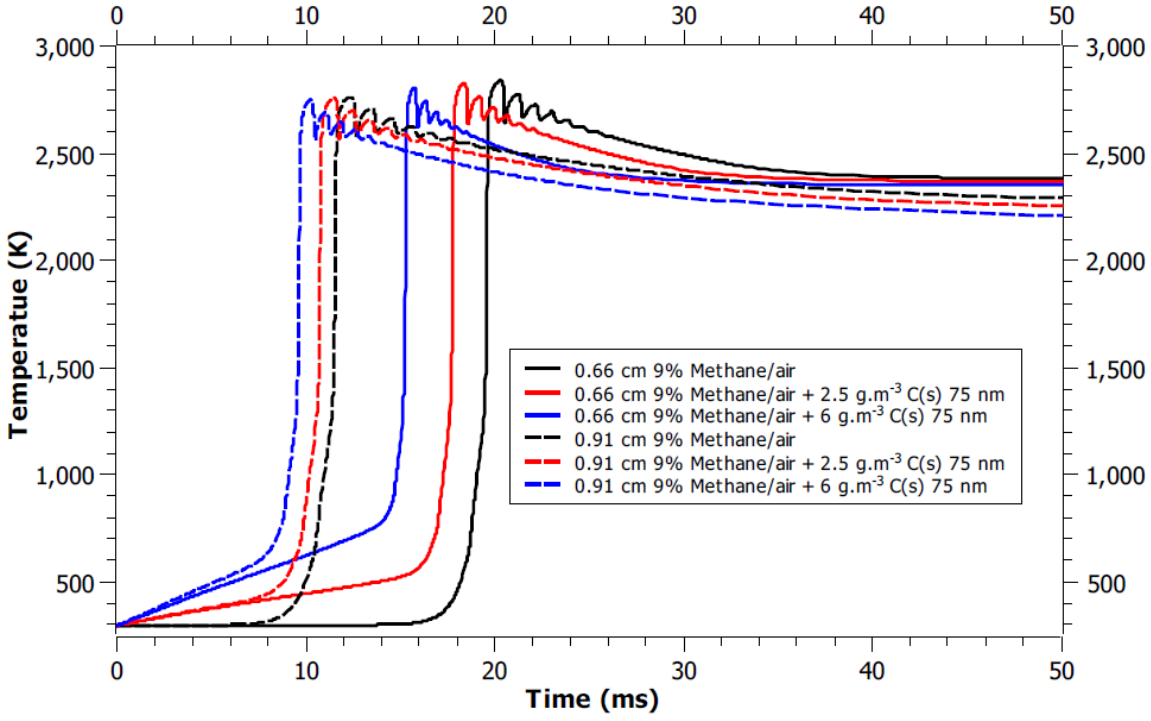

Figure 103. Influence of carbon black nanoparticles concentration at two positions of the numerical domain.

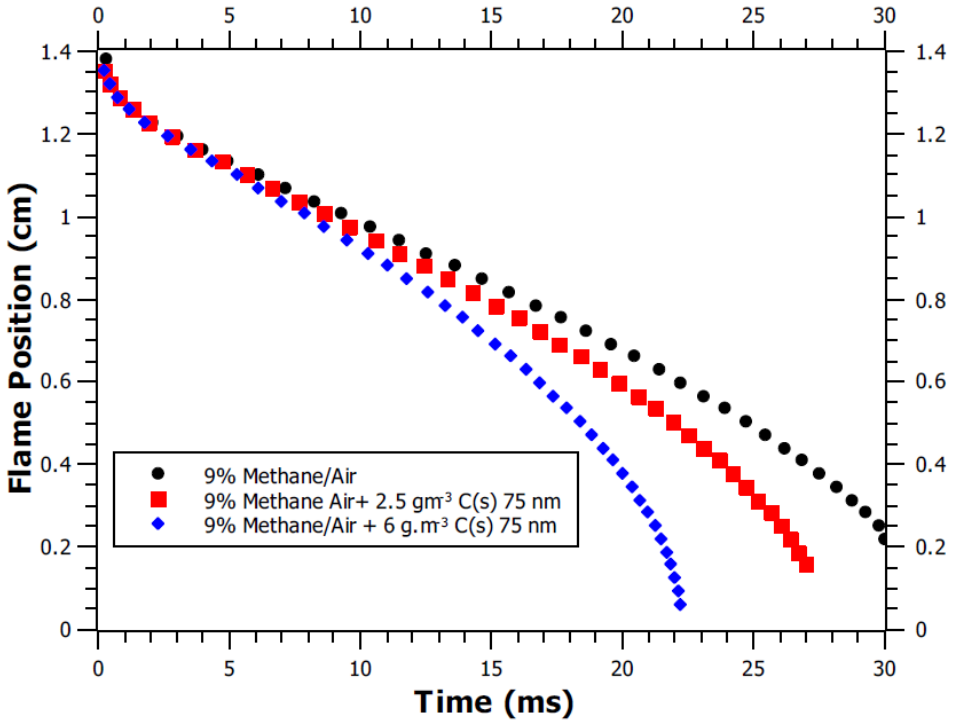

Figure 104. Influence of carbon black concentration on the flame position in the numerical domain over the time.

The explosion severity and flame velocity experimental results presented in previous chapters suggest that the dispersion of carbon black has a complex effect on the explosion of methane/air mixtures. It should be reminded that the explosion severity parameters seem to increase fuel lean conditions but decrease for stoichiometric and rich mixtures (chapter 2). Indeed, the modifications of explosion severity can be associated with changes in the chemical contribution of the nanoparticles, modifications of the flame stretch and thickness, changes on the heat for radiation and a contribution of the particles to soot nucleation. For instance, the numerical model suggests that the positive contribution of the addition of carbon black to the explosion severity parameters and burning velocity obtained experimentally can be associated with the radiative heat transfer between the burnt and unburnt gases, which is considerably augmented by the dispersion of carbon black nanoparticles. Likewise, the reduction in the explosion severity and burning velocity obtained for some mixtures may be primarily due to flame surface modifications and turbulent quenching observed during the turbulent propagation.

Despite the increase of approximately 23% in the flame velocity when 6 $g.m^{-3}$ of carbon black nanoparticles are added into the combustible mixture, which may explain the rise on the explosion severity parameters, some precautions must be taken into account when analyzing this result. Firstly, in order to better conclude on the effect of dispersion of carbon black nanoparticles in the flame velocity, the numerical model should take into account the initial size particle distribution, which will modify the absorption and scattering coefficient. In addition, the transitory behavior of the total surface of the dust as a result of agglomeration and sedimentation should reduce the contribution of the thermal radiation of the mixture. Finally, it should be reminded that, regardless the high stability of dispersion, the dust concentration in the cloud is lower than the initial concentration placed in the system to be dispersed. This means that the thermal and reactive

properties of the cloud will have a less important influence on the flame propagation than the estimations done with the model.

In this work, the effect of the addition of alumina inert particles on the explosion severity parameters and burning velocity has been also studied (Table 28). In Figure 105, the flame evolution of carbon black and alumina hybrid mixtures is compared for 2.5 $g.m^{-3}$ concentrations. The results suggest that alumina dust does not have any effect on the flame propagation of methane/air mixture, due to the very low emissivity of this material (0.07). However, flame propagation tests performed in alumina/methane/air mixture (see section 3.3.2) shows a slight increase on the flame brightness. Therefore, the properties of alumina implemented in the numerical model may not be representative of the properties of the APD – alumina in the experimental measurements. As for carbon black nanoparticles, the experimental differences between gas and alumina hybrid mixtures for flame propagation velocities and maximum overpressures are more likely to be a result of the flame surface modifications than to heat transfer contributions. In addition, the presence of alumina nanoparticles can favor the radical combination and plays a role as soot nuclei, which can explain some modifications on the experimental parameters. Analyses (X-Ray Diffraction XRD or Thermo-Gravimetric Analysis TGA for instance) should be performed in the future on the soot collected post-combustion in order to determine if alumina can act as a nuclei.

Figure 106 shows the evolution of the temperature of alumina and carbon black hybrid mixtures at concentrations equal to 6 $g.m^{-3}$ (75 nm). It had been found that an increase of the alumina concentration does not contribute to an acceleration of the methane/air flame.

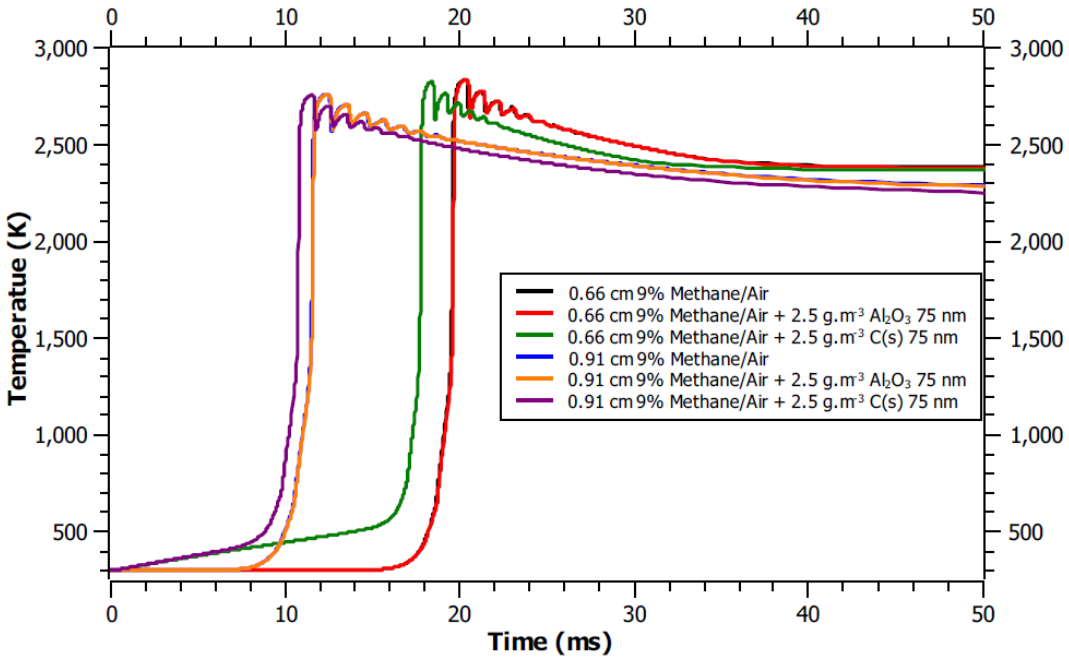

Figure 105. Temperature evolution of 9% Methane/Air, 9% Methane/Air+2.5g.m-3 Al2O3 (75 nm) and 9% Methane/Air+2.5g.m-3 C(s) (75 nm) at two points in the space.

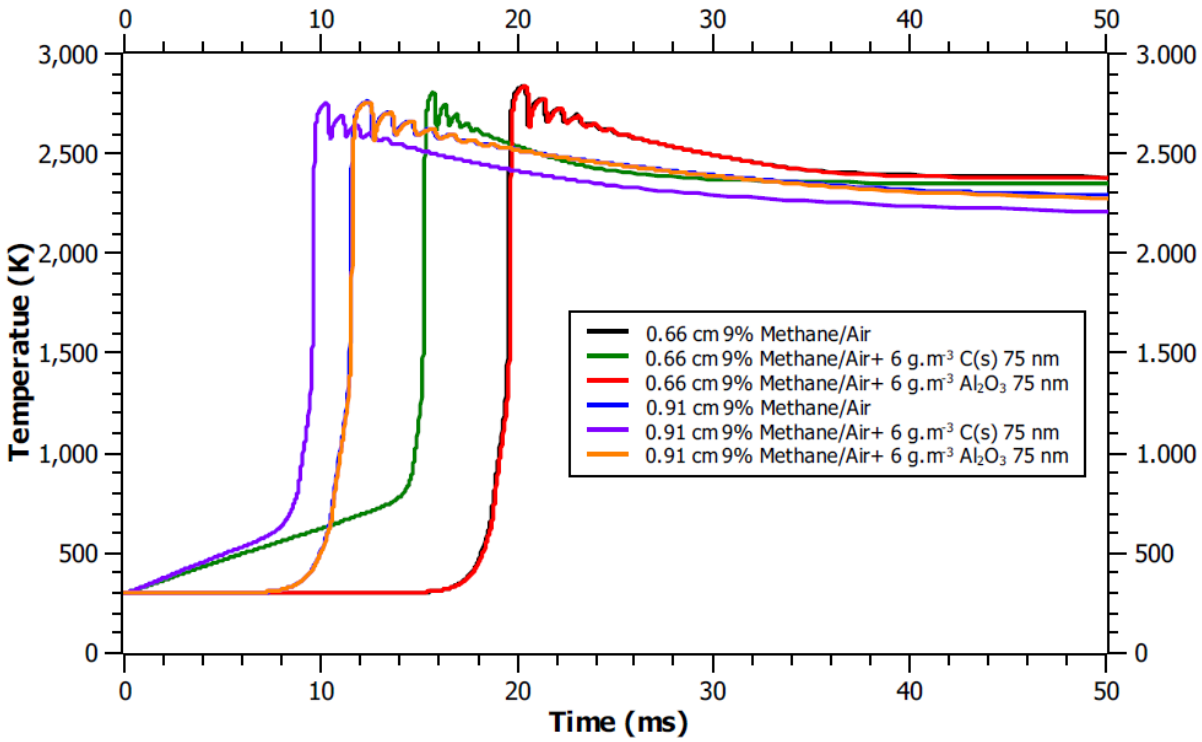

Figure 106. Comparison between carbon black and alumina particles on the flame propagation.

4.3.3 Hybrid mixture Flame – Contribution of the chemical reaction of the solid

4.3.3.1 Carbon black kinetic model

The solid carbon oxidation has been widely studied during the last years due to its key role in some industrial processes as the coal combustion, iron-making and gasification of coal, biomass or solid waste processes (Hurt and Calo, 2001). The heterogeneous combustion of the carbon particles is a complex phenomenon because the kinetics is influenced by the oxygen diffusion through the particle (notably at its surface), the formation of oxides in the active site, the migration of oxides and the changing characteristics of the surface during the reaction. Some studies had focused on the determination of global and semi-global reaction kinetics of different types of carbon particles and with different methods of estimation (Croiset et al., 1996; Field, 1969; Hurt and Calo, 2001; Ranish and Walker, Jr, 1993; Sørensen et al., 1996). However, these global expressions are unable to describe the global reactivity of the carbon as principal fuel and their applications are limited in pressure and temperature. Complex kinetics have been developed for combustion and gasification applications of char that have been found more accurate in the prediction of the yield of the reaction (Tilghman and Mitchell, 2015; Zoulalian et al., 2015).

The objective of this study is to analyze the effect of the dispersion of nanoparticles on the explosion properties of gas explosions, analyzing the influence of the specificities of these particles (specific surface, emissivity, reactivity, etc.). For this reason, the methane/air mixture is defined as the principal fuel of the reaction and the dispersed solid particles will modify the properties of the flame propagation. Thus, a simple kinetic mechanism has been chosen to describe the carbon black combustion and it is assumed that, for carbon black nanoparticles, the diffusion limitations can be neglected. Nevertheless, in the case of pure dust explosions (i.e. nanoparticles as principal fuel), a complex model should be implemented, taking in account the active site modifications and the

modifications on the size particle distribution. The carbon oxidation is assumed to produce only carbon monoxide and to follow the reaction rate proposed by Bews et al. (2001):

$$C(s) + \frac{1}{2}O_2 \rightarrow CO$$

$$\frac{\partial \varphi}{\partial t} = -W_C k_C \rho^{0.5} \frac{y_{O_2}^{0.5}}{W_{O_2}{}^{0.5}} \frac{S_{ext}}{V} \qquad \text{Eq 75}$$

The total external surface changes due to the reaction of the carbon black nanoparticles. Assuming that the carbon black nanoparticles are perfect spherical particles with the same mean diameter and by developing the total external surface, Eq. 75 becomes:

$$\frac{\partial \varphi}{\partial t} = -W_C k_C \rho^{0.5} \frac{y_{O_2}^{0.5}}{W_{O_2}{}^{0.5}} \frac{6\varphi}{\rho_p d_p} \qquad \text{Eq 76}$$

The rate consumption of carbon was assumed to follow the behavior proposed by Bews et al. (2001):

$$k_C = 1.1x10^4 \exp\left(\frac{-179\ \text{kJ mol}^{-1}}{RT}\right) [\text{mol}^{0.5}.\text{s}^{-1}\text{m}^{-0.5}] \qquad \text{Eq 77}$$

4.3.3.2 Numerical Model Results

The conservation equation for the concentration of carbon black nanoparticles (Eq 76) has been implemented in the numerical model, and by this means, the influence of methane reaction, of the carbon black reaction and of radiation heat transfer contributions are taken simultaneously into account to estimate the front flame propagation velocity. Figure 107 compares the temperature evolution at two points of the initial preheat zone for a gas mixture, a carbon black/methane hybrid mixture without the reaction of the particles and the same hybrid mixture taking into account the reaction of the solid particles. It should be reminded that the flame reaction was initially established between 1.22 and 1.45 cm, so, the behavior of the temperature at a point very close to the flame (0.91 cm) is first analyzed. At this point (Figure 107), not considerable differences has been obtained between the reactive carbon black numerical model and the hybrid mixture model taking into account only the radiative thermal contribution of the nanoparticles. This behavior can be explained analyzing the carbon black concentration and oxygen mass fraction evolution over time (Figure 108 and Figure 109). It can be observed that the oxygen mass fraction is very low when the carbon black reaction starts (i.e. the carbon black reaction begins at 10.5 ms and the mass fraction of oxygen is only of 1%). This result suggests that for the very early stage of the propagation, the carbon black reaction does not have an influence on the flame propagation, due to the slower carbon black kinetics compared to methane reaction. That means that the influence of the carbon black particles at those stages of the propagation is mostly attributed to the radiative heat transfer.

On the contrary, a slight difference is observed on the control volume located at the half of the initial preheat zone (x = 0.66 cm), where the carbon black reaction seems to reduce the flame propagation compared to the model taking in account only the radiative heat transfer contribution. It was expected that the exothermicity of the carbon black reaction will generate an increase in the

flame temperature and as a result, the flame propagation will be faster. However, the numerical result suggests that the carbon black contribution decreases the radiative heat transfer contribution owing to the reduction on the dust concentration. This means that the absorption and emission contribution are considerably changed by the diminution of the dust concentration over the time. Despite the differences observed between the flame temperature of the solid reactive model and the radiative model, the flame velocity of the mixture decreases only by 0.2 $cm.s^{-1}$ because of the carbon black reaction. This result suggests that the contribution of the carbon black reaction on the flame propagation of a hybrid mixture can be neglected for a concentration of 2.5 $g.m^{-3}$ of carbon black, but not its radiative effect.

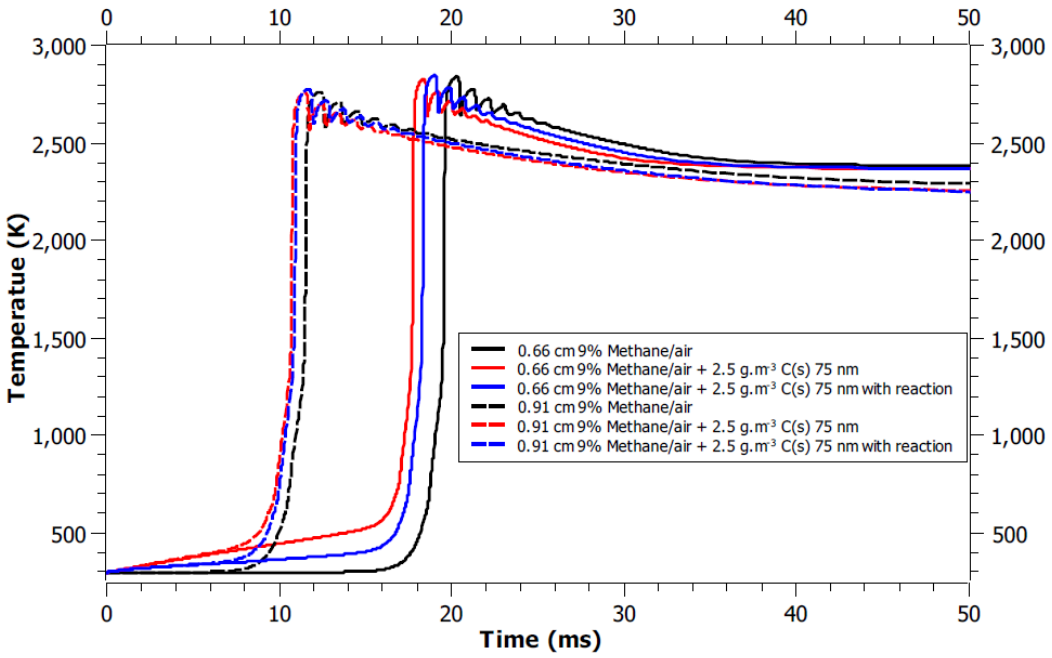

Figure 107. Effect of the carbon black reaction on the 2.5 $g.m^{-3}$ carbon black/methane/air flame propagation.

In Figure 110, the temperature evolution of methane/air and carbon black hybrid mixtures (for a dust concentration of 6 $g.m^{-3}$) are shown. A slight difference is evidenced in the temperature behavior when the carbon black reaction is included in the numerical model. The result suggests that at a position of x = 0.91 cm, the carbon black reaction takes place and the flame velocity is higher compared to methane/air mixtures, but lower than a non-reactive dispersed carbon black (Figure 111). Likewise, analyzing the control volume placed at x = 0.66 cm, a remarkable difference is observed when the reaction of carbon black is considered in the numerical model. It should be remembered that, in this study, low concentrations of carbon black have been analyzed (low compared to the Minimal Explosive Concentration of carbon black, i.e. 60 $g.m^{-3}$) in order to analyze the possible effect of dispersed particles on the explosion parameters, and to minimize the reactive contribution of the combustible dust. For the concentrations analyzed in this work, the carbon black does not seem to have a considerable influence on the final fractions of the burnt gases and in the temperature increase due to the carbon combustion. However, the main influence of the carbon black reaction is related to the properties of the non-transparent media, which are dependent on the emission and absorption properties. By this means, the reaction of carbon black should be taken into account in order to avoid over-estimation of the heat radiation contribution on

the flame propagation (e.g. the front flame propagation velocity decreases from 41 to 39.2 cm.s^{-1} when the reaction is taken into account).

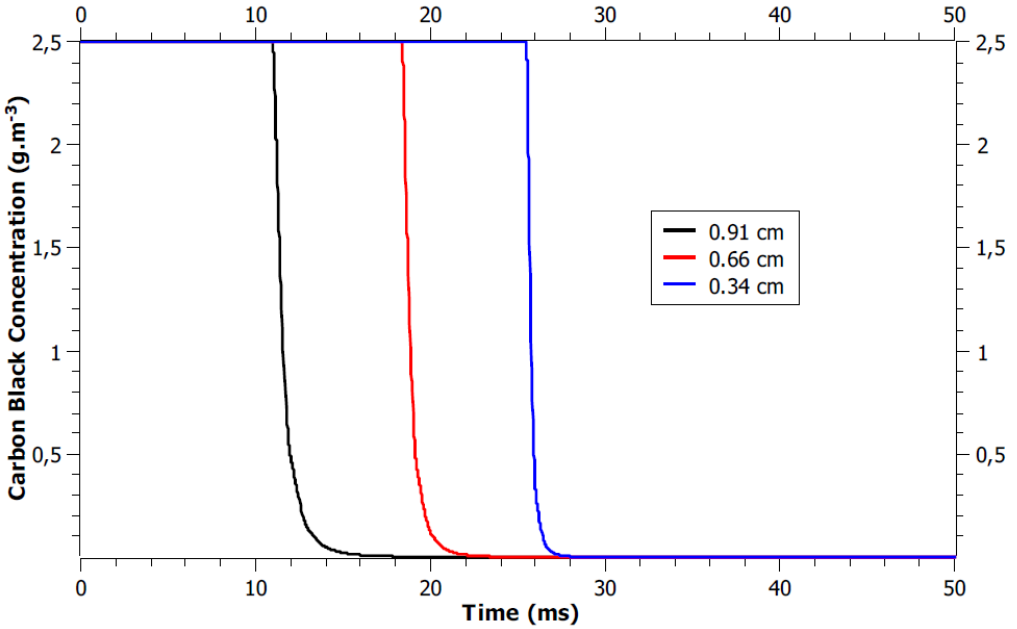

Figure 108. Carbon black concentration behavior for 2.5 g.m^{-3}/methane/air hybrid mixture.

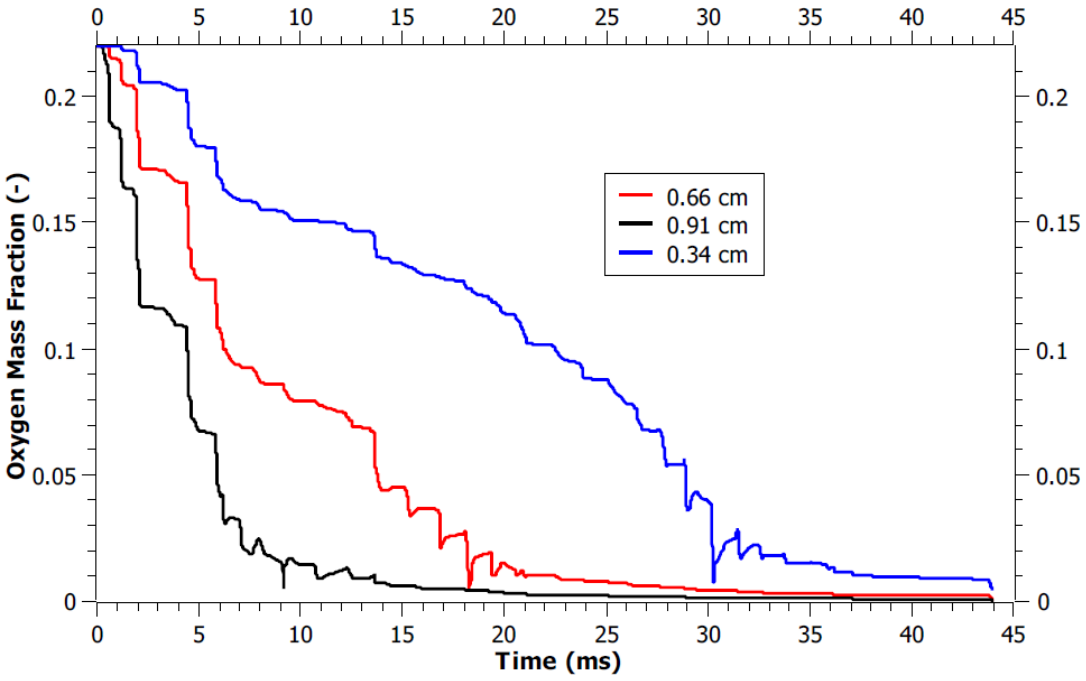

Figure 109. Oxygen mass fraction behavior for 2.5 g.m^{-3}/methane/air hybrid mixture.

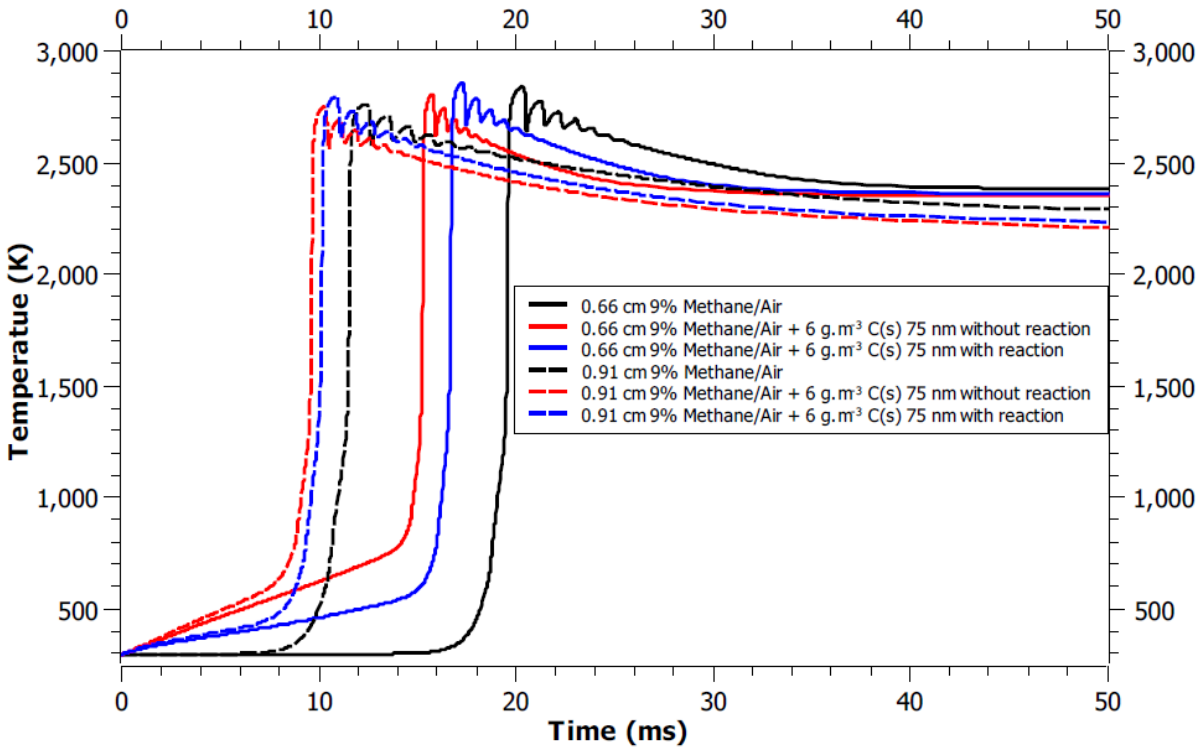

Figure 110. Effect of the carbon black reaction on the 6 g.m^{-3} carbon black/methane/air flame propagation.

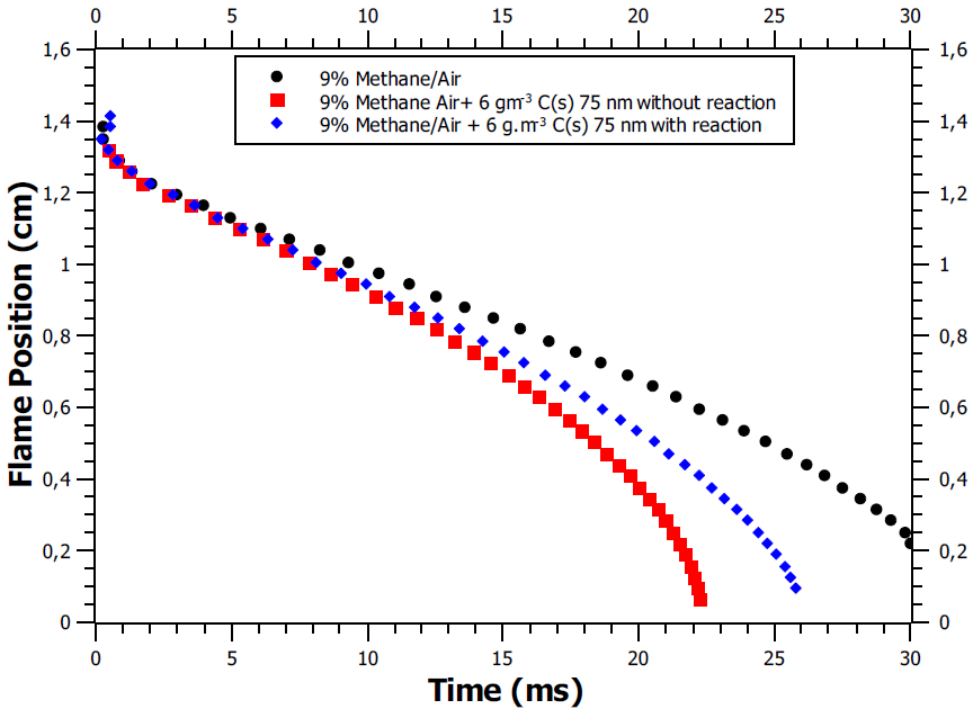

Figure 111. Influence of carbon black reaction on the flame position in the numerical domain over the time.

Besides the weak contribution of the carbon black reaction on the flame propagation at the studied concentrations, careful attention should be paid to the fuel solid combustion mechanism

implemented in the model. As it has been highlighted in the literature (Bews et al., 2001; Field, 1969), global reaction kinetic for carbon combustion has been found inaccurate to predict the real yield fractions and heat reaction energy. In this model, the simultaneous oxidation of methane and carbon black produces a weak contribution of the reaction of solid due to the considerable differences on the characteristic reaction times. Nevertheless, for higher carbon black concentrations or for a numerical model in which the principal fuel is the combustible dust, a semi-global combustion model should also be implemented for the dust reaction.

4.5. Conclusions

The experimental results have shown that insertion of low concentrations of carbon black nanoparticles modifies the maximum overpressure, the maximum rate of pressure rise and the burning velocity. The explosion sphere and tube propagation suggest that the dispersion of carbon black nanoparticles generates modifications of the explosion parameters, which depends on the fuel concentration and turbulence conditions. The main causes of these modifications are a chemical contribution of the carbon black nanoparticles, modifications on the particles and flame interactions that may modify the flame surface, the rise of radiative heat transfer due to the modification of the absorption, emission and scattering properties of the cloud.

For these reasons, the understanding of the predominant phenomena that modifies the explosion parameters is compulsory to manage such risk and improve the design of prevention and protection devices. In this chapter, a numerical model aiming to estimate the velocity of the flame front propagation has been developed, and the influence of the radiative heat transfer and carbon black reaction is also addressed. Even in previous chapters it has been demonstrated the important role of the turbulence in the flame propagation of hybrid mixtures, the system is assumed to be quiescent conditions. The main results of the numerical model evidence:

a) The flame propagation model shows a good agreement with commercial software to estimate the final temperature, the mass fraction of burnt gases and the flame velocity. The flame temperature of a stoichiometric methane/air mixture obtained by the model is equals to 2271 K compared to a theoretical adiabatic temperature of 2236 K. In addition, the flame velocity found by the numerical model for this mixture is 34 $cm.s^{-1}$, which is close to the experimental values of methane/air burning velocity from 34 to 38 $cm.s^{-1}$ (Dirrenberger et al., 2011; Proust, 2006). The semi-global mechanism implemented in this numerical model seems to be appropriate in order to evaluate of the methane combustion.
b) The study of the effect of carbon black particles dispersion is initially limited to the radiative heat transfer generated by the non-transparent dust cloud. If a dispersion of particles with a diameter equal to 10 µm (e.g. the Corax N550 agglomerates diameter), the model results show that the particles do not have any influence on the flame velocity. Nevertheless, if the particle diameter of the dispersed dust is equals to 75 nm (e.g. BET diameter of the elementary Corax N550 particle), a considerable increase of 23% of the flame propagation velocity is obtained when only 6 $g.m^{-3}$ are added to the combustible mixture. Even if an ideal dispersion of a homogeneous dispersion of elementary nanoparticles is very difficult to achieve, a clear flame acceleration is observed due to radiative contributions. Indeed, in order to have a more precise prediction of the interaction reaction – heat radiation transfer, the influence of the distribution on the absorption and emission coefficient, in addition to an initial gradient concentration, should be included in the numerical model.
c) The results of the numerical model suggest that the heat radiation contribution has a promoting effect on the flame propagation and it is consistent with the experimental increase on the explosion severity for some hybrid mixtures. However, further research must be done in order to understand the turbulence/reaction/heat thermal interactions that increases the flame propagation.
d) Moreover, the reaction contribution of the concentrations of carbon black can be neglected if the concentrations remains lower than the Minimal Explosive Concentration (MEC). But the reaction of carbon black nanoparticles modifies significantly the radiative heat transfer

between the reaction zone and the post flame zone, generating a diminution in the flame velocity, as it has been observed in the flame propagation tube for the highest concentrations of carbon black studied in this work.

e) A future work should be addressed to validate the numerical model over a wider range of fuel equivalent ratios and to optimize the reaction mechanism in order to obtain a predictive model. By this means, the flame propagation velocity of this hybrid mixtures would be -ideally- predicted without the necessity of further laboratory tests. This type of model will help to predict the explosive behavior of specific hybrid mixtures by limiting the number of tests and focusing only on a few validation experiments.

4.6. Conclusions (Français)

Pour rappel, les résultats expérimentaux ont montré que l'insertion de faibles concentrations de nanoparticules de noir de carbone modifie la surpression maximale, le taux maximal d'augmentation de la pression et la vitesse de combustion. Les essais menés en sphère d'explosion et en tube semi-ouvert suggèrent que la dispersion des nanoparticules de noir de carbone génère des modifications des paramètres d'explosion, qui dépendent de la concentration de méthane et des conditions de turbulence. Les causes principales de ces modifications sont la contribution chimique des nanoparticules de noir de carbone, des modifications sur la surface de la flamme, les modifications du transfert de chaleur par rayonnement en raison de la modification des propriétés d'absorption, d'émission et de diffusion du nuage.

Pour ces raisons, la compréhension des phénomènes prédominants qui modifient les paramètres d'explosion est obligatoire pour gérer ce risque et améliorer la conception des dispositifs de prévention et de protection. Dans ce chapitre, un modèle numérique 1D visant à estimer la vitesse de la propagation de la flamme a été développé et les influences du transfert de chaleur par rayonnement et de la réaction du noir de carbone sont également abordées. Il faut noter que, si dans les chapitres précédents, le rôle important de la turbulence dans la propagation de la flamme des mélanges hybridesa été démontré, le système étudié est ici au repos. Les principaux résultats du modèle numérique sont les suivants :

a) Le modèle de propagation de la flamme montre un bon accord avec des logiciels commerciaux pour estimer la température finale, les fractions de masse des gaz brûlés et la vitesse de la flamme des explosions de méthane. Ainsi, la température de la flamme d'un mélange stœchiométrique de méthane / air obtenu par le modèle est égale à 2271 K par rapport à une température adiabatique théorique de 2236 K. En outre, la vitesse de flamme trouvée par le modèle numérique pour ce mélange est de 34 $cm.s^{-1}$, ce qui est proche des valeurs expérimentales de la vitesse de combustion du méthane/air de 34 à 38 $cm.s^{-1}$ obtenues dans le tube de propagation ou reportés dans la littérature (Dirrenberger et al., 2011; Proust, 2006). Le mécanisme semi-global mis en œuvre dans ce modèle numérique semble donc approprié pour évaluer la combustion du méthane.
b) L'étude de l'effet de la dispersion des particules de noir de carbone est initialement limitée au transfert de chaleur par rayonnement généré par le nuage de poussière non transparent. Si une dispersion de particules d'un diamètre égal à 10 μm est générée (ce qui correspond, par exemple, au diamètre des agglomérats Corax N550), les résultats du modèle montrent que les particules n'ont aucune influence sur la vitesse de la flamme. Néanmoins, si le diamètre de particule du nuage dispersé est égal à 75 nm (ce qui correspond au diamètre BET des particules élémentaires de Corax N550), une augmentation considérable de 23% de la vitesse de propagation de la flamme est obtenue lorsque seulement 6 $g.m^{-3}$ sont ajoutés. Même s'il faut signaler qu'une dispersion idéale homogène de nanoparticules élémentaires est très difficile à réaliser à ces concentrations (phénomènes d'agglomération), une accélération claire de la flamme est observée en raison du rayonnement du milieu. En effet, afin d'avoir une prédiction plus précise des interactions réactions - transferts radiatifs, l'influence de la distribution de taille de particule sur les coefficients d'absorption et d'émission devra être incluse dans le modèle numérique.
c) Les résultats du modèle numérique suggèrent également que le rayonnement favorise la propagation de la flamme, ce qui est conforme à l'augmentation notée lors des

expérimentations pour certains mélanges hybrides. Cependant, d'autres recherches doivent être effectuées afin de comprendre les interactions turbulence / réaction / transferts thermiques qui impactent fortement la propagation de la flamme.

d) La contribution réactive des noirs de carbone peut être négligée si les concentrations restent inférieures à la Concentration Minimale d'Explosion (CME). Par contre, la réaction de nanoparticules de noir de carbone modifie de manière significative le transfert de chaleur radiatif entre la zone de réaction et la zone de post-flamme/postcombustion par diminution de la zone rayonnante, ce qui provoque une diminution de la vitesse de la flamme. Ce comportement est conforme à ce qui a été observé dans le tube de propagation de la flamme pour les concentrations élevées de noir de carbone étudiées dans le cadre de ce travail.

Un travail ultérieur devra être conduit afin de valider le modèle numérique sur une gamme plus large de concentrations de méthane et pour optimiser le mécanisme de réaction afin d'obtenir un modèle encore plus prédictif. Ce type de modèle aidera à prédire le comportement explosif de mélanges hybrides spécifiques en limitant le nombre de tests et en les choisissant de manière appropriée.

Nomenclature

Symbol	Description
C_p	Specific heat capacity at constant pressure [J.kg^{-1}.K^{-1}].
D	Molecular diffusivity [m^2.s^{-1}].
d_p	Particle diameter [m].
e_t	Total energy [J.m^{-3}].
E_i	Activation energy [cal.mol^{-1}].
h_f^0	Standard enthalpy of formation [kJ.mol^{-1}].
h_s	Sensible enthalpy [kJ.mol^{-1}].
I	Thermal radiation intensity [W.m^{-2}].
I_f	Flame thermal radiation intensity [W.m^{-2}].
I_{bp}	Black body thermal radiation intensity [W.m^{-2}].
j_i	Mass diffusion component i
k_j^f	Pre-exponential factor of the forward j reaction.
k_j^r	Pre-exponential factor of the reverse j reaction
K_a	Absorption coefficient [m^{-1}].
K_s	Scattering coefficient [m^{-1}].
P	Pressure [Pa]
Q_{abs}	Absorption efficiency [-].
Q_{sca}	Scattering efficiency [-].
Q_{rad}	Radiative Heat Transfer [J.m^{-3}.s^{-1}].
r_j	Molar reaction rate **[**kg.m^{-3}s^{-1}**]**
S_{ext}	External surface area [m^2]
T	Temperature [K].
T_f	Flame temperature [K].
u	Velocity [m.s^{-1}]
V	Volume [m^3]
V_i	Diffusion velocity [m s^{-1}].
$v_{i,j}$	Stoichiometric coefficient component i in reaction j [-]
y_i	Mass fraction component i [-].
x_i	Molar fraction component i [-].

W	Molecular Weight [kg.mol^{-1}]

Greek letters Description

γ	Expansion factor [-].
λ	Thermal conductivity **[**W.m^{-1}.K^{-1}**].**
β	Temperature exponent in the pre-exponential factor [-].
ρ	Density **[**kg.m^{-3}**]**
ρ_p	Particle density **[**kg.m^{-3}**].**
$\dot{\omega}_i$	Mass reaction rate component i **[**kg.m^{-3}s^{-1}**]**
ϕ	Molar concentration **[**mol.m^{-3}**]**
φ	Dust concentration **[**kg.m^{-3}**]**
ε_P	Particle Emissivity **[-]**
Ω	Solid angle **[-]**

References

Adzerikho, K., 1987. RADIATION HEAT TRANSFER IN TWO-PHASE MEDIA. J. Eng. Phys. 1306–1311.

Andersen, J., Rasmussen, C.L., Giselsson, T., Glarborg, P., 2009. Global Combustion Mechanisms for Use in CFD Modeling under Oxy-Fuel Conditions. Energy Fuels 23, 1379–1389.

Auerkari, P., 1996. Mechanical and physical properties of engineering alumina ceramics.

Bauffman, J., Cox, K., 2008. Measurement of laminar burning velocity of methane-air mixtures using a slot and Bunsen burner (Major qualifying project). Worcester Polytechnic Institute, Worcester, United States.

Bews, I.M., Hayhurst, A.N., Richardson, S.M., Taylor, S.G., 2001. The order, Arrhenius parameters, and mechanism of the reaction between gaseous oxygen and solid carbon. Combust. Flame 124, 231–245.

Bidabadi, M., Azad, A.V., 2015. Effects of radiation on propagating spherical flames of dust–air mixtures. Powder Technol. 276, 45–59.

Bidabadi, M., Haghiri, A., Rahbari, A., 2010. The effect of Lewis and Damköhler numbers on the flame propagation through micro-organic dust particles. Int. J. Therm. Sci. 49, 534–542.

Bidabadi, M., Shakibi, A., Rahbari, A., 2011. The radiation and heat loss effects on the premixed flame propagation through lycopodium dust particles. J. Taiwan Inst. Chem. Eng. 42, 180–185.

Bidabadi, M., Zadsirjan, S., Mostafavi, S.A., 2013. Radiation heat transfer in transient dust cloud flame propagation. J. Loss Prev. Process Ind. 862–868.

Bird, R.B., Stewart, W.E., Lightfoot, E.N., 2007. Transport Phenomena, Edición: 2 Rev ed. ed. John Wiley and Sons Ltd, New York.

Burden, R.L., Faires, J.D., 2010. Numerical Analysis. Cengage Learning.

Castellanos, D., Skjold, T., van Wingerden, K., Eckhoff, R.K., Mannan, M.S., 2013. Validation of the DESC Code in Simulating the Effect of Vent Ducts on Dust Explosions. Ind. Eng. Chem. Res. 52, 6057–6067. d

Croiset, E., Mallet, C., Rouan, J.-P., Richard, J.-R., 1996. The influence of pressure on char combustion kinetics, in: Symposium (International) on Combustion. Elsevier, pp. 3095–3102.

Dahoe, A., 2000. Dust Explosions: a Study of Flame Propagation.

Dirrenberger, P., Le Gall, H., Bounaceur, R., Herbinet, O., Glaude, P.-A., Konnov, A., Battin-Leclerc, F., 2011. Measurements of Laminar Flame Velocity for Components of Natural Gas. Energy Fuels 25, 3875–3884

Dormand, J.R., Prince, P.J., 1980. A family of embedded Runge-Kutta formulae. J. Comput. Appl. Math. 6, 19–26.

Eckhoff, R.K., 2011. Are enhanced dust explosion hazards to be foreseen in production, processing and handling of powders consisting of nano-size particles? J. Phys. Conf. Ser. 304, 012075.

Field, M.A., 1969. Rate of combustion of size-graded fractions of char from a low-rank coal between 1 200 K and 2 000 K. Combust. Flame 13, 237–252.

Frassoldati, A., Cuoci, A., Faravelli, T., Ranzi, E., Candusso, C., Tolazzi, D., 2009. Simplified kinetic schemes for oxy-fuel combustion, in: 1st International Conference on Sustainable Fossil Fuels for Future Energy. pp. 6–10.

Gosse, J., 2012. Propriétés de transport des gaz à pression modérée. Tech. L'Ingénieur.

Haghiri, A., Bidabadi, M., 2011. Dynamic behavior of particles across flame propagation through micro-iron dust cloud with thermal radiation effect. Fuel 90, 2413–2421.

Haghiri, A., Bidabadi, M., 2010. Modeling of laminar flame propagation through organic dust cloud with thermal radiation effect. Int. J. Therm. Sci. 49, 1446–1456.

Haynes, W.M., 2012. CRC Handbook of Chemistry and Physics, 93rd Edition. CRC Press.

Hurt, R.H., Calo, J.M., 2001. Semi-global intrinsic kinetics for char combustion modeling. Combust. Flame 125, 1138–1149.

Jones, W.P., Lindstedt, R.P., 1988. Global reaction schemes for hydrocarbon combustion. Combust. Flame 73, 233–249.

Kahaner, D.K., Ng, E., Schiesser, W.E., Thompson, S., 1991. Experiments with an ordinary differential equation solver in the parallel solution of method of lines problems on a shared-memory parallel computer. J. Comput. Appl. Math. 38, 231–253.

MathWorks, 2017. MATLAB Documentation [WWW Document]. URL https://fr.mathworks.com/help/matlab/?requestedDomain=fr.mathworks.com (accessed 6.14.17).

Meinköhn, E., Kanschat, G., Rannacher, R., Wehrse, R., 2007. Numerical methods for multidimensional radiative transfer, in: Reactive Flows, Diffusion and Transport. Springer, pp. 485–526.

Modest, M.F., 2013. Radiative heat transfer. Academic press.

Murillo, C., 2016. Experimental and numerical approaches to particles dispersion in a turbulent flow: application to dusts explosion. Université de Lorraine.

Murillo, C., Dufaud, O., López, O., Perrin, L., Vignes, A., Muñoz, F., 2013. CFD modelling of nanoparticles dispersion in a dust explosion apparatus. Chem. Eng. Trans. 889–894.

Omega, 2017. Emissitivity of Common Materials [WWW Document]. URL https://www.omega.com/literature/transactions/volume1/emissivitya.html (accessed 7.15.17).

Patankar, S., 1980. Numerical Heat Transfer and Fluid Flow, 1 edition. ed. CRC Press.

Poinsot, T., Veynante, D., 2005. Theoretical and numerical combustion. RT Edwards, Inc.

Proust, C., 2006. Flame propagation and combustion in some dust-air mixtures. J. Loss Prev. Process Ind. 19, 89–100.

Ranish, J.M., Walker, Jr, P.L., 1993. High pressure studies of the carbon oxygen reaction. Carbon 135–141.

Saatdjian, E., 2009. Les bases de la mécanique des fluides et transferts de chaleur et de masse pour l'ingénieurSaatdjian. Sapienta.

Sarmin, E.N., Chudov, L.A., 1963. On the stability of the numerical integration of systems of ordinary differential equations arising in the use of the straight line method. USSR Comput. Math. Math. Phys. 3, 1537–1543.

Schiesser, W.E., 1991. The Numerical Method of Lines: Integration of Partial Differential Equations, 1st edition. ed. Academic Press, San Diego.

Shampine, L.F., Gladwell, I., Thompson, S., 2003. Solving ODEs with matlab. Cambridge University Press.

Skjold, T., Castellanos, D., Olsen, K.L., Eckhoff, R.K., 2014. Experimental and numerical investigation of constant volume dust and gas explosions in a 3.6-m flame acceleration tube. J. Loss Prev. Process Ind. 30, 164–176.

Smith, J.., Van Ness, H., Abbott, M., 2004. Introduction to Chemical Engineering Thermodynamics.

Solomon, E., 1955. Molecular theory of gases and liquids. Joseph O. Hirschfelder, Charles F. Curtiss, and R. Byron Bird. John Wiley & Sons, Inc., New York (1954). 1219 pages. $20. AIChE J. 1, 272–272.

Sørensen, L.H., Gjernes, E., Jessen, T., Fjellerup, J., 1996. Determination of reactivity parameters of model carbons, cokes and flame-chars. Fuel 75, 31–38.

Thellmann, A., 2010. Impact of Gas Radiation on Viscous Flows, in particular on Wall Heat Loads, in Hydrogen-Oxygen vs. Methane-Oxygen Systems, based on the SSME Main Combustion Chamber. Universität München.

Tilghman, M.B., Mitchell, R.E., 2015. Coal and biomass char reactivities in gasification and combustion environments. Combust. Flame 162, 3220–3235.

Zoulalian, A., Bounaceur, R., Dufour, A., 2015. Kinetic modelling of char gasification by accounting for the evolution of the reactive surface area. Chem. Eng. Sci. 138, 281–290.

CONCLUSIONS

This research work describes the influence of the insertion of carbon black nanoparticles on the explosion parameters of methane/air mixtures. The effect of dust concentration, methane concentration, of the initial turbulence level and of the elementary particle diameter have been analyzed in this work. Different approaches had been implemented in this thesis. First, experiments in a 20L sphere have shown the influence of carbon black nanoparticles on the maximum overpressure and maximum rate of pressure rise, and the influence of the most relevant variables has been studied. Second, different methodologies have been implemented in order to determine the burning velocity of hybrid mixtures, aiming to elucidate the contribution of nanoparticles in gas explosions and to estimate modifications in the flame surface. Finally, a numerical model aiming to estimate the velocity of the flame front propagation has been developed, and the influence of the radiative heat transfer and carbon black reactivity is also addressed.

The contribution of this work is then threefold. It has allowed the development of a new *experimental methodology* based on the combination of the explosion severity assessment from tests in closed vessels and the determination of the flame propagation characteristics taking into account both the turbulence/combustion interactions and the radiative transfer. Such experimental procedures will be developed further on and applied on similar hybrid mixtures but also on dust/air mixtures. It has also led to the development of a *numerical model*, which aims to highlight the influence of the chemical reaction, the radiation transfer and the particle size distribution on the flame propagation characteristics. At last, it brings *new insights* on the phenomenology of dusts and hybrid mixtures explosions, and, will help to develop adequate strategies in order to assess and reduce such explosion risk.

In the following paragraphs, the main results obtained in this study are summarized.

5.1. MAIN RESULTS

Explosion severity test

The various modifications caused by the addition of carbon black nanoparticles on the maximum overpressure and on the maximum rate of pressure rise have been measured in a 20L sphere. The results evidence that the explosion severity changes when low concentrations of carbon black nanoparticles are incorporated into the system. However, the explosion severity will increase or decrease depending on the initial conditions of the system. For these reasons, the main influences observed are described below.

Addition of carbon black nanoparticles:

The maximum overpressure of the explosion slightly increases when 0.1 % mole of solid carbon are incorporated to the system in lean mixtures. However, for stoichiometric and rich methane mixtures, the maximum pressure after the explosion decreases for the same concentration of carbon black. In addition, for a carbon black concentration increased to 0.5% mole, the maximum overpressure decreases whatever the gas concentration.

The maximum rate of pressure rise seems to be more sensitive to the addition of carbon black nanoparticles on the explosion severity. A considerable decrease has been obtained on this variable for fuel lean mixture when 0.1% mole carbon black are incorporated to the systems. The result suggests that the diminution of the explosion severity is more important for particles with a smaller elementary particle diameter (Printex XE2 in this work).

In this study, the main causes that explain the modifications of dispersed nanoparticles on methane/air explosions are: I) a reaction of the carbon black nanoparticles occurs simultaneously with the gas reaction, II) the dispersed nanoparticles disrupts the flame propagation, resulting in an increase of the flame stretch and of the flame surface. III) the nanoparticles ahead the front flame modify the radiative heat transfer between the unburnt mixture and the burnt gases. IV) the dispersed particles enhance the soot nucleation.

An effort to validate each hypothesis has been made in this work and the main conclusions are presented in the following subsections.

Low turbulence level:

The cloud of carbon black nanoparticles remains highly stable some minutes after the dispersion. Dispersion stability test has shown that after three minutes the mean mobility diameter does not change (approximately 240 nm and 370 nm for Printex XE2 and Corax N550, respectively), with a dust concentration considerably higher ($2.4x10^5$ particles.cm^{-3}) in comparison to the environmental/reference initial concentration ($6.3x10^3$ particles.cm^{-3}).

Explosion severity tests have shown that even at low turbulence levels, the presence of carbon black nanoparticles modifies the violence of the explosion. This means that for lean fuel mixture, the explosion severity can be increased if there is a stable dispersion of nanoparticles, and a turbulent dispersion is not compulsory to have a contribution of the nanoparticles to the explosion.

High turbulence level:

At high turbulence levels, the diminution of the maximum rate of pressure rise is higher than for low turbulent systems, especially for dust with a smaller particle diameter. These results suggest that the deagglomeration of the particles is obtained at high turbulence levels, increasing the total surface and amplifying the effect of the nanoparticle on the heat transfer or flame perturbations. Such deagglomeration phenomenon at high initial turbulence level has already been proven for microparticles (Murillo, 2016).

Hypothesis I – Contribution of carbon black nanoparticles on the combustion reaction

In order to test the possible chemical contribution of the carbon black nanoparticles on the hybrid mixtures explosions, two approaches had been implemented. First, the burnt gases have been analyzed by micro-gas chromatography. The second approach aims to compare the explosion severity of carbon black/methane to inert alumina/methane hybrid mixtures.

The addition of carbon black particles to fuel lean mixtures seems to promote the oxidation of CO into CO_2, which will generate a higher release of chemical energy and, consequently, an increase in the maximum rate of pressure rise. However, it has been shown that the final fraction of CO and H_2 are directly related to the initial turbulence level. In other words, carbon black nanoparticles probably react, but it is not possible to relate their combustion with the modifications of the explosion severity, due to the influence of the turbulence in the final concentration of burnt gases.

The addition of alumina particles (inert compound) generates similar trends for the explosion severity parameters dP/dt_m and P_m: these parameters increase when low concentrations of carbon black and alumina nanoparticles are injected on the methane/air mixtures at fuel lean mixtures conditions. These results suggest that effects of both particles seem to be generated by modifications of the front flame and radiative heat transfer. Eventually, the results do not allow to separate the chemical contribution from the other hypotheses.

Burning velocity determination

The estimation of the burning velocity is necessary because it is a fundamental measure of the combustion process and it is an essential input for the modelling of the explosion severity of these systems. Moreover, it is directly linked to the previous explosivity parameters. The measure for dust and hybrid mixtures is very difficult due to the turbulent nature of these phenomena and the interaction between the reaction, the heat transfer and the turbulence of the system. In this work, the experimental measure of the flame velocity had been performed by various approaches:

Thin model from explosion severity tests

A first approach has been implemented in order to understand the influence of the insertion of carbon black nanoparticles on the burning velocity of methane/air mixtures. The burning velocity was estimated by the thin spherical propagation model using the explosion severity tests. For methane/air mixture, the estimated values are very close to the reported values. Two main results must be highlighted for hybrid mixtures. First, the burning velocity seems to increase for lean mixtures when low concentrations of carbon black are added to the system (i.e. 0.1% mole fraction of carbon black), but decrease for stoichiometric and rich fuel mixtures. Secondly, a significant difference is obtained between the burning velocity of Printex XE2/methane and Corax N550/methane hybrid mixtures. This result suggests that the elementary particle diameter has a strong effect on the burning velocity.

This approach present the advantage that the results are estimated from a standardized equipment, in which the variability of the results are considerably reduced in comparison with the tube method. However, this estimation takes in account two important hypotheses that can generate an underestimation of the burning velocity: I) the flame thickness is assumed to be an infinitely sheet (which is also an hypothesis made in order to determine the K_{st} parameter used for vent sizing purposes), II) the maximum rate of pressure rise does not change with the global equivalence ratio, III) a spherical propagation is assumed, and the stretch and turbulence perturbations are neglected.

Flame propagation tube:

The flame velocity has been measured using the tube method. The front flame propagation was recorded using a high-speed video camera. In these videos, the flame propagation is recorded taking advantage of the brightness of the flame and enhancing the detection with numerical filters.

The reproducibility test shows similar values on the flame spatial velocity at low turbulence levels, however, the trends seems delayed in time, and a high variability is obtained at such conditions. The spatial velocity seems to decrease when the carbon black concentration increases in the initial mixture. The initial turbulence level has an important influence on the spatial velocity results, which seems to increase at high turbulence levels. Nevertheless, a reduction of the spatial velocity is evidenced for the highest turbulence levels analyzed in this study (i.e. at an ignition delay time of 60 ms).

The unstretched flame velocities obtained for gas and hybrid mixtures present a high variability, which make very difficult to establish influences of the different variables studied in this work. Nevertheless, for methane/air mixtures the results has been validated with the burning velocity reported by other authors (Dirrenberger et al., 2011; Proust, 2006). It can be concluded that:

Gas concentration influence: A clear evolution of the unstretched flame velocity is not obtained for neither gas nor hybrid mixtures.

Initial turbulence level influence: For almost all the gas concentrations studied in this work, the unstretched burning velocity seems higher at an initial turbulence level of $v_{rms} = 1.4\ m.s^{-1}/t_v$

= 120 ms (intermediate turbulence level). At the highest turbulence level studied in this work (v_{rms} = 1.6 $m.s^{-1}$/t_v = 60 ms), the unstretched velocity decreases in comparison with low turbulence levels (v_{rms} = 0.9 $m.s^{-1}$/t_v = 500 ms), which suggests that the flame is greatly destabilized by the turbulent flow. The stretch factor is considerable reduced for systems at initial low turbulence level, which suggest that the stretching is mostly due to the flame curvature instead of a strain contribution.

Dust concentration influence: At the lowest initial turbulence level (t_v = 500 ms) analyzed in this study, the unstretched flame velocity seems to increase for fuel lean mixtures but decreases for stoichiometric and fuel rich mixtures. This trend confirms the results obtained in the 20L severity tests. For high turbulent systems, it was not possible to establish a clear trend.

Schlieren technique

Schlieren images allow a better observation of the flame propagation and show a significant change of the flame surface when the initial turbulence level of the system increases, which it is initially smooth and became highly wrinkled under very turbulent conditions. As it was obtained for the unburning velocity of flame videos without physical filters, the results present a high variability and establish trends from the results is still difficult. Nevertheless the results suggest:

Gas concentration influence: A clear evolution of the unstretched flame velocity is not obtained for neither gas nor hybrid mixtures. Only for gas mixtures at quiescent conditions, the unstretched burning velocity is the highest at stoichiometric conditions, and decreases for lean and rich fuel mixtures.

Initial turbulence level influence: For gas mixtures, a considerable reduction in the unstretched burning velocity is observed when the initial turbulence level increase. For hybrid mixtures, it was not possible to determine a clear monotonous relation between the turbulence level and the unstretched flame velocity.

Dust concentration influence: Regardless the high variability of the system, it seems that the unstretched burning velocity increases when the concentration of carbon black is augmented in the initial mixture.

Considerable differences have been found between the unstretched velocity meaured from videos without physical filters and from videos recorded using the Schlieren images. The first conclusion is that for both methods, a significant variability in the results is obtained. As it was highlighted in the reproducibility tests, initial turbulence generates a high variability in the results that make difficult to establish if the results are related to an influence of a specific variable or they are the result of the randomness of the system. In addition, the unstretched velocity – stretch factor graphs suggest that the fast interactions between the walls and the flame increases the instability of the flame, and as a consequence, can increase the variability of the results.

Furthermore, the differences between the two methods of detection of the flame front suggest that the flame surface estimation is fundamental to have a good estimation of the flame velocity. A considerable enhancement on the flame surface is obtained by the Schlieren method. It has been demonstrated that the detection of the flame interface based on the luminosity generates an overestimation of the flame surface, and in addition, the irregularities on the surface were not taken into account in such analysis.

Hypothesis II – Flame perturbations by the dispersed nanoparticles

The results of the flame propagation tube had also been analyzed in order to study the possible modifications on the flame surface as a result of the dispersion of nanoparticles. As it was

performed in the severity explosion tests, the burning velocity of inert particles had been analyzed. The unstretched burning velocity estimated for AP-D alumina/methane/air mixtures are considerable higher than those obtained for gas mixture explosions. The previous results and specifically the fact that flames with similar spatial velocities can exhibit different unstretched burning velocities, suggest that the presence of solid particles such as alumina modifies the flame surface during the propagation. However, it was not possible to separate the influence of the modification of the flame front from the contribution of the radiative heat transfer and from the chemical contribution of carbon black nanoparticles. Moreover, the schlieren method has evidenced modifications of the flame surface and stretch factor due to the dispersion of nanoparticles, however a quantification of these phenomena was not possible.

Numerical Model

A numerical model to estimate the flame velocity of a gas mixture explosion through a two-phase media containing nanoparticles had been developed. With this context, the influence of the radiative heat transfer and of the reaction of carbon black has been also addressed.

The numerical model has been validated for methane/air mixtures. The results on the flame temperature and mass fractions are in good agreement with detailed chemical kinetic calculations in a commercial 1-D code (for instance the obtained flame temperature for 9% methane/air mixtures is 2271 K compared to a theoretical adiabatic temperature of 2236 K). The study of the effect of carbon black particles dispersion is initially limited to the heat radiation transfer generated by the non-transparent dust cloud. An increase of 23% on the flame propagation is obtained when a concentration of 6 $g.m^{-3}$ of carbon black particles (with an elementary particle diameter of 75 nm) is added to the initial gas mixture.

It was initially believed that the radiative heat transfer generates a diminution on the explosion severity due to the heat loss on the flame, resulting in a lower flame temperature. However, the results of the numerical model suggest that the heat radiation contribution has a promoting effect on the flame propagation due to the increase of the temperature in the preheat zone. This result is consistent with the experimental increase of the explosion severity for some hybrid mixtures. However, further research must be done in order to understand the turbulence/reaction/heat thermal interactions that increases the flame propagation.

Hypothesis III – Radiative heat transfer influence on the burning velocity

The insertion of nanoparticles modifies greatly the radiative heat transfer, as it has been observed in the flame propagation videos and Schlieren images. However, the quantification of the radiative heat transfer is still a challenge. As previously highlighted, the numerical model suggests a considerable flame acceleration due to the radiative contribution of a non – transparent media.

In addition, the unstretched flame propagation differences between alumina/methane and carbon black mixture, suggest that the radiative heat transfer may have a considerable influence on the flame propagation. However, a differentiation of the individual contribution of flame surface modification and of the radiative heat transfer is compulsory to understand the predominant phenomenon during the flame propagation.

5.2. PERSPECTIVES

New insights on process safety

The results of this research work suggest that careful attention must be paid for the sizing of protection devices involving hybrid mixtures. The modifications evidenced on the explosion severity parameters (P_m, dP/dt_m and K_{st}) due to the presence of nanoparticles can imply differences on the relief surface of the protection devices compared to pure gas mixtures. As it

has been highlighted in the introduction of this work, the gasification process is an example of the generation of carbonaceous particles/gas hybrid mixtures. In Figure 112, a schema a circulating fluidized bed gasifier followed by the high temperature filtration of the obtained gases is shown. The explosion severity test results suggest that a different protection device dimensioning should be performed for the hybrid mixture present inside the gasifier (char or ashes/syngas) compared to the syngas after filtration.

In addition, the flame propagation study shows modifications on the flame surface and an increase of radiation transfer when carbon black nanoparticles are dispersed into the initial mixture. The previous results suggest that the dispersed particles generate modifications of the flame thickness that invalid the hypotheses implemented in the cubic law, and imply the reconsideration of this law for the sizing of protection devices for hybrid mixtures.

Furthermore, the explosion severity tests have shown turbulent quenching of hybrid mixtures with nanoparticles having a very small particle diameter. This results open the opportunity to study for different type of applications the addition of particles that at turbulent conditions will generate flame extinction.

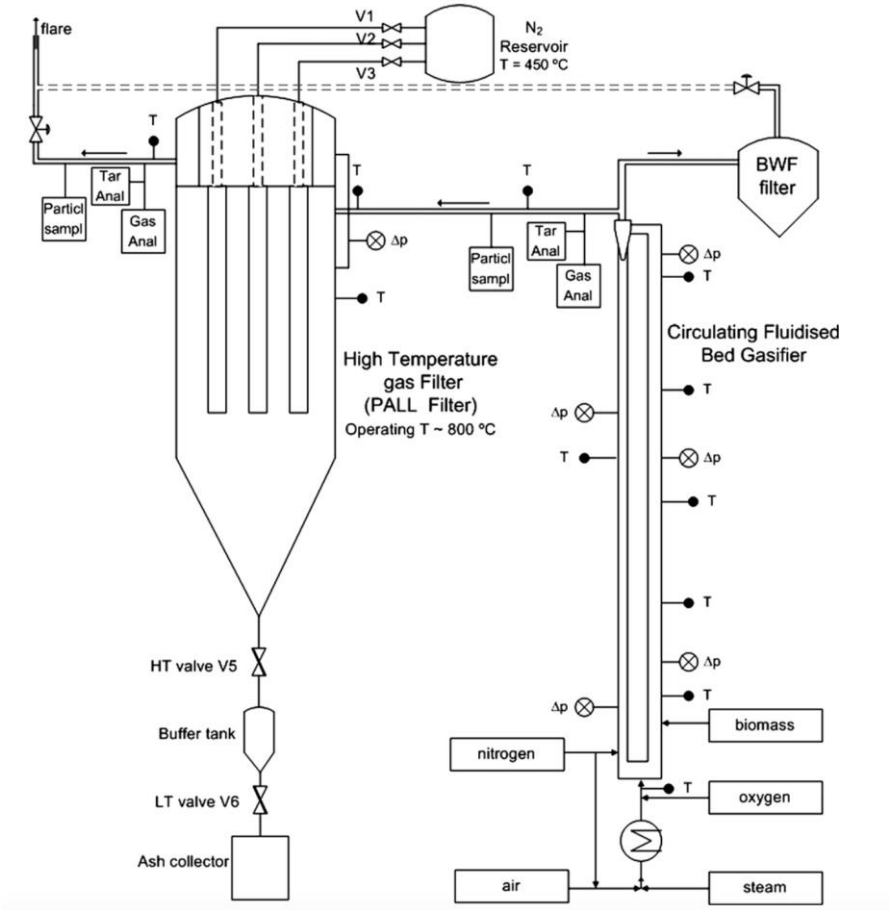

Figure 112. Schematic diagram of gasification and filtration (Simeone et al., 2011).

Perspectives for further research works

The results of this work have evidenced modification of the explosion severity parameters of methane/air mixtures due to the dispersion of carbon black nanoparticles. However, further research on the experimental determination of the flame burning velocity of hybrid mixtures is still necessary. In addition, the simultaneous phenomena, which take place during the explosion of hybrid mixtures, must be characterized and their contributions should be quantified. This

section aims to highlight the main future work already underway or that will be soon implemented in the LRGP laboratory.

Experimental approach:

The flame propagation tube has been used to determine the flame velocity of hybrid mixtures. However, the fast interaction of the flame with the walls of the tube generates problems for the flame detection, increases the flame stretch and can increase the variability of the results. Such experimental set-up will be of use in order to determine the impact of obstacles or flame arresters (quenching) on the flame propagation within the tube.

During the research work of Murillo (2016), a replica of the 20L explosion sphere was built to visualize and quantify the dust dispersion inside the equipment. Within the context of this work, some modifications have been made in order to incorporate an ignition source and pressure relief system in order to perform explosion at atmospheric conditions in this vessel (Figure 113). Flame propagation tests are currently being performed on methane/air mixture (Figure 114) in order to study the spherical propagation of the flame kernel, and to record flame propagation without the influence of walls nor the influence of the pressure relief. This flame propagation set-up will improve the characterization of the flame stretching during its propagation. In addition, the Schlieren technique will be also implemented in this vessel for a better flame front flame detection.

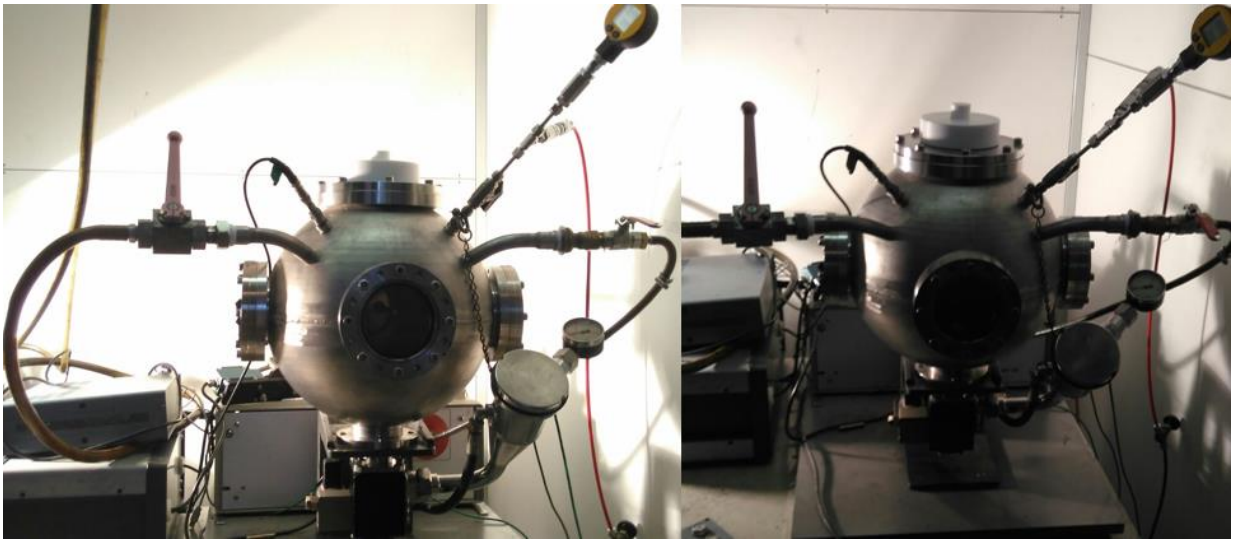

Figure 113. Explosion sphere adaptation to the study of the flame propagation.

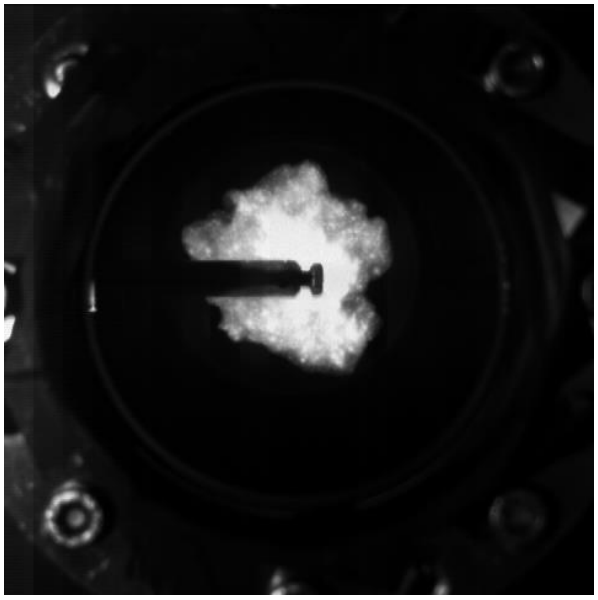

Figure 114. Flame propagation on the 20L sphere.

The quantification of the suspended mass of nanoparticles during the dispersion should be incorporated to the analysis of the effect of nanoparticles on the front flame propagation, at different turbulence levels. Laser extinction techniques based on the Beer-Lambert law should be implemented to this purpose.

Hypothesis IV – Nanoparticles as soot nuclei

The probable effect of carbon black nanoparticles (or other dust particles in suspension, e.g. alumina) as soot nuclei must be also analyzed. A system allowing the rapid collection of dust/soot samples after explosion must be implemented in order to study them by Scanning Electron Microscopy, X-Ray Diffraction XRD or Thermo-Gravimetric Analysis (TGA).

Numerical approach:

In this work a numerical method has been developed in order to estimate the flame propagation velocity of hybrid mixtures. However, this numerical model does not take into account the initial turbulence, is limited to one direction in the space and supposes a monomodal particle size distribution. Further developments are needed in that way.

Moreover, the CFD simulation of the flame propagation of hybrid mixture on STAR-CCM V11.02 is currently being done in collaboration with la Universidad de los Andes in Bogotá, taking into account the simultaneous reactions, heat transfer and turbulent system. A future work should be addressed to combine the previous numerical model with the CFD approach. It will then possible to validate the numerical CFD model and to optimize the reaction mechanism in order to obtain a predictive model. This type of model will help to predict the explosive behavior of specific hybrid mixtures by limiting the number of tests and focusing only on a few validation experiments.

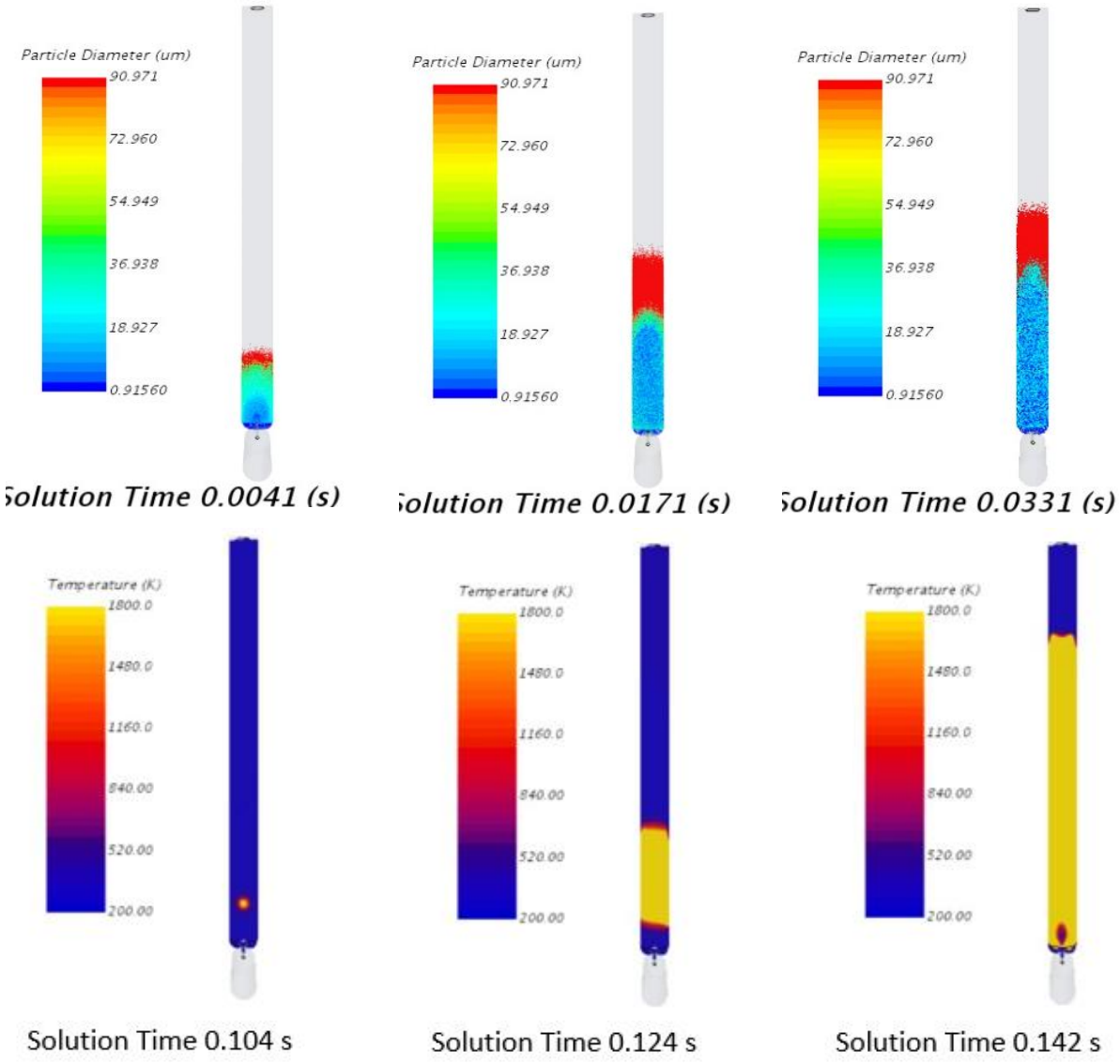

Figure 115. CFD simulation in STAR-CCM+ of carbon black dispersion and flame propagation in the 1m flame propagation tube (results of research project currently performed by Andrés Pinilla, Universidad de los Andes).

Finally, this research work can also find an application in the design of hybrid metal/gas burners combined to heat conversion for propulsion systems i.e. for terrestrial transportation or aerospatial applications (Julien et al., 2017 ; Lomba, 2016; Soo et al., 2013).

CONCLUSIONS

Ce travail de recherche décrit l'influence de l'insertion de nanoparticules de noir de carbone sur les paramètres d'explosion des mélanges méthane/air. Les effets de la concentration en poussière, de la concentration en méthane, du niveau de turbulence initiale et du diamètre des particules élémentaires et agglomérats ont été analysés dans ce travail. Différentes approches ont été mises en œuvre dans cette thèse. Tout d'abord, les expériences dans une sphère standardisée de 20L ont démontré l'influence des nanoparticules de noir de carbone sur la surpression maximale et la vitesse maximale de montée en pression. De plus, une étude paramétrique a été menée. Deuxièmement, différentes méthodologies permettant de déterminer la vitesse de combustion des mélanges hybrides ont été mises en place afin d'élucider la contribution des nanoparticules dans les explosions de gaz et d'estimer les modifications de la surface de la flamme. Enfin, un modèle numérique visant à estimer la vitesse de propagation de la flamme avant a été développé et les impacts du transfert de chaleur radiatif et de la réactivité du noir de carbone ont également été abordés.

Au global, ce travail a permis le développement d'une ***nouvelle méthodologie expérimentale*** basée sur la combinaison de l'évaluation de la sévérité de l'explosion et la détermination des caractéristiques de propagation de la flamme en tenant compte à la fois des interactions turbulence/combustion et du transfert radiatif. De telles procédures expérimentales seront développées à l'avenir et appliquées sur des mélanges hybrides similaires, mais aussi sur des mélanges poussière / air. Il a également conduit au développement d'un ***modèle numérique*** qui vise à mettre en évidence l'influence de la réaction chimique, du transfert de rayonnement et de la distribution de la taille de particule sur les caractéristiques de propagation de la flamme. Enfin, il apporte de ***nouvelles contributions sur la phénoménologie des poussières*** et des explosions de mélanges hybrides et aidera à développer des stratégies adéquates afin d'évaluer et de réduire ce risque d'explosion.

Dans les paragraphes suivants, les principaux résultats obtenus dans cette étude sont résumés.

6.1. SYNTHESE DES PRINCIPAUX RÉSULTATS

Test de sévérité de l'explosion

Les différentes modifications causées par l'insertion de nanoparticules de noir de carbone sur la surpression maximale et sur la vitesse de montée en pression ont été mesurées dans une sphère de 20L. Les résultats prouvent que la sévérité de l'explosion change lorsque de faibles concentrations de nanoparticules de noir de carbone sont incorporées dans le système. Cependant, la gravité de l'explosion augmentera ou diminuera en fonction des conditions initiales du système. Dans ce contexte, les principales influences observées sont décrites ci-dessous.

Ajout de nanoparticules de noir de carbone :

La surpression maximale de l'explosion augmente légèrement lorsque 0,1% mol. de noir de carbone est incorporé au système dans des mélanges pauvres en méthane. Cependant, pour les mélanges stœchiométriques ou riches en méthane, la pression maximale après l'explosion diminue pour cette même concentration de noir de carbone. En outre, pour une concentration en noir de carbone supérieure, i.e. 0,5% mol., la surpression maximale diminue quelle que soit la concentration de gaz.

La vitesse maximale de montée en pression semble plus sensible à l'insertion de nanoparticules de noir de carbone. Une diminution considérable a été obtenue sur cette variable pour les

mélanges pauvres en méthane lorsque 0,1% mol. de noir de carbone sont incorporés dans le système réactif. Le résultat suggère que la diminution de la sévérité de l'explosion est plus importante pour les particules avec un plus petit diamètre de particule élémentaire (ici, le Printex XE2).

Dans cette étude, les principales causes qui peuvent expliquer les modifications apportées par les nanoparticules dispersées sur les explosions de méthane/air sont: i) une réaction des nanoparticules de noir de carbone se produit simultanément avec la réaction gazeuse, ii) les nanoparticules dispersées perturbent la propagation de la flamme, ce qui entraîne une augmentation de l'étirement de la flamme et de la surface de la flamme, iii), les nanoparticules présentes en amont du front de flamme modifient le transfert de chaleur radiatif entre le mélange non brûlé et les gaz brûlés, iv) les particules dispersées promeuvent le phénomène de nucléation de la suie.

Un effort pour valider chaque hypothèse a été fait dans ce travail et les principales conclusions sont présentées dans les sous-sections suivantes.

Faible niveau de turbulence :

Le nuage de nanoparticules de noir de carbone reste très stable quelques minutes après la dispersion. Le test de stabilité à la dispersion a notamment démontré qu'après trois minutes, le diamètre moyen de mobilité électrique ne change pas (environ 240 nm et 370 nm pour le Printex XE2 et le Corax N550, respectivement), avec une concentration de poussière considérablement plus élevée ($2{,}4.10^{5}$ particules.cm^{-3}) que la concentration initiale environnementale (bruit de fond) ($6{,}3.10^{3}$ particules.cm^{-3}).

Les tests de sévérité de l'explosion ont montré que, même à faible taux de turbulence, la présence de nanoparticules de noir de carbone modifie la violence de l'explosion. Cela signifie que pour un mélange pauvre en méthane, la sévérité de l'explosion peut être augmentée s'il existe une dispersion stable de nanoparticules. Par conséquent, il a été prouvé qu'une dispersion turbulente n'est pas obligatoire pour avoir une contribution significative des nanoparticules sur l'explosion.

Niveau de turbulence élevé :

À des niveaux élevés de turbulence, la diminution de la vitesse maximale de montée en pression est plus élevée que pour les systèmes à faible turbulence, en particulier pour la poudre possédant un plus faible diamètre de particule. Ces résultats suggèrent que la désagglomération des particules est obtenue à des niveaux élevés de turbulence, augmentant la surface totale et amplifiant l'effet des nanoparticules sur le transfert de chaleur ou les perturbations de la flamme. Un tel phénomène de désagglomération lié au niveau de turbulence initiale du nuage a déjà été démontré pour les microparticules (Murillo, 2016).

Hypothèse I - Contribution des nanoparticules de noir de carbone sur la réaction de combustion

Afin de tester la contribution chimique possible des nanoparticules de noir de carbone sur les explosions de mélanges hybrides, deux approches ont été mises en œuvre. Tout d'abord, les gaz brûlés ont été analysés par micro-chromatographie en phase gazeuse. La deuxième approche visait à comparer la sévérité de l'explosion du noir de carbone/méthane aux mélanges hybrides inerte d'alumine/méthane.

L'insertion de particules de noir de carbone pour des mélanges pauvres en méthane semble favoriser l'oxydation du CO en CO_2, ce qui génére une libération plus élevée d'énergie et, par conséquent, une augmentation de la vitesse de montée en pression. Cependant, il a été démontré que les fractions finales de CO et H_2 sont directement liées au niveau de turbulence initiale. En

d'autres termes, si la contribution réactive des nanoparticules de noir de carbone n'est pas négligeable, il n'est pas possible – par ce seul moyen - de relier leur combustion aux modifications de la gravité de l'explosion en raison de l'influence marquée de la turbulence dans la concentration finale de gaz brûlés.

Il a donc été imaginé d'utiliser des particules inertes afin d'identifier l'impact de la réaction des nanopoudres. L'insertion de particules d'alumine génère des tendances similaires pour les paramètres de sévérité d'explosion $(dP/dt)_m$ et P_m : ces paramètres augmentent lorsque de faibles concentrations de nanoparticules de noir de carbone et d'alumine sont injectées au sein de mélanges méthane/air dans des conditions de mélange pauvre en carburant. Ces résultats suggèrent que les effets des deux particules semblent être générés par des modifications du front de flamme et du transfert radiatif.

Détermination de la vitesse de combustion

L'estimation de la vitesse de combustion est intéressante car c'est une mesure fondamentale du processus de combustion et c'est, par ailleurs, une entrée essentielle pour la modélisation de la sévérité de l'explosion de ces systèmes. La mesure de cette variable sur des explosions des poussières et des mélanges hybrides est très difficile en raison de la nature turbulente de ces phénomènes et de l'interaction entre la réaction, le transfert de chaleur et la turbulence du système. Dans ce travail, la mesure expérimentale de la vitesse de la flamme a été réalisée par diverses approches :

Modèle de flamme mince issu des tests de sévérité par explosion

Une première approche a été mise en place afin de comprendre l'influence de l'insertion de nanoparticules de noir de carbone sur la vitesse de combustion des mélanges méthane/air. La vitesse de combustion a été estimée par le modèle de propagation sphérique d'une flamme mince en utilisant les tests de sévérité de l'explosion (Dahoe et al., 2002). Pour le mélange méthane / air, les valeurs estimées sont très proches des valeurs reportés dans la littérature (Proust, 2006). Deux principaux résultats doivent être mis en évidence pour les mélanges hybrides. Tout d'abord, la vitesse de combustion semble augmenter pour des mélanges pauvres en méthane lorsque de faibles concentrations de noir de carbone sont ajoutées au système (c'est-à-dire pour 0,1% mol. de noir de carbone), mais diminuent pour les mélanges stoechiométriques ou riches en carburant. Deuxièmement, une différence significative est obtenue entre la vitesse de combustion des mélanges hybrides Printex XE2/méthane et Corax N550/méthane. Ce résultat suggère que le diamètre des particules élémentaires a un fort effet sur la vitesse de combustion.

Cette approche présente l'avantage d'obtenir des données à partir d'un équipement standardisé, dans lequel la variabilité des résultats est considérablement réduite par rapport à la méthode du tube. Cependant, cette estimation prend en compte trois hypothèses importantes qui peuvent engendrer une sous-estimation de la vitesse de combustion: i) l'épaisseur de la flamme est supposée être négligeable (ce qui est également une hypothèse faite pour déterminer le paramètre Kst utilisé pour le dimensionnement des évents), ii) les faibles changements de richesse globale (gaz + poudre) n'impactent pas significativement la vitesse de montée en pression, iii) on suppose une propagation sphérique de la flamme et les perturbations de l'étirement et de la turbulence sont négligées.

Tube de propagation de la flamme :

La vitesse de la flamme a été mesurée à l'aide de la méthode du tube. La propagation de la flamme avant a été enregistrée à l'aide d'une caméra ultra rapide. Dans ces vidéos, la propagation de la flamme est enregistrée en profitant de la luminosité de la flamme et en améliorant la détection avec des filtres numériques.

Les tests de reproductibilité montrent une variabilité faible sur la vitesse spatiale de la flamme à faible taux de turbulence, mais les courbes distance versus temps semblent décalées dans le temps (i.e. plus forte variabilité) pour des niveaux des turbulences élevés. La vitesse spatiale semble diminuer lorsque la concentration en noir de carbone augmente dans le mélange initial. Le niveau de turbulence initiale a une influence importante sur les résultats de la vitesse spatiale, qui semble augmenter à des niveaux élevés de turbulence. Néanmoins, cette évolution n'est pas monotone et une réduction de la vitesse spatiale est mise en évidence pour les niveaux de turbulence très élevés (i.e., dans cette étude, pour un délai d'inflammation de 60 ms).

Les vitesses de flamme non étirées obtenues pour le gaz et les mélanges hybrides présentent une grande variabilité globale, ce qui rend très difficile l'établissement d'influences nettes des différentes variables étudiées dans ce travail. Néanmoins, il faut souligner que pour les mélanges méthane/air, les résultats ont été validés au regard des données de la littérature (Dirrenberger et al., 2011; Proust, 2006). On peut ainsi tirer quelques enseignements importants de ces essais :

Influence du niveau de turbulence initiale : pour presque toutes les concentrations de gaz étudiées dans ce travail, la vitesse de flamme non étirée semble plus élevée pour un niveau initial de turbulence intermédiaire (v_{rms} = 1,4 $m.s^{-1}$ / tv = 120 ms). Pour des niveaux de turbulence très élevés (v_{rms} = 1,6 ms^{-1} / tv = 60 ms), la vitesse non étirée diminue par rapport à celles observées aux faibles niveaux de turbulence (vrms = 0,9 ms^{-1} / tv = 500 ms), ce qui suggère que la flamme est fortement déstabilisée par le flux turbulent. Le facteur d'étirement est considérablement réduit pour les systèmes au niveau initial de faible turbulence, ce qui suggère que l'étirement est alors principalement dû à la courbure de la flamme plutôt qu'aux contraintes hydrodynamiques.

Influence de la concentration de poussière : Au niveau de turbulence initiale le plus bas (tv = 500 ms) analysé dans cette étude, la vitesse de la flamme non étirée semble augmenter pour les mélanges pauvres en carburant, mais diminue pour les mélanges stœchiométriques et riches en carburant. Cette tendance confirme les résultats obtenus dans les tests de sévérité conduits en sphère de 20 L. Pour les systèmes très turbulents, il n'a pas été possible d'établir une tendance claire.

<u>Apport de la technique dite de Schlieren</u>

Les images Schlieren permettent une meilleure observation de la propagation de la flamme et montrent un changement significatif de la surface de la flamme lorsque le niveau de turbulence initiale du système augmente : des flammes initialement lisses deviennent très plissées dans des conditions très turbulentes. Du fait du caractère stochastique de la turbulence, les résultats présentent une forte variabilité et l'établissement de tendances claires est encore difficile. Néanmoins, il est possible d'établir les conclusions suivantes :

Influence de la concentration en gaz : Pour les mélanges de gaz au repos (quiescent), la vitesse de combustion non étirée est plus élevée aux conditions stœchiométriques et diminue pour les mélanges pauvres ou riches en méthane.

Influence du niveau de turbulence initial : pour les mélanges de gaz, une réduction considérable de la vitesse de combustion non étirée est observée lorsque le niveau de turbulence initiale augmente. Pour les mélanges hybrides, il n'a pas été possible de déterminer une relation monotone claire entre le niveau de turbulence et la vitesse de la flamme non étirée.

Influence de la concentration de poussière : indépendamment de la grande variabilité du système, il semble que la vitesse de combustion non étirée augmente lorsque la concentration de noir de carbone augmente dans le mélange initial.

Des différences considérables ont été trouvées entre la vitesse non étirée obtenue à partir de vidéos sans filtres physiques et celle extraite à partir des vidéos enregistrées à l'aide des images Schlieren. En plus des considérations liées à la variabilité des résultats du fait de la turbulence, les interactions rapides entre les parois du tube et la flamme augmentent grandement son instabilité, par conséquent, peuvent limiter la reproductibilité des tests.

En outre, les différences entre les deux méthodes de détection du front de flamme suggèrent que l'estimation de la surface de la flamme est fondamentale pour avoir une bonne estimation de la vitesse de la flamme. Une amélioration considérable de la surface de la flamme est obtenue par la méthode de Schlieren. Il a été démontré que la détection de l'interface de flamme basée sur la luminosité génère une surestimation de la surface de la flamme. Il faut par ailleurs souligner que les irrégularités de surface de flamme n'ont pas été prises en compte dans cette analyse.

Hypothèse II - Les perturbations de la flamme par les nanoparticules dispersées

Les résultats du tube de propagation de la flamme ont également été analysés afin d'étudier les modifications éventuelles sur la surface de la flamme en raison de la dispersion des nanoparticules. La vitesse de combustion non étirée estimée pour les mélanges d'alumine/méthane/air est considérablement supérieure à celle obtenue pour les explosions de mélanges de gaz. Les résultats précédents combinés au fait que des flammes avec des vitesses spatiales similaires peuvent présenter des vitesses de combustion non étirées différentes, suggèrent que la présence de particules solides telles que l'alumine modifie la surface de la flamme pendant la propagation. Cependant, il n'a pas été possible de séparer l'influence de la modification du front de flamme de la contribution du transfert de chaleur radiatif et de la contribution chimique des nanoparticules de noir de carbone. En outre, la méthode de Schlieren a mis en évidence des modifications de la surface de la flamme et du facteur d'étirement dû à la dispersion des nanoparticules, mais la quantification de ces phénomènes reste sujette à caution.

Modèle numérique

Un modèle numérique pour estimer la vitesse de la flamme d'une explosion de mélange de gaz et de nanoparticules a été développé. Dans ce contexte, l'influence du transfert de chaleur radiatif et de la réaction du noir de carbone a également été incluse.

Le modèle numérique a été validé pour les mélanges méthane/air. Les résultats obtenus sur la température de la flamme et les fractions massiques de composés sont en bon accord avec ceux issus des logiciels commerciaux 1-D (par exemple, la température de flamme obtenue pour 9% de mélanges de méthane / air est de 2271 K par rapport à une température adiabatique théorique obtenue par PREMIX de 2236 K). L'étude de l'effet de la dispersion des particules de noir de carbone est initialement limitée au transfert de rayonnement thermique généré par le nuage de poussière non transparent. Une augmentation de 23% de la propagation de la flamme est obtenue lorsqu'une concentration de 6 $g.m^{-3}$ de particules de noir de carbone (avec un diamètre de particule élémentaire de 75 nm) est ajoutée au mélange gazeux initial.

On a d'abord pensé que le transfert de chaleur radiatif génère une diminution de la sévérité de l'explosion du fait de la perte de chaleur dans la zone réactive, ce qui entraîne une température de flamme plus faible. Cependant, les résultats du modèle numérique suggèrent que la contribution du rayonnement thermique a un effet favorisant la propagation de la flamme dû à l'augmentation de la température dans la zone de préchauffage. Ce résultat est conforme à l'augmentation observée expérimentalement au niveau de la sévérité de l'explosion de certains mélanges hybrides.

Hypothèse III - Influence du transfert de chaleur par rayonnement sur la vitesse de combustion

L'insertion de nanoparticules modifie considérablement le transfert de chaleur radiatif, comme cela a été observé dans les vidéos de propagation de la flamme et les images Schlieren. Cependant, la quantification du transfert de chaleur par rayonnement est encore un défi. Comme souligné précédemment, le modèle numérique suggère que l'accélération de la flamme peut être considérable en raison de la contribution radiative d'un média non transparent.

De plus, les différences de vitesse de flamme non étirées entre les mélanges méthane / alumine et méthane / noir de carbone confirment l'impact significatif du transfert de chaleur radiatif sur la propagation de la flamme. Cependant, une différenciation de la contribution individuelle de la modification de la surface de la flamme (hydrodynamique) et du transfert de chaleur radiatif est encore nécessaire pour mieux isoler le phénomène prédominant pendant la propagation de la flamme.

6.2. PERSPECTIVES

Applications en sécurité des procédés

Les résultats de ce travail de recherche suggèrent qu'une attention particulière doit être accordée au dimensionnement des dispositifs de protection impliquant des mélanges hybrides. Les modifications mises en évidence sur les paramètres de gravité de l'explosion (P_m, dP/dt_m et K_{st}) en raison de la présence de nanoparticules (ou plus largement de particules en suspension) peuvent induire des différences notables sur la surface des évents par rapport aux mélanges de gaz pur. Comme souligné en introduction de ce travail, le processus de gazéification est un exemple de génération de mélanges hybrides de particules carbonées/gaz. Sur la Figure 116, le schéma d'un gazéifieur à lit fluidisé circulant incluant une étape de filtration à haute température des gaz obtenus est représenté. Les résultats du test de sévérité de l'explosion suggèrent qu'un dimensionnement différent du dispositif de protection devrait être effectué pour le mélange hybride présent dans le gazéifieur (noir de carbone ou suies/gaz de synthèse) par rapport au gaz de synthèse après filtration (accroissement possible de la surface d'évent).

En outre, l'étude de propagation de la flamme montre des modifications sur la surface de la flamme et une augmentation du transfert de rayonnement lorsque des nanoparticules de noir de carbone sont dispersées dans le mélange initial. Les résultats précédents suggèrent que les particules dispersées génèrent des modifications de l'épaisseur de la flamme qui invalident les hypothèses implémentées dans la loi cubique (utilisée pour le dimensionnement d'évent) et impliquent une remise en cause de cette loi pour le dimensionnement des dispositifs de protection pour des mélanges hybrides.

De plus, les tests de gravité de l'explosion ont montré une extinction turbulente (quenching) de mélanges hybrides avec des nanoparticules ayant un très petit diamètre de particule. Cela donne ainsi l'occasion d'étudier cet effet pour différents types d'applications, comme par exemple l'injection rapide de nanoparticules inertes qui, dans des conditions turbulentes, engendrerait une extinction de flamme par effet thermique, mais également par recombinaison de radicaux.

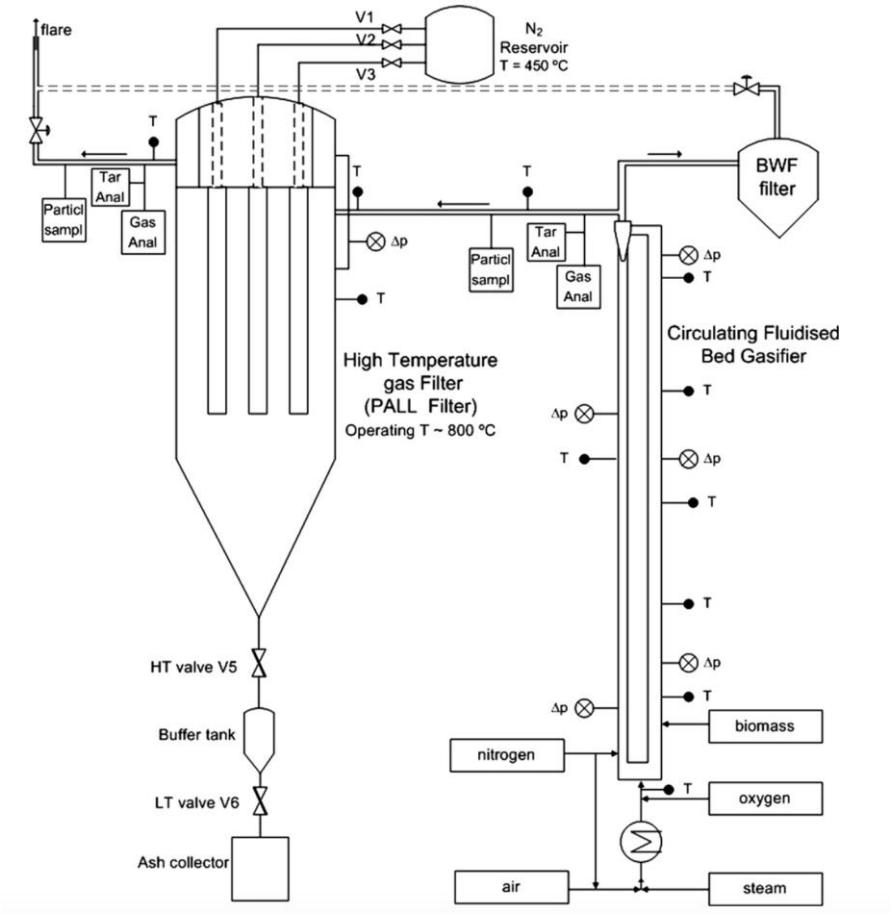

Figure 116. Diagramme schématique d'un dispositif de gazéfication et de filtration (Simeone et al., 2011).

Perspectives pour d'autres travaux de recherche

Les résultats de ce travail ont démontré la modification des paramètres de gravité de l'explosion des mélanges méthane/air en raison de la dispersion des nanoparticules de noir de carbone. Cependant, des recherches supplémentaires sur la détermination expérimentale de la vitesse de combustion de la flamme des mélanges hybrides sont encore nécessaires. En outre, les phénomènes simultanés, qui se produisent lors de l'explosion des mélanges hybrides, doivent être caractérisés et leurs contributions doivent être quantifiées. Cette section vise à mettre en évidence les principaux travaux futurs, ou déjà initiés, ou qui seront bientôt mis en œuvre dans le laboratoire LRGP.

Approche expérimentale:

Le tube de propagation de la flamme a été utilisé pour déterminer la vitesse de la flamme des mélanges hybrides. Cependant, l'interaction rapide de la flamme avec les parois du tube génère des problèmes pour la détection de la flamme, augmente l'étirement de la flamme et peut augmenter la variabilité des résultats. Une telle mise en place expérimentale sera néanmoins utile pour déterminer l'impact des obstacles ou des arrêtes-flammes (trempe/quenching) sur la propagation de la flamme dans le tube.

Au cours du travail de recherche de Murillo (2016), une réplique de la sphère d'explosion 20L a été construite pour visualiser et quantifier la dispersion de poussière à l'intérieur de l'équipement. Dans le cadre de ce travail, certaines modifications y ont été apportées pour incorporer une source d'allumage (étincelle permanente) et un système de décompression (soupape) afin d'effectuer une explosion aux conditions atmosphériques (Figure 117). Des

essais de propagation de la flamme sont actuellement effectués sur le mélange de méthane/air (Figure 118) afin d'étudier la propagation sphérique du noyau de flamme et d'enregistrer la propagation de la flamme sans l'influence des parois, ni celle de la libération de pression par ouverture de soupape. Cette configuration de propagation de la flamme améliorera la caractérisation de l'étirement de la flamme pendant sa propagation. En outre, la technique Schlieren sera également implémentée pour cet équipement afin d'obtenir une meilleure détection de flamme avant de flamme.

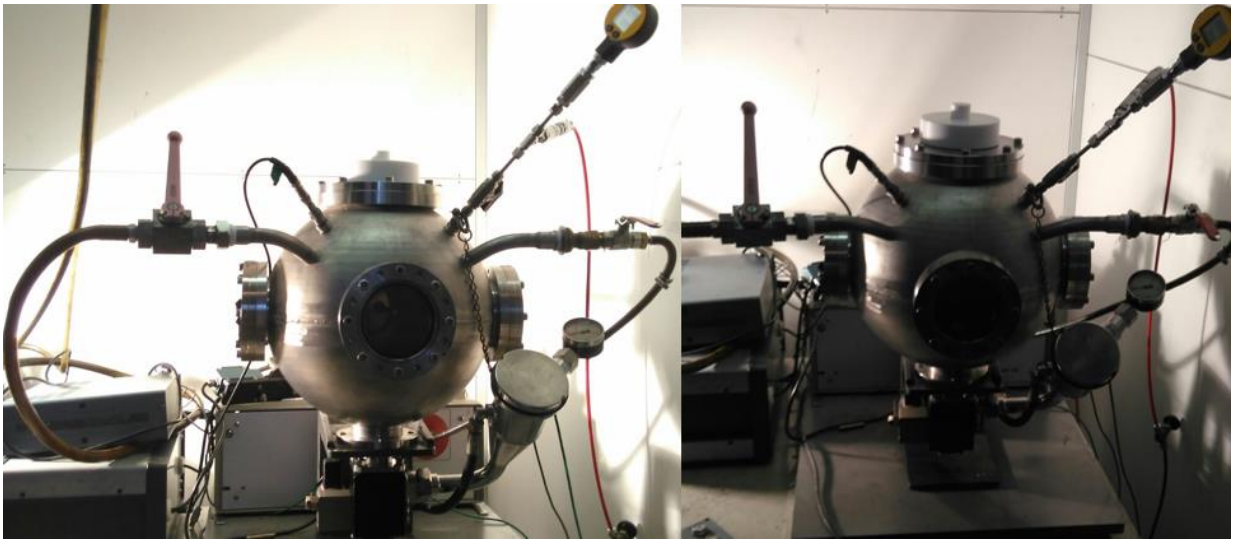

Figure 117. L'adaptation de la sphère d'explosion à l'étude de la propagation de la flamme.

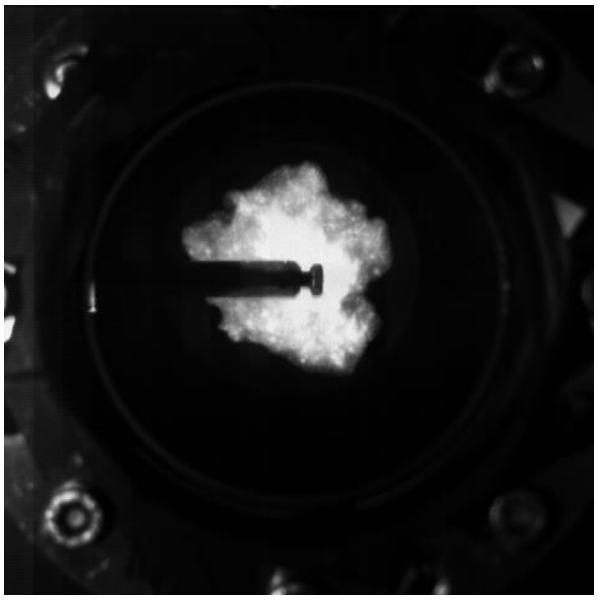

Figure 118. Propagation d'une flamme de méthane en sphère éventée de 20L.

La quantification de la masse suspendue de nanoparticules pendant la dispersion devrait être incorporée à l'analyse de l'effet des nanoparticules sur la propagation de la flamme, à différents niveaux de turbulence. Les techniques d'extinction du laser basées sur la loi de Beer-Lambert devraient être mises en œuvre à cette fin.

Hypothèse IV - Nanoparticules comme noyaux de condensation des suies

L'effet probable des nanoparticules de noir de carbone (ou d'autres particules de poussière en suspension, par exemple l'alumine) en tant que noyaux de condensation des suies doit également être analysé. Un système permettant la collecte rapide d'échantillons de poussière / suie après

explosion (en en présence d'inerte afin de différencier la nature du noyau et des condensats) doit être mis en place afin de les étudier par microscopie électronique à balayage, rayonnement XRR ou analyse thermo-gravimétrique (TGA).

Approche numérique :

Dans ce travail, une méthode numérique a été développée afin d'estimer la vitesse de propagation de la flamme des mélanges hybrides. Cependant, ce modèle numérique ne prend pas en compte la turbulence initiale, est limité à une seule direction dans l'espace et suppose une distribution de taille de particules monomodale. D'autres développements sont donc nécessaires afin d'améliorer ces points.

En outre, la simulation CFD de la propagation de la flamme du mélange hybride sur STAR-CCM V11.02 est en cours en collaboration avec l'Université de los Andes à Bogotá, en prenant en compte les réactions simultanées, le transfert de chaleur et le système turbulent. Un travail futur devrait être initié afin de combiner le modèle numérique précédent avec l'approche CFD. Il sera alors possible de valider le modèle CFD numérique et d'optimiser le mécanisme de réaction afin d'obtenir un modèle 'prédictif'. Ce type de modèle aidera à prédire le comportement explosif de mélanges hybrides spécifiques en limitant le nombre de tests et en se concentrant uniquement sur quelques expériences de validation.

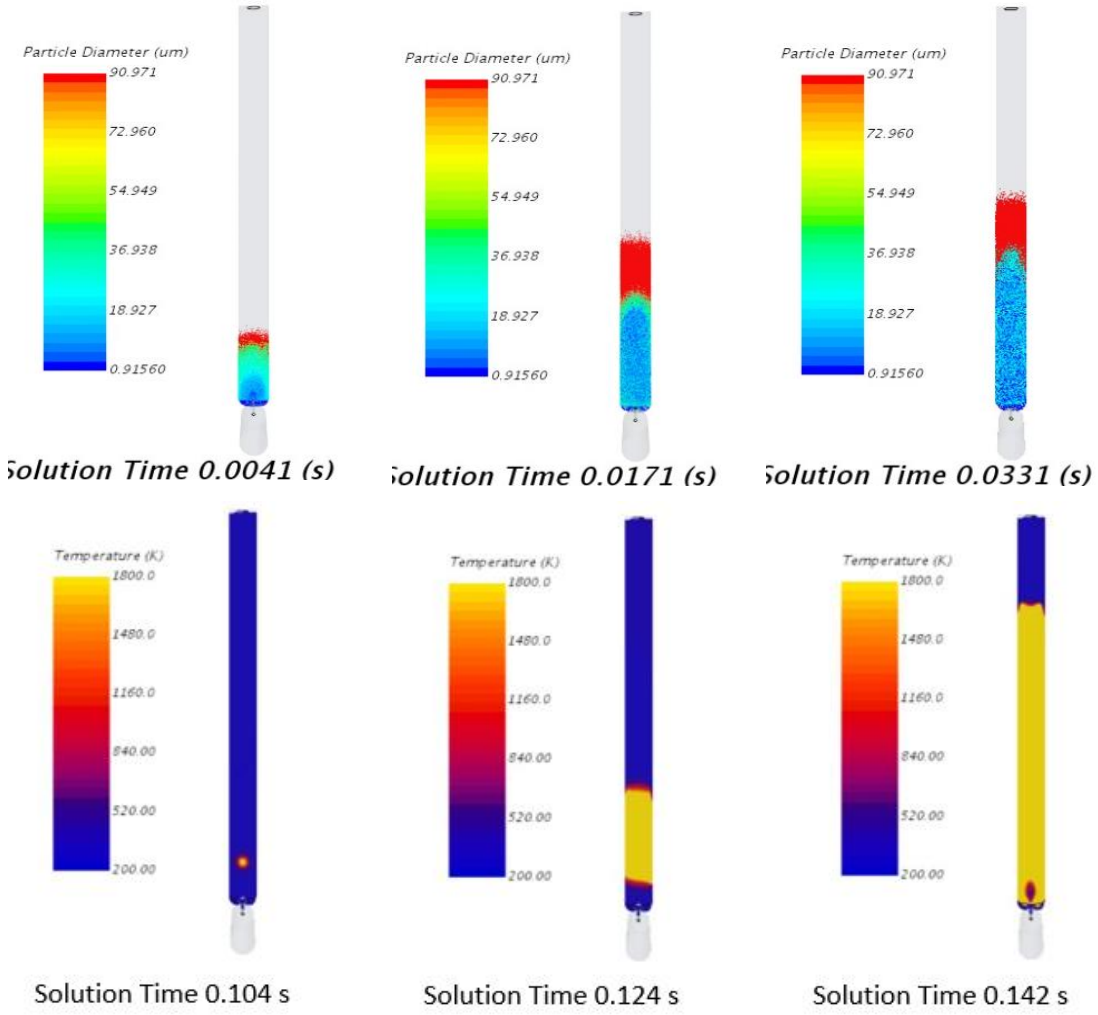

Figure 119. Simulation CFD dans STAR-CCM + de la dispersion du noir de carbone et de la propagation de la flamme dans le tube de propagation de la flamme de 1 m (résultats du projet de recherche actuellement réalisé par Andrés Pinilla, Universidad de los Andes).

Enfin, ce travail de recherche pourra également trouver une application dans la conception de brûleurs de métal / gaz hybrides combinés à la conversion de chaleur pour des systèmes de propulsion, c'est-à-dire pour le transport terrestre ou les applications aérospatiales (Julien et al., 2017 ; Lomba, 2016; Soo et al., 2013).

References

Dirrenberger, P., Le Gall, H., Bounaceur, R., Herbinet, O., Glaude, P.-A., Konnov, A., Battin-Leclerc, F., 2011. Measurements of Laminar Flame Velocity for Components of Natural Gas. Energy Fuels 25, 3875–3884.

Julien, P., Whiteley, S., Soo, M., Goroshin, S., Frost, D.L., Bergthorson, J.M., 2017. Flame speed measurements in aluminum suspensions using a counterflow burner. Proc. Combust. Inst. 36, 2291–2298.

Lomba, R., 2016. Utilisation de la combustion métallique dans les machines thermiques. PhD thesis. Université d'Orleans.

Murillo, C., 2016. Experimental and numerical approaches to particles dispersion in a turbulent flow: application to dusts explosion. Université de Lorraine.

Proust, C., 2006. A few fundamental aspects about ignition and flame propagation in dust clouds. J. Loss Prev. Process Ind. 19, 104–120.

Simeone, E., Nacken, M., Haag, W., Heidenreich, S., de Jong, W., 2011. Filtration performance at high temperatures and analysis of ceramic filter elements during biomass gasification. Biomass Bioenergy, CHRISGAS 35, S87–S104.

Soo, M., Julien, P., Goroshin, S., Bergthorson, J.M., Frost, D.L., 2013. Stabilized flames in hybrid aluminum-methane-air mixtures. Proc. Combust. Inst. 34, 2213–2220.

Appendix A: Flame propagation Results

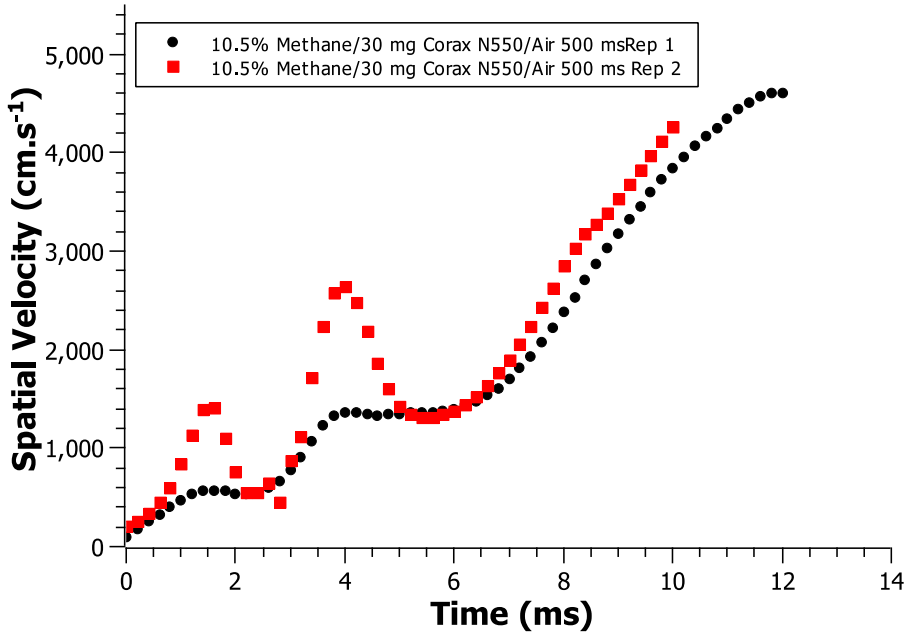

Figure 120. Reproductibility test for 10.5% methane/ 30 mg Corax N550/ air at v_{rms} = 0.9 m.s^{-1}

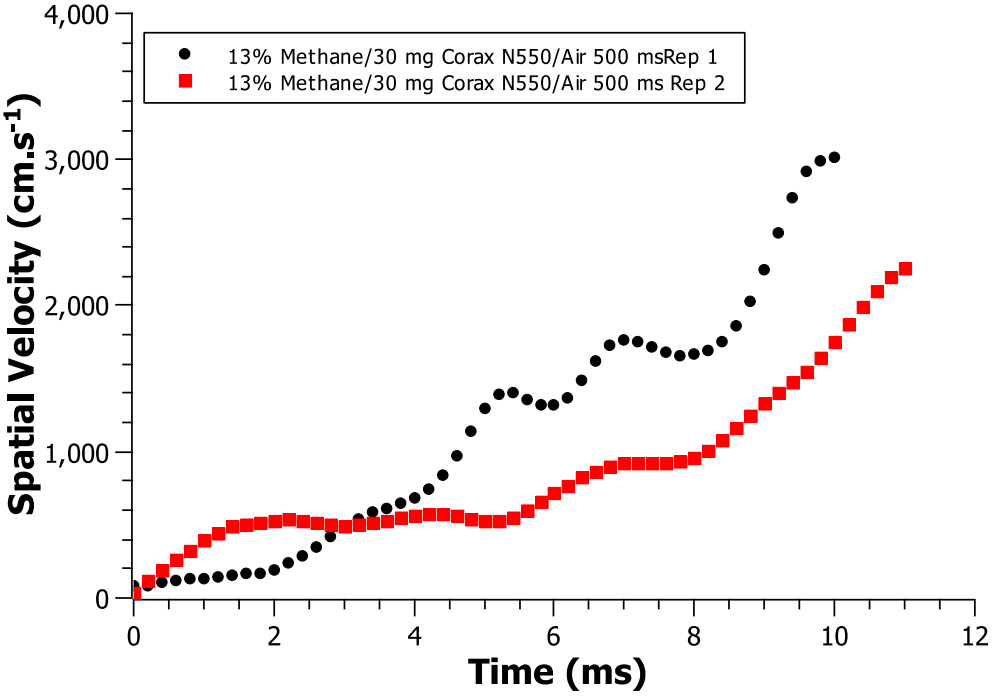

Figure 121. Reproductibility test for 13% methane/ 30 mg Corax N550/ air at v_{rms} = 0.9 m.s^{-1}

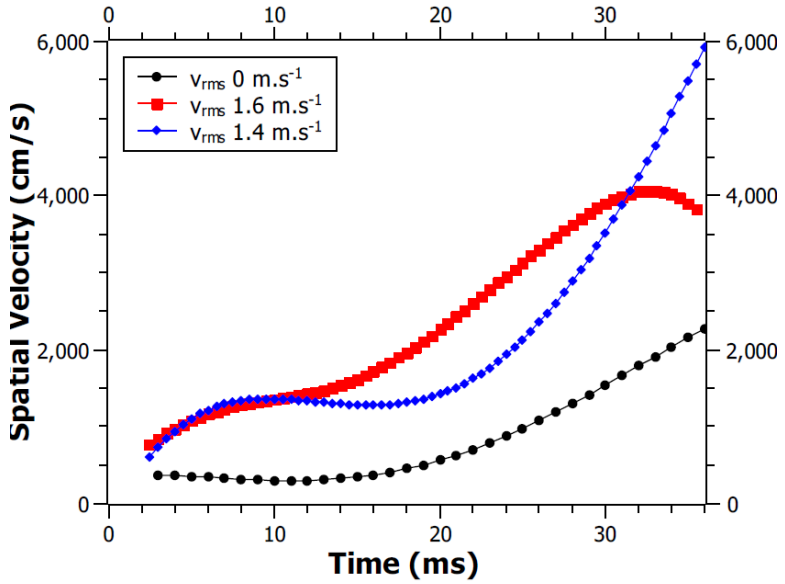

Figure 122. Spatial velocity of 9% Methane/air explosion at different initial turbulence level.

Appendix B: Conservation Energy Balance

The total energy balance of a system is described by (Poinsot and Veynante, 2005):

$$\partial_t(\rho e_t) + div(\rho e_t u) + div(Pu) + div(q) = div(\tau(u) \cdot u) \quad \text{Eq 78}$$

The total energy can be expressed as the mechanical and chemical + sensible energy:

$$e_t = \frac{1}{2}|u|^2 + e$$

Taking in account the total energy definition, equation 78 became:

$$\frac{1}{2}\partial_t(\rho|u|^2) + \partial_t(\rho e) + \frac{1}{2}div(pu \cdot |u|^2) + div(\rho eu) + div(Pu) + div(q) = div(\tau(u) \cdot u) \quad \text{Eq 79}$$

$$\frac{1}{2}\partial_t(\rho|u|^2) + \partial_t(\rho e) + \frac{1}{2}div(pu \cdot |u|^2) + div(\rho eu) + Pdiv(u) + u \cdot \nabla P + div(q) - div\big(\tau(u)\big) \cdot u = \tau(u) : \nabla u \quad \text{Eq 80}$$

The conservation equation establish the following relation (Poinsot and Veynante, 2005):

$$\frac{1}{2}\partial_t(\rho|u|^2) + \frac{1}{2}div(pu \cdot |u|^2) = u[\partial_t(\rho u) + div(pu \otimes u)] = -u \cdot \nabla P + div\big(\tau(u)\big) \cdot u$$

Inserting this relationship into the energy balance:

$$\partial_t(\rho e) + div(\rho eu) + Pdiv(u) + div(q) = \tau(u) : \nabla u \quad \text{Eq 81}$$

The energy balance must be written in terms of the temperature of the system, so the definition of the total enthalpy of the system is used:

$$e = h - \frac{P}{\rho} = \sum y_i h_i - \frac{P}{\rho}$$

$$\partial_t\left(\rho(h - \frac{P}{\rho})\right) + div\left(\rho(h - \frac{P}{\rho})u\right) + Pdiv(u) + div(q) = \tau(u) : \nabla u$$

$$\partial_t(\rho h) + \partial_t P + div(\rho hu) - u \cdot \nabla P - Pdiv(u) + Pdiv(u) + div(q) = \tau(u) : \nabla u$$

$$\partial_t(\rho h) + \partial_t P + div(\rho hu) - u \cdot \nabla P + div(q) = \tau(u) : \nabla u$$

The total enthalpy is divided in sensible and chemical energy as follows:

$$h = h_s + \sum_{i=1}^{Nspecies} y_i h_{f,i}^0 \quad \text{Eq 82}$$

The energy balance could be related to the sensible enthalpy as follows:

$$\partial_t(\rho h_s) + \sum_{i=1}^{Nspecies} h_{f,i}^0 \left[\partial_t(\rho y_i) + div(\rho y_i u)\right] + \partial_t P + div(\rho h_s u) - u \cdot \nabla P + div(q) = \tau(u) : \nabla u \quad \text{Eq 83}$$

Using the equation 37 (the species balance), we have

$$\frac{\partial}{\partial t}(\rho y_i) + div(\rho y_i u) = \dot{\omega}_i - div(j_i)$$

So the energy balance became (Poinsot and Veynante, 2005):

$$\partial_t(\rho h_s) + div(\rho h_s u) + \sum_{i=1}^{Nspecies} h_{f,i}^0 \dot{\omega}_i - \sum_{i=1}^{Nspecies} div(h_{f,i}^0 j_i) + \partial_t P - u \cdot \nabla P + div(q) = \tau(u) : \nabla u$$

If the energy flux q is defined as:

$$q = -\lambda \nabla \mathrm{T} + \sum_{i=1}^{Nspecies} h_i j_i$$

$$\partial_t(\rho h_s) + div(\rho h_s u) + \sum_{i=1}^{Nspecies} h_{f,i}^0 \dot{\omega}_i - \sum_{i=1}^{Nspecies} div\left(h_{f,i}^0 j_i\right) + \partial_t P - u \cdot \nabla P - div(\lambda \nabla \mathrm{T}) + \sum_{i=1}^{Nspecies} div(h_i j_i) = \tau(u) : \nabla u$$

The equation 82 is rewritten for the specie i as:

$$h_i = h_{s,i} + h_{f,i}^0$$

By this relation, the diffusion flux is expressed in terms of the sensible energy of the system as:

$$\partial_t(\rho h_s) + div(\rho h_s u) + \sum_{i=1}^{Nspecies} h_{f,i}^0 \dot{\omega}_i + \partial_t P - u \cdot \nabla P - div(\lambda \nabla \mathrm{T}) + \sum_{i=1}^{Nspecies} div\left(h_{s,i} j_i\right) = \tau(u) : \nabla u$$

Assuming that the mean heat capacity of the mixture is constant with the temperature, the sensible energy is (Poinsot and Veynante, 2005):

$$h_s = \sum_{i=1}^{Nspecies} C_{p,i} y_i T$$

$$\sum_{i=1}^{Nspecies} C_{p,i} \partial_t(\rho y_i T) + \sum_{i=1}^{Nspecies} C_{p,i}\, div(\rho y_i T u) + \sum_{i=1}^{Nspecies} h_{f,i}^0 \dot{\omega}_i + \partial_t P - u \cdot \nabla P - div(\lambda \nabla \mathrm{T}) + \sum_{i=1}^{Nspecies} C_{p,i} div(j_i T) = \tau(u) : \nabla u$$

$$\sum_{i=1}^{Nspecies} C_{p,i}[\partial_t(\rho y_i T) + div(\rho y_i T u) + div(j_i T)] + \sum_{i=1}^{Nspecies} h_{f,i}^0 \dot{\omega}_i + \partial_t P - u \cdot \nabla P - div(\lambda \nabla \mathrm{T}) = \tau(u) : \nabla u$$

$$\sum_{i=1}^{Nspecies} C_{p,i}[\rho y_i \partial_t(T) + \rho y_i u div(T) + j_i div(T) + T\partial_t(\rho y_i) + T div(\rho y_i u) + T div(j_i)] + \sum_{i=1}^{Nspecies} h_{f,i}^0 \dot{\omega}_i + \partial_t P + -u \cdot \nabla P - div(\lambda \nabla \mathrm{T}) = \tau(u) : \nabla u$$

Using again the species balance, the energy balance is simplified as follows:

$$\sum_{i=1}^{Nspecies} C_{p,i}[\rho y_i \partial_t(T) + \rho y_i u div(T) + j_i div(T) + T\dot{\omega}_i] + \sum_{i=1}^{Nspecies} h_{f,i}^0 \dot{\omega}_i + \partial_t P - u \cdot \nabla P - div(\lambda \nabla \mathrm{T}) = \tau(u) : \nabla u$$

Assuming constant pressure and neglecting viscous terms, the energy balance is (Poinsot and Veynante, 2005);

$$\sum_{i=1}^{Nspecies} C_{p,i}[\rho y_i \partial_t(T) + \rho y_i u div(T) + j_i div(T)] = -\dot{\omega}_i \left[\sum_{i=1}^{Nspecies} \left[h_{f,i}^0 + C_{p,i} T \right] \right] + div(\lambda \nabla \mathrm{T})$$

Effect of carbon black nanoparticles on the explosion severity of gas mixtures

Flammable gas/solid hybrid mixture explosions are not well understood because of the interaction of the thermal transfer process, the combustion kinetics mechanisms and the interactions between turbulence and combustion. The main objective on this work is to study the explosion severity and flame burning velocities of carbon black nanoparticles/methane to better understand the influence of added nanopowders in gas explosions.

Tests have been performed in a flame propagation tube and in the standard 20 L explosion sphere. The influence of carbon black particles on the explosions severity and in the front flame propagation has been appreciated by comparing the results obtained for pure gas mixtures. It appeared that the carbon black nanoparticles insertion increases around 10% the explosion severity for lean methane mixtures. Therefore, it seems that nanoparticles has an impact on the severity of the explosion even for quiescent systems, contrary to systems involving micro-sized powders that requires a dispersion at high turbulence levels. The increment on the maximum rate of pressure rise is higher for powders with lower elementary particle diameter, which is notably due to the fragmentation phenomena. A flame propagation numerical model associated to a gas/carbon black mixture has been developed to examine the influence of carbon blacks on the flame propagation. The results of the numerical model suggest that the radiative heat contribution promotes the flame acceleration. This result is consistent with the experimental increase on the explosion severity for some hybrid mixtures.

Keywords: *Nanoparticles, hybrid mixtures, dust explosions, soot formation*

Effet de nanoparticules de noir de carbone sur la sévérité d'explosions de mélanges des gaz

Les explosions de mélanges de gaz inflammables/solides combustibles ne sont pas bien comprises en raison de la complexité des transferts thermiques, des mécanismes de cinétiques et des interactions entre la turbulence /combustion. L'objectif principal de ce travail est d'étudier la sévérité des explosions des nanoparticules de carbone noir/méthane afin de comprendre l'influence de l'insertion des nanoparticules sur les explosions de gaz.

Des tests ont été effectués sur ces mélanges dans un tube de propagation de la flamme et dans une sphère d'explosion standard de 20 L. L'influence de la turbulence initiale et de la taille de particule élémentaire du noir de carbone a également été étudiée. Il semble que l'insertion de nanoparticules de noir de carbone augmente d'environ 10% la sévérité de l'explosion pour les mélanges pauvres en méthane. Par conséquent, il semble que les nanoparticules ont un impact sur la sévérité de l'explosion même pour les systèmes à basse turbulence, contrairement aux systèmes impliquant des poudres de taille micrométrique qui nécessitent une dispersion à des niveaux élevés de turbulence. L'augmentation de la vitesse maximale de montée en pression est plus élevée pour des poudres avec un petit diamètre de particule, notamment en raison des phénomènes de fragmentation. En outre, un modèle numérique de propagation de front de flamme associé à un mélange gaz/noir de carbone a été développé pour examiner l'influence du noir de carbone sur la propagation de la flamme. Les résultats du modèle numérique suggèrent que la contribution de la chaleur radiative favorise l'accélération de la flamme. Ces résultats sont en accord avec les résultats expérimentaux de sévérité de l'explosion pour certains mélanges hybrides.

Mot clés : *Nanoparticules, mélanges hybbirdes, explosion de poussières, particules des suies*